

**NONLINEAR TIME HISTORY AND PUSH-OVER ANALYSES
FOR SEISMIC DESIGN AND EVALUATION**

by

Yonghui Roger Li, M.Sc.

Dissertation

Presented to the Faculty of the Graduate School of

the University of Texas at Austin

in Partial Fulfillment

of the Requirements

for the Degree of

Doctor of Philosophy

The University of Texas at Austin

December 1996

**NONLINEAR TIME HISTORY AND PUSH-OVER ANALYSES
FOR SEISMIC DESIGN AND EVALUATION**

**Approved by
Dissertation Committee:**

James G. ...

Paul E. ...

Michael W. ...

Jose M. ...

Kenneth ...

To my dearest wife, Fan Liu

ACKNOWLEDGMENTS

The author is deeply indebted to Dr. James O. Jirsa for his continuous encouragement, guidance, friendly advice and support throughout this research. I am so fortunate to have worked under the supervision of Dr. Jirsa who has not only enriched my education in structural engineering, but more importantly, inspired my belief in myself. Without the mentorship from Dr. Jirsa, I could not have completed my Ph.D. degree.

I also wish to express my sincere gratitude to the dissertation committee members: Dr. M. D. Engelhardt, Dr. M. E. Kreger, Dr. K. M. Liechti and Dr. J. M. Roesset for their time and advice given to my research work. I enjoyed the friendly conversations with Dr. Engelhardt and Dr. Kreger. The course I took from Dr. Liechti was one of my favorites. The help from Dr. Roesset is highly appreciated. Also the advice from Dr. S. Wood is very valuable. In addition, I wish to thank Dr. C. P. Johnson, Dr. J. L. Tassoulas, and Dr. R. E. Klingner for their help at the beginning of my study here at Austin.

Special thanks are extended to the staff of the Civil Engineering Department and Phil M. Ferguson Structural Engineering Laboratory, in particular, to Lena M. Brooks, Laurie Golding and April Jenkins.

I would also like to give my thanks to fellow graduate students who helped me and made working at Ferguson Laboratory such a joyful experience. To name a few, I like to thank Scott Luckiesh, Abdelhakim Bouadi, Robert Frosch, Wanzhi Li, Yonggang Zhang and David Gwie.

Finally, my deepest thanks goes to my wife, Fan Liu, for her love and understanding, for providing me with so much needed support and encouragement. She always believed in me and stood behind me. Without her, I would not be able to go through all the difficult days.

**NONLINEAR TIME HISTORY AND PUSH-OVER ANALYSES
FOR SEISMIC DESIGN AND EVALUATION**

Publication No. _____

Yonghui Roger Li, Ph.D.
The University of Texas at Austin, 1996

Supervisor: James O. Jirsa

The extensive damage and economic losses which occurred during the 1994 Northridge and other recent moderate earthquakes have stimulated structural engineers to consider how to protect economic investment in addition to meeting life safety requirements of buildings.

The equivalent lateral force procedure for seismic design is based on implicit consideration of inelastic response of structures in earthquakes. Experience with past earthquakes has indicated that this procedure is inadequate in controlling damage in buildings. Nonlinear dynamic time history analyses explicitly provide information on the magnitude and change of internal forces and deformations in structures.

The objective of this study is to demonstrate the capacity of nonlinear programs to predict performance of reinforced concrete structures subjected to various earthquake ground motions, and to provide guidance on use of nonlinear analyses for seismic design and evaluation. Two buildings subjected to three different earthquakes are analyzed using two nonlinear programs: DRAIN-2D and IDARC, and the analysis results are compared with recorded response data. Both nonlinear dynamic time history and nonlinear static push-over analyses are performed, and correlations between these two nonlinear analysis methods are studied. A simplified shear failure model is proposed in the study. A number of parameters affecting the results, such as damping coefficients, actual strength of materials, effective stiffness and residual shear capacity are investigated. Also the performance of the buildings subjected to various representative earthquake ground motions is studied. Design-spectrum-compatible artificial earthquakes are generated and the most critical design earthquakes are discussed.

TABLE OF CONTENT

CHAPTER 1: INTRODUCTION	1
1.1 General	1
1.2 Objective	3
1.3 Scope	4
CHAPTER 2: LITERATURE REVIEW AND BACKGROUND INFORMATION ..	6
2.1 General	6
2.2 Computation of Inelastic Response	9
2.2.1 Linear Elastic Analysis Methods	10
2.2.2 Inelastic Analysis Methods	20
2.3 Earthquake Response from Instrumented Buildings	31
2.4 Performance Based Seismic Engineering	35
2.4.1 Performance Level Definitions	40
2.4.2 Earthquake Design Levels	46
CHAPTER 3: BUILDING AND INSTRUMENTATION DATA COLLECTION ..	48
3.1 General	48
3.2 Seven-Story Hotel at 8244 Orion Avenue	48
3.2.1 General Building Description	49
3.2.2 Northridge Earthquake (1994)	60
3.2.2.1 Building Instrumentation	60
3.2.2.2 Building Earthquake Damage	67
3.2.3 San Fernando Earthquake (1971)	72
3.2.3.1 Building Instrumentation	73
3.2.3.2 Building Earthquake Damage	78
3.3 Ten-Story Building at 7215 Bright Avenue	79
3.3.1 General Building Description	79

3.3.2 Whittier Narrows Earthquake (1987)	89
3.3.2.1 Building Instrumentation	89
3.3.2.2 Building Earthquake Damage	90
CHAPTER 4: NONLINEAR PROGRAMS AND ANALYTICAL MODELS	94
4.1 General	94
4.2 Nonlinear Programs	95
4.2.1 DRAIN-2D	95
4.2.1.1 Dynamic Equilibrium and Integration Procedure	96
4.2.1.2 Damping Coefficients	97
4.2.1.3 Reinforced Concrete Member Modeling	98
4.2.1.4 Extended Takeda's Model	99
4.2.2 IDARC	101
4.2.2.1 Dynamic Equilibrium and Integration Procedure	104
4.2.2.2 Viscous Damping	104
4.2.2.3 Reinforced Concrete Member Modeling	104
4.2.2.4 Hysteretic Modeling	108
4.3 Analytical Model	110
4.3.1 DRAIN-2D	110
4.3.1.1 Material Properties	111
4.3.1.2 Element Stiffness	112
4.3.1.3 Shear Failure Model	121
4.3.2 IDARC	126
4.3.2.1 Material Properties	127
4.3.2.2 Shear Failure	127
CHAPTER 5: NONLINEAR DYNAMIC TIME HISTORY ANALYSES	130
5.1 General	130
5.2 Seven-Story Hotel in the Northridge Earthquake	130

5.2.1 Evaluation of Response Records	132
5.2.1.1 Torsional Effects	132
5.2.1.2 Periods of Vibration	135
5.2.2 Parametric Study	138
5.2.2.1 Damping Coefficients	138
5.2.2.2 Actual Strength of Materials	138
5.2.2.3 Effective Stiffness of Members $(EI)_{\text{eff}}$	140
5.2.2.4 Residual Shear Capacity	142
5.2.3 Analysis Results	142
5.3 Seven-Story Hotel in the San Fernando Earthquake	155
5.3.1 Evaluation of Response Records	155
5.3.2 Analysis Results	157
5.3.2.1 DRAIN-2D Analyses	157
5.3.2.2 IDARC Analyses	167
5.4 Ten-Story Building in the Whittier Narrows Earthquake	168
5.4.1 Evaluation of Response Records	173
5.4.2 Analysis Results	173
CHAPTER 6: NONLINEAR STATIC (PUSH-OVER) ANALYSES	180
6.1 General	180
6.2 Seven-Story Hotel	182
6.2.1 Current Seismic Design Criteria	183
6.2.2 1994 Northridge Earthquake	184
6.2.2.1 Loading Patterns	184
6.2.2.2 Effects of Effective Stiffness $(EI)_{\text{eff}}$	190
6.2.3 1971 San Fernando Earthquake	193
6.3 Ten-Story Building	199
6.3.1 Seismic Design Criteria	199

6.3.2 Loading Patterns	200
6.3.3 Effects of Effective Stiffness $(EI)_{\text{eff}}$	202
CHAPTER 7: DISCUSSION OF RESULTS AND DESIGN IMPLICATIONS	205
7.1 General	205
7.2 Selection of Representative Ground Motions	205
7.3 Artificially Generated Earthquake Ground Motions	211
7.3.1 Design-Spectrum-Compatible Artificial Earthquake	212
7.3.2 Site-Dependent, Spectrum-Compatible Artificial Earthquake	214
7.4 Effects of Different Earthquake Ground Motions on Building Responses .	217
7.4.1 Seven-Story Hotel	217
7.4.2 Ten-Story Building	227
CHAPTER 8: CONCLUSIONS	240
8.1 Summary	240
8.2 Conclusions	246
8.2.1 Nonlinear Dynamic Time History Analyses	247
8.2.2 Nonlinear Static Push-Over Analyses	248
8.2.3 Most Critical Earthquake Ground Motions	249
8.3 Suggestions for Further Research	250
REFERENCES	251
VITA	259

CHAPTER 1

INTRODUCTION

1.1 General

The general philosophy of earthquake resistant design for buildings is well established¹: (1) to prevent non-structural damage in minor earthquakes which may occur frequently in the service life of a structure; (2) to prevent structural damage and minimize non-structural damage in moderate earthquakes which may occasionally occur; and (3) to avoid collapse or serious damage in major earthquakes which may rarely occur. However, codes only require buildings to be designed for one ultimate force level. In effect, buildings are explicitly designed only for the third criterion. The extensive damage and unprecedented economic losses caused by the 1994 Northridge Earthquake², have stimulated designers and owners to consider how the design philosophy outlined above can be implemented to meet criteria (1) and (2), and to protect a building owner's economic investment.

The equivalent lateral force procedure for seismic design, as embodied in building codes of the United States and most other countries, is based on implicit consideration of inelastic structural response in the event of severe earthquakes. This approach has a number of deficiencies as summarized below:

- (1) The internal forces determined from elastic analysis under code-specified static forces are quite different from those produced during the inelastic earthquake response of the structure.
- (2) Although inelasticity may actually occur only at certain levels and in certain locations, there is no way of determining those locations or the extent of inelasticity in any of these locations through elastic analysis under code-prescribed static loads. As a result, special ductility details must be provided in every structural member and every connection. Also, there is no way to ascertain that the ductility provided through conformance with prescribed detailing requirements will always suffice.
- (3) Elastic story drifts under code-specified forces, amplified by such multiplication factors as may be prescribed, will be quite different from the actual inelastic story drifts. Thus, keeping the amplified story drifts within prescribed limits may not result in the intended damage control and safety against instability.

Information on the amount and distribution of internal forces and deformations in yielding structures can be obtained through inelastic response history analyses of structures subjected to earthquake motions. Over the past 20 years, several nonlinear time history analysis programs have been developed. However, the

applicability and accuracy of those programs need to be evaluated before they can be used in routine design.

Structural acceleration records produced by earthquakes are one of the few sources of quantitative information about the response of large structures to damaging, or potentially damaging, earthquakes. They not only allow modern design practices in earthquake engineering to be checked, but also they can play an important role in research to improve these practices. As a consequence, considerable effort has been made by earthquake engineers to record structural accelerations in addition to ground accelerations during an earthquake. Over the last two decades, or so, these efforts have been rewarded by the increasing number of sets of strong-motion acceleration records which have been obtained in buildings. These data provide excellent resources for calibrating the accuracy of those nonlinear programs.

1.2 Objective

The objective of this study is to demonstrate capacity of available programs to predict performance of reinforced concrete structures subjected to various earthquake ground motions, and to provide guidance on use of nonlinear time history analyses for evaluating and designing new, existing, or retrofitted buildings in seismic zones to meet various performance requirements.

1.3 Scope

The buildings used for calibration and analysis in this study are restricted to reinforced concrete moment resisting frames. In order to achieve the objective, the following tasks were undertaken:

- (1) Collection of all the necessary data regarding the design and construction of two reinforced concrete structures, instrumentation information, and response records of the buildings to the most significant earthquake motions experienced since construction.
- (2) Analyses of the response records of the buildings during the most significant earthquake ground motions experienced.
- (3) Prediction of the behavior of the building when subjected to the recorded earthquake ground motions using two nonlinear time history analysis programs: modified DRAIN-2D³ and IDARC2D version 3.1⁴. Computed responses are compared with responses recorded during significant earthquakes to evaluate the reliability and accuracy of the analytical models used in the time history analyses.
- (4) Evaluation of nonlinear static analyses of structures subjected to lateral incremental loads. A Nonlinear Static Procedure (NSP) has been proposed in the FEMA supported project to produce guidelines for the seismic rehabilitation of buildings (ATC-33)⁵.

(5) Analyses of the probable performance of the buildings under various representative earthquake ground motions. Five earthquake records are used in the present study. Also design-spectrum-compatible artificial earthquakes are generated and the most critical design earthquakes are discussed.

CHAPTER 2

LITERATURE REVIEW AND BACKGROUND INFORMATION

2.1 General

Almost all building construction in the United States today is regulated under building codes that include provisions for construction in seismic zones. The major building codes currently in effect include the Uniform Building Code (ICBO-1994)⁶, BOCA Code (BOCA-1993)⁷ and Standard Building Code (SBCCI-1993)⁸. Each of these in turn is based either on the SEAOC Blue Book (SEAOC-1990)¹ or NEHRP Provisions (BSSC-1991)⁹, resource documents which themselves are closely tied to ATC 3-06 (ATC-1978)¹⁰. Each of these codes is therefore very similar with regard to seismic design and construction provisions.

The primary goal of these codes is to provide life-safety by requiring buildings to have sufficient integrity, strength and ductility to resist collapse or generation of large falling debris, in very severe, but relatively infrequent earthquakes. Secondary goals include control of property damage and maintenance of function through drift limitations in moderate events, which are expected to occur more often. These codes have been developed empirically, based on observations of actual damage which has occurred to structures in past earthquakes and extensive research at various institutions. Following each major earthquake, engineers have observed the damage sustained by buildings, with particular interest in the performance of structures

conforming to the code in force at the time of construction. Where unacceptable damage has been observed, the building code provisions have been modified to prevent the recurrence of such damage in future events. As a result, current building codes enforced in seismically active regions of the United States are believed to provide good levels of life-safety protection in buildings which are properly designed and constructed. However, these codes appear less reliable with regard to the secondary goals of minimizing property damage in moderate and small events for some types of construction.

In recent years, California, due to its active seismicity and relatively modern inventory of buildings, has provided a good laboratory in which to judge the effectiveness of these building codes in meeting their intended performance goals. In 1989, the M7.1 Loma Prieta Earthquake affected the San Francisco Bay area. Although this was a relatively large magnitude event, the location and fault rupture characteristics were such that strong ground motion had a relatively short duration and the most densely developed regions of the San Francisco Bay area experienced ground accelerations that were 1/4 to 1/2 that anticipated in the largest expected earthquake. Despite the relatively limited levels of ground shaking, the Loma Prieta Earthquake caused more than \$7 billion in damage with some modern structures, designed according to recent editions of the building code, damaged so severely that extended loss of use occurred. Although no loss of life occurred in modern buildings designed

to recent building codes, the economic loss which occurred was judged both by the structural engineering profession and public policy makers as too large for this moderate event¹¹. A need was identified for new building design and construction procedures, which could better meet society's requirement that property and business interruption losses in moderate earthquakes be controlled to acceptable levels. Also identified was the need to expand the scope of procedures used to evaluate and rehabilitate existing buildings.

In January of 1994, the M6.7 Northridge Earthquake occurred, resulting in even more severe losses, estimated at approximately \$20 billion, than the Loma Prieta Earthquake. Engineers and public policy makers again determined that it is unacceptable to experience this magnitude of loss in such relatively frequent and moderate events. Faced with a need to repair and reconstruct hundreds of buildings, the California Office of Emergency Services contracted with SEAOC to develop recommendations for performance based design and construction procedures which could be implemented as rapidly as possible.

SEAOC has been actively engaged in the development of seismic design and construction provisions contained in the UBC Code for more than 40 years. In 1992, the SEAOC board of directors established the Vision 2000 Committee to develop a framework for a next generation, performance based, seismic resistive building code. During the period 1992-1993, the committee developed a preliminary framework for a

performance based building code, which incorporated the adoption of newly developing analytical techniques and methodologies for characterizing the behavior of structural systems subjected to strong ground motion, including energy balance and non-linear analysis methods.

Information on the amount and distribution of internal forces and deformations in yielding structures can be obtained explicitly through inelastic response time history analyses of structures subjected to earthquake input motions. Inelastic response time history analysis by direct integration of the coupled equations of motion has often been used in research studies of earthquake response of yielding structures^{12,13,14}. The commentary to the NEHRP Provisions recognizes two- and three-dimensional inelastic response analyses as the most rigorous analysis procedures for seismic design.

2.2 Computation of Inelastic Response

The analysis of the response of building structures to dynamic loads is a difficult task, especially if the response is nonlinear, as in the case of reinforced concrete buildings subjected to strong seismic ground shaking. Making a reliable estimate of response is one of the most difficult tasks facing the structural engineer.

2.2.1 Linear Elastic Analysis Methods

Since linear elastic analysis is the basis for nonlinear analysis, and most current seismic codes and specifications are based on linear elastic analysis theory, a background review of linear elastic analysis methods will be presented first.

Linear elastic analysis is a relatively routine process and involves the application of well-established computational techniques. These are used in many of the well-known and widely used commercial software systems and are described in numerous texts on structural dynamics^{15,16,17,18}. Therefore, only a brief summary of these methods shall be given here.

(1). *Equivalent Static Lateral Load Analysis.* Static analyses of building structures for lateral loads are readily performed by standard frame analysis programs, and this approximate method is the only one feasible for hand calculations. The vast majority of structures are designed in accordance with the Uniform Building Code or other model codes such that the dynamic characteristics of the structures are accounted for approximately by determining the equivalent static lateral loads.

For example, the procedures for the design of structures by the UBC-94 Code are determined considering zoning, site characteristics, occupancy, configuration, structural system, building height, and building weight. Lateral forces are determined

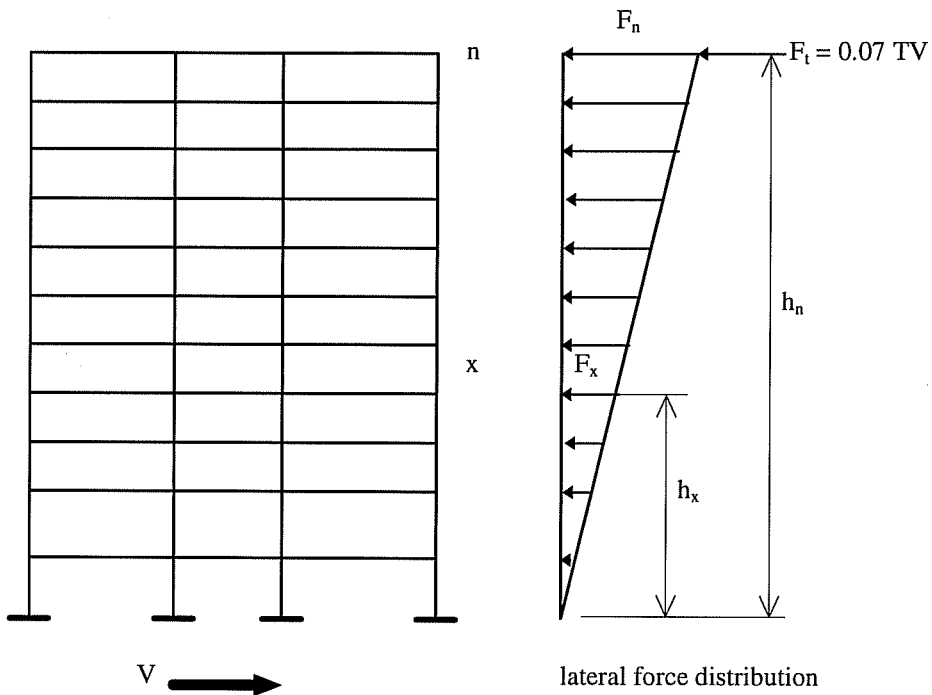
by first calculating design base shear, which is proportional to the weight of the building as described in equation (2.1):

$$V = \frac{ZIC}{R_w} W \quad (2.1)$$

- where Z = seismic zone coefficient.
I = importance factor.
C = site coefficient.
R_w = structural system coefficient.
W = total seismic dead load.

The design base shear is distributed along the height of a building. A portion of the design base shear is concentrated at the top of a flexible building (if building fundamental period of vibration is $T > 0.7$ sec.), to account for higher mode response. The rest of the design base shear is distributed linearly, varying from a maximum value at the top to a minimum at the bottom, in correspondence with fundamental mode response. Therefore story shear can be calculated using equation (2.2), and this is graphically represented in Figure 2.1.

$$V_x = F_t + \sum_{i=x}^n F_i \quad (2.2)$$



- F_i, F_n, F_x = lateral force applied to level i, n or x, respectively.
- F_t = portion of V considered concentrated at top of structure in addition to F_n .
- h_i, h_x = height in ft above base to level i, or x, respectively.
- w_i, w_x = that portion of w which is located at or assigned to level i or x, respectively.
- W = total seismic dead load.
- T = fundamental period of vibration of structure in seconds in direction of analysis.
- V = total lateral force or shear at the base for which a building is to be designed.

Figure 2.1 Lateral Force Distribution

Finally the building is designed according to applicable combinations of factored lateral forces and gravity loads or related internal moments and forces from equations (2.3) and (2.4):

$$U = 1.4 (D + L + E) \quad (2.3)$$

$$U = 0.9 D \pm 1.4 E \quad (2.4)$$

where U = required strength to resist factored loads.

D = dead loads.

L = live loads.

E = load effects of earthquake.

(2) *Response Spectrum Analysis.* The importance of the response spectrum in seismic analysis and design of structures is well known to earthquake design engineers. The response spectrum introduced by Biot^{19,20}, and Housner²¹ describes the maximum response of a damped single-degree-of-freedom oscillator at various frequencies or periods. The procedure for computing and constructing the response spectrum is illustrated in Figure 2.2.

Typical acceleration, velocity, and displacement response spectra for the S00E component of El Centro, the Imperial Valley Earthquake of May 18, 1940, are shown in Figure 2.3.

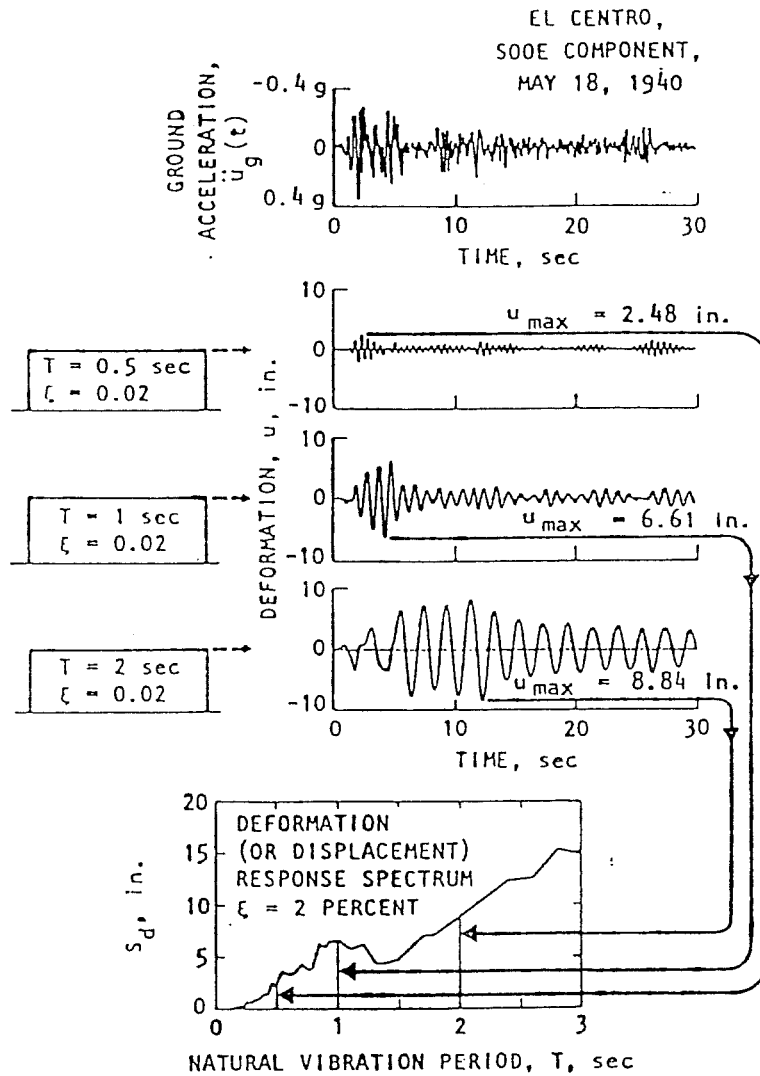


Figure 2.2 Computation of Deformation (or Displacement) Response Spectrum¹⁵

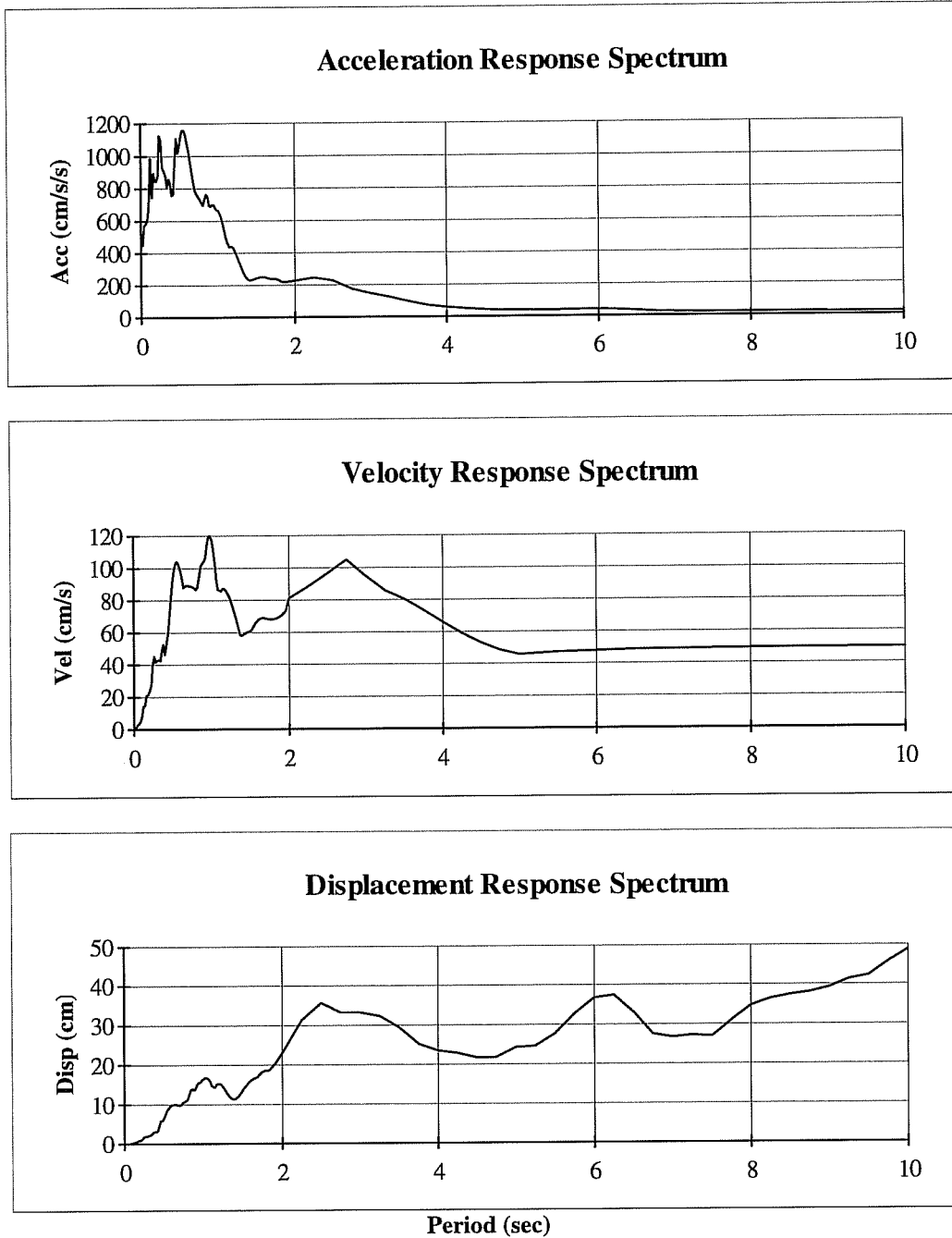


Figure 2.3 Response Spectra for 5% Damping for the S00E Component of El Centro, the Imperial Valley Earthquake of May 18, 1940

The frequency contents of earthquake ground motions are illustrated very graphically by response spectra. The random nature of such ground motions prompted the generation of design spectra, which reflect the averaged frequency content of expected ground motions. In 1978, the Applied Technology Council¹⁰ recommended that a smooth version of the normalized spectral shapes proposed by Seed et al.²² be used for developing seismic regulations for buildings. The ATC spectra, which have also been adopted by the Seismology Committee of the Structural Engineers Association of California¹, are presented in Figure 2.4. Site soil categories are grouped into three types: rock and stiff soils (soil type 1), deep cohesionless or stiff clay soils (soil type 2), and soft to medium clays and sands (soil type 3).

For multiple-degree-of-freedom systems, a number of independent displacement coordinates are required to describe the displacement of the structure at any instant of time. The response of the structure is represented in terms of a linear superposition of mode shapes, and for each mode shape, the structure is treated as a single-degree-of-freedom structure. After the determination of the important natural modes and frequencies of a building, its response to ground motions, as synthesized in the design spectrum, is readily determined. However, any realistic determination of a structure's modes and frequencies calls for a detailed mathematical model that can only be solved feasibly using computer analyses. In addition, techniques for combining the different modal responses are needed. Most common is the use of the square root

of the sum of the squares method (SRSS). However, if some of the frequencies of the structure are very close or even identical, then the individual modal maxima have to be combined by techniques which take this fact into account^{18,23}. Also, the response spectrum method can only be used to calculate the maximum responses of structures.

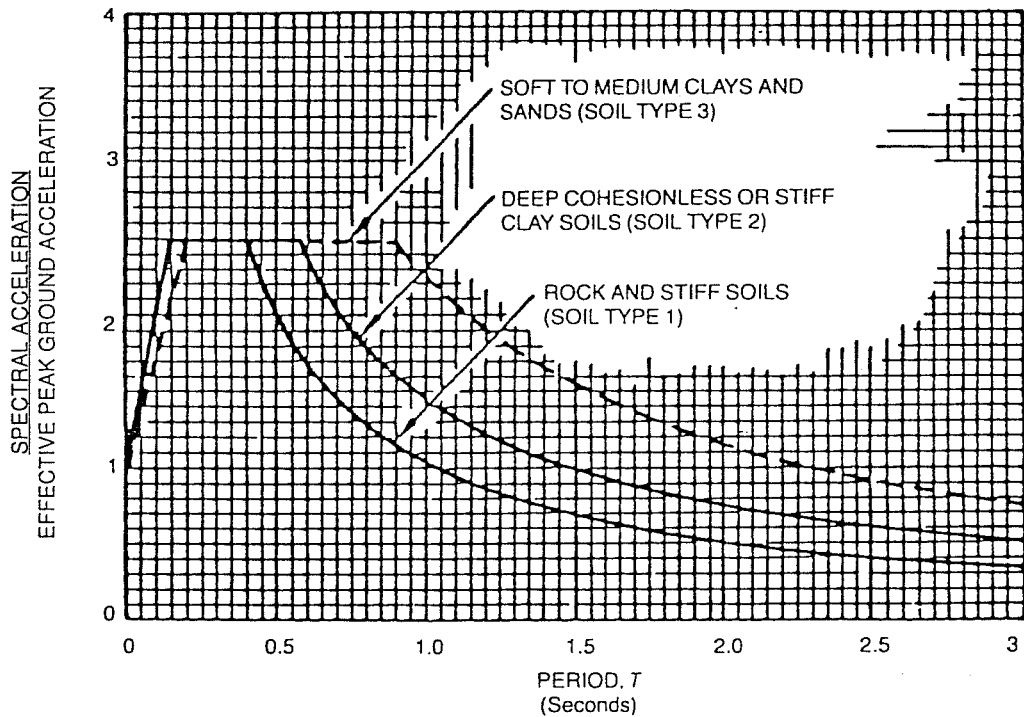


Figure 2.4 Normalized Design Response Spectra⁶

(3) *Time History Analysis by Modal Superposition.* To eliminate the difficulties in combining the different modal responses, and to obtain time history information, time history analysis by modal superposition uses a deterministic acceleration history such as one recorded during an actual earthquake as the input ground motion. Equations of motion are established for as many degrees of freedom as are needed to describe the stiffness and mass characteristics of the building. The seismic response of a building can usually be described by a few important lateral deformation modes. For example, the maximum roof displacement of a high-rise building during an earthquake is typically determined largely (up to 90%) by the first, or fundamental, mode as shown in Figure 2.5. Therefore it is very efficient to transform the equations of motion from physical to natural coordinates¹⁶. In this new coordinate system, the equations are uncoupled and therefore readily solved for the modal responses.

The accuracy demand of the mathematical model of the structure's stiffness, mass and damping properties for this analysis method is comparable to that for the response spectrum method. Time history analysis is only slightly more accurate than the response spectrum method because of the more accurate superposition of the various modal responses.

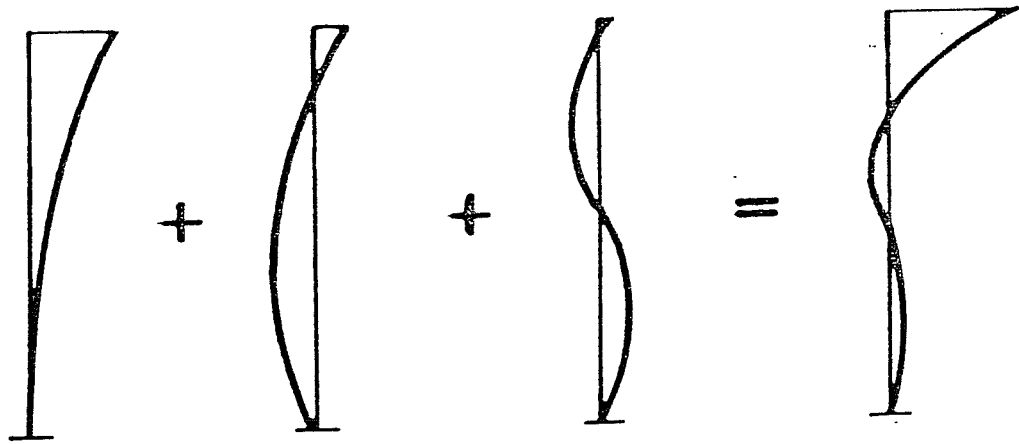


Figure 2.5 Superposition of Mode Shapes

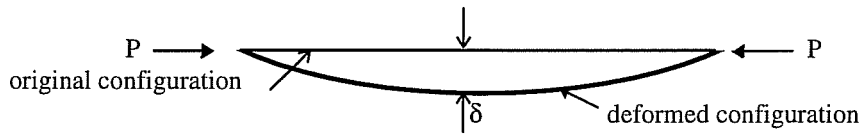
(4) *Time History Analysis by Direct Integration.* The transformation of variables from physical to modal coordinates implies that linear superposition of individual modal response is applicable. If this assumption is not valid (as is the case for inelastic analysis or non-proportional damping), it is more appropriate to solve the equations of motion directly, without transforming them first to modal coordinates. Thus the method of integration has to be used for nonlinear analysis. For linear elastic structures it is also sometimes desirable to solve the equations of motion by direct integration, such as when the response cannot be synthesized from a few dominant

natural modes. Time history analysis by direct integration will be fully explored in section 2.2.2.

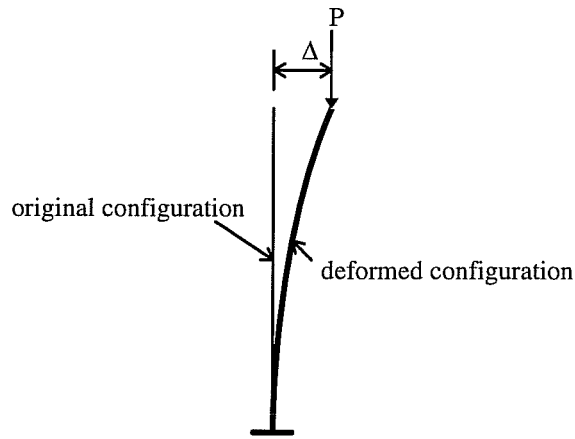
(5) *Frequency Response Analysis.* Instead of integrating the equations of motion in the time domain, it is possible to solve them by integrating in the frequency domain, which offers computational advantages when random vibration analyses are performed^{18,24,25}. The representation of earthquake loads as a random process is more meaningful for predicting structural response to future events than the use of single deterministic forcing functions. In particular, frequency content estimates of ground acceleration histories in the form of power spectrum density functions are less uncertain than the predictions of other loading characteristics. Thus, random vibration analysis techniques are suitable for earthquake response predictions, especially if structures can be represented by linear elastic models.

2.2.2 Inelastic Analysis Methods

Nonlinear structural behavior may be caused either by geometric or material nonlinearities. Geometric nonlinearities are typically associated with large deformations. Two forms of geometric nonlinearity, namely the P- δ (member curvature) effect and the P- Δ (chord rotation) effect are illustrated in Figure 2.6.



P- δ effect



P- Δ effect

Figure 2.6 P- δ and P- Δ Effects

The P- Δ effect reduces the element flexural stiffness against sidesway. The P- δ effect reduces the element flexural stiffness in both sidesway and non-sidesway modes of deformation. Except for tall and slender structures, concrete buildings are rather rigid and typically do not undergo very large deformations. However, the P- Δ

effect is known to affect the safety of compression members and can have an influence on the overall stability of structures and therefore should not be ignored.

Material nonlinearities are associated with inelastic behavior, exhibited by members strained beyond their yield capacities as depicted in Figure 2.7. Plastic hinges formed in the process have a considerable effect on the structural response. Designers utilize this effect to limit the structural response through controlled energy dissipation. Inelastic analysis accounts for material inelasticity or yielding when a material is stressed beyond its yield stress.

The structural analysis problem is greatly complicated by nonlinear behavior. The presence of plastic hinges changes the effective structural stiffness at numerous, if not most time steps, thereby greatly increasing the numerical effort required for solution of the problem. In the following paragraphs, several approximate nonlinear methods will be discussed, then the method of nonlinear time history analysis by direct integration, a more accurate analysis technique, will be introduced.

(1) *Approximate Analysis Methods*

If the analysis objective is simply to demonstrate that a design has sufficient capacity, especially in conjunction with preliminary design tasks, approximate analysis methods are fully adequate and a number of these have been developed over the years. A special word of caution is in order concerning approximate analysis

methods. They give reasonable results only if proper consideration is given to all limiting assumptions. They arguably require more experience on the part of the analyst than standard, more accurate methods. In many cases it is difficult to assess the degree of approximation involved or the effect of those approximations on response.

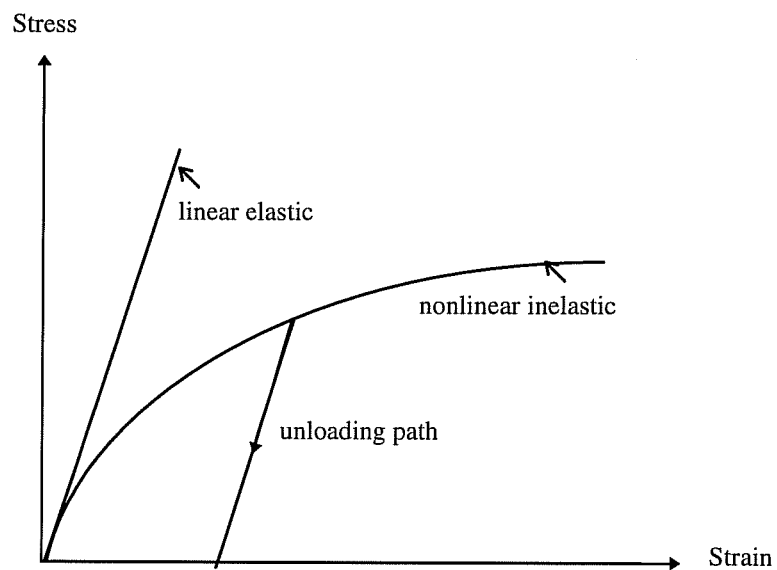


Figure 2.7 Elastic and Inelastic Material Behavior

(a) *Inelastic response spectra.* The most common approximate methods employ inelastic response spectra. Spectra for linear elastic analysis were discussed earlier. In order to adapt these to inelastic analysis of reinforced concrete buildings,

two approaches are possible. In the first method, the unmodified elastic response spectrum defines a given earthquake, but in order to estimate the nonlinear response, the actual effective frequency of the nonlinear structure f_1 is used, which is smaller than the elastic frequency of the structure as shown in Figure 2.8 (tripartite logarithmic plot). In the other method, the frequency of vibration f_2 is based on the elastic properties of the structure, but it is used in conjunction with a modified inelastic response spectrum, Figure 2.8. Such a spectrum is generated by analyzing the time history response of a single-degree-of-freedom oscillator with a nonlinear force-deformation behavior to the given ground motion history. Newmark and Hall²⁶ devised a simple technique for converting an elastic spectrum into an inelastic one, using the ductility ratio μ as the only parameter.

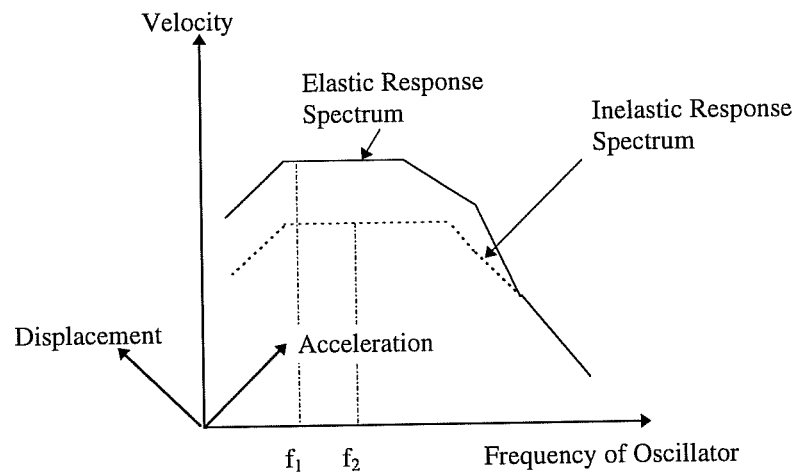


Figure 2.8 Inelastic Response Spectrum Methods

While the use of response spectra for linear structural analysis is relatively straight forward, it should be applied to nonlinear analysis only with great caution. First, the method is valid only for systems with limited ductility and becomes increasingly inaccurate for large inelastic deformations. In an analysis requiring the structure's inelastic period, determination of inelastic period is not straight forward. The inelastic period is not clearly defined because it is a function of loading and ductility. In addition, it is difficult to assess the degree of simplification inherent in constructing an elastic or inelastic response spectrum. Also the relationship between a structural ductility ratio and individual element ductility ratios is not unique or fixed. As an approximation, an overall structural ductility of 3 to 5 may correspond to member ductility ratios of up to 15²⁶.

Most important is the fact that the principle of linear superposition, on which the response spectrum method for multi-degree-of-freedom systems is based, does not apply to nonlinear systems. In other words, inelastic response spectra may help in determining the approximate response of nonlinear single-degree-of-freedom systems, but not of multi-degree-of-freedom systems. Mode shapes in the conventional sense are meaningless with respect to nonlinear structures. It is noteworthy that the Uniform Building Code and ATC methods are indirectly based on inelastic response spectra²⁷.

(b) *Substitute structure method.* This method was originally proposed by Shibata and Sozen²⁸ as an approximate method for the seismic design of concrete frames. The method employs linear elastic analysis of a modified version of the actual structure. The substitute structure is defined by replacing the actual member stiffness EI_a by a reduced stiffness,

$$EI_s = \frac{EI_a}{\mu} \quad (2.5)$$

where subscripts “s” and “a” refer, respectively, to the substitute and actual structure, and “ μ ” is the acceptable damage ratio, which is comparable to but not identical with the ductility ratio. Modes and frequencies for the undamped substitute structure are obtained using linear dynamic analysis. Equivalent modal damping ratios are computed as:

$$\beta_s = 0.2(1 - \mu^{-2}) + 0.02 \quad (2.6)$$

Studies have shown²⁹ that this amount of viscous damping leads approximately to the same response as hysteretic damping in inelastic analysis. Design forces are computed with the help of linear response spectra. Under the assumption that the mode shapes and frequencies of the substitute structure retain the same significance and meaning as in a linear elastic structure, the various modal responses are combined using the square root of the sum of the squares method.

This method has been shown to give results that are sufficiently accurate for preliminary design purposes²⁸. However, when applying it to final designs, it is

important to recognize its limitations and its inability to accurately determine the inelastic response of the structure and the ductility demands of the individual members.

(c) *Q-Model Method*. The Q-model³⁰ is based on two types of simplifications:

1) reduction of a multi-degree-of-freedom model of a structure to a single-degree-of-freedom oscillator, and 2) approximation of the incremental stiffness properties of the entire structure by a single nonlinear spring. The reduction to the SDOF oscillator follows the derivation by Biggs¹⁷. The mass of the oscillator is equal to that of the MDOF system, adjusted with an appropriate factor, and the oscillator stiffness is derived from the force necessary to deform the MDOF system in a particular way. The nonlinear spring force of the SDOF system is based on the nonlinear force-displacement relationship obtained for the properties of the actual structure analyzed, with the assumption that it is subjected to a set of monotonically increasing external forces. For some of the scale models that were tested at the University of Illinois, agreement between experiment and computations using the Q-model was found to be good.

It should be noted that all of these simplified methods are based on the assumptions that there are no abrupt changes in stiffness or mass along the building height. Their highly approximate nature and low computational cost make them suitable for preliminary analyses of regular buildings.

(2) *Nonlinear Time History Analysis by Direct Integration.* Nonlinear time history analysis by direct integration method is the most accurate analysis method available. The basic analysis problem is characterized by the requirement that the incremental dynamic forces acting on a structure during some small time step Δt have to be in equilibrium,

$$M\Delta\ddot{x}(t) + C\Delta\dot{x}(t) + K\Delta x = \Delta F(t) \quad (2.7)$$

For the numerical solution of these equations in the time domain, there are two fundamentally different groups of algorithms available: explicit and implicit integration schemes³¹. In explicit integration, the equation of motion, Eq.(2.7) is established for time t . An important example of an explicit scheme is the central difference operator, wherein accelerations and velocities at time t are approximated as follows,

$$\ddot{x}_t = \frac{1}{\Delta t^2} (x_{t-\Delta t} - 2x_t + x_{t+\Delta t}) \quad (2.8)$$

$$\dot{x}_t = \frac{1}{2\Delta t} (-x_{t-\Delta t} + x_{t+\Delta t}) \quad (2.9)$$

Substitution of Eqs. (2.8) and (2.9) into Eq. (2.7) leads to

$$\left(\frac{1}{\Delta t^2} M + \frac{1}{2\Delta t} C\right)x_{t+\Delta t} = F_t - \left(K - \frac{2}{\Delta t^2} M\right)x_t - \left(\frac{1}{\Delta t^2} M - \frac{1}{2\Delta t} C\right)x_{t-\Delta t} \quad (2.10)$$

This set of equations can be solved directly for $x_{t+\Delta t}$, the unknown displacements at time $t+\Delta t$. For diagonal matrices M and C , this task is trivial and does not require the factorization of the structures stiffness matrix K .

In implicit integration, the equation of motion, Eq. (2.7), is written not in terms for time t but for time $t+\Delta t$. For example, in the widely used Newmark method, accelerations and velocities are approximated as follows:

$$\ddot{x}_{t+\Delta t} = \frac{6}{\Delta t^2} (x_{t+\Delta t} - x_t) - \frac{6\dot{x}_t}{\Delta t} - 2\ddot{x}_t \quad (2.11)$$

$$\dot{x}_{t+\Delta t} = \frac{3}{\Delta t} (x_{t+\Delta t} - x_t) - 2\dot{x}_t - \frac{\Delta t}{2} \ddot{x}_t \quad (2.12)$$

Substitution of Eqs. (2.11) and (2.12) into Eq. (2.7) leads to

$$K^* x_{t+\Delta t} = F_{t+\Delta t}^* \quad (2.13)$$

where

$$K^* = K + \frac{6}{\Delta t^2} M + \frac{3}{\Delta t} C \quad (2.14)$$

$$F_{t+\Delta t}^* = F_{t+\Delta t} + \left(\frac{6}{\Delta t^2} x_t + \frac{6}{\Delta t} \dot{x}_t + 2\ddot{x}_t \right) M + \left(\frac{3}{\Delta t} x_t + 2\dot{x}_t + \frac{\Delta t}{2} \ddot{x}_t \right) C \quad (2.15)$$

Eq. (2.13) can be solved for the displacements $x_{t+\Delta t}$. But this task involves factorization of the effective stiffness matrix K^* , which is a computationally expensive task. Moreover, K^* changes whenever K changes, such as due to inelastic behavior or when Δt is varied. The piecewise linearization of response histories causes unbalanced forces at each time step which can be resolved using various numerical analysis techniques³¹.

Explicit algorithms have to satisfy the so-called Courant condition, $\Delta t < T_n / \pi$, i.e. the time step of integration has to be less than a certain fraction of the structure's smallest natural period T_n , otherwise the algorithm will be unstable. Physically, this requirement means that Δt should be of the order of the time required by sound waves to travel through the smallest member or element in the structure. This time step can be extremely small. For example, the sound velocity in steel is 16,800 ft/sec. Thus, a sound wave travels along a 12 ft column in 0.7×10^{-3} sec, so that the stability criterion requires $\Delta t < 0.2 \times 10^{-3}$ sec. In the case of structures with massless degrees of freedom, the method breaks down because $T_n = 0$, unless such degrees of freedom are condensed out prior to the time step solution. Thus, even though the solution of Eq. (2.10) requires relatively little effort, a time history analysis of a 10 sec earthquake record may involve at least 50,000 time steps.

Implicit algorithms are generally unconditionally stable, i.e., the solution remains stable, even though the Courant condition is violated. The time step size may

be several orders of magnitude larger than T_n . Physically, these algorithms have the effect of suppressing the higher modes through artificial damping. It is of interest to note that these higher modes generally contribute little to the structural response. But when an unstable integration method is used, a violation of the stability criterion causes these high frequency modes to drown out the responses of the significant lower modes, thus making the results useless.

In sum, the choice of a numerical solution algorithm has to balance accuracy and stability requirements. The apparent computational advantage associated with the larger time steps of an implicit integration scheme can in general be realized only by sacrificing accuracy. Fortunately in the case of building structures, the role of higher modes is usually not very significant.

2.3 Earthquake Response from Instrumented Buildings

The first set of structural accelerograms was obtained as early as 1933 in the basement and on the roof of the Hollywood Storage Building, a box-like reinforced concrete 14-story structure. The records were produced during an earthquake ($M_L = 5.4$) in Los Angeles. No published studies of these records are known. Indeed, they seem to have been overlooked, despite their historic importance.

It was almost another 20 years, during the 1952 Kern County Earthquake ($M_L = 7.2$), before the next set of significant records was obtained in a structure.

Housner³² has studied the basement and parking lot records to investigate possible soil-structure interaction, but there appear to be no published studies of the relationship between either of these accelerograms and the measured roof accelerations.

During the period 1952-1970, several other sets of building records were obtained. Hudson³³, in one of the first studies of measured seismic response, examined the accelerograms produced in the 15-story Alexander Building during the 1957 San Francisco Earthquake ($M_L = 5.3$). He obtained reasonable agreement between the measured peak accelerations, 0.06g and 0.09g in the N09W direction at the 11th and 16th floors respectively, and those obtained from a model using the response spectra calculated from the N09W basement accelerations by an electric analog method. The properties of the three modes used in the model came from forced vibration tests using a shaking machine. Unfortunately, further studies of the Alexander Building have not been possible since only the basement record has been digitized, although a complete set of digital accelerograms for the basement, 11th, and 16th floors are available for an aftershock ($M_L = 4.4$) of the 1957 San Francisco Earthquake.

An assessment of the situation up to 1970 is that strong-motion accelerations had been measured in several buildings during earthquakes in the preceding 40 or so years, but few researchers had attempted to utilize them. No doubt research was inhibited by the lack of corrected digital versions of the accelerograms. In 1968,

Caltech launched an extensive program to digitize and process the backlog of all significant U.S. strong-motion accelerograms, and this program should have spurred more studies of the structural records. However, it was the 1971 San Fernando Earthquake in California which actually generated interest in such studies.

As a result of a Los Angeles City ordinance enacted in 1965, all the newer high-rise buildings in the city were instrumented at the time of the San Fernando Earthquake ($M_L = 6.4$) whose epicenter was just outside the northern boundary of the city. As a consequence, records were obtained from more than 50 buildings designed according to modern building codes and practices, with roof accelerations peaking at levels of 0.4 - 0.5g in several buildings. None of the instrumented buildings suffered heavy damage, although there was modest structural damage in at least three of them, the Holiday Inns at 8244 Orion Blvd and 1640 S Marengo St., and the Bank of California at 15250 Ventura Blvd.

The importance of the San Fernando records of both ground and structural motions was immediately recognized and considerable effort was expended to produce corrected digital versions as rapidly as possible. Within two years of the earthquake, a NOAA report was published³⁴, which contains analyses of many of the structural records together with other engineering studies of the earthquake. Another early study is an analysis of the two accelerograms produced in Building 180, a nine-story

steel-frame structure located on the campus of the Jet Propulsion Laboratory, Pasadena³⁵.

The early studies of the earthquake response were typically of the following type. A linear model, often one used in dynamic design, was synthesized from the structural plans, a guess being made of the amount of damping in each mode, typically taken as 5% of critical damping. The response of the model to the measured base acceleration was then computed and compared with the earthquake records from the mid-height or roof accelerographs. Calculated peak response quantities were generally in reasonable agreement with the measured values. However, detailed agreement between the time histories of the model and recorded responses was lacking.

Records of interest obtained since 1971 include those from Whittier Tower, a ten-story modern reinforced concrete building, during the 1976 Whittier Earthquake in California³⁶. This event had a local magnitude of only 4.2 and Whittier Tower is 14 km from the epicenter, yet the peak accelerations in the transverse direction were surprisingly large, 0.28g and 0.19g at the fifth floor and at the tenth floor respectively. The duration of the strong motion was only one to two seconds. No structural damage was reported.

In 1992, the United States Geological Survey released a CD-ROM containing 4270 uncorrected strong motion accelerograms from about 500 earthquakes representing all of the available North American and Hawaiian records from ground-

level instruments for the period of 1933 through 1986⁴¹. These data then were passed through a preliminary correction process by Naeim and Anderson⁴² which included base-line correction, instrument correction, band-pass filtering, and integration to calculate velocity and displacement. Later, the 1933-1986 selection was complemented with virtually all corrected ground-level accelerograms released by the California Strong Motion Instrumentation Program of the California Department of Mines and Geology (SMIP/CDMG) for California earthquakes since 1987⁴³.

A list of earthquakes contributing records of engineering significance ($M > 5.5$, Peak Ground Acceleration $> 0.05g$) is presented in Table 2.1. A histogram of the chronological distribution of earthquake records contained in this selection is shown in Figure 2.9. Figures 2.10 and 2.11 show histograms of focal depth and epicentral distance for records in the selection.

2.4 Performance Based Seismic Engineering

Severe earthquakes are relatively infrequent events, which may or may not ever occur within the life of a building. While it may be feasible technically to design and construct buildings such that they do not experience any damage in the most severe earthquake events, it is generally considered unnecessary and uneconomical to do so. Therefore, an engineering design philosophy has evolved over the years in which design is performed with the anticipation that severe earthquakes will cause some

Table 2.1 Earthquake Contributing Records to the 1933-1992 Database⁴³

No.	Year	Earthquake name	Magnitude
1	1933	Long Beach, California	6.3
2	1934	Baja, California	6.5
3	1935	Helena, Montana	6.0
4	1938	NW California	5.5
5	1940	El Centro	7.0
6	1941	NW California	6.6
7	1941	Santa Barbara, California	5.9
8	1941	Northern California	6.4
9	1942	Borrego Valley	6.5
10	1949	Western Washington	7.1
11	1952	Kern County	7.4
12	1952	Northern California	5.5
13	1952	Southern California	6.0
14	1954	Wheeler Ridge, California	5.9
15	1954	Northern California	6.5
16	1955	San Jose	5.8
17	1956	El Alamo	6.8
18	1960	Northern California	5.7
19	1961	Hollister	5.6
20	1965	Puget Sound, Washington	6.5
21	1966	Parkfield, California	6.1
22	1966	Mexico	5.6
23	1967	Northern California	5.8
24	1968	Borrego Mountain	6.7
25	1971	San Fernando	6.6
26	1971	Andreanof Islands	7.1
27	1972	Mexico	5.5
28	1972	Alaska	7.5
29	1972	Managua, Nicaragua	6.2
30	1973	Michoacan, Mexico	7.5
31	1973	Point Mugu, California	5.9
32	1973	Honolulu, Hawaii	6.0
33	1973	Mexico	5.6
34	1973	Mexico	6.8
35	1973	Mexico	6.0
36	1974	Alaska	5.6
37	1974	Mexico	5.5
38	1975	Alaska	6.0
39	1975	Northern California	5.7
40	1975	Oroville	5.7
41	1975	Mexico	5.9
42	1975	Island of Hawaii	5.7
43	1976	Mexico	5.7
44	1978	Mexico	6.4
45	1978	Santa Barbara, California	5.5
46	1978	Mexico	7.7
47	1979	Southern Alaska	7.3
48	1979	Mexico	7.6
49	1979	Coyote Lake, California	5.7
50	1979	Imperial Valley, California	6.5
51	1979	Imperial Valley, California	5.5
		a.s.	

(Continued)

Table 2.1 (Continued)⁴³

No.	Year	Earthquake name	Magnitude
52	1980	Livermore, California	5.9
53	1980	Anza	5.5
54	1980	Mammoth Lakes, California	6.5
55	1980	Mammoth Lakes, California	5.7
56	1980	Mammoth Lakes, California	6.3
57	1980	Victoria	6.1
58	1980	Mexico	6.4
59	1980	Trinidad, California, offshore	7.2
60	1981	Westmoreland, California	5.6
61	1981	Mexico	7.1
62	1983	Alaska	6.3
63	1983	Coalinga, California	6.7
64	1983	Alaska	5.8
65	1983	Alaska	6.4
66	1983	Coalinga aftershock	6.0
67	1983	Trinidad, California, offshore	5.7
68	1983	Alaska	6.2
69	1983	Mexico	5.6
70	1983	Hawaii	6.6
71	1983	Mexico	5.5
72	1984	Morgan Hill, California	6.2
73	1984	Round Valley	6.1
74	1985	Mexico	8.1
75	1985	Michoacan, Mexico	8.1
76	1985	Guerrero, Mexico	7.6
77	1985	Alaska	6.5
78	1985	Mexico	5.6
79	1985	Nahanni, NWT, Canada	6.9
80	1985	Nahanni, NWT, Canada	5.7
81	1985	Alaska	5.6
82	1986	Hollister	5.5
83	1986	Mt. Lewis, California	5.8
84	1986	Michoacan, Mexico	7.0
85	1986	Michoacan, Mexico	5.6
86	1986	Alaska	7.9
87	1986	North Palm Springs, California	5.9
88	1986	Chalfant Valley	6.0
89	1987	Whittier	6.1
90	1989	Loma Prieta	7.1
91	1990	Upland	5.0
92	1991	Sierra Madre	5.8
93	1992	Landers	7.5
94	1992	Petrolia	6.9

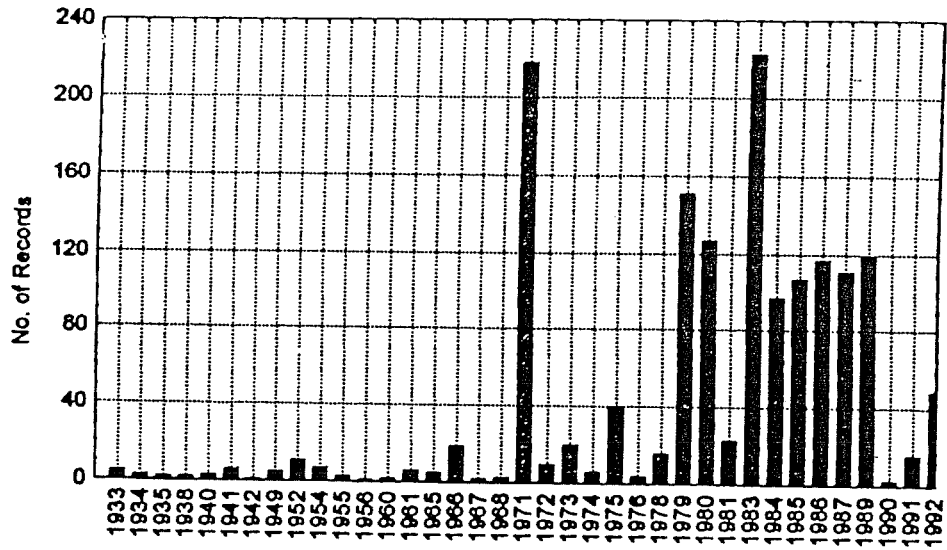


Figure 2.9 Annual Distribution of Records in the 1933-1992 Database⁴³

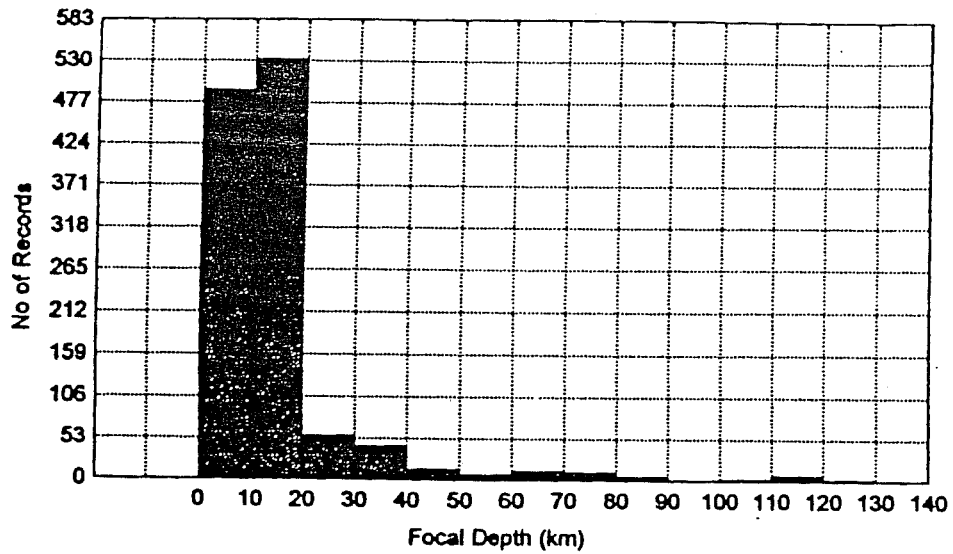


Figure 2.10 Distribution of Focal Depth of Records Contained in the 1933-1992 Database⁴³

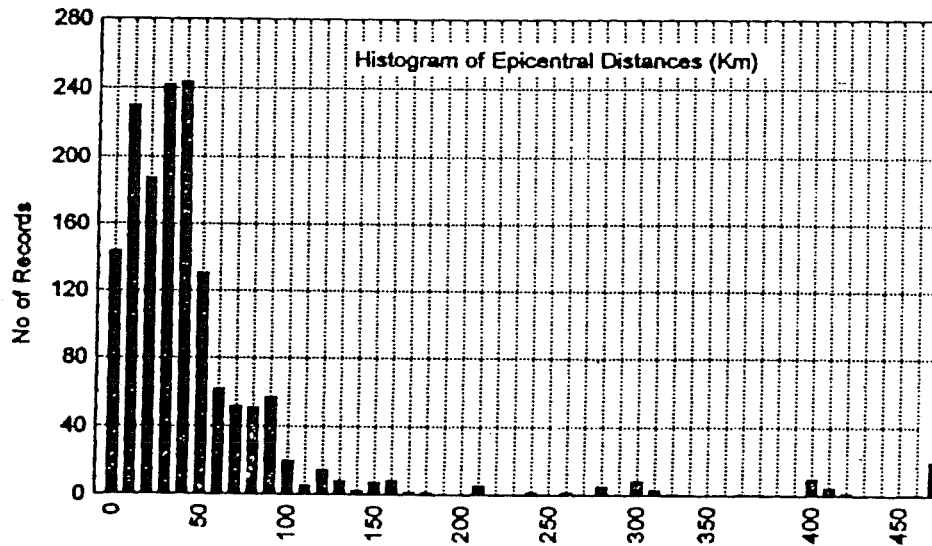


Figure 2.11 Distribution of Epicentral Distance of Records Contained in the 1933-1992 Database⁴³

damage to most buildings. The intent of earthquake resistive design therefore has become one of attempting to limit the damage experienced by a building to levels which are considered acceptable by structural engineers. Historically, damage which would not result in loss of life was deemed acceptable for most structures.

Under the concept of performance based engineering, the acceptability of various levels of damage is determined based on the consequences of this damage to the user community and the frequency with which such damage occurs. If a structure is provided with enhanced earthquake resistance, this reduces costs over its life related

to loss of life, business interruption, and repair/reconstruction following earthquakes. In an optimal situation, the costs related to providing initial earthquake resistance in a structure would be balanced against the costs related to damage in future earthquakes. The goal is to minimize earthquake related cost to the building owner over the life of the building. This is done by considering a set of performance levels.

2.4.1 Performance Level Definitions

(1) Fully Operational

A performance level in which essentially no damage has occurred. If a building responds to an earthquake within this performance level, the consequences to the building user community are negligible. The building remains safe to occupy and it is expected that post-earthquake damage inspectors utilizing the ATC-20 (ATC-1989)⁴⁴ methodology would post the building with a green placard. The building is occupiable and all equipment and services related to the building's basic occupancy and function are available for use. In general, repair is not required.

(2) Operational

A performance level in which moderate damage to non-structural elements and contents, and light damage to structural elements has occurred. The damage is limited

and does not compromise the safety of the building for occupancy. Post-earthquake damage inspectors utilizing the ATC-20 methodology would be expected to post the building with a green placard. It would be available for occupancy for its normal intended function, immediately following the earthquake, however, damage to some contents, utilities and non-structural components may disrupt some normal functions. Back-up systems and procedures may be required to permit continued use. Repairs may be instituted at the owners' and tenants' convenience.

(3) Life-safe

A performance level (damage state) in which moderate damage to structural and non-structural elements, and contents has occurred. The structure's lateral stiffness and ability to resist additional lateral loads have been reduced, possibly to a great extent, however, some margin against collapse remains. No major falling debris hazards have occurred. Egress from the building is not substantially impaired, albeit elevators and similar electrical and mechanical devices may not function. In the worst case, post-earthquake damage inspectors, using the ATC-20 methodology, would be expected to post such a building with a yellow placard. In such cases the building would not be available for immediate post-earthquake occupancy. The building would probably be repairable, although it may not be economically practical to do so.

(4) Near Collapse

An extreme damage state in which the lateral and vertical load resistance of the building have been substantially compromised. Aftershocks could result in partial or total collapse of the structure. Debris hazards may have occurred and egress may be impaired, however, all significant vertical load carrying elements (beams, columns, slabs, etc.) continue to function. In the worst case, post-earthquake damage inspectors, using the ATC-20 methodology, would be expected to post such a building with a red placard. The building will likely be unsafe for occupancy and repair may not be technically or economically feasible.

Figure 2.12 illustrates the entire spectrum of damage states which a building may experience when subjected to ground motions of increasing severity. This figure was developed by SEAOC's Vision 2000 Committee⁵⁹ and also relates the various ranges of damage which are permissible within the intent of each of the limiting performance level and, for easy reference, defines a numerical damage index.

Table 2.2 describes permissible levels of damage to the various systems and sub-systems in buildings, for each of the four performance levels⁵⁹ as established by Vision 2000. Also shown are typical transient (during the earthquake response) and permanent (after the earthquake response) drift levels which may be sustained by a building in meeting these performance levels. Permissible drift levels are functions of the structural as well as non-structural systems.

Damage Range &
Damage Index

Damage States and Performance Level Thresholds

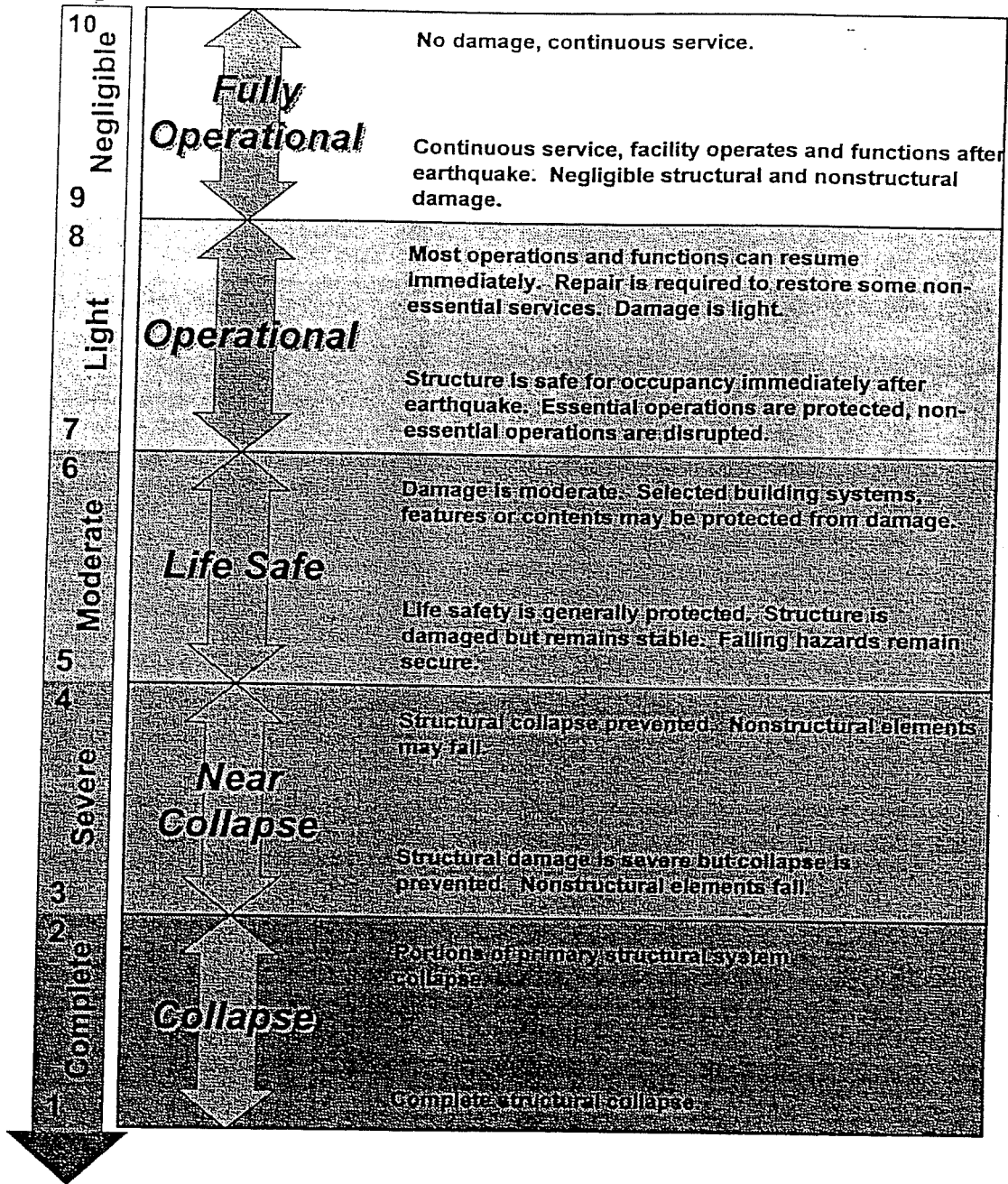


Figure 2.12 Spectrum of Damage States⁵⁹

Table 2.2 General Damage Descriptions by Performance Levels and System⁵⁹

System Description	Performance Level									
	10 Fully Operational	9	8 Operational	7	6 Life Safe	5	4 Near Collapse	3	2 Collapse	1
Overall building damage	Negligible		Light		Moderate		Severe		Complete	
Permissible transient drift	< 0.2%+/-		< 0.5%+/-		< 1.5%+/-		< 2.5%+/-		> 2.5%+/-	
Permissible permanent drift	Negligible.		Negligible.		< 0.5%+/-		< 2.5%+/-		> 2.5%+/-	
Vertical load carrying element damage	Negligible.		Negligible.		Light to moderate, but substantial capacity remains to carry gravity loads.		Moderate to heavy, but elements continue to support gravity loads.		Partial to total loss of gravity load support.	
Lateral Load Carrying Element damage	Negligible - generally elastic response; no significant loss of strength or stiffness.		Light - nearly elastic response; original strength and stiffness substantially retained. Minor cracking/yielding of structural elements; repair implemented at convenience.		Moderate - reduced residual strength and stiffness but lateral system remains functional.		Negligible residual strength and stiffness. No story collapse mechanisms but large permanent drifts. Secondary structural elements may completely fail.		Partial or total collapse. Primary elements may require demolition.	
Damage to architectural systems	Negligible damage to cladding, glazing, partitions, ceilings, finishes, etc. Isolated elements may require repair at users convenience.		Light to moderate damage to architectural systems. Essential and select protected items undamaged. Hazardous materials contained.		Moderate to severe damage to architectural systems, but large falling hazards not created. Major spills of hazardous materials contained.		Severe damage to architectural systems. Some elements may dislodge and fall.		Highly dangerous falling hazards. Destruction of components.	
Egress systems	Not impaired.		No major obstructions in exit corridors. Elevators can be restarted perhaps following minor servicing.		No major obstructions in exit corridors. Elevators may be out of service for an extended period.		Egress may be obstructed.		Egress may be highly or completely obstructed.	

Table 2.2 (Continued)⁵⁹

System Description	Performance Level									
	10 Fully Operational	9	8 Operational	7	6 Life Safe	5	4 Near Collapse	3	2 Collapse	1
Mechanical/Electrical/ Plumbing/Utility Systems	Functional.		Equipment essential to function and fire/life safety systems operate. Other systems may require repair. Temporary utility service provided as required.		Some equipment dislodged or overturned. Many systems not functional. Piping, conduit ruptured.		Severe damage and permanent disruption of systems.		Partial or total destruction of systems. Permanent disruption of systems.	
Damage to contents	Some light damage to contents may occur. Hazardous materials secured and undamaged.		Light to moderate damage. Critical contents and hazardous materials secured.		Moderate to severe damage to contents. Major spills of hazardous materials contained.		Severe damage to contents. Hazardous materials may not be contained.		Partial or total loss of contents.	
Repair	Not required.		At owners/tenants convenience.		Possible - building may be closed.		Probably not practical.		Not possible.	
Effect on occupancy	No effect.		Continuous occupancy possible.		Short term to indefinite loss of use.		Potential permanent loss of use.		Permanent loss of use.	

2.4.2 Earthquake Design Levels

Earthquake design levels are expressed in terms of a mean recurrence interval or a probability of exceedance as shown in Table 2.3⁵⁹. The mean recurrence interval (e.g. 475 years) is an expression of the average period of time, expressed in years, between the occurrence of earthquakes which produce effects of the same, or greater, severity. The probability of exceedance (e.g. 10% in 50 years) is a statistical representation of the chance that earthquake effects exceeding a given severity, will be experienced at the site within a specified number of years. Recurrence interval can be directly related to a probability of exceedance in a specified number of years.

Figure 2.13⁵⁹ summarizes the recommendations for minimum design performance objectives for buildings of different occupancies and uses.

Table 2.3 Earthquake Design Levels⁵⁹

Earthquake Design Level	Recurrence Interval	Probability of Exceedance
Frequent	43 years	50% in 30 years
Occasional	72 years	50% in 50 years
Rare	475 years	10% in 50 years
Very Rare	970 years ^{10,44}	10% in 100 years ^{10,44}

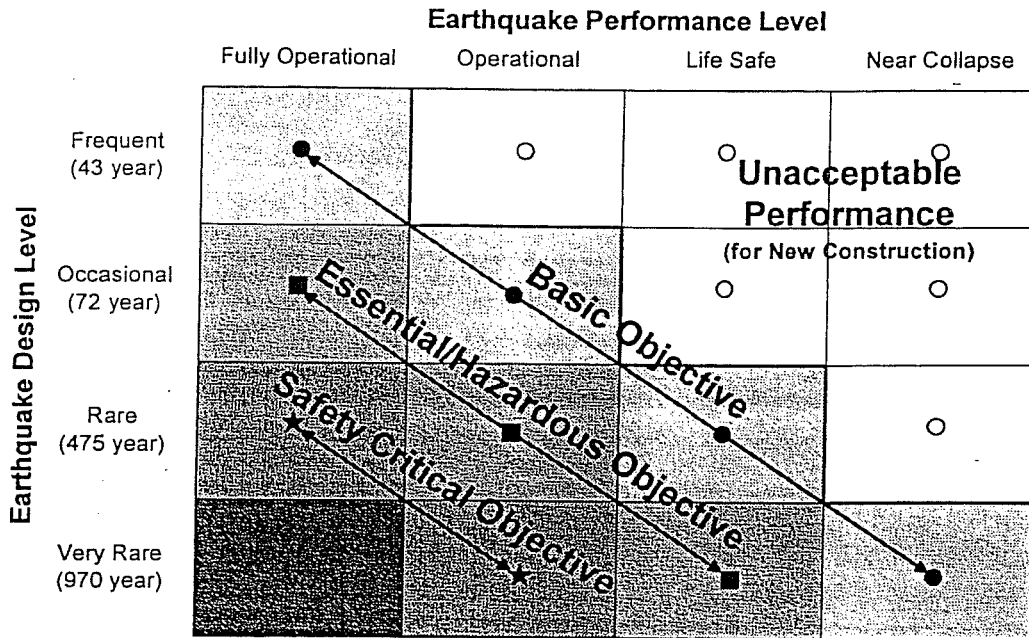


Figure 2.13 Recommended Performance Objective for Buildings⁵⁹

Performance based seismic design and rehabilitation is currently a very active area of study. Many performance objectives are not well-defined and they depend on computational tools to determine the response with appropriate accuracy.

CHAPTER 3

BUILDING AND INSTRUMENTATION DATA COLLECTION

3.1 General

Two buildings were analyzed in this study. The first building is a seven-story reinforced concrete hotel at 8244 Orion Avenue, Van Nuys, California, which was severely damaged during the 1994 Northridge Earthquake, although it did not collapse. The building is unique because it had documented minor structural damage in the 1971 San Fernando Earthquake. A ten-story reinforced concrete building located at 7215 Bright Avenue, Whittier, California, which survived the 1987 Whittier Narrows Earthquake with no visible damage reported⁴⁸ was also analyzed. In the following sections, building details and response data recorded during the earthquakes are presented. Post earthquake damage observations are also provided.

3.2 Seven-Story Hotel at 8244 Orion Avenue

The seven-story hotel is a reinforced concrete frame structure designed in 1965 at a construction cost of 1.3 million dollars. An elevation of the building is shown in Figure 3.1. The building is located in the center of the San Fernando Valley. Geologic source data show that the site lies on recent alluvium. The typical soil boring logs show the underlying soil to be primarily fine sandy silts and silty fine sands⁴⁶.



Figure 3.1 Seven-Story Hotel at Orion Avenue. Northwest Elevation⁶⁸

3.2.1 General Building Description

The structure, which is about 62 feet by 160 feet in plan dimensions, consists of roughly 63,000 square feet of floor area. In Table 3.1, general information of the building is summarized.

Table 3.1 General Information - Seven-Story Hotel⁴⁵

Date of Construction:	1966
Date of Design:	1965
Design Code:	L.A. City Building Code 1964
Number of Story:	7
Plan Dimensions:	62 ft - 8 in (NS) × 151 ft - 2 in (EW)
Building Height:	65 ft - 8 $\frac{1}{2}$ in
Story Heights	
Ground floor:	13 ft - 6 in
Second through sixth floor:	8 ft - 8 $\frac{1}{2}$ in
Seventh floor:	8 ft - 8 in

The foundation of the building consists of groups of friction piles with caps connected by foundation beams as shown in Figure 3.2. The pile groups are concentric with building columns.

The floor plan is the same for every floor except ground floor level where one story canopies connect to the main building. The structure is nearly symmetrical. In the longitudinal direction, columns are spaced at 19 feet center to center, and in the

transverse direction, at 20 feet. The weak axis of the columns is in the longitudinal direction. The floor system is flat plate construction. The floor slab is 10 inches thick at the second floor, 8-1/2 inches thick at the third through seventh floors, and 8 inches thick at the roof (Figures 3.3-3.5). Typical details of beam and column sections are shown in Figure 3.6. The structure was constructed of normal weight reinforced concrete. Properties of the materials specified for the construction are given in Table 3.2.

Interior partitions, in general, consist of gypsum wall-board. One inch thick plaster was used for exterior partitions at each end of the building and at the stair and elevator bays in the longitudinal direction of the building. Some additional cement plaster walls were located on the south side of the building at the first floor. Four bays at the east end of the structure were infilled with brick masonry walls at the first story (Figure 3.7). One inch wide expansion joints separated these walls from exterior columns. Between the walls and the second floor spandrel beams, separation joints were 1/2 inch wide. In the original design, the masonry infill walls were not considered part of the lateral load resisting system. Lateral forces in each direction are resisted by perimeter spandrel beam-column frames and interior slab-column frames,. Interior columns are 18" × 18" and exterior columns are 14" × 20". Figure 3.8 and Figure 3.9 show the south and north perimeter frame elevations, respectively.

Typical beam reinforcement above the third floor consists of 2-#6 bars at the bottom, 3-#8 at the top and #3 ties varying from 3 inches on center near the ends and

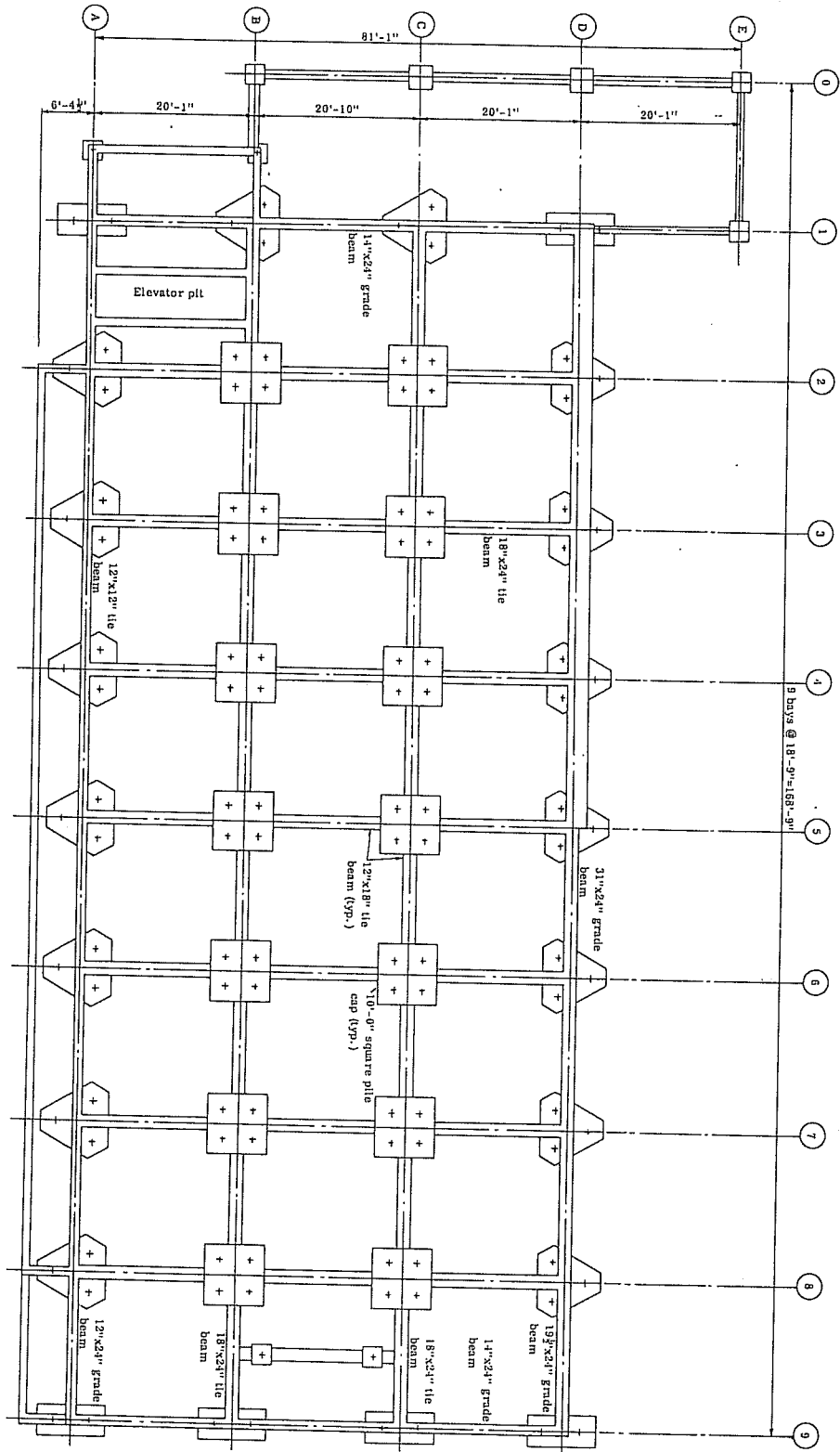


Figure 3.2 Seven-Story Hotel. Foundation Plan⁶⁸

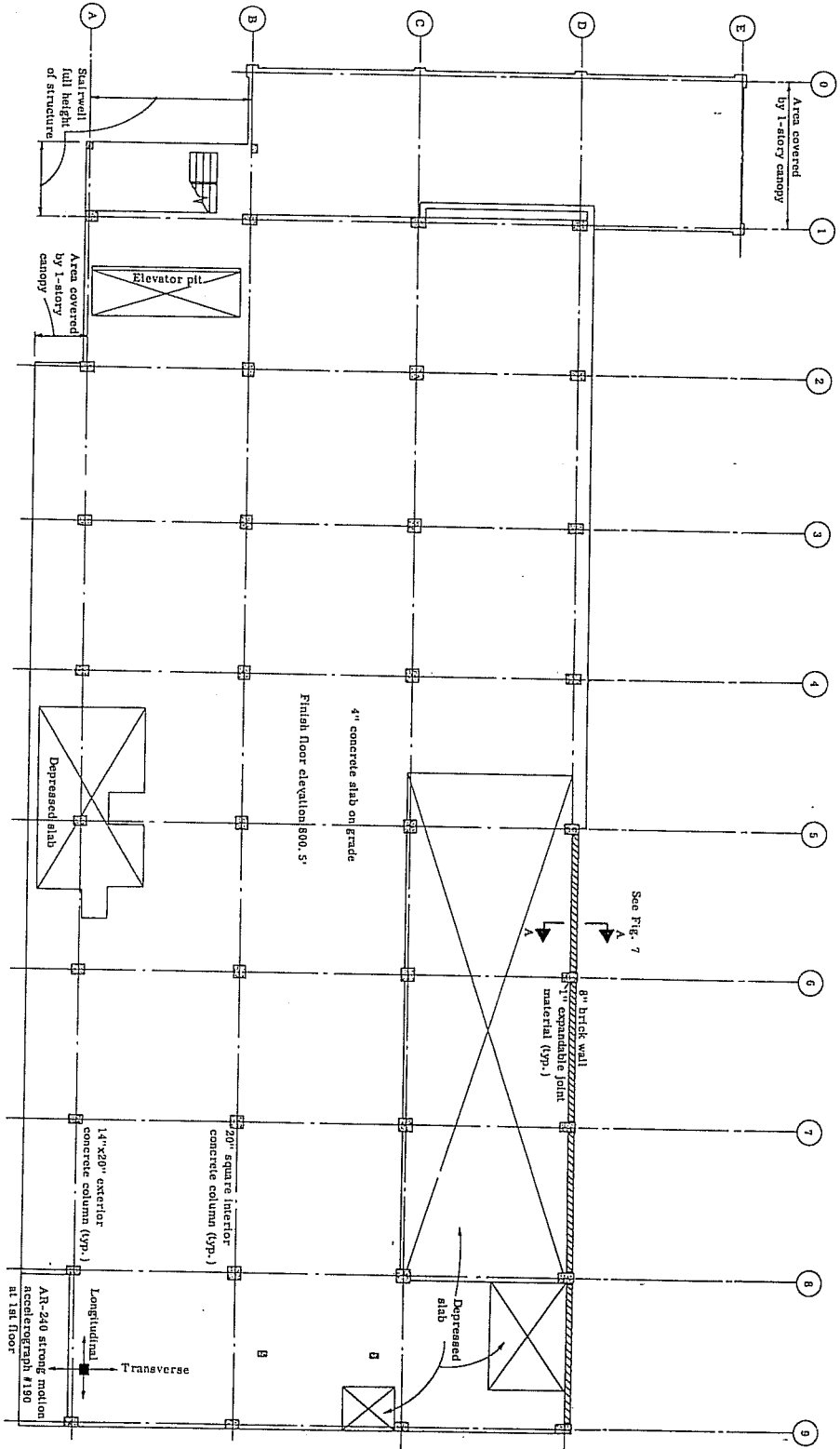


Figure 3.3 Seven-Story Hotel. First-Floor Plan⁶⁸

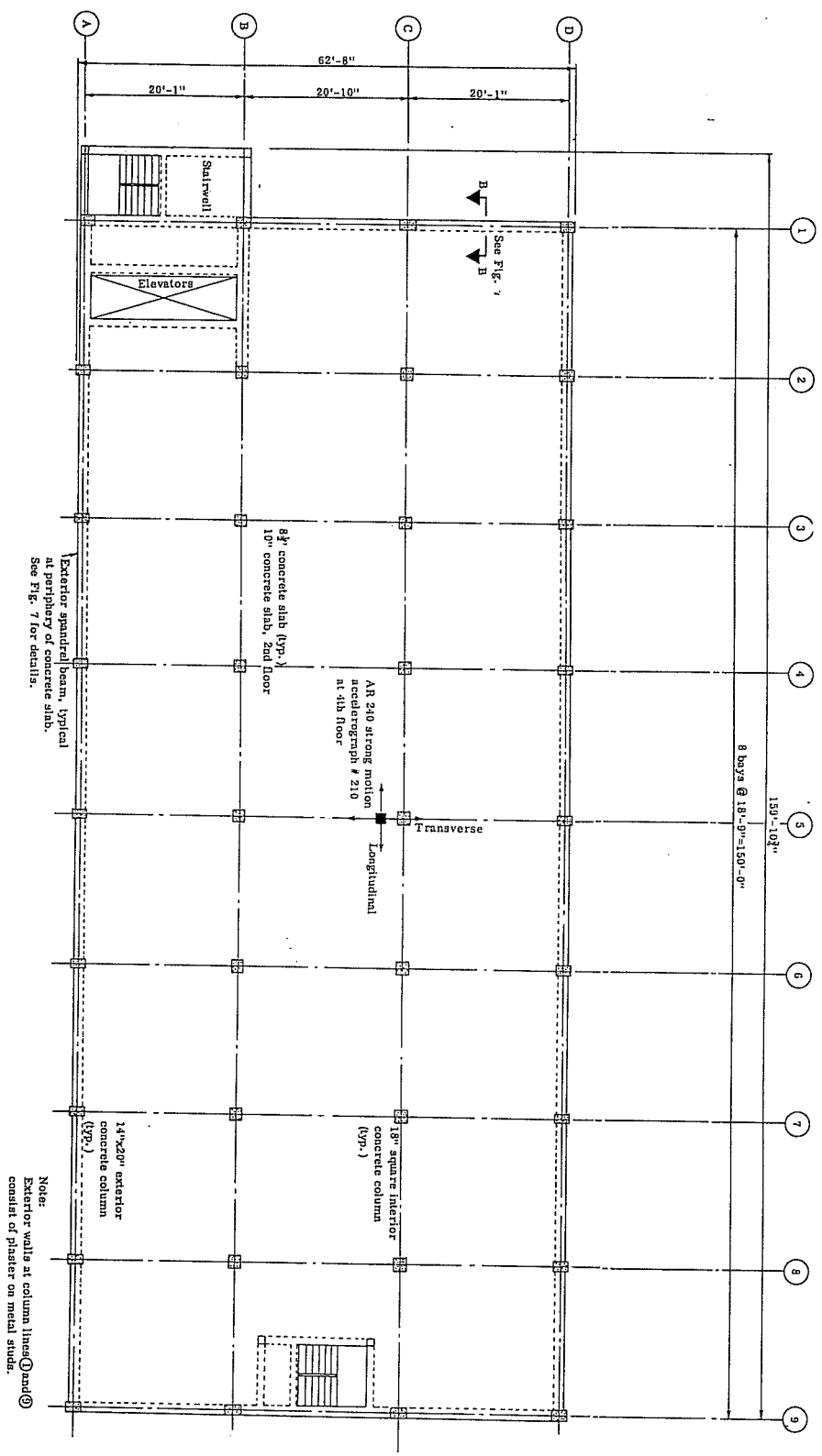


Figure 3.4 Seven-Story Hotel. Typical Floor Framing Plan⁶⁸

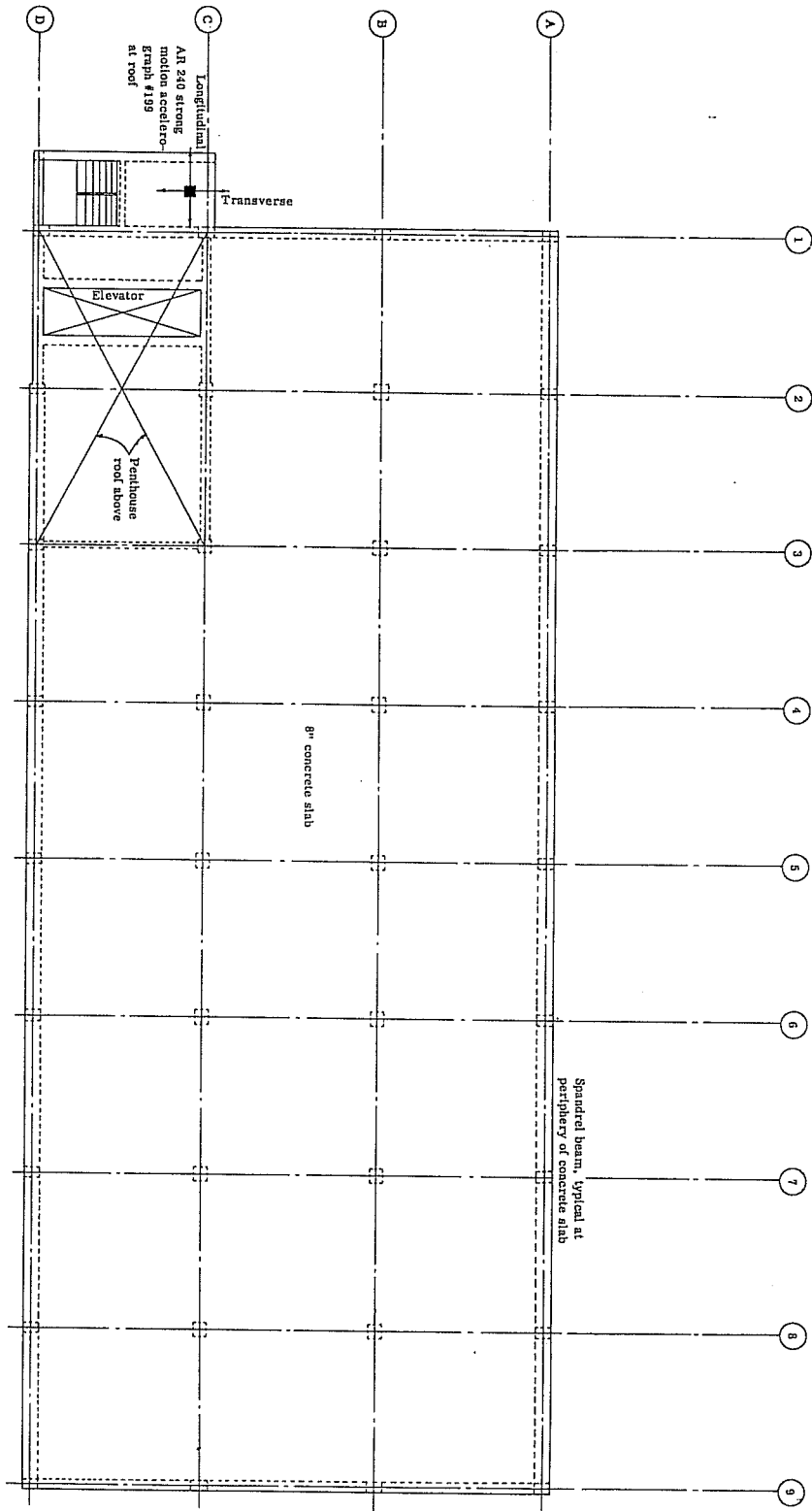


Figure 3.5 Seven-Story Hotel. Roof Framing Plan⁶⁸

TYPICAL COLUMN DETAIL

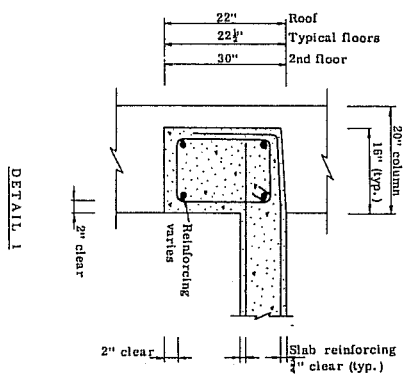
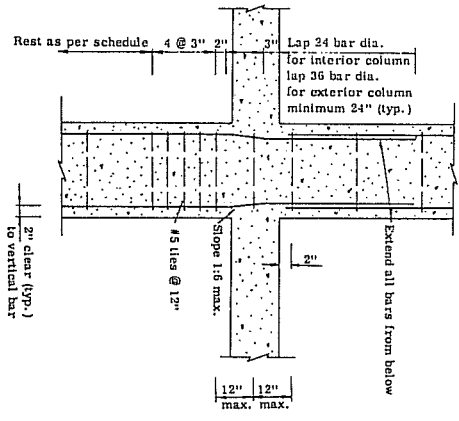


Figure 3.6 Seven-Story Hotel Sections and Details 68

TYPICAL TRANSVERSE SECTION

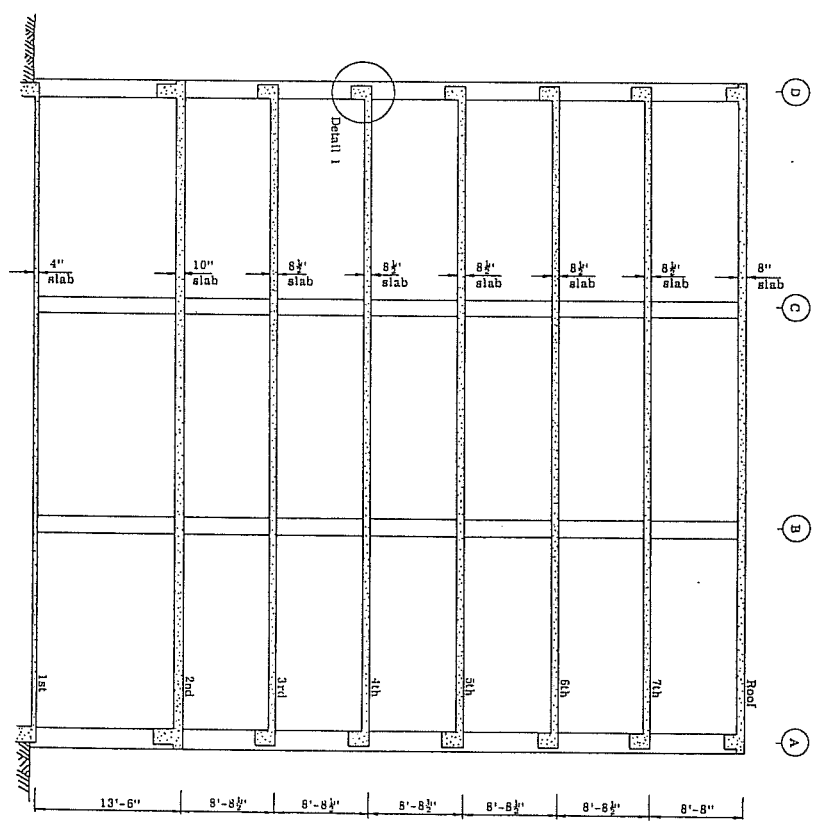


Table 3.2 Properties of Construction Materials⁶⁸

Concrete (normal weight, 150 pcf unit weight)		
Location in structure	Minimum specified compressive strength (f'_c) in ksi	
Columns, 1st to 2nd floors	5	
Columns, 2nd to 3rd floors	4	
Beams and slabs, 2nd floor	4	
All other concrete, 3rd floor to roof	3	
Reinforcing steel		
Location in structure	Grade	Minimum specified yield strength (f_y) in ksi
Beams and slabs	Intermediate-grade deformed billet bars (ASTM A-15 and A-305)	40
Column bars	Deformed billet bars (ASTM A-432)	60

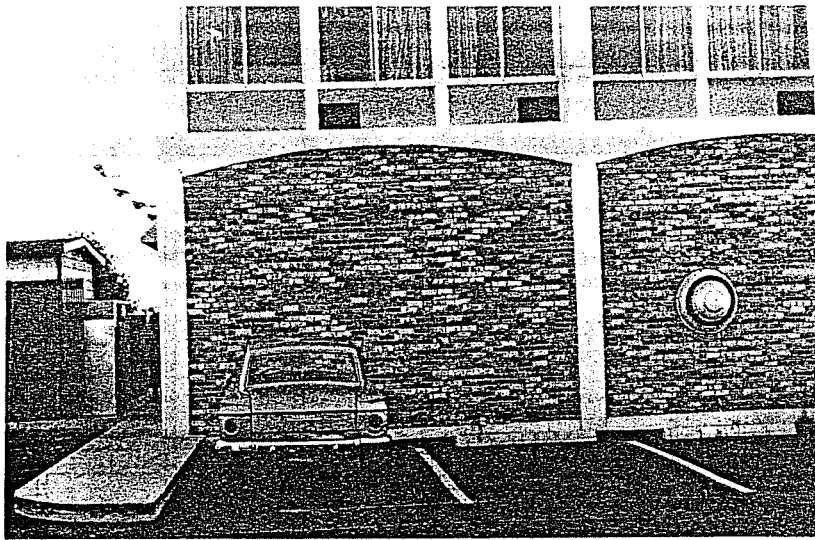


Figure 3.7 Seven-Story Hotel. East End of North Side of Building⁶⁸

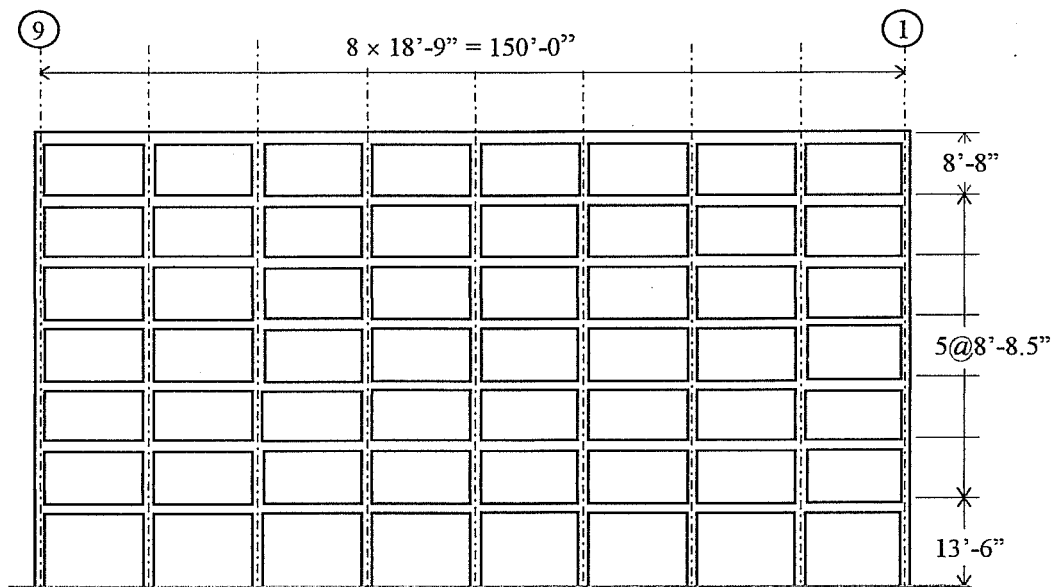


Figure 3.8 Seven-Story Hotel South Perimeter Frame Elevation

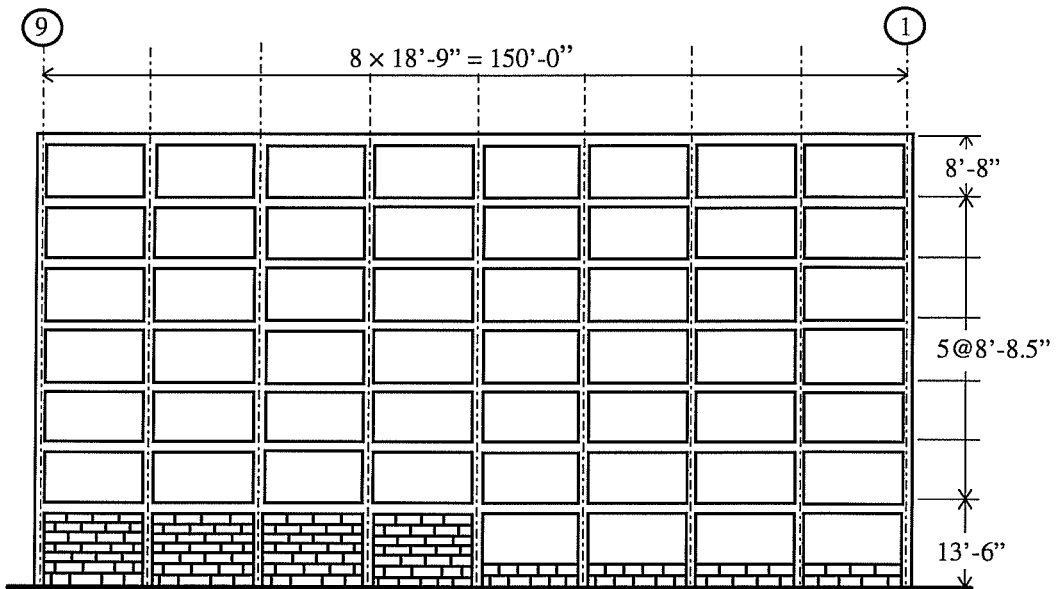


Figure 3.9 Seven-Story Hotel North Perimeter Frame Elevation

increasing to 5 and 10 inch spacings in the middle portion. Because the structure was cast-in-place construction, part of the slab adjacent to the spandrel beam was considered to act as a T-beam flange and 2#6 reinforcing bars within the slab flange were included in the negative reinforcement for analyses. The added bars were not included in the original design of the spandrels. Above the fourth floor, columns were reinforced with 6-#7 vertical bars and #2 ties (2 sets per location) at 12 inches on center. Below the fourth floor, columns consisted of 6-#9 vertical bars with #3 ties

(2 sets per location) at 12 inches on center. As noted earlier (Table 3-2), higher strength concrete was used for the lower floor columns.

3.2.2 Northridge Earthquake (1994)

The Northridge Earthquake occurred on January 17, 1994 at 4:31 a.m. local time, about 20 miles west-northwest of Los Angeles in Northridge. The epicenter, which was about 1 mile south-southwest of Northridge, was located at 34°12'N, 118°32'W. The local Richter magnitude was $M_L = 6.4$ determined from TERRAScope data by H. Kanamori². The National Earthquake Information Center has calculated the surface wave magnitude of the quake as $M_S = 6.8$. The focal depth was estimated at about 9-12 miles⁴⁷. The strong shaking lasted about 15 seconds in the epicentral area.

3.2.2.1 Building Instrumentation

The building is located approximately 4.5 miles east of the epicenter. It suffered severe damage during the earthquake and was red-tagged after post-quake inspection. The building was extensively instrumented at the time the earthquake struck and motions were recorded by sixteen sensors. Among these sensors, ten sensors recorded North-South motion, five sensors recorded East-West motion, and one recorded vertical motion. The sensor locations are shown in Figure 3.10.

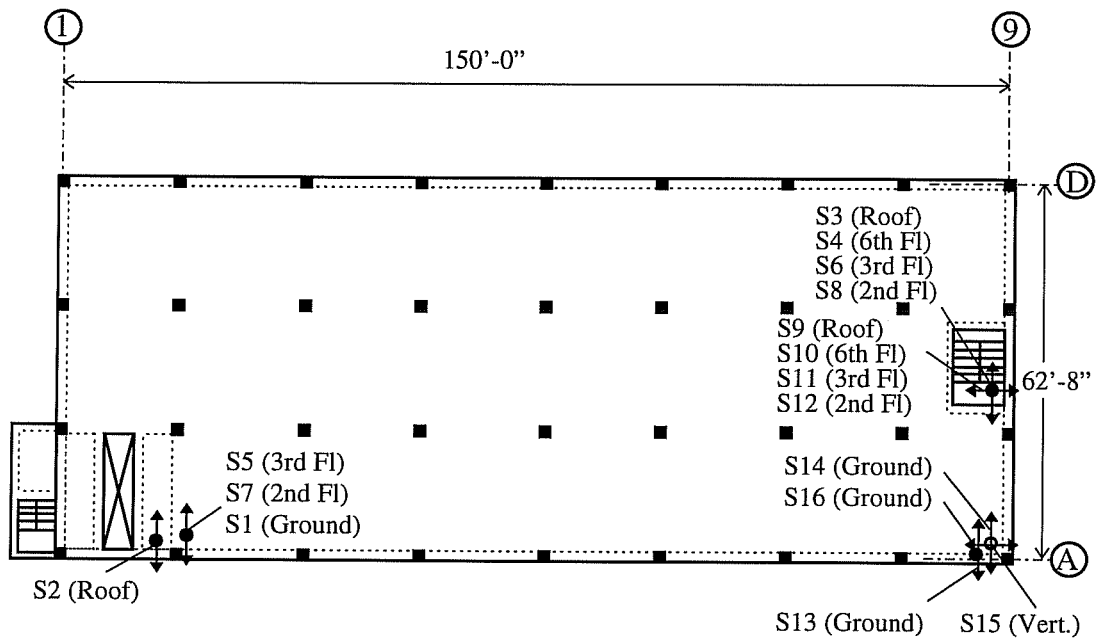


Figure 3.10 Seven Story Hotel Sensor Location at the 1994 Northridge Earthquake

Figures 3.11, 3.12, 3.13, and 3.14 show recorded acceleration records at all the sensors. Peak ground accelerations in the East-West, North-South, and vertical direction were 0.45g, 0.42g, and 0.27g, respectively. The recorded peak accelerations and approximate times of occurrence are listed in Table 3.3.

Table 3.3 Recorded Peak Acceleration and Approximate Time of Occurrence During the 1994 Northridge Earthquake:
Seven-Story Hotel

Station Location	Longitudinal (east/west) direction		Transverse (north/south) direction		Vertical (up/down) direction	
	Station Number	Peak Acceleration and Time of Occurrence	Station Number	Peak Acceleration and Time of Occurrence	Station Number	Peak Acceleration and Time of Occurrence
Roof	S9	0.58g at 9.22 sec.	S2 S3	0.56g at 4.64 sec. 0.57g at 7.36 sec.		
6th Floor	S10	0.46g at 9.12 sec.	S4	0.33g at 7.28 sec.		
3rd Floor	S11	0.36g at 10.06 sec.	S5 S6	0.41g at 4.84 sec. 0.45g at 4.44 sec.		
2nd Floor	S12	0.33g at 8.44 sec.	S7 S8	0.38g at 4.12 sec. 0.40g at 4.58 sec.		
Ground Floor	S16	0.45g at 8.86 sec.	S13 S1	0.42g at 5.54 sec. 0.39g at 5.58 sec.	S15	0.27g at 4.18 sec.

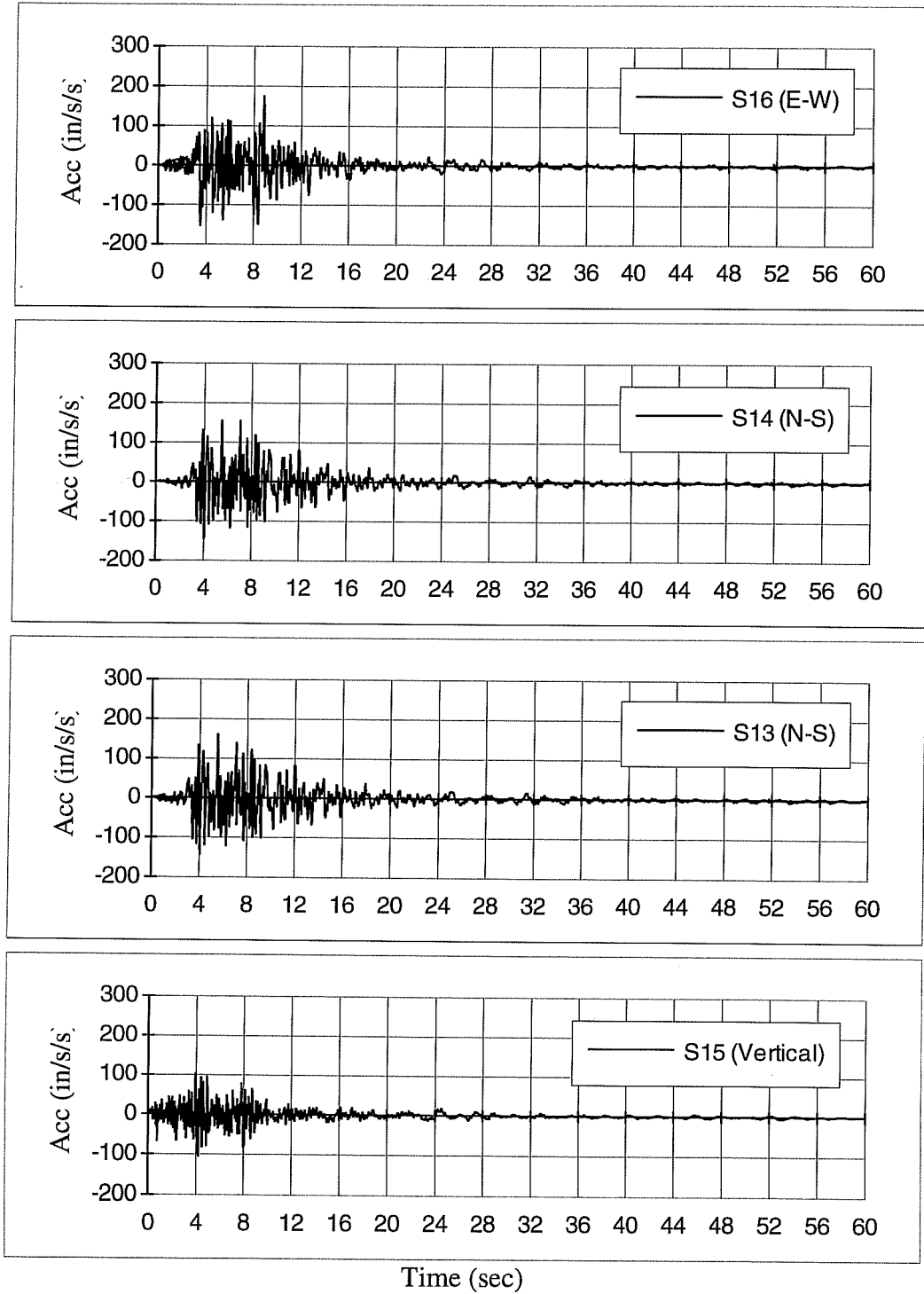


Figure 3.11 Acceleration Recorded at East End at Ground Level

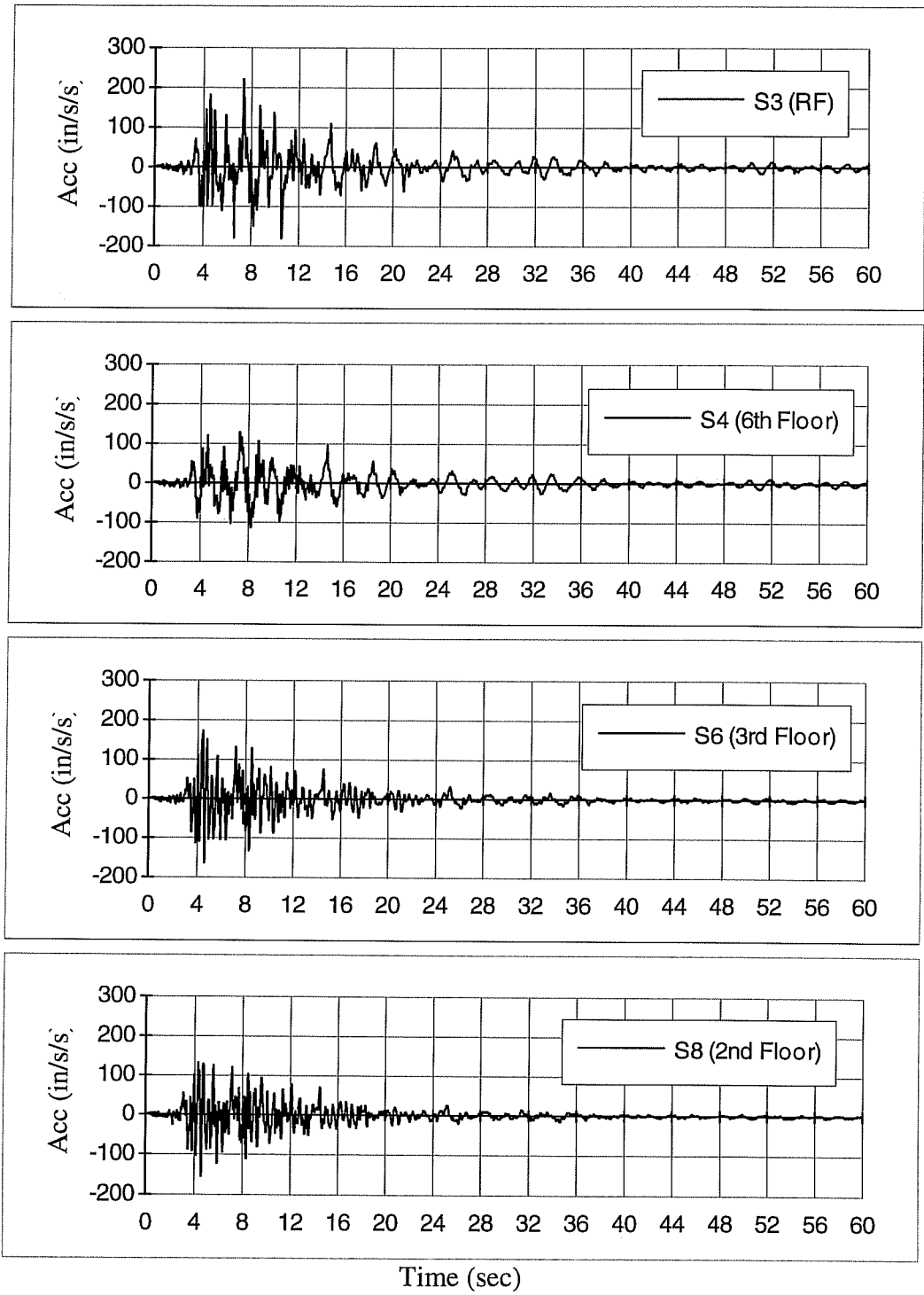


Figure 3.12 Acceleration Recorded at East End in North-South Direction

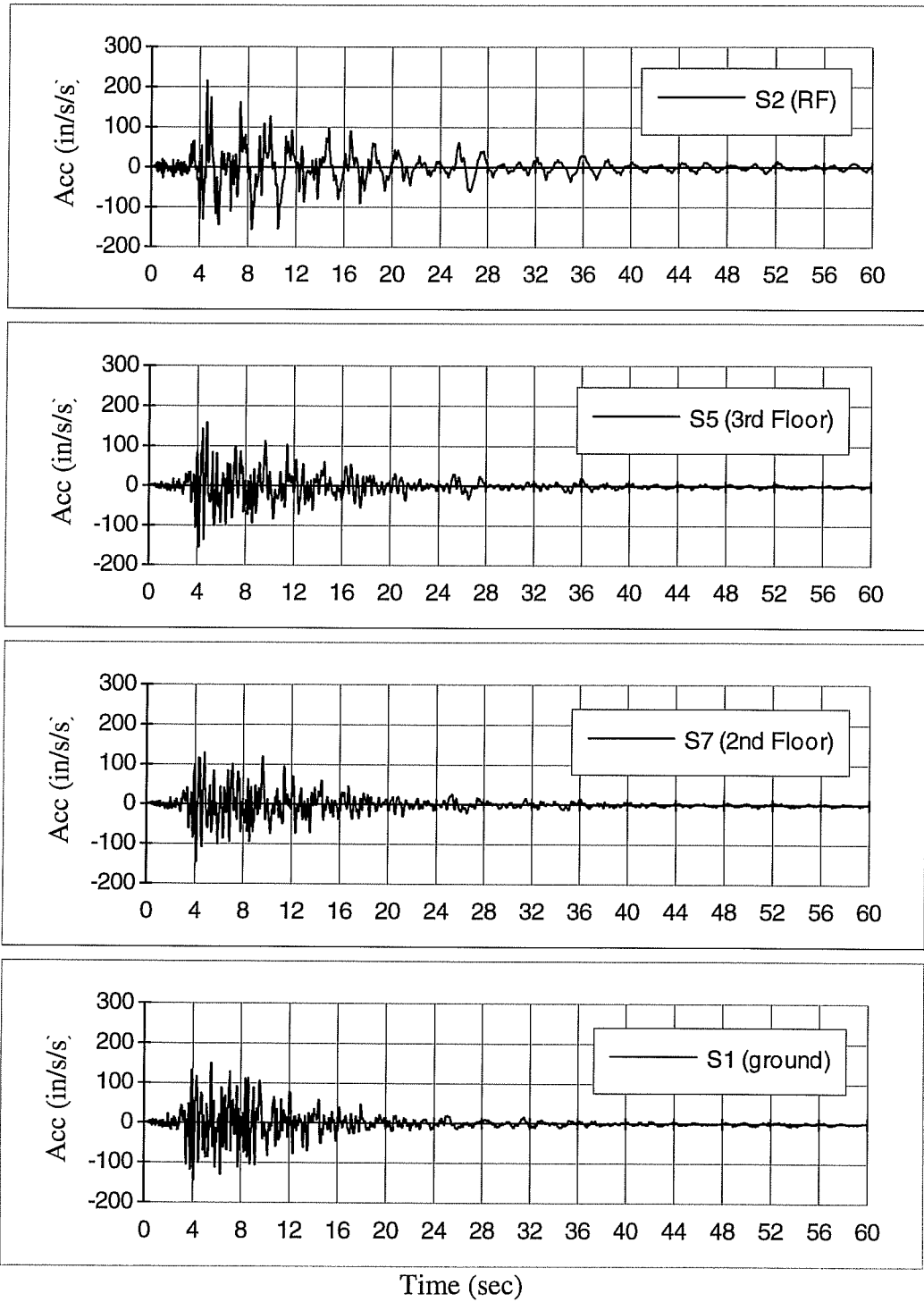


Figure 3.13 Acceleration Recorded at West End in North-South Direction

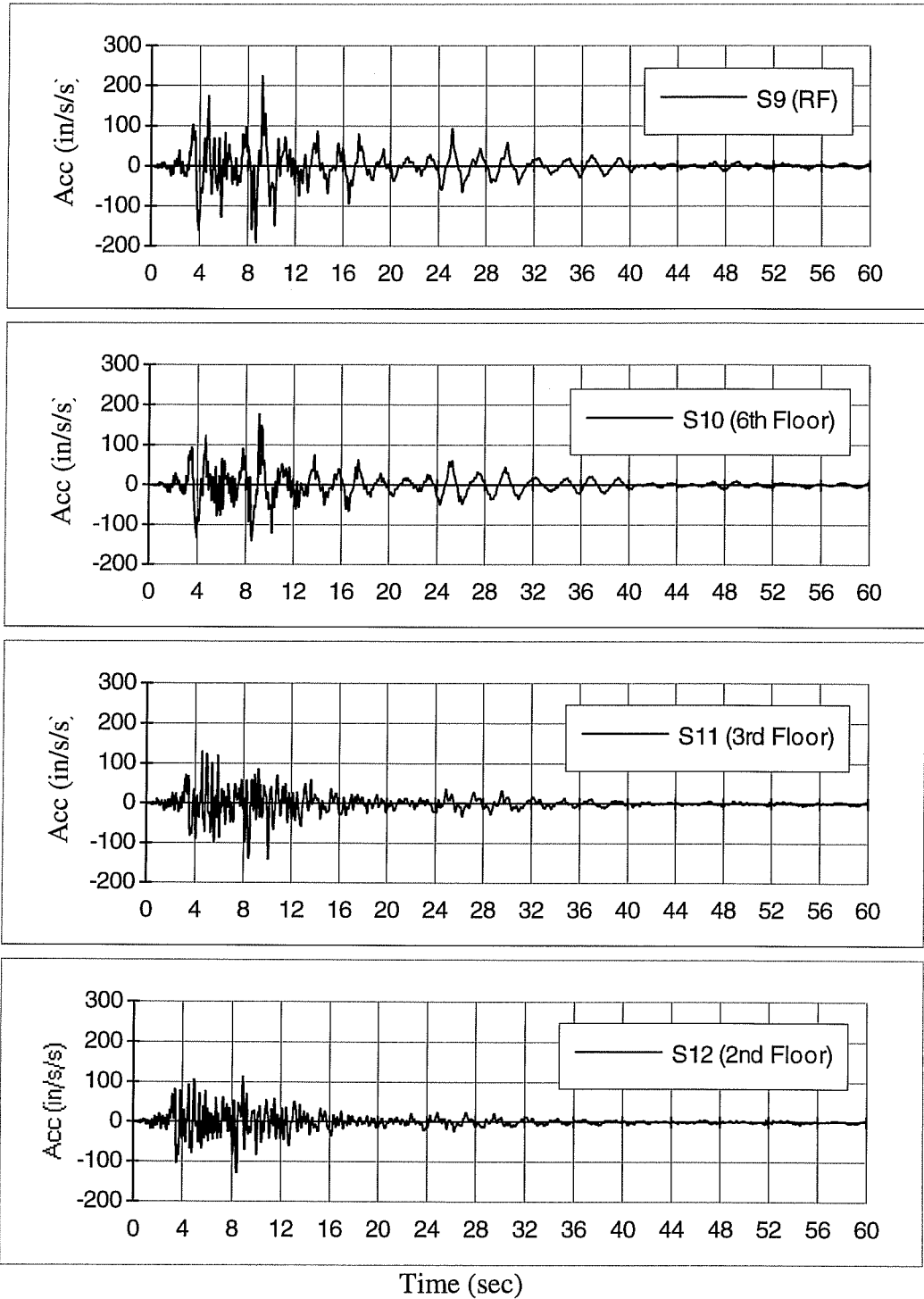
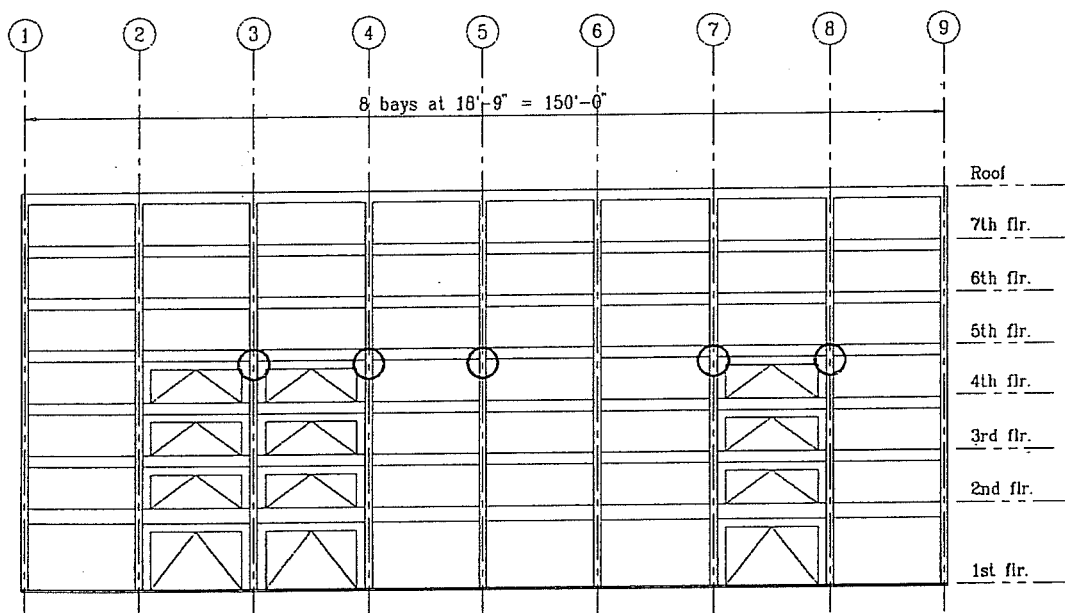


Figure 3.14 Acceleration Recorded at East End in East-West Direction

3.2.2.2 Building Earthquake Damage

The building suffered extensive structural damage during the Northridge Earthquake. Several columns between the fourth and fifth floors failed in shear (Figures 3.15 and 3.16) and temporary shoring was provided to prevent collapse.



Legend:


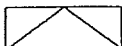
-  Indicates location of the most severe damage
-  Indicates temporary shoring

Figure 3.15 South Perimeter Frame Elevation after the 1994 Northridge Earthquake⁴⁵

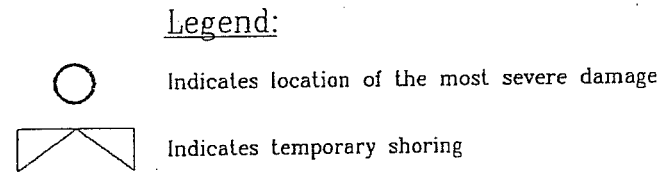
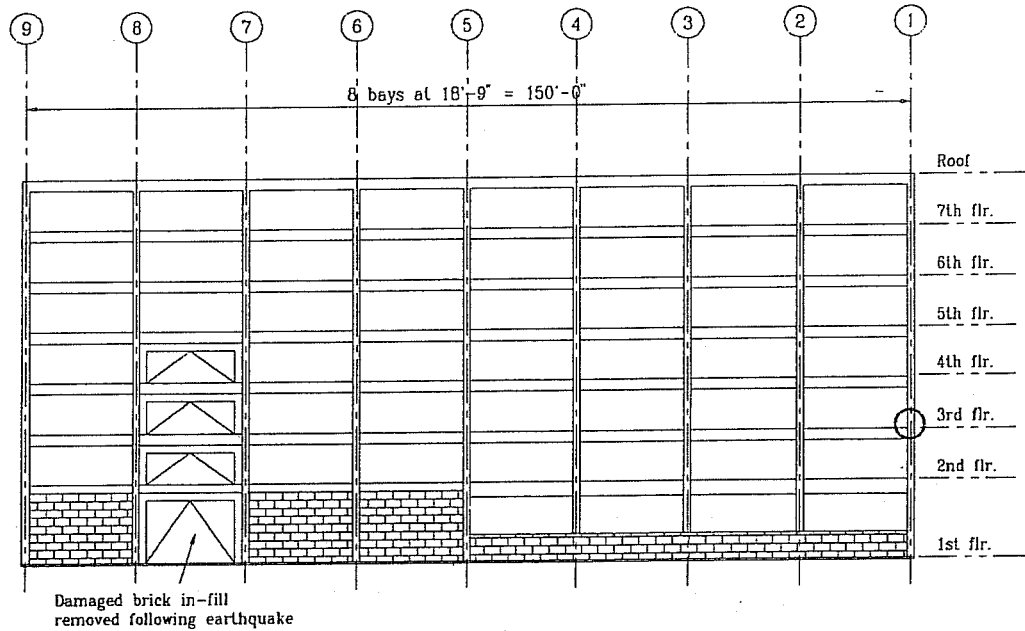


Figure 3.16 North Perimeter Frame Elevation after the 1994 Northridge Earthquake⁴⁵

Most of the structural damage were observed in the longitudinal perimeter frames, with the south perimeter frame suffering more damage than the north perimeter frame. Damage consisted primarily of shear failure at the top of the columns beneath spandrel beams. Column vertical reinforcement between ties buckled due to

loss of confinement after the column failed in shear. Figure 3.17 shows temporary shoring in the south perimeter frame of the building and Figure 3.18 shows the north perimeter frame after the earthquake. Most of the shear failures occurred between the fourth and the fifth floors in south perimeter frame. Figure 3.19 is a close up view of

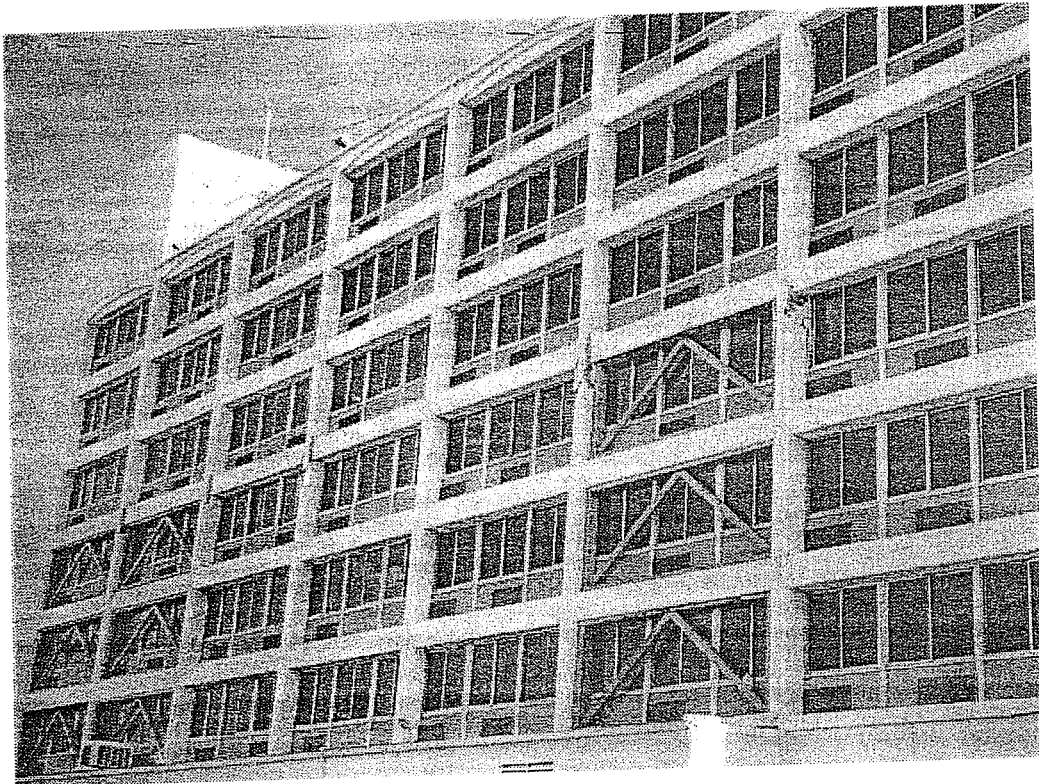


Figure 3.17 South Perimeter Frame Elevation with Temporary Shoring after the 1994 Northridge Earthquake⁴⁵



Figure 3.18 North Perimeter Frame Elevation with Temporary Shoring after the 1994 Northridge Earthquake⁴⁵

damaged columns below the fifth floor spandrel beam. Figure 3.20 shows a typical failure region at the end of a column. Flexural cracks and minor concrete spalling were visible in several spandrel beams⁴⁵, suggesting possible yielding of the beam flexural reinforcement. Cracks were also observed in masonry infill walls located in

the first story of the north perimeter frame, and indicated that these non-structural walls might have acted as part of the lateral force resisting system, at least in the first few seconds of the earthquake.



Figure 3.19 Close View of Damaged Columns Below fifth Floor Spandrel Beam
(Column A-7 and A-8)⁴⁵

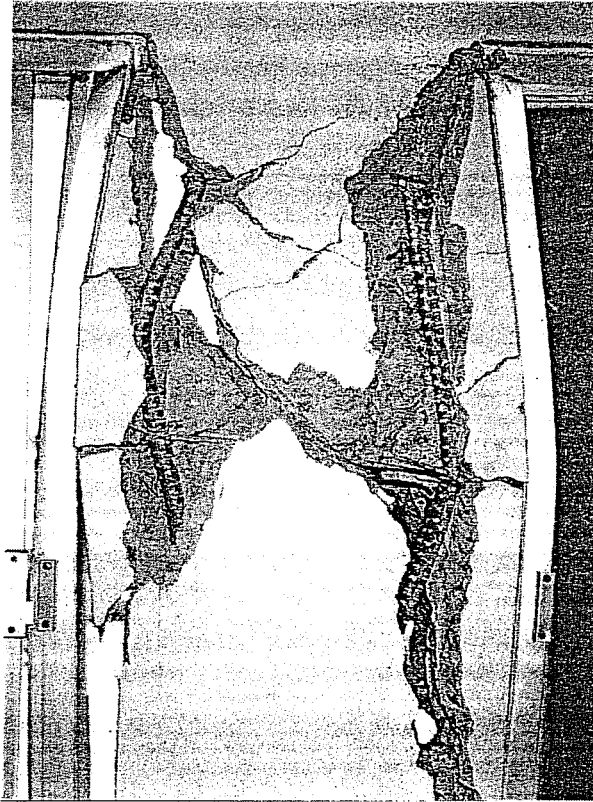


Fig. 3.20 Failure Region of Column A-8 Between Fourth and Fifth Floor
Viewed From Inside of the Building⁴⁵

3.2.3 San Fernando Earthquake (1971)

The San Fernando Earthquake occurred on February 9, 1971 at 6:01 a.m. local time. The epicenter was located about 9 miles east of Newhall-Saugus, California, at $34^{\circ} 24' N$ and $118^{\circ} 24' W$. The magnitude was 6.6 on the Richter scale. The focal depth was estimated at about 8 miles⁷².

3.2.3.1 Building Instrumentation

Motions caused by the San Fernando Earthquake were recorded by Earth Sciences AR-240 strong-motion accelerographs located at the roof, fourth floor, and ground level (Figure 3.21).

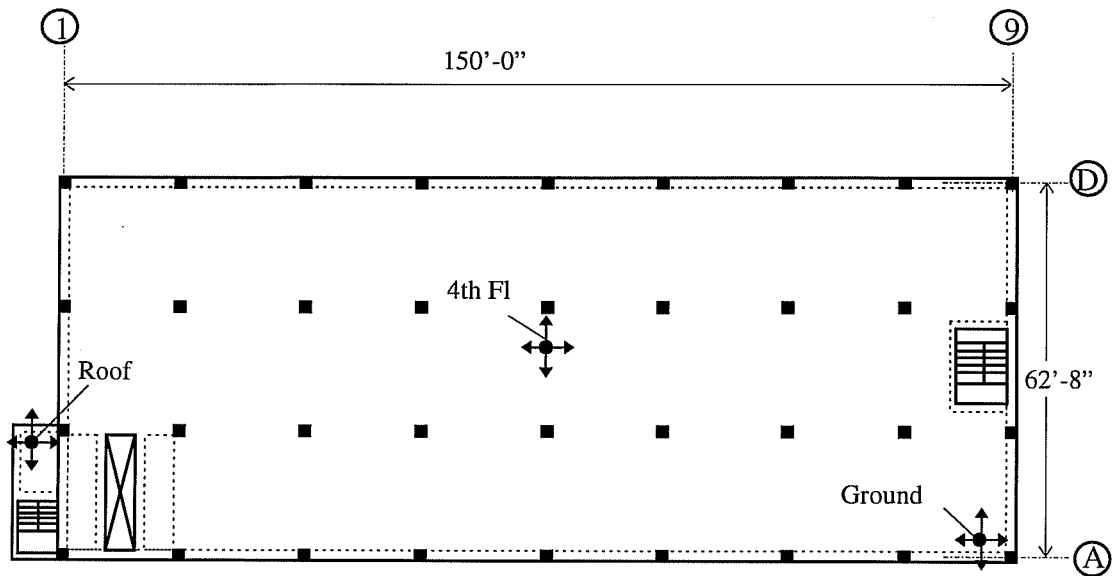


Figure 3.21 Seven-Story Hotel Sensor Location at the 1971 San Fernando Earthquake

At each location, motions were recorded along the three principal axes, parallel to the long direction of the building (longitudinal), parallel to the short side of the building (transverse), and vertical. Approximately 40 seconds of motion were recorded for each component at each location. The peak measured accelerations and times of occurrence for each recording are given in Table 3-3.

Table 3-3 Recorded Peak Acceleration and Approximate Time of Occurrence during the 1971 San Fernando Earthquake. Seven-Story Hotel

Station	Transverse (north/south) component	Longitudinal (east/west) component	Vertical component
Roof	0.406g at 9.9 sec.	0.327g at 9.2 sec.	0.24g at 3.6 sec.
4th Floor	0.203g at 9.1 sec.	0.253g at 7.9 sec.	0.24g at 3.47 sec.
Ground Floor	0.251g at 12.5 sec.	0.134g at 9.0 sec.	0.18g at 3.62 sec.

Figures 3.22, 3.23, and 3.24 are plots of acceleration time history recorded at the roof, 4th floor, and ground floor levels, respectively. In each figure, there are accelerograms in the longitudinal, transverse, and vertical direction. The duration of strong motion was about 10 to 20 seconds.

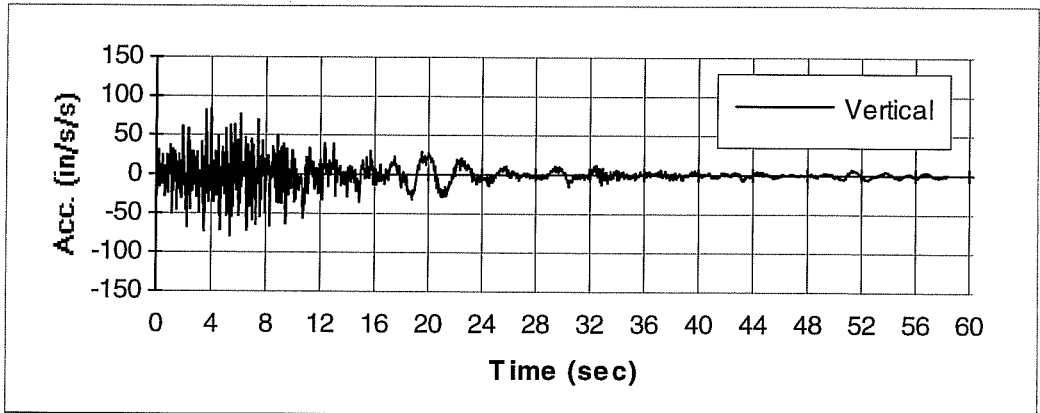
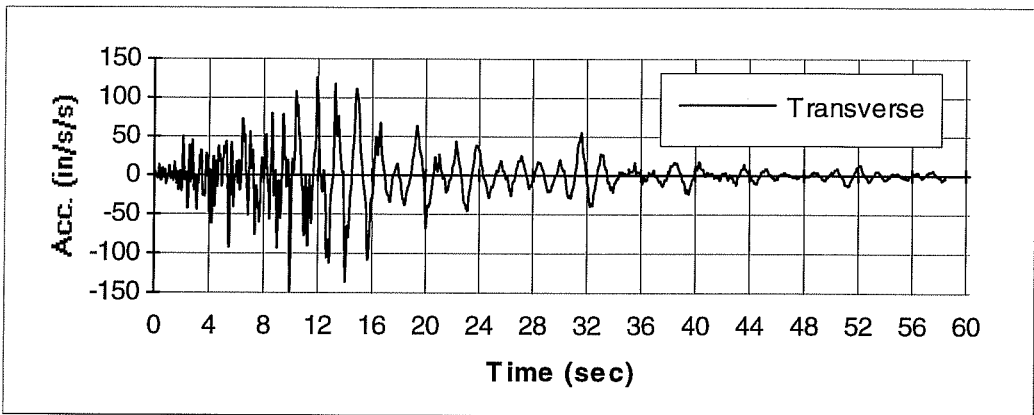
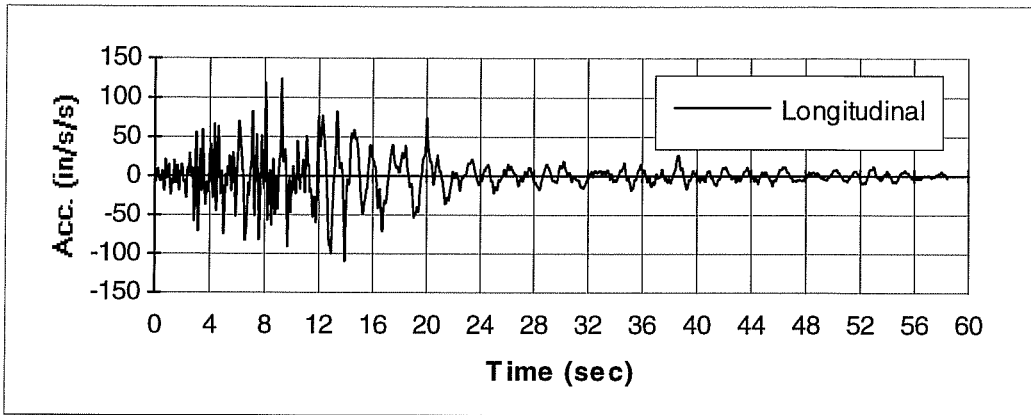


Figure 3.22 Seven-Story Hotel. Recorded acceleration at the Roof during the 1971 San Fernando Earthquake

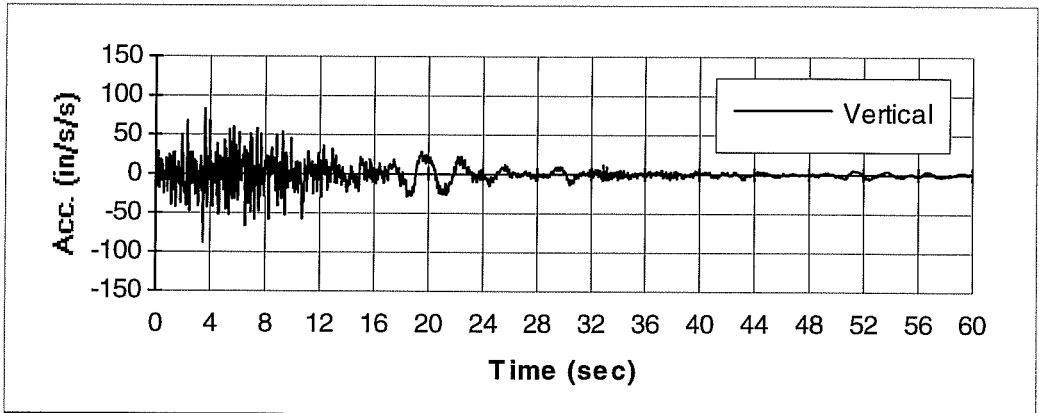
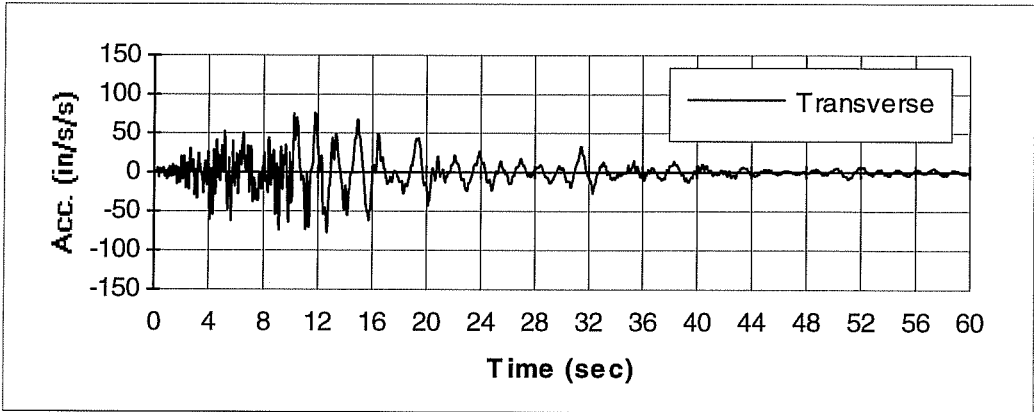
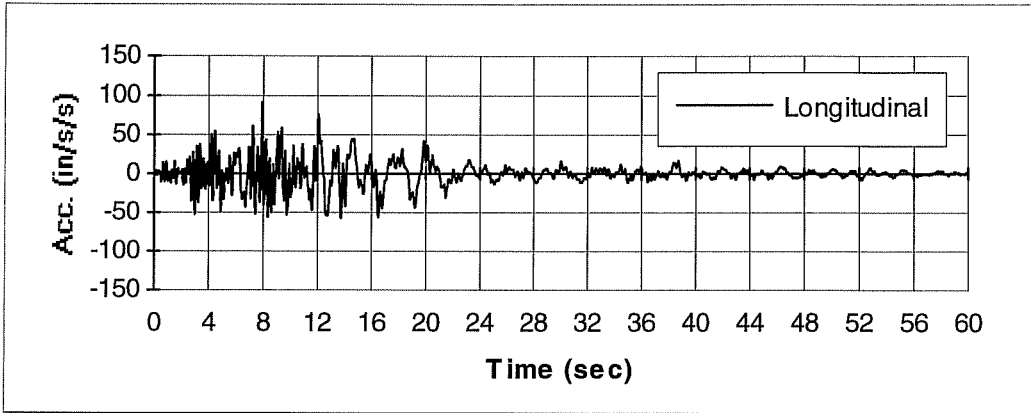


Figure 3.23 Seven-Story Hotel. Recorded Acceleration at the Fourth Floor during the 1971 San Fernando Earthquake

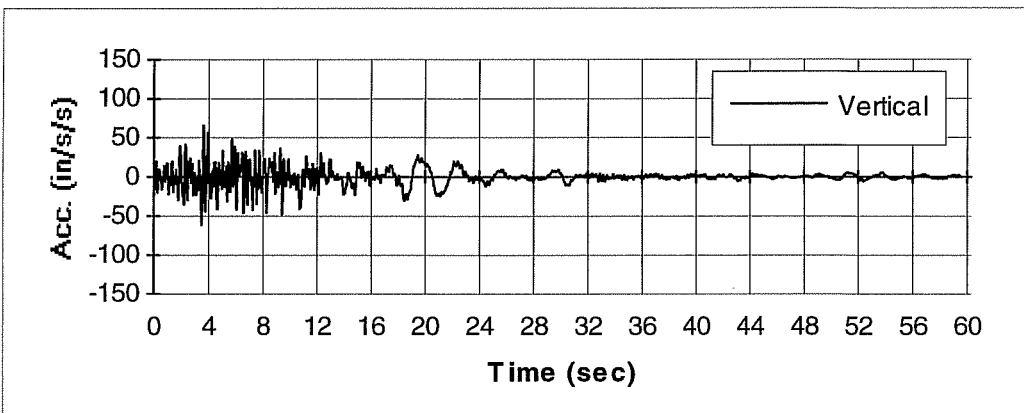
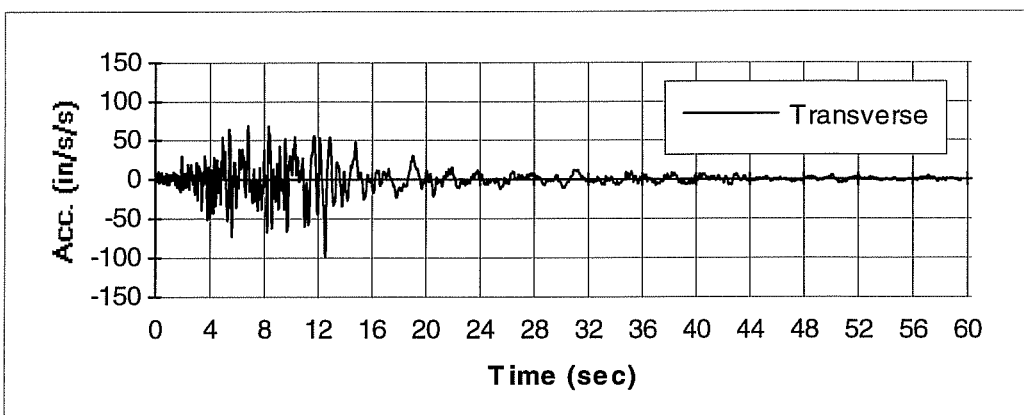
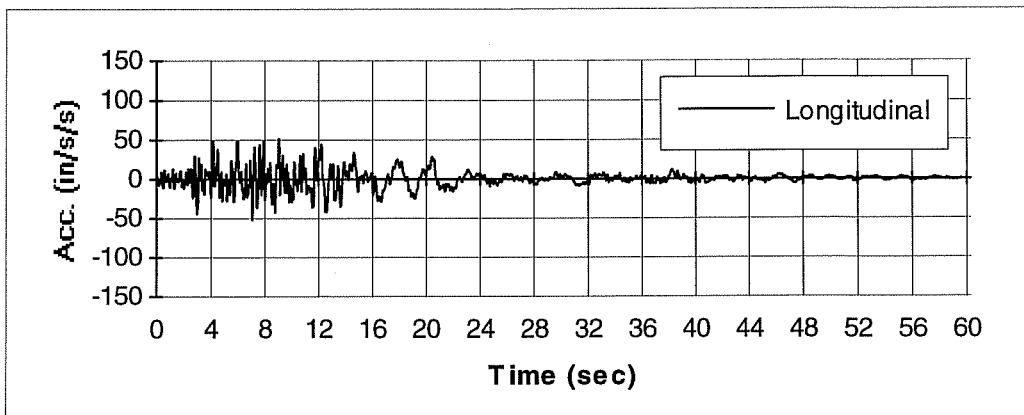


Figure 3.24 Seven-Story Hotel. Recorded Acceleration at the Ground Level during the 1971 San Fernando Earthquake

3.2.3.2 Building Earthquake Damage

Repair of non-structural damage cost approximately 10 percent of the initial construction cost of the building⁶⁸. Structural damage was minor and was repaired by patching the second floor beam-column joint on the north side (east-end) of the structure (Figure 3.25).

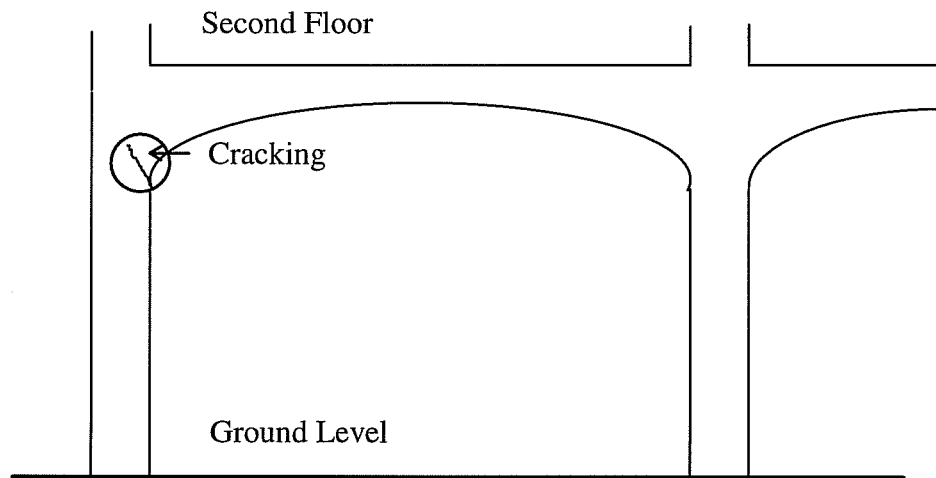


Figure 3.25 Cracking Pattern at the Second Floor Beam-Column Joint on the North Side (East-End) of the Structure

There was non-structural damage primarily to partitions, bathroom tiles, and plumbing pipelines. The second and the third floors suffered the most severe damage while the sixth and the seventh floors suffered the least damage⁶⁸.

3.3 Ten-Story Building at 7215 Bright Avenue

3.3.1 General Building Description

The ten story building is a reinforced concrete structure (Figure 3.26) with plan dimensions of 52 ft 8 in by 183 ft 4 in⁴⁸. The building, located in the City of Whittier in Southern California, was designed and constructed in 1972. Table 3.4 is a summary of general information about the building.

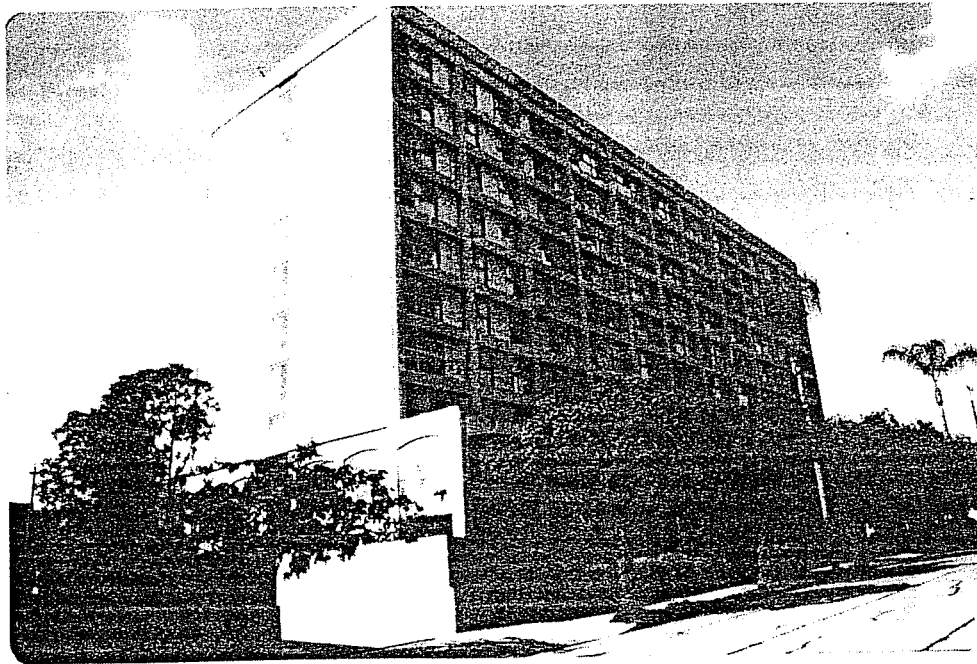


Fig. 3.26 General View of the Ten Story Building⁴⁹

Table 3.4 Ten-Story Building General Information Summary

Date of Construction:	1972	
Date of Drawings:	1972	
Design Code:	Uniform Building Code (1970 ed.)	
Number of Stories:	Above Ground Level	10
	Below Ground Level	1
Plan Dimensions:	52 ft - 8 in (NS) × 183 ft - 4 in (EW)	
Building Height:	90 ft	
Story Heights		
Basement:	9 ft - 8 in	
First story:	12 ft - 0 in	
Second through roof floor:	8 ft - 8 in	

Plan views of the foundation and first floor are shown in Figures 3.27 and 3.28. Plan views of the second floor and typical floors are shown in Figures 3.29 and 3.30. Cast-in-place shear walls with coupling beams were located at the north and south ends of the building along Grid lines 2 and 13 (Figure 3.27). Also two smaller shear walls surrounded the elevators at lines 7 and 8 (Figures 3.28 and 3.31). There were additional shear walls at the second story on all lines between G and E (Figure 3.29).

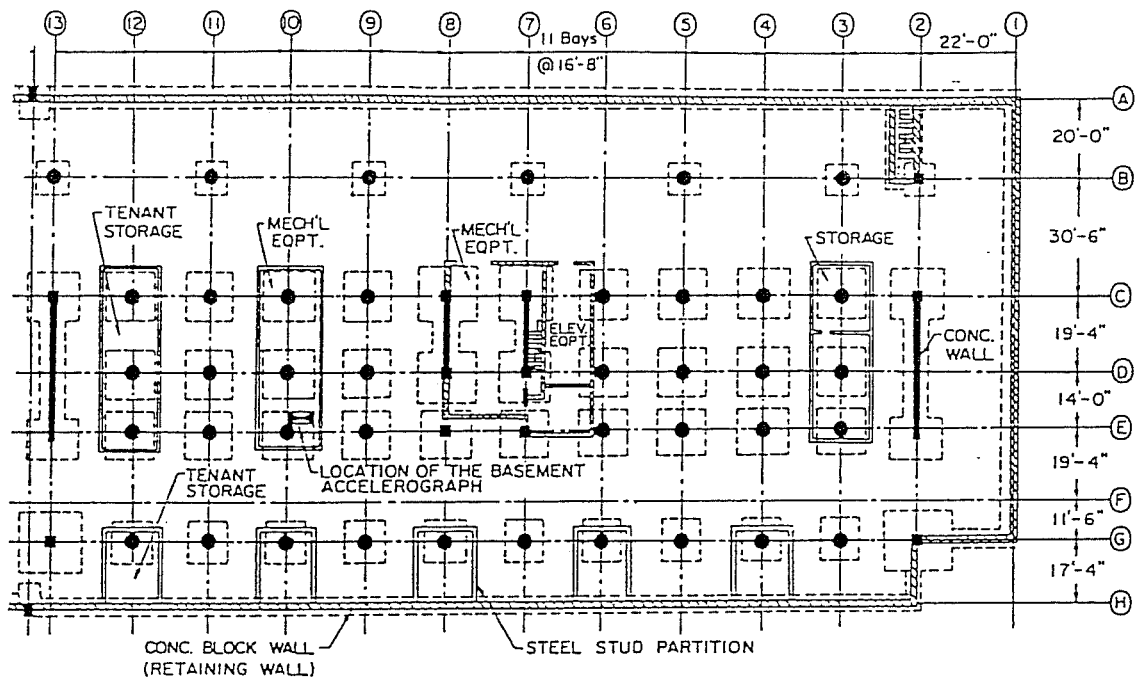


Figure 3.27 Basement-Foundation Plan³⁶

The foundation of the building consists of spread footings (Figure 3.27). There is a parking facility on the west and north sides of the structure at the basement level (Figure 3.28). Figure 3.31 shows an elevation of the structure on Grid C and Figure 3.32 shows an elevation of the transverse direction of the building. Normal weight concrete was used and Table 3.5 is a summary of the material properties specified for the construction.

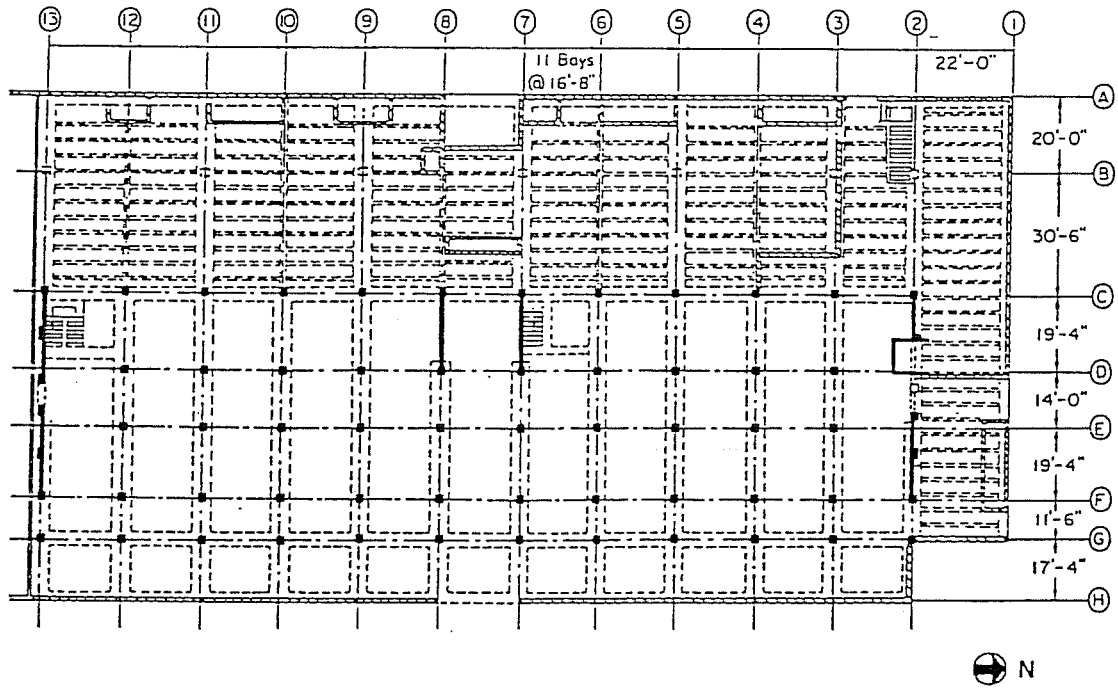


Figure 3.28 First Floor Framing Plan³⁶

Typical exterior columns are 20" by 20", and typical interior columns are 16" by 16". Spandrel beams have the dimensions of 24" by 24". Slabs are 6.5 inches thick for all floors.

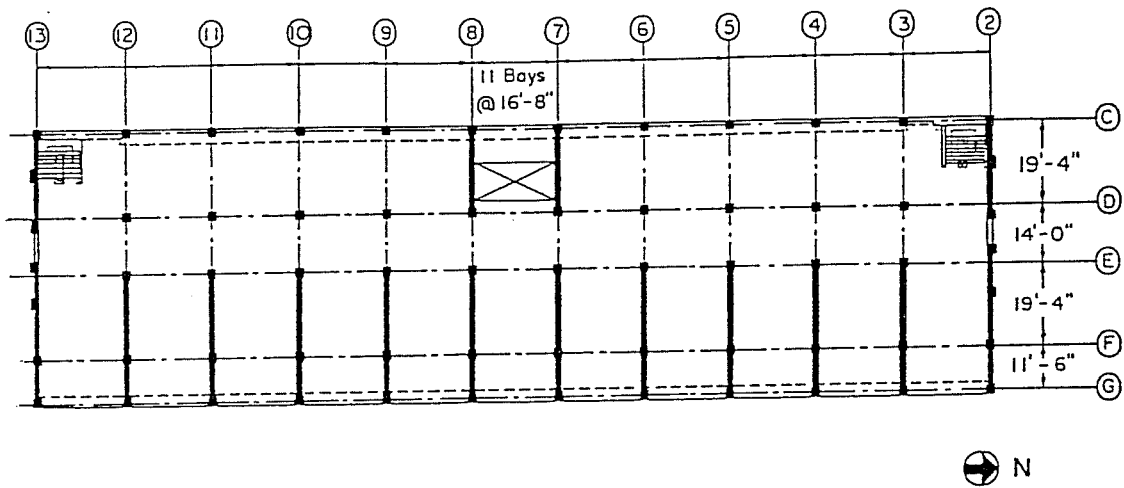


Figure 3.29 Second Floor Plan³⁶

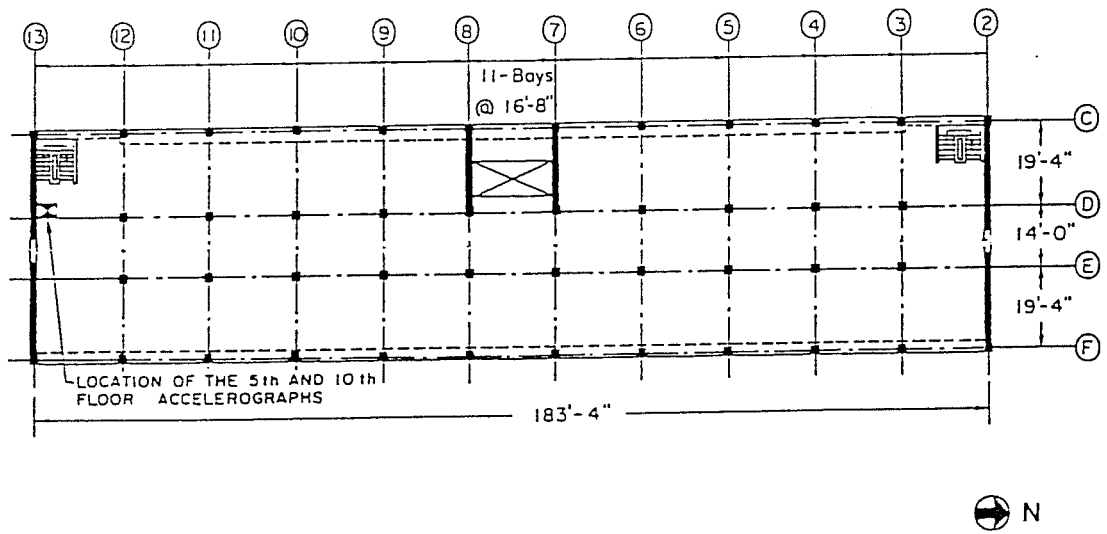


Figure 3.30 Typical Floor Plan³⁶

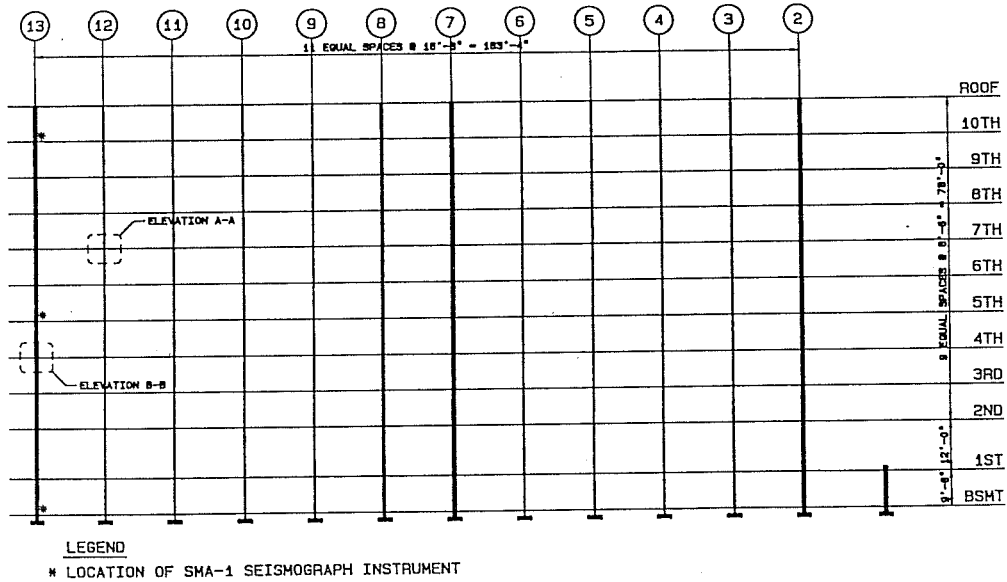


Fig. 3.31 Elevation of Building on Grid C in Longitudinal Direction⁴⁸

Details of the reinforcement in the moment-resisting frame on Grid line C are shown in Figure 3.33. Although there is no joint shear reinforcement in the beam-column region, a quick check shows that joint shear is not a problem. Table 3.6 is a summary of the reinforcement for the structural members of the building.

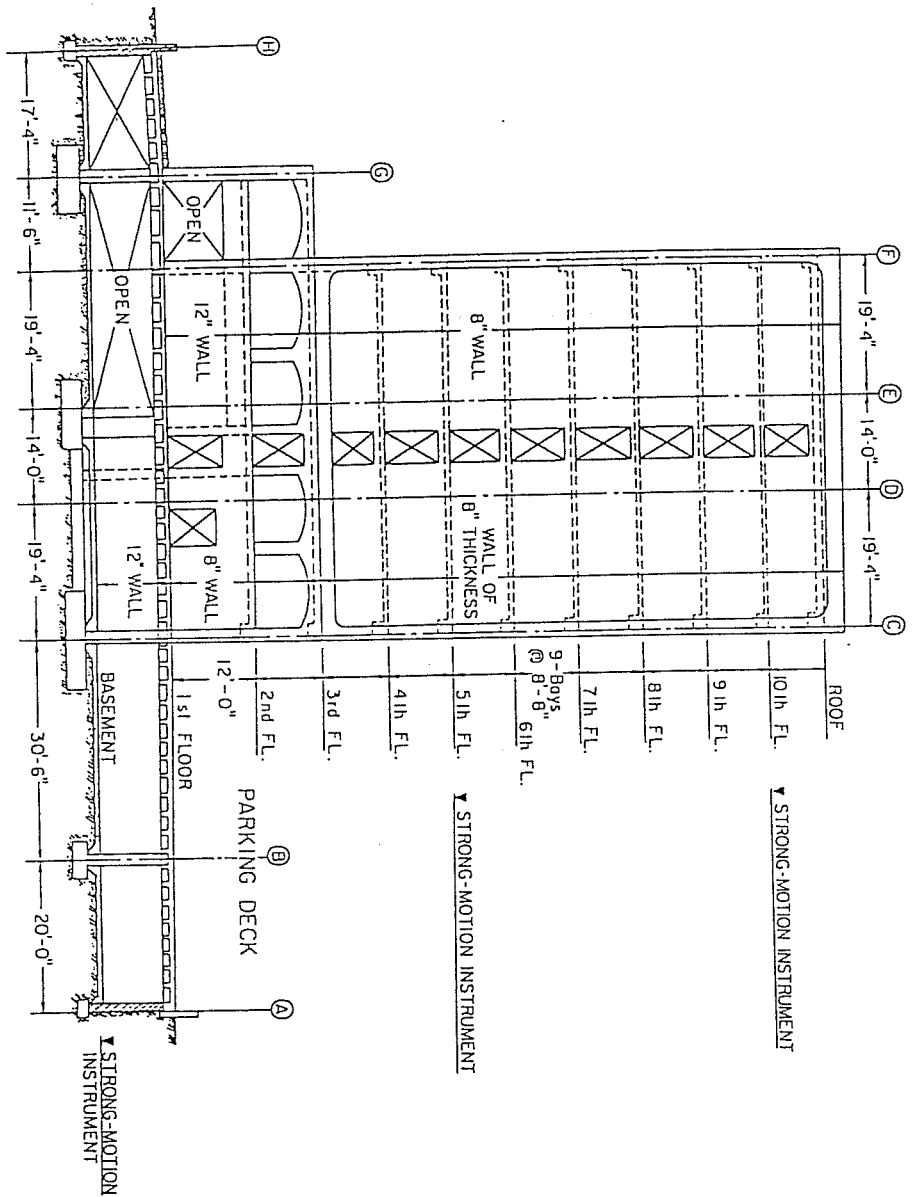


Figure 3.32 Elevation of the building in Transverse Direction⁴⁹

Table 3.5 Material Properties for Construction. Ten-Story Building

Concrete (regular weight, 150 pcf unit weight)		
Location in structure	Minimum specified compressive strength (f'_c) in ksi	
Columns, 1st to 6th floors	4	
Columns, 6th to roof floors	3	
Beams and slabs, all floors	3	
Reinforcing steel		
Location in structure	Grade	Minimum specified yield strength (f_y) in ksi
All reinforcing steel in beams and columns	deformed Grade 60 (ASTM A-615)	60

The seismic lateral resisting system in the longitudinal direction (north-south) consists of moment frames in which most of the lateral capacity is to be provided by perimeter column-spandrel beam frames and interior column-slab frames. In the transverse direction (east-west), the seismic lateral resistance is provided by a dual system consisting of two reinforced concrete coupled shear walls at both ends of the building.

Table 3.6 Summary of the Steel Reinforcement. Ten- Story Building

Beams			
Floor	Longitudinal Reinforcement		
	Top	Bottom	
1st-3rd	6#10	6#10	
4th-6th	6#8	6#8	
7th-8th	6#7	6#7	
9th-Roof	6#6	6#6	
Columns			
Story	Corner Columns	Exterior Columns	Interior Columns
Basement-1st	14#11	10#11	4#11
2nd	14#11	6#11	4#8
3rd	14#11	4#11	4#8
4th-5th	10#11	4#10	4#8
6th	8#11	4#10	4#8
7th	6#11	4#9	4#8
8th	6#10	4#9	4#8
9th-10th	4#9	4#9	4#8
Shear Walls			
Story	Boundary Element Longitudinal Reinforcement	Web Reinforcement	
Basement	16#11	#4 at 18" vert., #5 at 13" horiz.	
1st-3rd	14#11	#4 at 18" vert., #4 at 16" horiz.	
4th-5th	10#11	#4 at 16" vert., #5 at 12" horiz.	
6th	8#11	#4 at 16" vert., #5 at 12" horiz.	
7th	6#11	#4 at 16" vert., #5 at 12" horiz.	
8th	6#10	#4 at 16" vert., #5 at 12" horiz.	
9th-10th	4#9	#4 at 16" vert., #5 at 12" horiz.	

3.3.2 Whittier Narrows Earthquake (1987)

The Whittier Narrows Earthquake occurred on October 1, 1987 at 7:42 a.m. local time, at about 9.3 miles northeast of downtown Los Angeles. The epicenter was estimated at $34^{\circ}3'N$, $118^{\circ}5'W$, at a focal depth of about 8.7 miles. The earthquake ruptured part, 4 km by 5 km, of a previously unidentified buried thrust fault that strikes east-west and dips 25° down to the north⁵⁰. The local Richter magnitude was determined as $M_L = 5.9$.

3.3.2.1 Building Instrumentation

The building is located south of the epicenter at a distance of approximately 6.2 miles. The SMA-1 seismographs (each capable of recording three components of motion) were located at basement, fifth and tenth floor levels as shown in Figures 3.27, 3.30, 3.31, and 3.32. The building instrumentation is part of the National Strong-Motion Instrumentation Network (NSMIN) operated by the U.S. Geological Survey (USGS). Table 3.7 summarizes the peak values for the recorded accelerations in each direction. Figures 3.34, 3.35 and 3.36 show the recorded accelerograms in the longitudinal, transverse and vertical directions at the basement, 5th floor and 10th floor levels. Although the duration of the earthquake was about 30 seconds, strong shaking only lasted about 4 seconds.

Table 3.7 Recorded Peak Acceleration and Approximate Time of Occurrence During the 1987 Whittier Narrows Earthquake. Ten-Story Building:

Station Location	Longitudinal (North-South) direction	Transverse (East-West) direction	Vertical (Up-Down) direction
10th Floor	0.43g at 4.64 sec.	0.52g at 4.04 sec.	0.50g at 4.38 sec.
5th Floor	0.55g at 4.02 sec.	0.61g at 4.00 sec.	0.28g at 3.90 sec.
Basement	0.39g at 3.98 sec.	0.62g at 4.02 sec.	0.24g at 4.04 sec.

3.3.2.2 Building Earthquake Damage

No structural or significant non-structural damage was observed during post earthquake visual inspection⁴⁸.

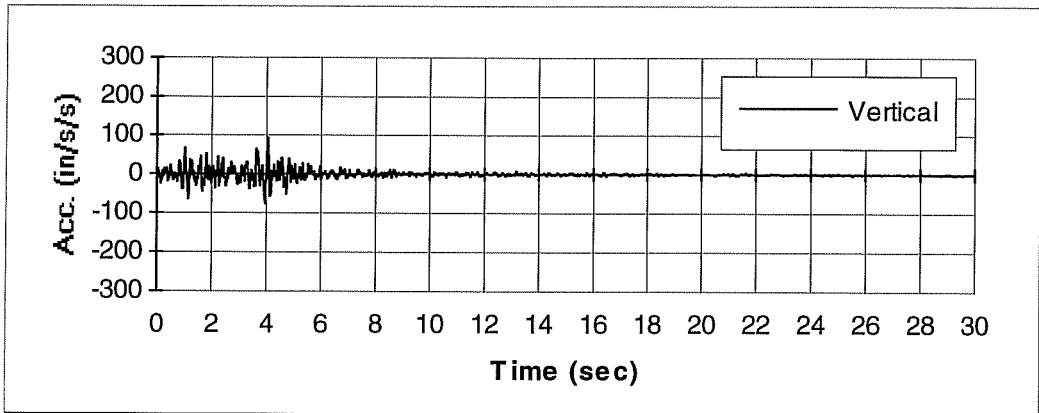
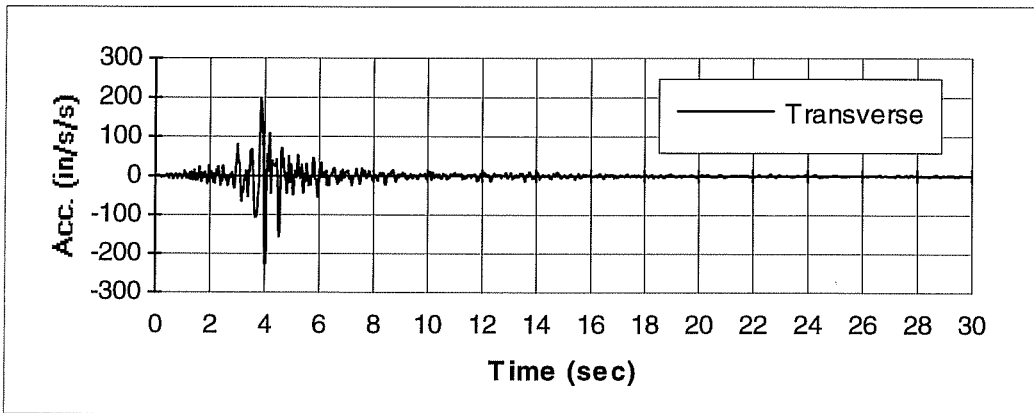
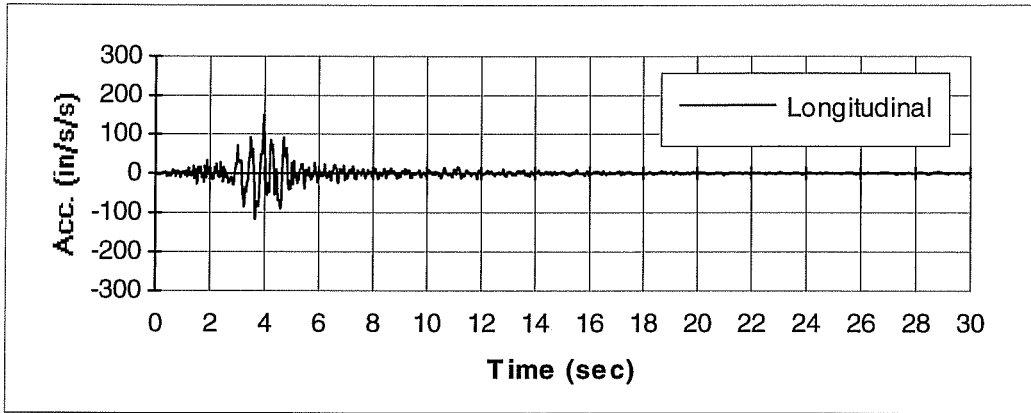


Figure 3.34 Ten-Story Building. Recorded Acceleration at the Basement in the 1987 Whittier Narrows Earthquake

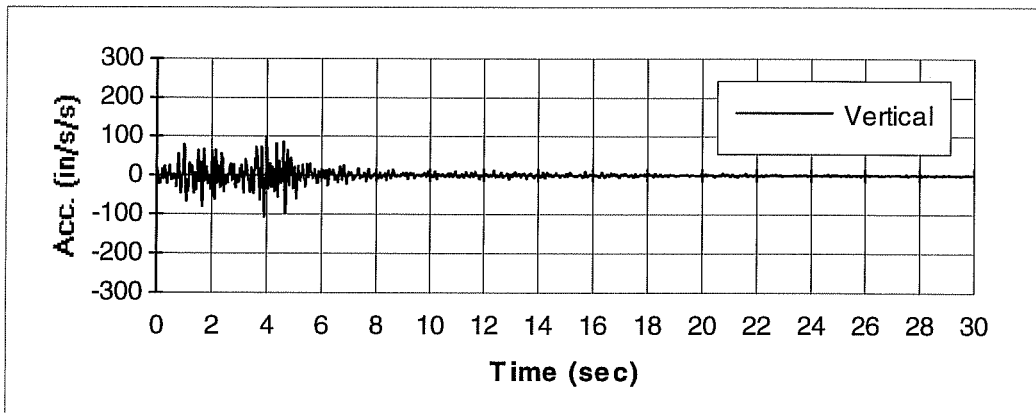
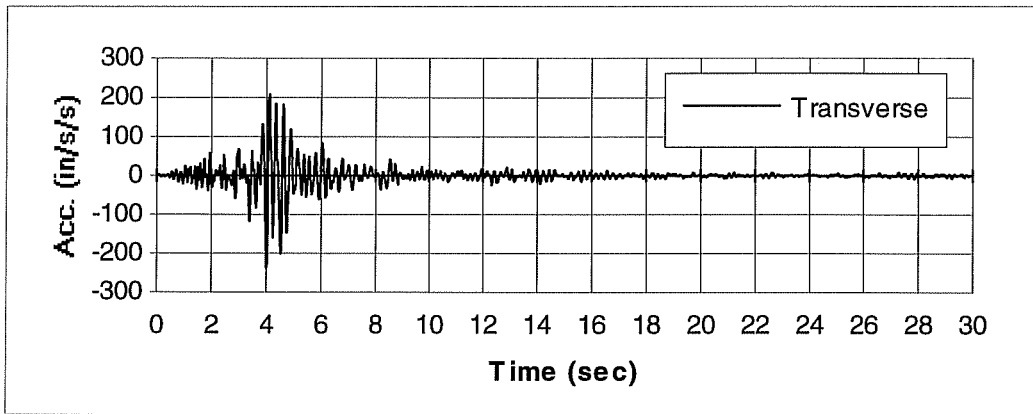
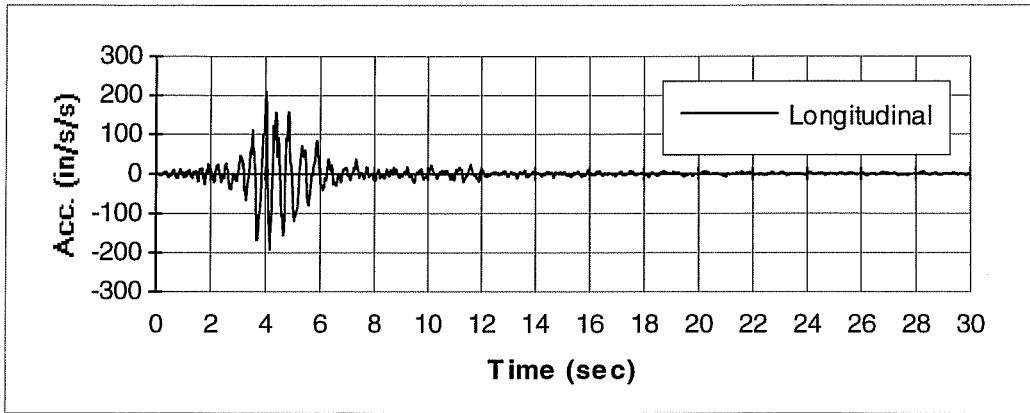


Figure 3.35 Ten-Story Building. Recorded Acceleration at the 5th Floor in the 1987 Whittier Narrows Earthquake

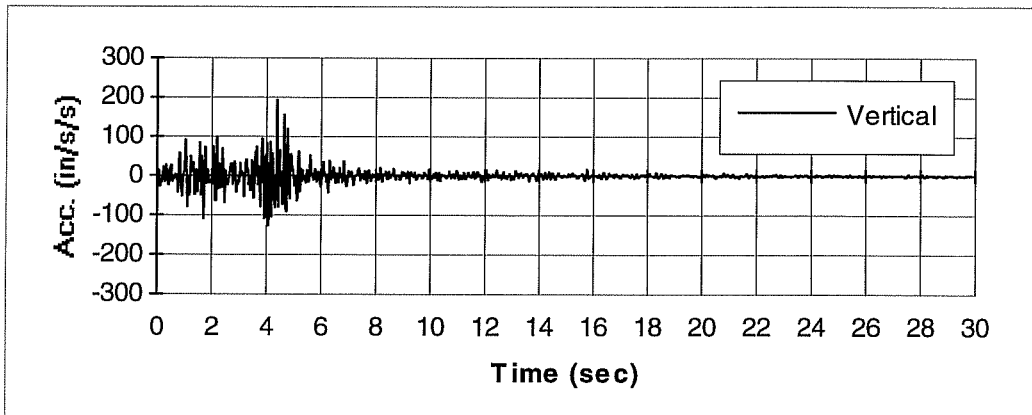
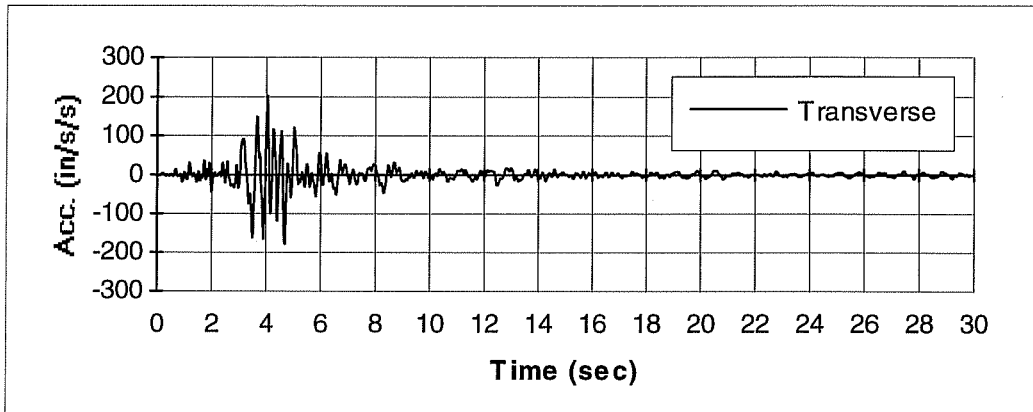
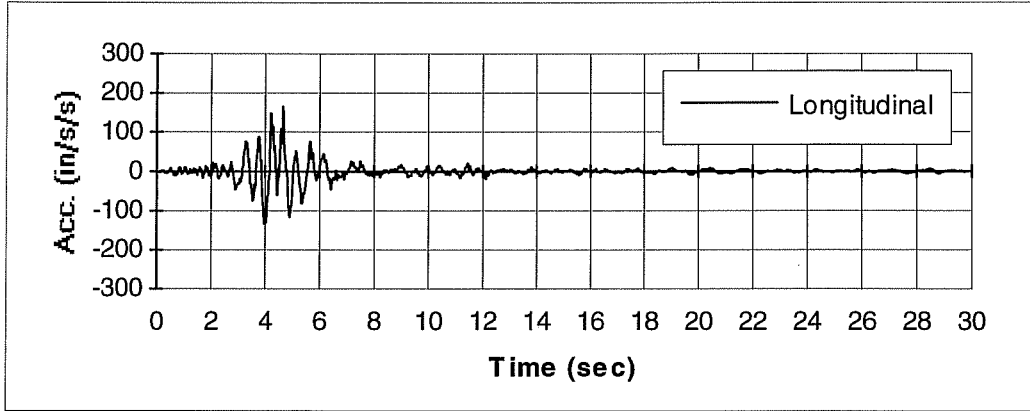


Figure 3.36 Ten-Story Building. Recorded Acceleration at the 10th Floor in the 1987 Whittier Narrows Earthquake

CHAPTER 4

NONLINEAR PROGRAMS AND ANALYTICAL MODELS

4.1 General

There are numerous approaches for modeling inelastic behavior of structures. Ideally, inelastic models should follow the gradual spread of cracking and yielding throughout the structure. The distribution of inelasticity is modeled by discretization of members into a number of “fibers”⁵³. The stiffness of sections is obtained by numerically integrating the stiffness of the cross-section of elements in which fibers may be in the elastic, inelastic, or strain-hardening range. This technique is computationally intensive. For dynamic analyses of structures under earthquake excitations, simplified modeling techniques are generally employed. For moment resisting frame structures, inelastic behavior is, in general, concentrated at the two ends of structural elements (beams or columns). As a result, most simplified modeling techniques assume that inelastic behavior occurs at member ends only. Between the ends, elements are assumed to behave elastically. In this chapter, two most commonly used nonlinear programs are discussed. Analytical models used for buildings selected for this study are presented.

4.2 Nonlinear Programs

Over the past 20 years or so, a number of nonlinear time history analysis programs have been developed at various research institutions. One of the most commonly used programs, DRAIN-2D was originally developed in the 1970's at the University of California at Berkeley by Kanaan and Powell³. Another program for reinforced concrete structure analysis, IDARC, was originally developed in the 1980's at the State University of New York at Buffalo by Park, Reinhorn and Kunnath⁵². Numerous modifications have been made to both programs since their initial release.

4.2.1 DRAIN-2D

A structure is idealized as a planar assemblage of discrete elements connected at every floor level with a rigid diaphragm. Analysis is carried out by the Direct Stiffness Method, with nodal displacements as unknowns. Each node possesses up to three displacement degrees of freedom. The earthquake excitation is defined by time histories of ground acceleration. Static loads may be applied prior to the dynamic loading, but no yielding is permitted under static loads.

The dynamic response is determined by step-by-step integration, with a constant acceleration assumption within any step. The tangent stiffness of the structure is used for each step, and linear structural behavior is assumed during the step. If an element yields or unloads, information will be returned from the element

subroutine. Changes are then made to the tangent stiffness matrix and the triangularization operation of Gauss elimination is repeated. Any unbalanced loads resulting from errors in the assumed linear behavior within the step will be eliminated by applying corrective loads in the subsequent time step. Second order effects can be taken into account by including geometric stiffness in the element stiffness matrix.

The structure mass is assumed to be lumped at nodes so that the mass matrix is diagonal. Axial deformations and shear deformations of structural elements are included in the analysis. Beam-column joint regions are assumed infinitely rigid.

4.2.1.1 Dynamic Equilibrium and Integration Procedure

At any finite time step, Δt , the equation of dynamic equilibrium is satisfied approximately as:

$$[M]\{\Delta \ddot{x}\} + [C_T]\{\Delta \dot{x}\} + [K_T]\{\Delta x\} = \{\Delta F\} \quad (4.1)$$

in which, $\{\Delta \ddot{x}\}$, $\{\Delta \dot{x}\}$ and $\{\Delta x\}$ are the increments of acceleration, velocity and displacement, respectively, at nodes; $\{\Delta F\}$ is the increment in applied loading; $[M]$ is the mass matrix; and $[C_T]$ and $[K_T]$ are tangent values of the damping and stiffness matrices for the structure at the beginning of the time step.

The dynamic equilibrium Equation (4.1) is solved by using an approximation that within the time step acceleration remains constant. As discussed in Chapter 3,

this method has the advantage of being stable for all periods and time steps. However, the accuracy of the results depends on the integration time step used. The smaller the time step, the more accurate are the expected results. Previous research has shown that a time step of 0.005 second will generally yield enough accuracy^{14,54}.

4.2.1.2 Damping Coefficients

DRAIN-2D assumes that viscous damping results from a linear combination of the mass and tangent stiffness matrices according to Equation (4.2):

$$[C_T] = \alpha [M] + \beta [K_T] \quad (4.2)$$

where α and β are called damping coefficients. These coefficients can be selected in one way by assuming that the system is uncoupled into normal modes⁵⁵. For any two modes of vibration i and j :

$$\alpha = \frac{4\pi(T_j\xi_j - T_i\xi_i)}{T_j^2 - T_i^2} \quad (4.3)$$

$$\beta = \frac{T_i T_j (T_j \xi_i - T_i \xi_j)}{\pi(T_j^2 - T_i^2)} \quad (4.4)$$

in which T_i , T_j are the respective periods of two modes of vibration selected, and ξ_i , ξ_j are the respective damping ratios for these two modes. Typically, the first two modes of vibration are selected, because they dominate the dynamic behavior of

building structures. Although the mass matrix remains the same during the analysis, the stiffness matrix varies with time. Therefore, the damping matrix needs to be updated whenever the stiffness of a structure changes.

4.2.1.3 Reinforced Concrete Member Modeling

A beam element with degrading stiffness was formulated to model reinforced concrete frame elements.

In DRAIN-2D, the one-component model proposed by Giberson⁵⁶ was adopted to represent reinforced concrete frame members (beams and columns) as shown in Figure 4.1. The element was assumed to consist of a linear elastic beam element with non-linear rotational springs at each end. Yielding may only take place in concentrated plastic hinge regions at the element ends. All plastic deformations, including the effects of stiffness degradation, were introduced by means of the moment-rotation relationships for the inelastic springs.

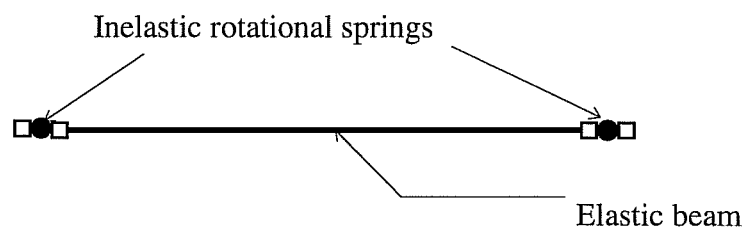


Figure 4.1 Element Idealization - One Component Model

4.2.1.4 Extended Takeda's Model

An extended version of Takeda's model⁵⁷, illustrated in Figure 4.2, was adopted for the moment-rotation relationship for each inelastic spring.

The modifications made to Takeda's original model are shown in Figures 4.3 and 4.4. There were two major changes: (1) a reduction of the unloading stiffness, by an amount which depends on the largest previous spring rotation, and (2) an increase in reloading stiffness, which also depends on previous spring rotations.

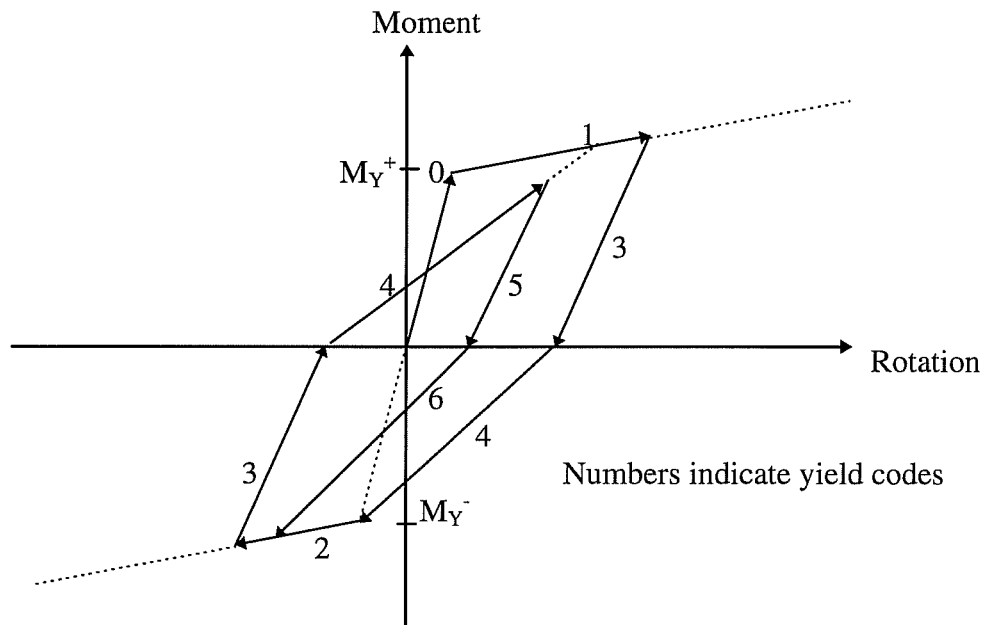


Figure 4.2 Inelastic Spring Moment-Rotation Relationship
Extended from Takeda's Model

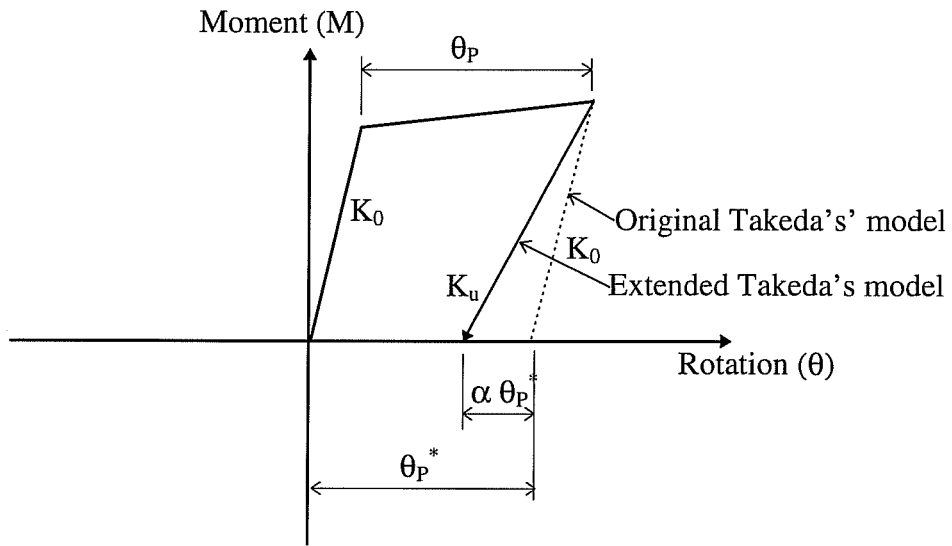


Figure 4.3 Unloading Stiffness for Extended Takeda's Model

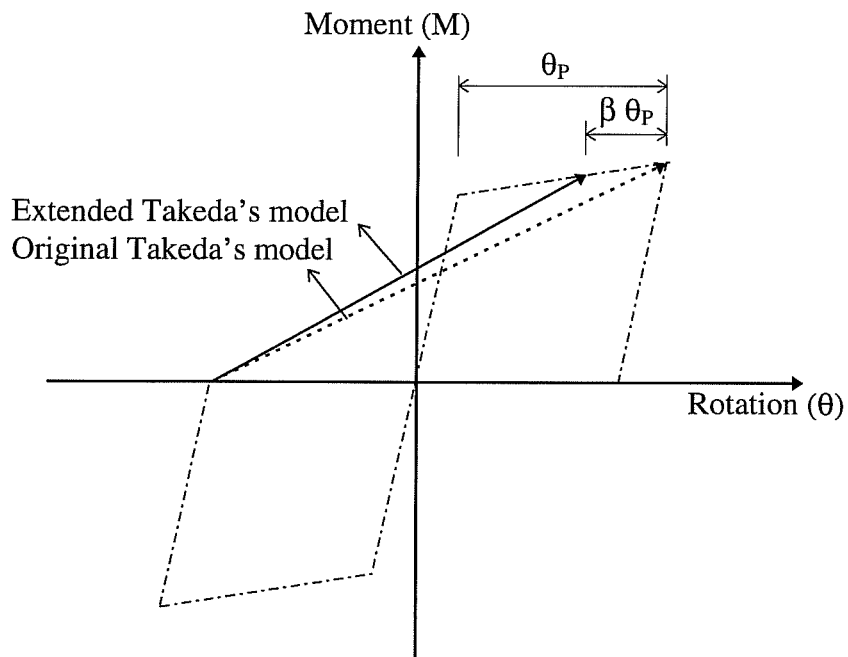


Figure 4.4 Reloading Stiffness for Extended Takeda's Model

4.2.2 IDARC

The first version of IDARC was developed in 1987 and released in 1988 by the National Center for Earthquake Engineering Research (NCEER) at the State University of New York at Buffalo. IDARC was programmed for Inelastic Damage Analysis of Reinforced Concrete building structures. The motivation for developing such a program was the lack of analytical tools to predict inelastic behavior of structures in past earthquakes and in dynamic experimental tests, especially for reinforced concrete structures.

Although IDARC was designed for two-dimensional analyses, it can take into account three-dimensional effects by connecting a set of parallel frames with transverse elements as shown in Figure 4.5. A reinforced concrete building is idealized as a series of plane frames connected together by transverse beams. Beams and columns are modeled as inelastic single component elements with distributed stiffness⁵⁸. Shearwalls are modeled using a combination of shear and flexure springs connected in series. The program can perform comprehensive analyses including: (1) nonlinear static analysis for initial stress due to gravity loads; (2) nonlinear static (push-over) analysis under monotonic lateral loads; (3) quasi-static cyclic analysis under load or displacement control; (4) inelastic dynamic analysis due to earthquake loads; (5) damage level analysis.

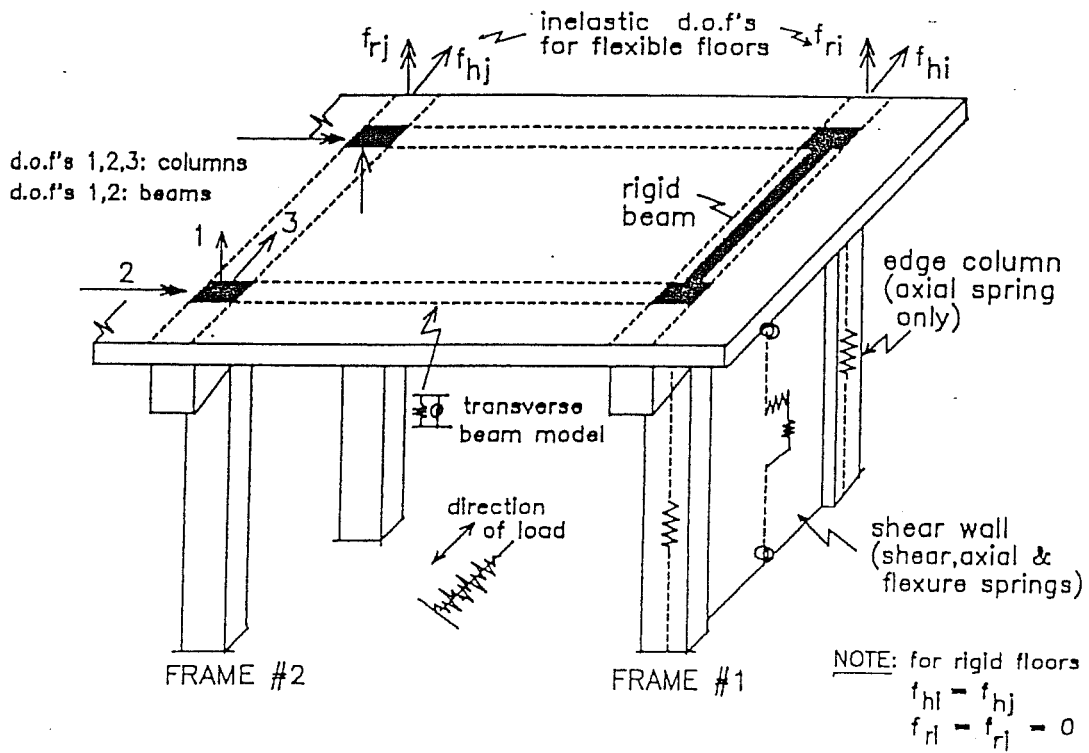


Figure 4.5 Structural Modeling Illustration⁶¹

As in DRAIN-2D, IDARC employs the Direct Stiffness Method, with nodal displacements as unknowns. The structure mass is lumped at nodes. Axial deformations and shear deformations of structural members are taken into account in the matrix formulation. Like in DRAIN-2D, the computation is performed incrementally assuming that the stiffness of the structure does not change during the

time step. However, if the stiffness of any element changes, equilibrium will not be satisfied at the end of the time step. Therefore, a restoring procedure is adopted to minimize this error by applying a one-step unbalanced force correction as shown in Figure 4.6. A simple equivalent force method is used to account for P-delta effects due to inter-story drift⁴.

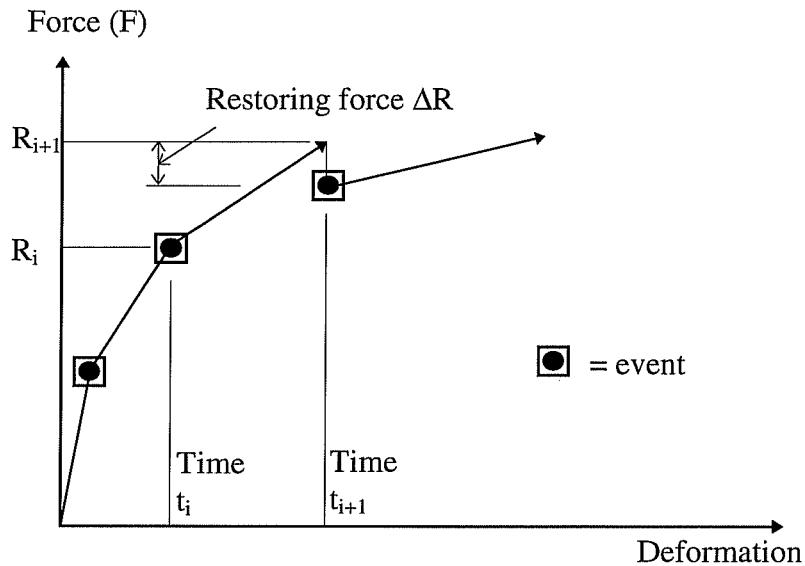


Figure 4.6 Unbalanced Force Correction

4.2.2.1 Dynamic Equilibrium and Integration Procedure

The incremental equation for dynamic equilibrium is the same as the one used in DRAIN-2D described in Equation (4.1). The dynamic equation is solved by a direct step-by-step integration procedure using Newmark's method⁶⁰ which assumes a constant-average-acceleration, the same method used in DRAIN-2D.

4.2.2.2 Viscous Damping

Viscous damping is assumed for the structural system. To calculate the damping matrix, the fundamental period of the structure is determined first using the conventional Stodola method. Then this period is used to compute a constant viscous damping factor for the dynamic analysis. The program designers claimed that although the actual mechanism of damping in a structure responding inelastically is not fully understood, the contribution of viscous damping is negligible compared to energy dissipation through hysteretic action⁶¹.

4.2.2.3 Reinforced Concrete Member Modeling

A single-component model was used for modeling beams and columns in IDARC. The basic objective in developing a member model for nonlinear analysis is to adequately characterize the varying stiffness properties of elements during a cyclic loading event. Two fundamental approaches are generally employed, one is based on

a finite plastic zone at ends of a member, like the one used in DRAIN-2D, and the other is based on a variation of the flexibility along the member, like the one used in IDARC. During earthquakes, lateral load moments are generally much greater than the gravity load moments and it is assumed that the moment distribution along a frame member is linear, as shown in Figure 4.7. Furthermore, the flexibility factor, $1/EI$, is assumed to vary linearly along the member between two ends and the point of inflection. If gravity load moments are found significant, the linear moment distribution assumption is still acceptable if the member is divided into an adequate number of sub-members.

Once the flexibility distribution is established, the 2 by 2 flexibility matrix is derived from virtual work principles as shown in Equation (4.5):

$$f_{ij} = \int_0^L m_i(x)m_j(x) \frac{1}{EI(x)} dx \quad (4.5)$$

Since members can bend in double curvature or in single curvature, the integration needs to be carried out for these two possible cases as shown in Figure 4.8.

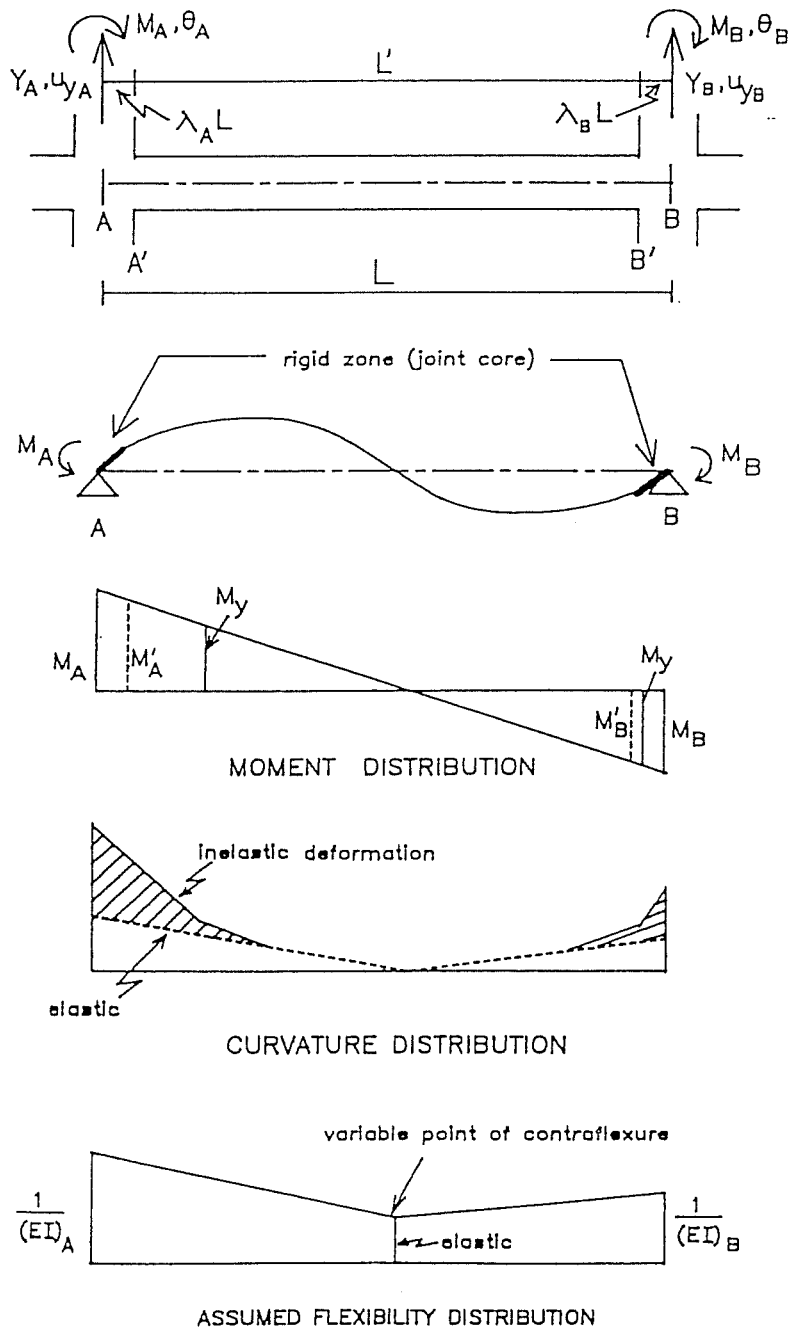


Figure 4.7 Modeling of Distributed Flexibility⁶¹

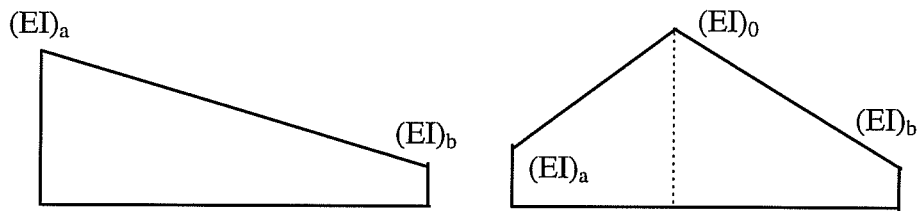
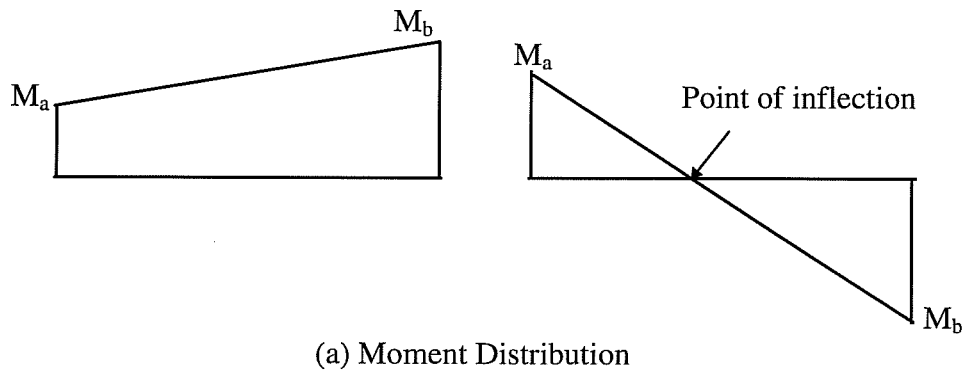


Figure 4.8 Variation of Flexibility along the Member

4.2.2.4 Hysteretic Modeling

A non-symmetric tri-linear curve was used for the hysteretic envelope shown in Figure 4.9. Three parameters α , β , and γ were utilized to produce effects of stiffness degradation, strength deterioration and pinching or slip behavior, respectively (Figure 4.10).

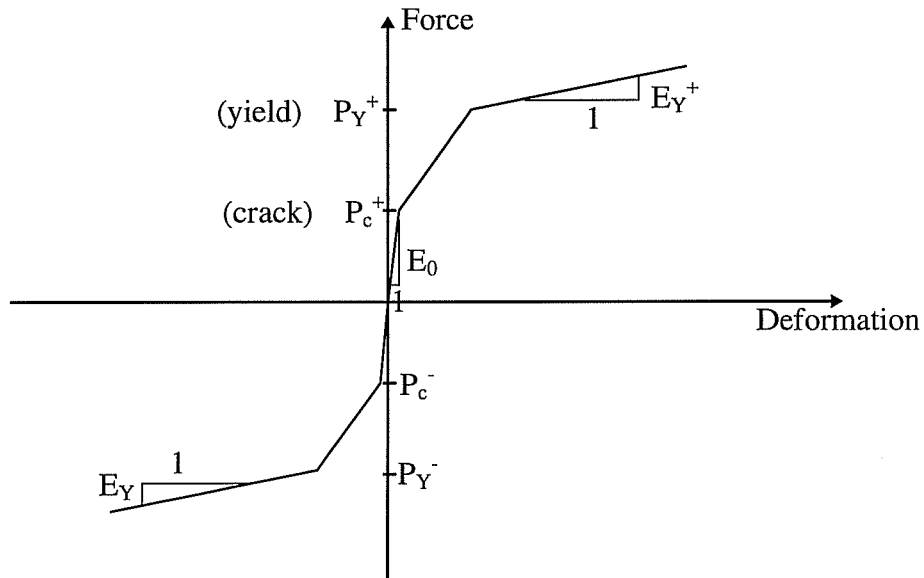
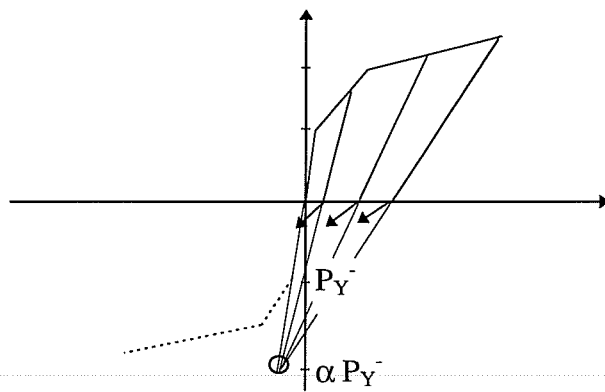
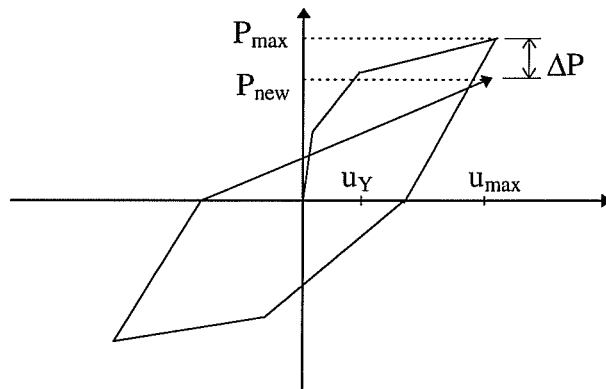


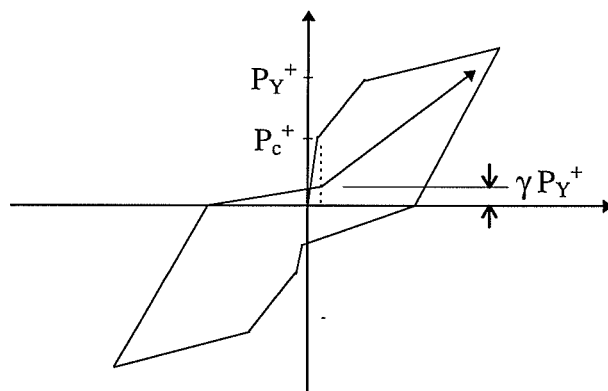
Figure 4.9 Non-Symmetric Tri-Linear Envelope



(a) Modeling of Stiffness Degradation



(b) Modeling of strength deterioration



(c) Modeling of Pinching or Slip Behavior

Figure 4.10 Hysteretic Model and Control Parameters

4.3 Analytical Model

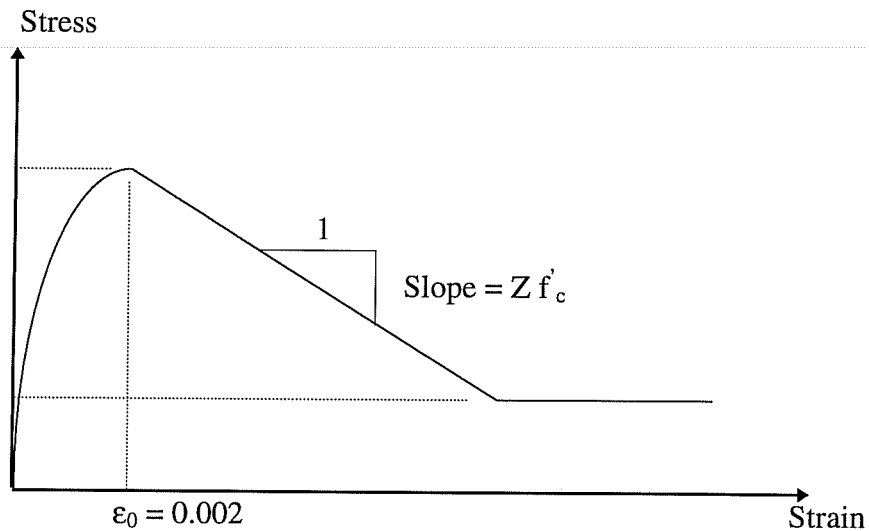
The analytical models used to idealize the inelastic behavior of the reinforced concrete members of buildings selected for this study are described in this section. Material properties as well as hysteretic behavior of such members are presented. Also, assumptions used in assigning member stiffness properties are discussed.

4.3.1 DRAIN-2D

The element subroutine 11 - reinforced concrete beam was used to model members in buildings. The degrading stiffness element has two additional deformation modes, namely additional rotational deformations associated with each of the two rotational springs, as shown in Figure 4.1. For each element, deformations consist of inelastic hinge rotations of springs and deformations of elastic beams connecting the springs. However the additional degrees of freedom due to spring rotations are condensed out in the element stiffness matrix formulation, so they do not appear as structural degrees of freedom. Yield moments specified at the ends of elements consider no interaction between axial force and bending moment in producing yield.

4.3.1.1 Material Properties

The stress-strain relationship for concrete material was assumed to follow the Park and Kent model⁶² as shown in Figure 4.11. The stress-strain relationship for reinforcing steel was idealized as presented in Figure 4.12.



$$Z = \frac{0.5}{\epsilon_{50u} + \epsilon_{50h} - 0.002}$$

in which, $\epsilon_{50u} = \frac{3 + 0.002 f'_c}{f'_c - 1000}$, (f'_c in psi)

$$\epsilon_{50h} = \frac{3}{4} \rho_s \sqrt{\frac{b''}{s}}$$

Note: ρ_s is the ratio of transverse reinforcement over the volume of confined concrete;
 b'' is the width of confined core;
 s is the transverse reinforcing steel spacing.

Figure 4.11 Stress-Strain Relationship for Concrete. DRAIN-2D

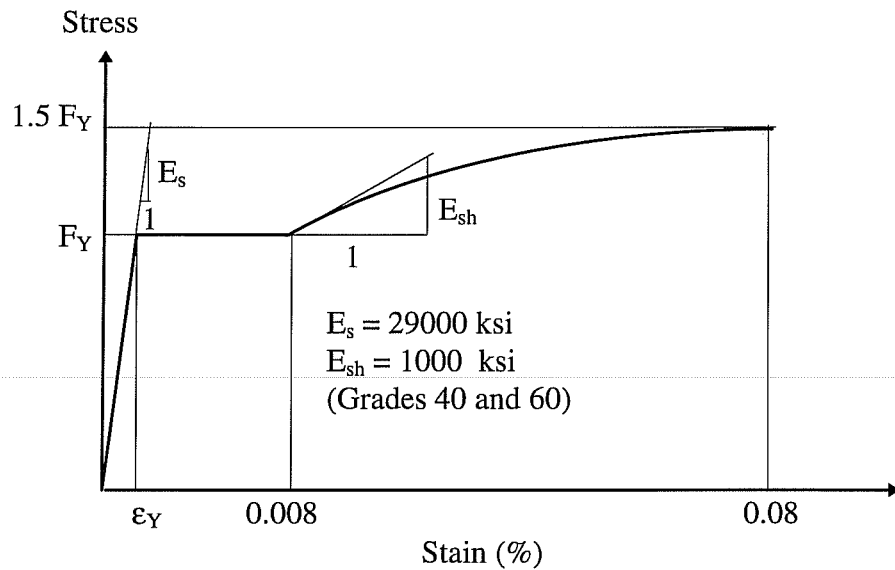


Figure 4.12 Stress-Strain Relationship for Reinforcing Steel. DRAIN-2D

4.3.1.2 Element Stiffness

In the analysis of reinforced concrete frame structures, difficulties inevitably arise in assigning cross section and material properties. The following assumptions were made in DRAIN-2D:

- (1) Materials are homogeneous;
- (2) Members bend in double curvature with equal moment at both ends as shown in

Figure 4.13;

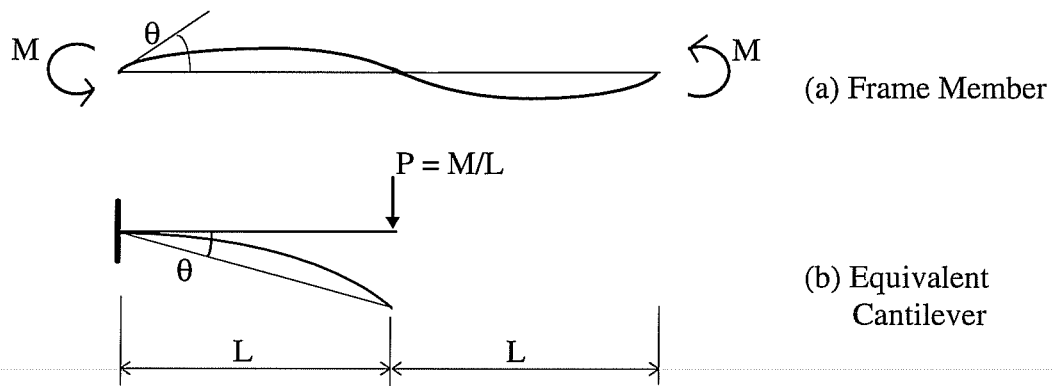


Figure 4.13 Equivalent Cantilever

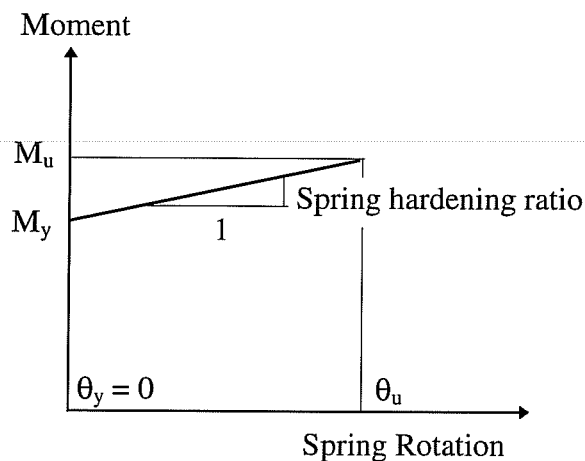
- (3) Within the equivalent cantilever, section properties, including material, dimension, and reinforcement do not change.

Two options are available in DRAIN-2D for assigning element stiffness properties³:

Option 1:

An effective flexural stiffness $(EI)_{\text{eff}}$, which takes into account cracking, is specified for the linear elastic element. Also an axial stiffness (EA) and a shear stiffness (GA') are specified based on gross section properties.

A very large initial elastic stiffness is assigned to the spring (10^{16} kip-inches), so that each hinge is practically rigid up to yield (Figure 4.14).



$$\text{Spring hardening ratio} = \frac{M_u - M_Y}{\theta_u - \theta_Y} = \frac{M_u - M_Y}{\theta_u}$$

Figure 4.14 Assumed Spring Moment-Rotation Relationship

The moment-curvature relationship of the cross-section was determined using the program RCCOLA⁶³, which calculates moment capacity, shear capacity, yield ductility and curvatures at a series of given axial loads, for different specified extreme compressive strains of concrete, in reinforced concrete cross sections. The multi-line moment curvature diagram obtained from the RCCOLA program was reproduced by a

bi-linear relationship (Figure 4.15). The yield point (M_Y, Φ_Y) and the ultimate point (M_u, Φ_u) for the bi-linear relationship are the same as in the original diagram. In calculating the moment-curvature relationship for columns, the column axial load was assumed to consist of gravity load only. The axial load in beams was neglected in calculating the moment-curvature relationship.

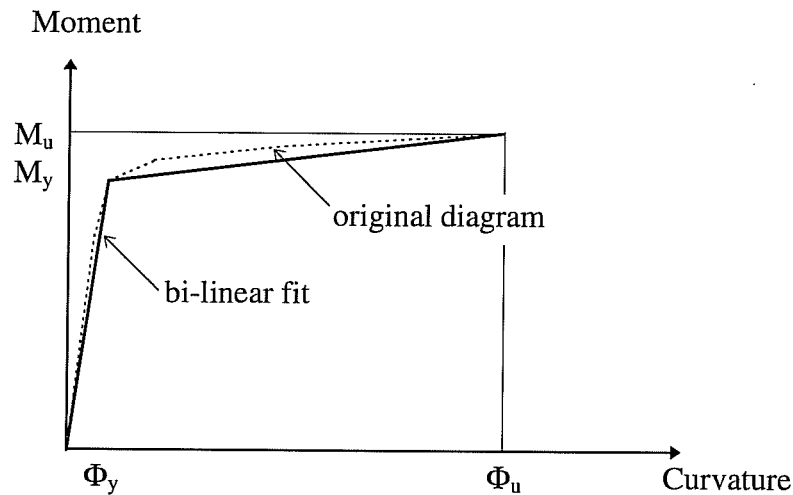


Figure 4.15 Bi-Linear Fit for the Moment-Curvature Relationship of Reinforced Concrete Sections

Plastic hinges were assumed to be concentrated along a distance d from the end (d is the effective depth of the cross section). Figure 4.16 shows the moment and curvature diagrams for the equivalent cantilever with a plastic hinge formed at the end.

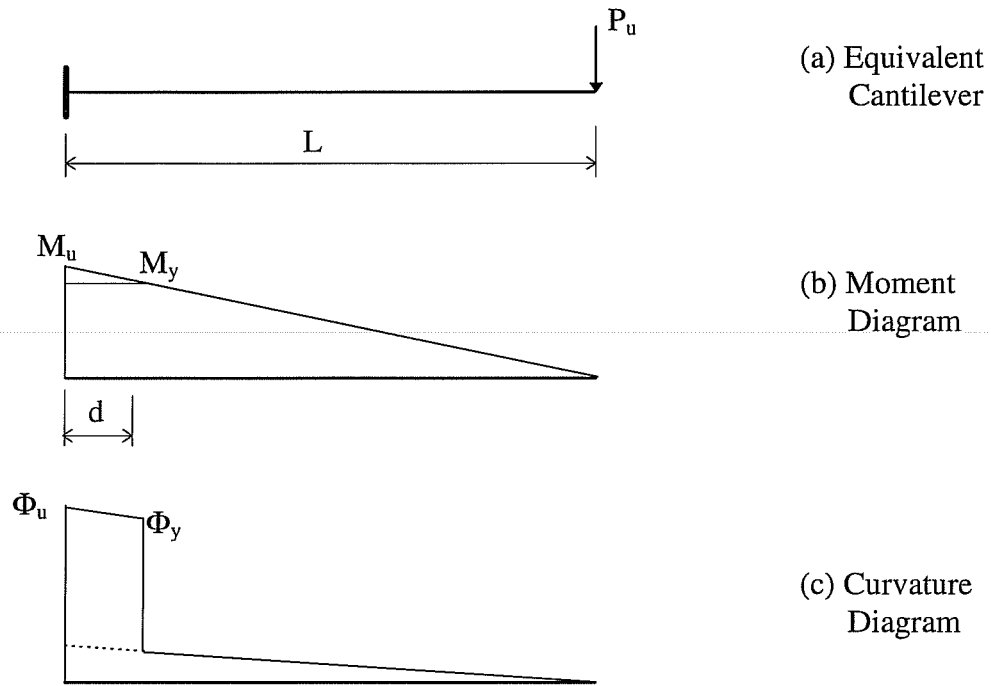


Figure 4.16 Moment and Curvature Diagrams for the Equivalent Cantilever

The hardening ratio of the spring after the plastic hinge forms (Figure 4.8) was computed by assuming that plastic deformation only occurred within the plastic hinge. Therefore, using the Conjugate Beam Method, the plastic hinge rotation θ_u was calculated as follows (Figure 4.17).

$$\theta_u = \frac{\delta_u}{L} \quad (4.6)$$

$$\delta = (\Phi_U - \Phi_Y)d(L - \frac{d}{2}) \quad (4.7)$$

After substituting (4.7) into (4.6):

$$\theta_U = \frac{(\Phi_U - \Phi_Y)d(L - \frac{d}{2})}{L} \quad (4.8)$$

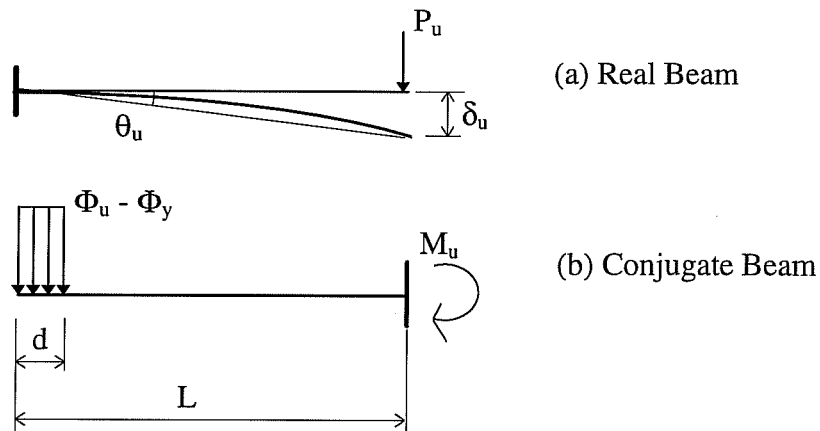


Figure 4.17 Calculation of Spring Hardening Ratio

Option 2:

First, the equivalent cantilever was represented with an idealized cantilever as shown in Figure 4.18. The effective stiffness (EI), initial spring stiffness K_{sp} , and

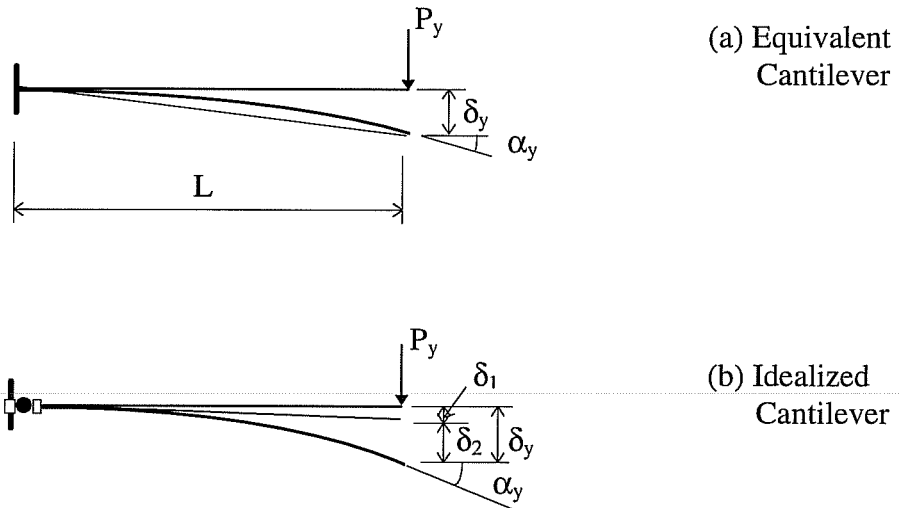
spring strain hardening ratio p were computed by setting the tip displacement δ_y and tip rotation α_y of the idealized cantilever equal to those of the equivalent cantilever as shown in Figure 4.18 when the fixed-end moment reaches yield. The following equations can be used to obtain the effective stiffness, initial spring stiffness and spring hardening ratio³:

$$EI = \frac{M_y L}{3(2\alpha_y - 2\frac{\delta_y}{L})} \quad (4.9)$$

$$K_{sp} = \frac{M_y L}{(\delta_y - \frac{M_y L^2}{3EI})} \quad (4.10)$$

$$p = \frac{(P_u L - M_y) L}{(\delta_u - \delta_y - \frac{(P_u L - M_y) L^2}{3EI})} \quad (4.11)$$

in which, δ_u is any cantilever tip displacement when the fixed-end moment is strain hardening; M_y is the yield moment at the fixed-end of the cantilever. Figure 4.19 shows the P - δ relationship of the cantilever and the M - θ relationship of the spring.



- P_y : Load when fixed-end moment $M = PL$ reaching yield;
 δ_y Cantilever tip displacement;
 δ_1 Cantilever tip displacement due to spring rotation only;
 δ_2 Cantilever tip displacement due to beam bending only;
 α_y Cantilever tip rotation;

Figure 4.18 Idealized Cantilever

By assuming the section moment-curvature relationship as shown in Figure 4.20, tip displacement and tip rotation for the equivalent cantilever can be calculated using Equations (4.12), (4.13) and (4.14).

$$\delta_y = \frac{1}{3} \Phi_y L^2 - \frac{1}{3} \left(\frac{M_{cr}}{M_y} \right)^2 L^2 \left(\frac{M_{cr}}{M_y} \Phi_y - \Phi_{cr} \right) \quad (4.12)$$

$$\alpha_y = \frac{1}{2} \Phi_y L - \frac{1}{2} \left(\frac{M_{cr}}{M_y} \right) L \left(\frac{M_{cr}}{M_y} \Phi_y - \Phi_{cr} \right) \quad (4.13)$$

$$\begin{aligned} \delta_u = & \frac{1}{3} \Phi_y \left(\frac{M_y}{M_u} L \right)^2 - \frac{1}{3} \left(\frac{M_{cr}}{M_y} \Phi_y - \Phi_{cr} \right) \left(\frac{M_{cr}}{M_u} L \right)^2 + \frac{1}{6} (\Phi_u - \Phi_y) \left(1 - \frac{M_y}{M_u} \right) \left(2 + \frac{M_y}{M_u} \right) L^2 \\ & + \frac{1}{2} \Phi_y \left(1 - \frac{M_y}{M_u} \right) \left(1 + \frac{M_y}{M_u} \right) L^2 \end{aligned} \quad (4.14)$$

Values for M_{cr} , M_y , M_u , and Φ_{cr} , Φ_y , Φ_u , were calculated using a pre-processor in IDARC.

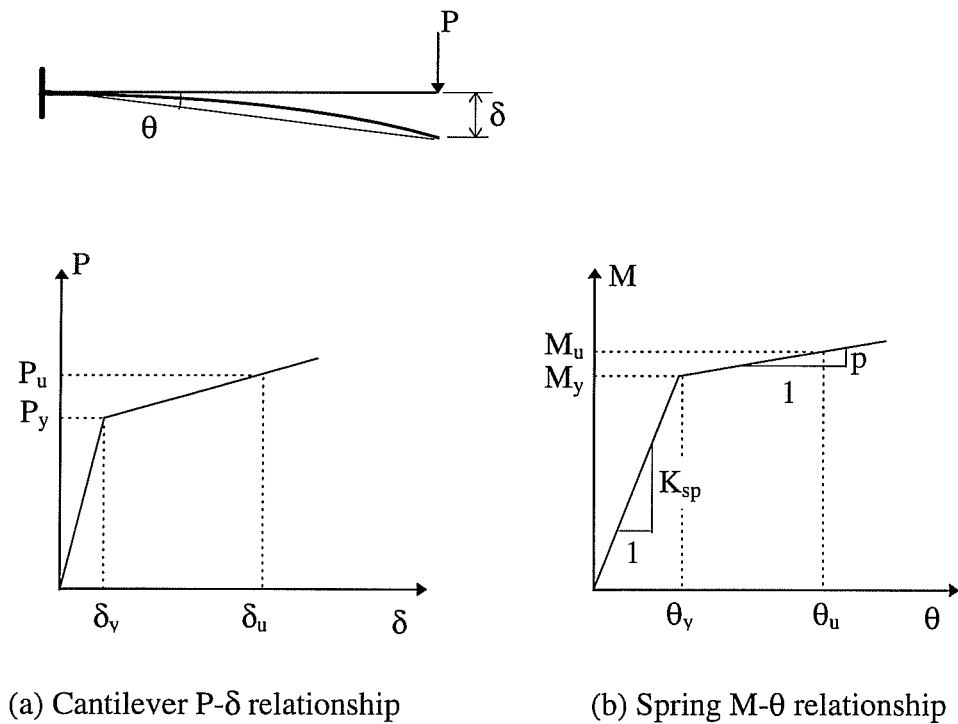


Figure 4.19 Idealized Cantilever Behavior

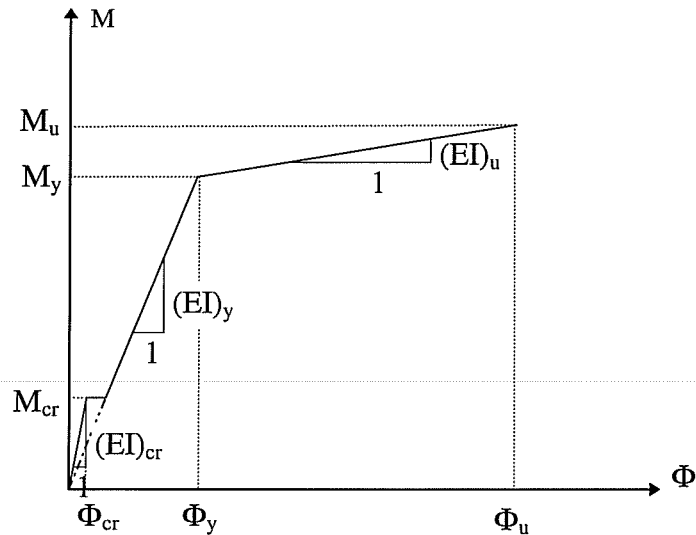


Figure 4.20 Section M- Φ Diagram

4.3.1.3 Shear Failure Model

Behavior of reinforced concrete columns after shear failure has been extensively studied in the past. Lu and Chen⁶⁴ summarized typical failure modes of reinforced concrete short columns as: (1) Shear compression failure. In the case of specimens with moderate axial load and large shear reinforcement ratio, shear compression failure takes place due to combined stress in the compressed region of the concrete reaching maximum capacity (Figure 4.21); (2) Shear bond failure. with large longitudinal reinforcement ratio, large bar sizes and low concrete strength, diagonal cracks appear first at the ends of columns, then bond cracks initiate at a distance h from the end of the column (h is the height of column cross sections). At

the later stages of loading, bond cracks extend through the entire height of the column (Figure 4.22); (3) Shear flexure failure. This type of failure may occur when the longitudinal reinforcement ratio and axial load are low. The failure is initiated by yielding of the longitudinal bars in tension. With further increase in deformation, crushing commences in the compressed region of the concrete (Figure 4.23). In this case, specimens can withstand large deformation.

Tests conducted by Umehara and Jirsa⁶⁵ showed that columns with axial loads of 20% of the ultimate compression capacity were able to sustain lateral drifts of at least twice that at peak shear capacity with no sign of axial failure. In this study, columns were assumed to maintain their axial stiffness and strength after reaching peak shear capacity.

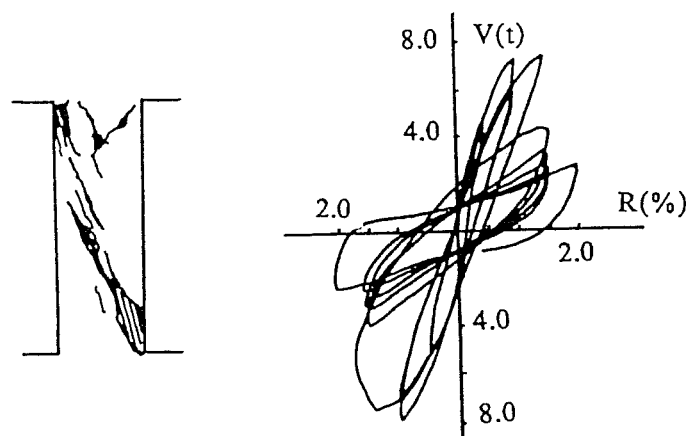


Figure 4.21 Shear Compression Failure⁶⁴

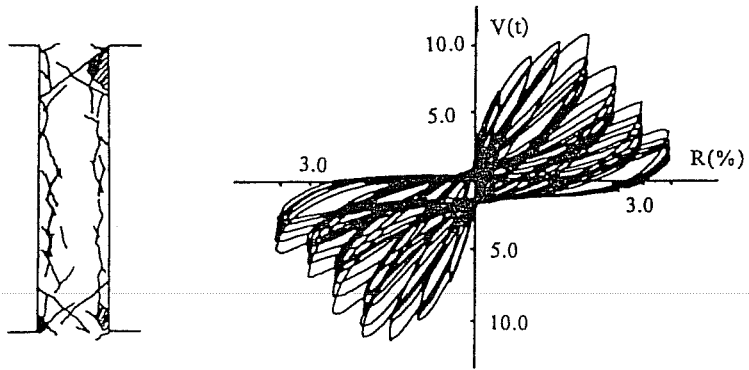


Figure 4.22 Shear Bond Failure⁶⁴

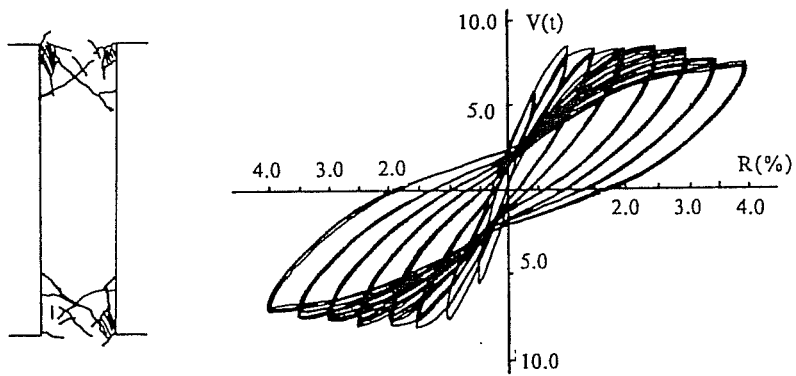
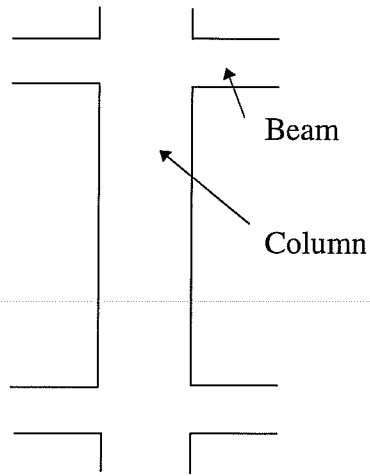


Figure 4.23 Shear Flexure Failure⁶⁴

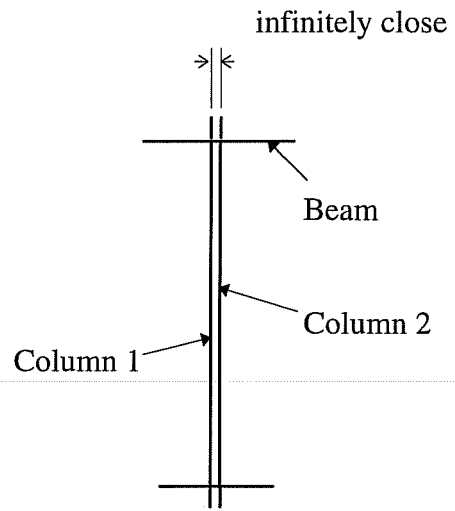
A simplified shear failure model called the parallel-element model was proposed in the analysis. As shown in Figure 4.24, every column element was divided into two sub-elements, namely, column 1 and column 2. After the shear capacity of the original column element is exceeded, column 2 loses its lateral load resisting capacity by changing to a truss member. The shear capacity of column 1 can be set to a very large value so that it does not fail in shear, and this shear capacity becomes a residual shear capacity after the original column element fails in shear. The hysteretic behavior of the column with shear failure is demonstrated schematically in Figure 4.25. After the shear failure occurs, a sudden loss of shear capacity from the peak capacity V_{\max} to a residual capacity V_{res} was assumed. By using different values for the residual shear capacity, different shear failure modes shown in Figures 4.21 through 4.23 can be modeled. From the actual failure mode of the columns, and the reinforcement and axial load condition, the column failure of the seven-story hotel during the 1994 Northridge Earthquake was characterized as shear flexure failure (Figure 4.23). Residual shear capacity was assumed to remain constant after shear failure occurred and the column was assumed to be able to sustain very large lateral deformations. The shear capacity V_{\max} was computed using ACI 318-95 Code⁶⁹ equation (11-4) for members subject to axial compression,

$$V_c = 2\left(1 + \frac{N_u}{2000A_g}\right)\sqrt{f'_c}b_wd \quad (4.15)$$

Before shear failure

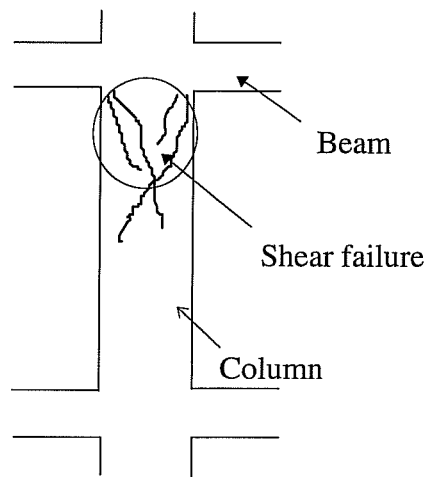


Actual member

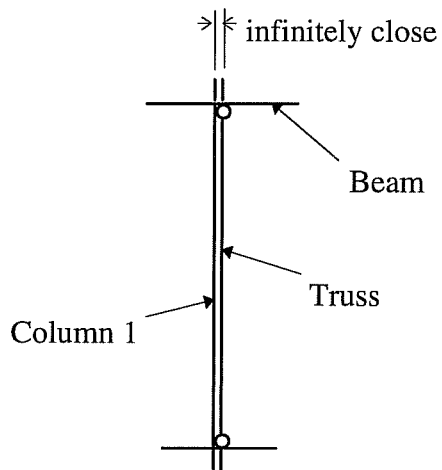


Idealized model

After shear failure



Actual member



Idealized model

Figure 4.24 Parallel-Element Model for Shear Failure

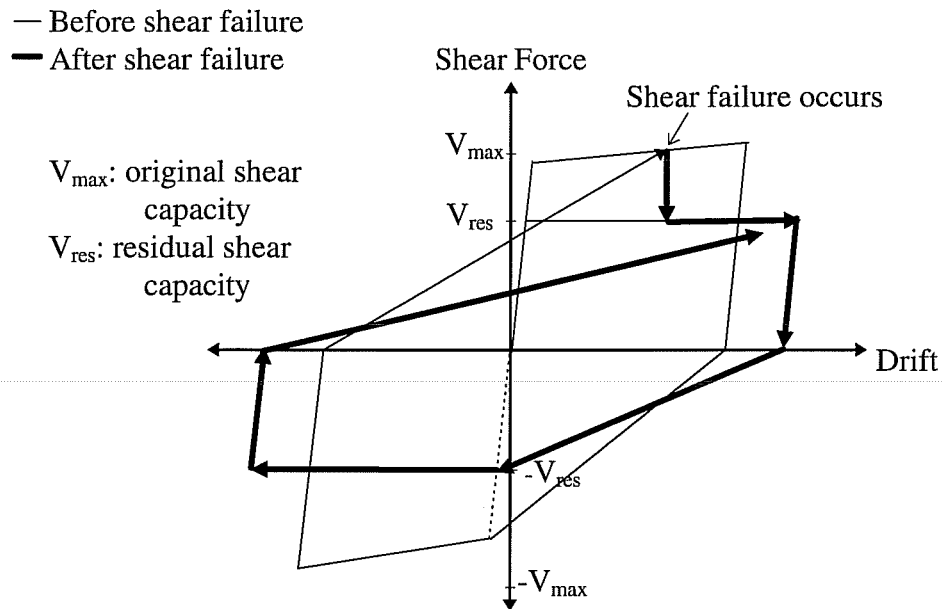


Figure 4.25 Model of hysteretic behavior of column failing in shear

4.3.2 IDARC

Because of the nature of the member modeling technique used in IDARC, the input data for IDARC are much simpler than those in DRAIN-2D. Gross section properties are used as the initial condition, and the program updates member flexibility (stiffness) according to moments produced in members due to earthquake excitation.

IDARC contains a pre-processor which can generate hysteretic envelopes for reinforced concrete members according to input material properties. Users can also

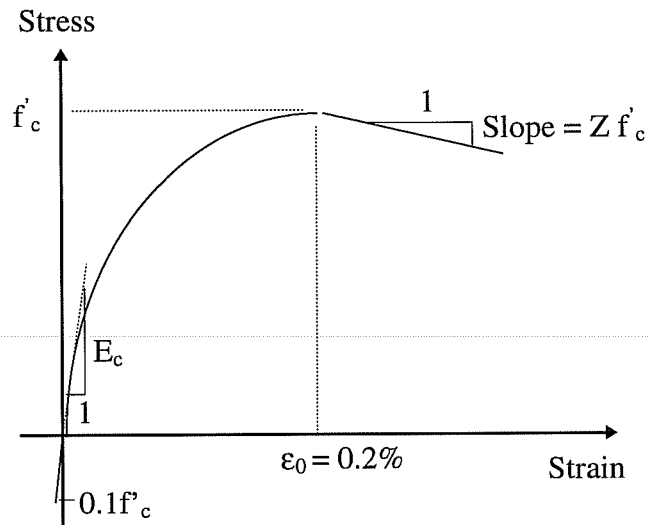
input hysteretic envelopes directly. In this study, hysteretic envelopes were generated using the pre-processor.

4.3.2.1 Material Properties

An unconfined concrete stress-strain relationship was adopted to represent behavior of concrete material as shown in Figure 4.26. A tri-linear model was adopted for steel stress-strain relationship (Figure 4.27).

4.3.2.2 Shear Failure

IDARC does not have the capacity for modeling sudden member shear failure, although it can model gradual strength deterioration as shown in Figure 4.10.



$$Z = \frac{0.5}{\epsilon_{50u} + \epsilon_{50h} - 0.002}$$

in which, $\epsilon_{50u} = \frac{3 + 0.002 f'_c}{f'_c - 1000}$, (f'_c in psi)

$$\epsilon_{50h} = \frac{3}{4} \rho_s \sqrt{\frac{b''}{s}}$$

Note: ρ_s is the ratio of transverse reinforcement over the volume of confined concrete;
 b'' is the width of confined core;
 s is the transverse reinforcing steel spacing.

Figure 4.26 Concrete Stress-Strain Relationship. IDARC

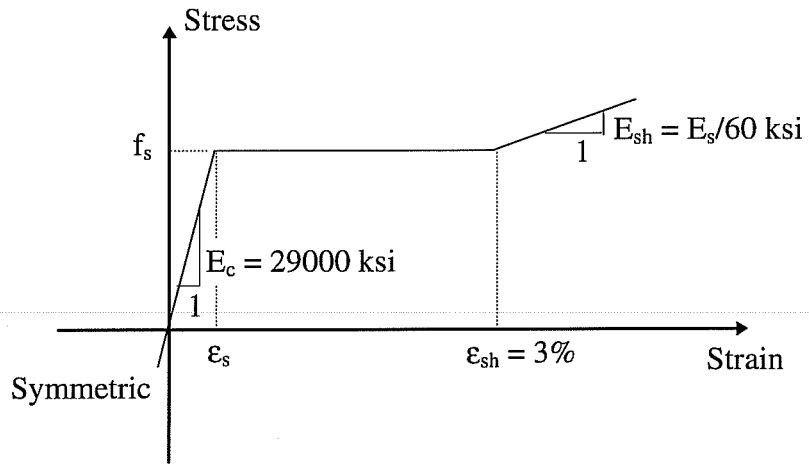


Figure 4.27 Steel Stress-Strain Relationship. IDARC

CHAPTER 5

NONLINEAR DYNAMIC TIME HISTORY ANALYSES

5.1 General

The response of two buildings under three different earthquakes were analyzed and compared with recorded data.

5.2 Seven-Story Hotel in the Northridge Earthquake

The building was analyzed only in the east-west (longitudinal) direction because most of the damage occurred in this direction. Lateral force is resisted in this direction by moment frames (Figure 3.4). An earlier study⁶⁸ established that the exterior frames were twice as stiff as interior frames. Two-dimensional nonlinear dynamic time history analyses were performed for the longitudinal frame along the south perimeter where most of column shear failure took place and 1/3 of the structural mass was assigned to this frame. Figure 5.1 shows the structural model of the south perimeter frame used for dynamic analyses. DRAIN-2D was used to model and analyze the response of this building under the 1994 Northridge Earthquake. Since the shear failure model could not be included in IDARC, it was not used for this building for the 1994 Northridge Earthquake.

	7	14	21	28	35	42	49	56	Roof
63 126	70 133	77 140	84 147	91 154	98 161	105 168	112 175	119 182	6th Fl
62 125	69 132	76 139	83 146	90 153	97 160	104 167	111 174	118 181	5th Fl
61 124	68 131	75 138	82 145	89 152	96 159	103 166	110 173	117 180	4th Fl
60 123	67 130	74 137	81 144	88 151	95 158	102 165	109 172	116 179	3rd Fl
59 122	66 129	73 136	80 143	87 150	94 157	101 164	108 171	115 178	2nd Fl
58 121	65 128	72 135	79 142	86 149	93 156	100 163	107 170	114 177	1st Fl
57 120	64 127	71 134	78 141	85 148	92 155	99 162	106 169	113 176	Ground Fl

Note: numbers indicate elements used in analyses.

Figure 5.1 Structural Model for Nonlinear Dynamic Analyses. Seven-Story Hotel

5.2.1 Evaluation of Response Records

The displacement response time history was also available from the California Strong Motion Instrumentation Program (CSMIP). The following observations regarding the building's torsional effects and periods of vibration were made according to these records.

5.2.1.1 Torsional Effects

There were sensors located at both east and west ends of the structure (Figure 3.14). As a result torsional effects can be evaluated from the recorded building response in the north-south (transverse) direction. Figures 5.2, 5.3 and 5.4 show the recorded roof, 3rd floor and 2nd floor displacement time histories at the east end (Stations S2, S5 and S7) and the west end (Stations S3, S6 and S8), respectively. In Table 5.1, the maximum differences in relative displacements between the east end and the west end at various floor levels are listed. To better measure the magnitude of this torsional movement, maximum relative displacements at corresponding floors were calculated from the recorded data. The percentage of maximum differences in relative displacements with respect to the maximum displacements was then computed and listed in Table 5.1.

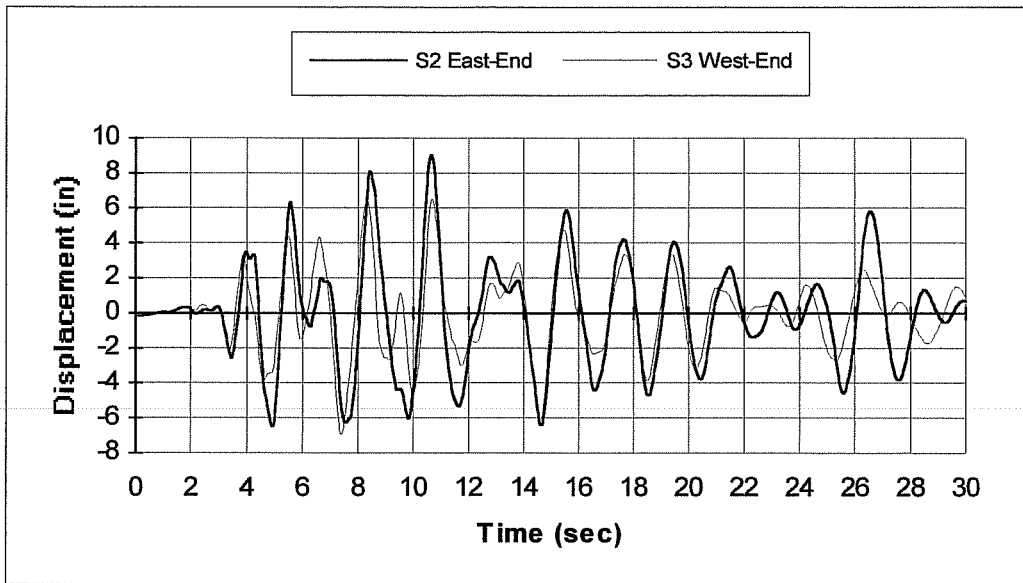


Figure 5.2 Comparison Between Roof Relative Displacement Time History in the North-South Direction at the East End and the West End of the Building

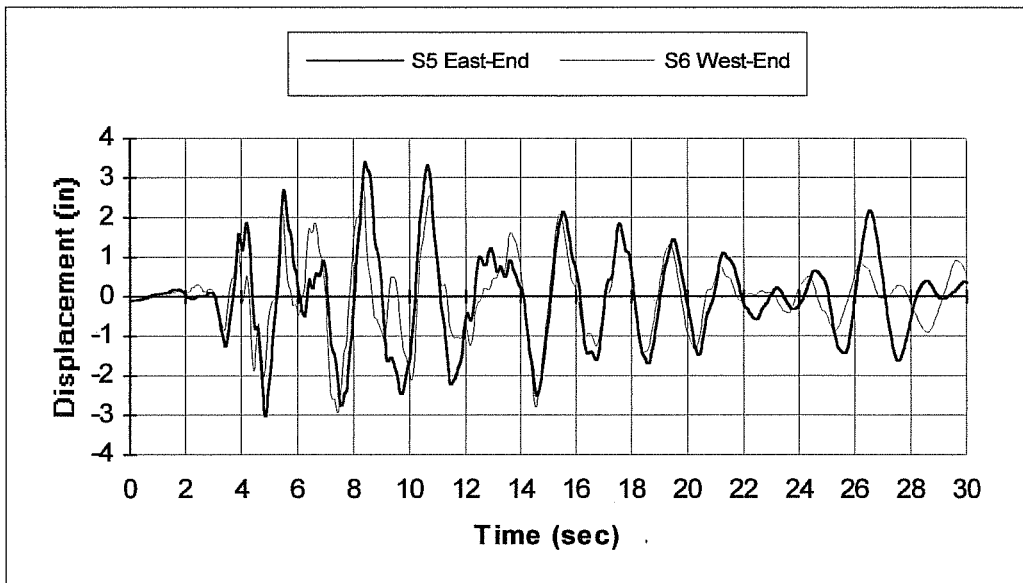


Figure 5.3 Comparison Between the 3rd Floor Relative Displacement Time History in the North-South Direction at the East End and the West End of the Building

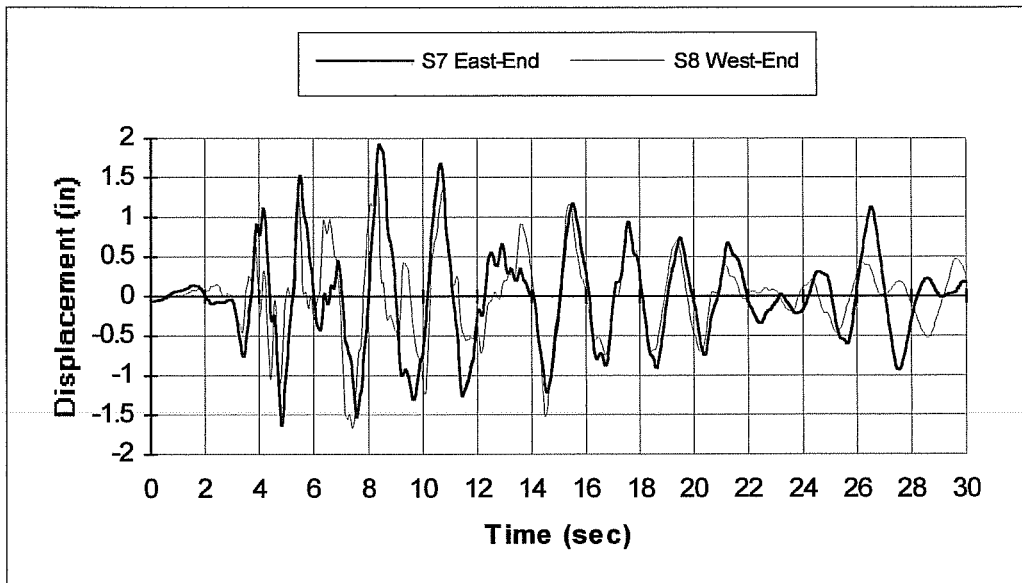


Figure 5.4 Comparison Between the 2nd Floor Relative Displacement Time History in the North-South Direction at the East End and the West End of the Building

Table 5.1 Maximum Horizontal Displacements in the North-South (Transverse) Direction at the East End and the West End

Level	Maximum Difference between two ends	Maximum Displacement	$\frac{\text{Maximum Difference}}{\text{Maximum Displacement}}$
Roof	5.54 in at 8.72 sec	9.04 in	61%
3rd Floor	2.59 in at 8.62 sec	3.41 in	76%
2nd Floor	1.69 in at 8.50 sec	1.93 in	88%

Figure 5.5 shows the horizontal ground displacement in the north-south (transverse) direction at the east end (Channel S1) and the west end (Channels S13 and S14). There was practically no torsional movement at the ground level of the building. However the torsional movement of the building recorded at floors above the ground level was rather significant. In the east-west (longitudinal) direction, the second floor underwent a maximum lateral displacement of 1.64 inches. This indicates that the one-inch joint separation between the first story brick walls and the adjacent columns was not enough to keep the walls from acting as part of the lateral force resisting system. The damage observed in the brick walls and the significant torsional response recorded during the earthquake in an otherwise symmetric structure support this hypothesis.

5.2.1.2 Periods of Vibration

Since the building was analyzed only in the east-west (longitudinal) direction, only the recorded periods of vibration in east-west direction were evaluated. Figure 5.6 shows the relative displacement time history of the roof, the 6th floor, the 3rd floor and the 2nd floor in the longitudinal direction.

As shown in Figure 5.6, the period of vibration in the east-west (longitudinal) direction changed significantly during the earthquake. At the beginning of ground shaking, the fundamental period was approximately 1.53 seconds. In the middle of

ground shaking, the fundamental period increased to approximately 2.10 seconds. In the later stages of the earthquake, the building responded at a fundamental period of approximately 2.39 seconds. The significant lengthening of building period of vibration clearly indicates the inelastic response and damage of the longitudinal frames in the earthquake. Also noticed in Figure 5.6 is some disturbance in the displacement response at lower floor levels, which suggests the participation of higher mode responses.

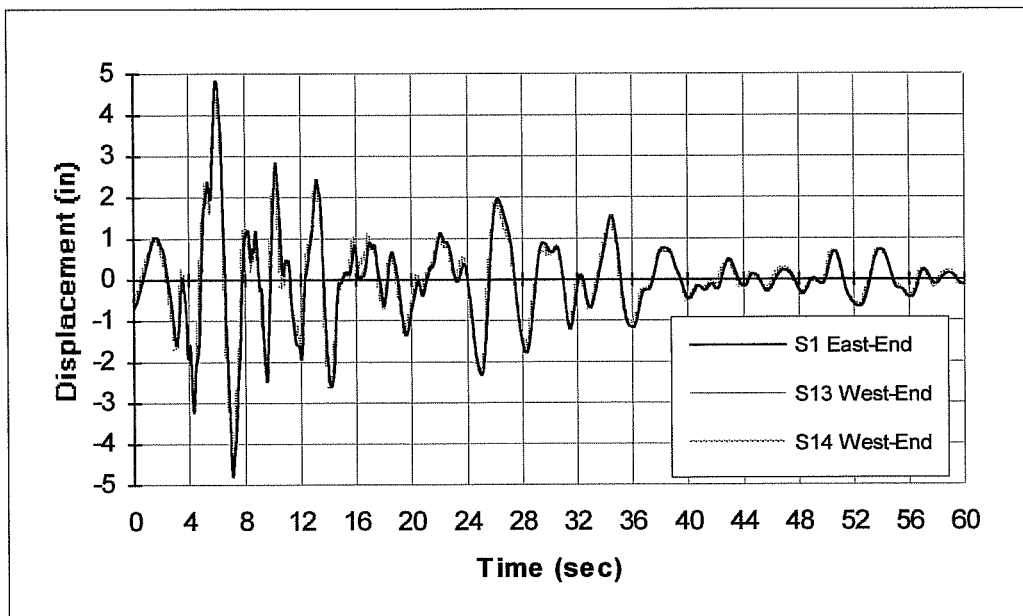


Figure 5.5 Horizontal Ground Movement in North-South (Transverse) Direction at East and West Ends

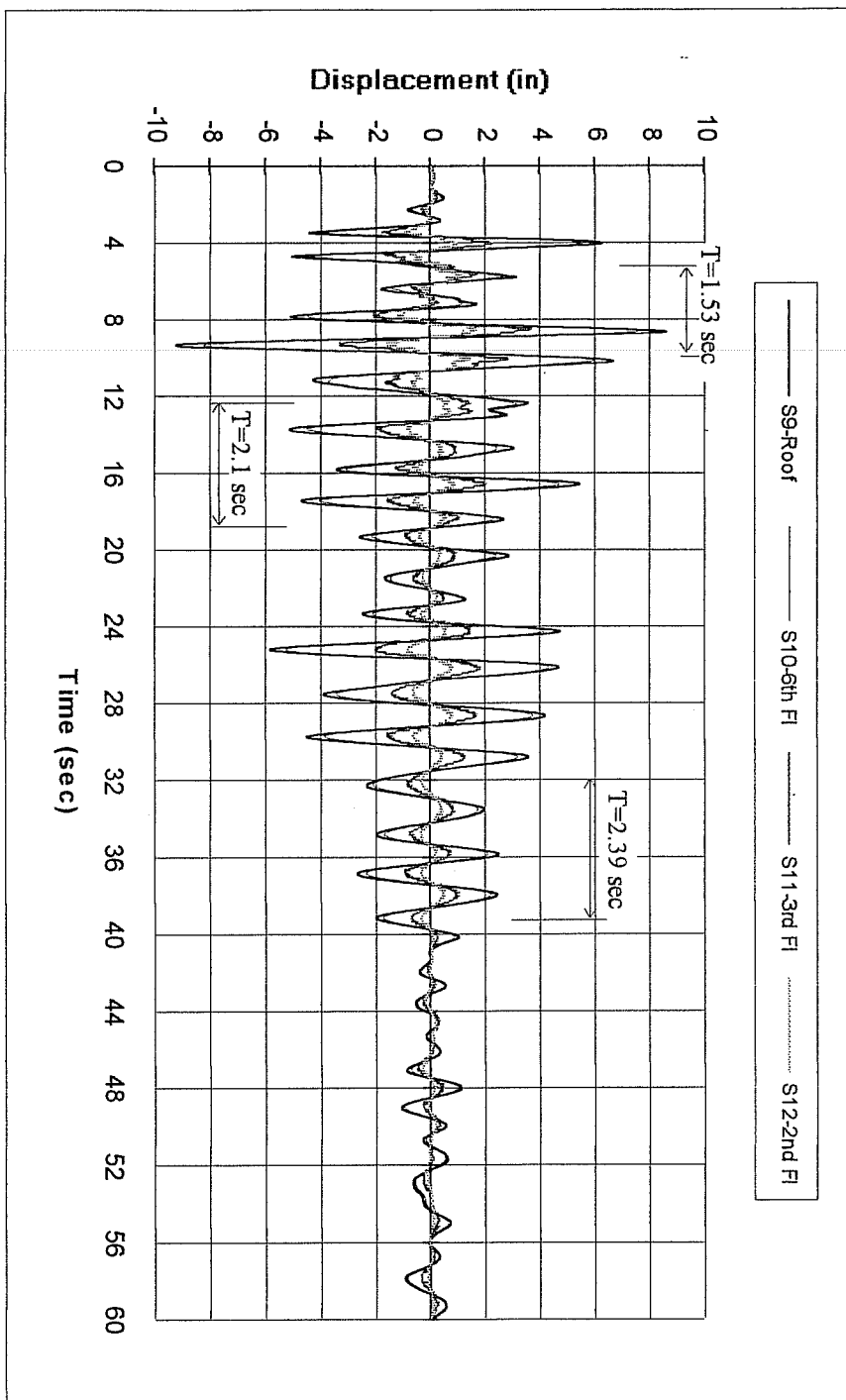


Figure 5.6 Recorded Floor Relative Displacement Time Histories in East-West (Longitudinal) Direction

5.2.2 Parametric Study

To better understand the results of analysis and what factors effect those results, several important parameters were studied first. From the results of this parametric study, proper parameters were chosen for this building. During the study of one parameter, all other parameters were kept the same. Only Option 1 (Section 4.3.1.2) for assigning element stiffnesses was used for the parametric study. Results of using other options to assign element stiffnesses were compared in Section 5.3.2.

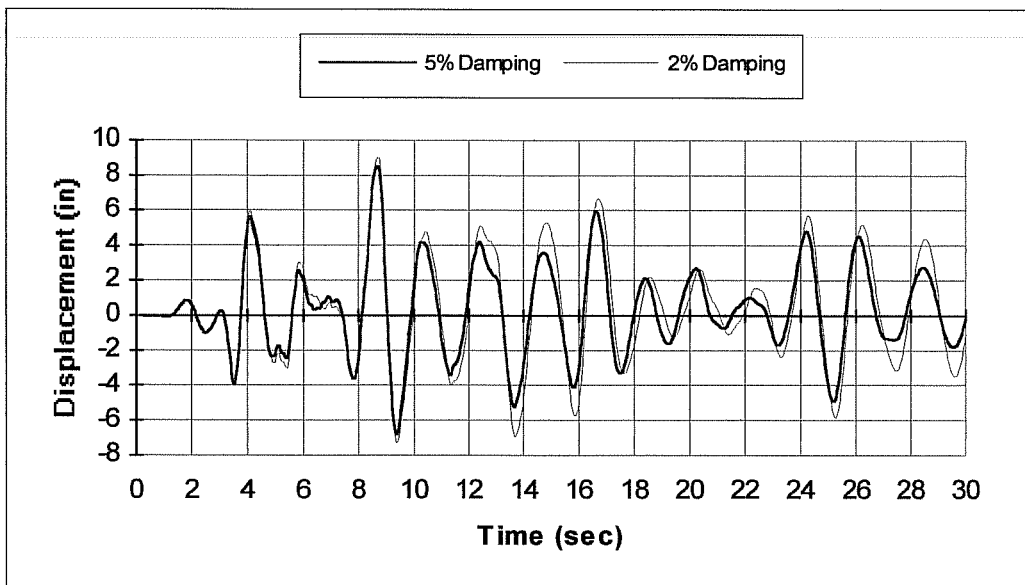
5.2.2.1 Damping Coefficients

Recommended values of viscous damping for reinforced concrete structures vary from 2% to 10%, depending on the level of deformation and strain induced in the structure. From analyses, it can be seen (Figure 5.7) that damping coefficients had little influence on the structural period, or on the shape of the roof displacement. Less damping caused slightly larger displacements, consequently, less damping could be expected to cause slightly more damage.

5.2.2.2 Actual Strength of Materials

The actual strength of concrete at the time of an earthquake is always larger than the design value given in the original drawings, because of the overstrength in original materials and strength gained over time. In addition, concrete and reinforcing

steel exhibit a significant increase in both strength and stiffness when loaded at increased strain rates, such as the strain rates expected during earthquakes. This higher rate of loading alone is estimated to increase the strength obtained from standard cylinder tests by as much as 15-20%^{66,67}.

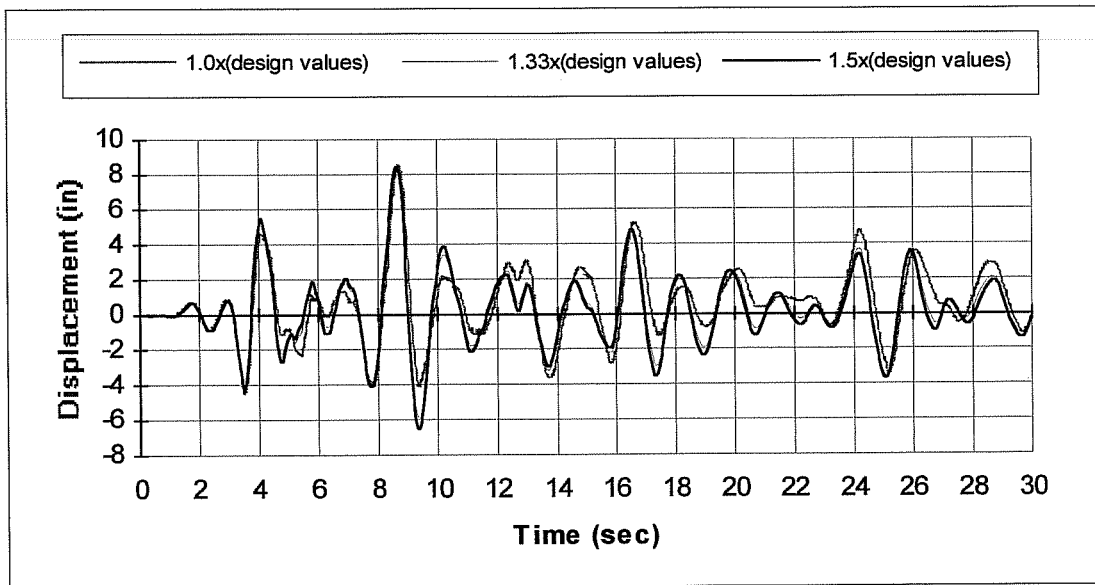


Ground motion:	1994 Northridge Earthquake.
Material strength:	$3/2x$ (design values).
Effective stiffness $(EI)_{\text{eff}}$:	$0.30(EI_g)$
Residual shear capacity:	$2/3$ of original shear capacity.

Figure 5.7 Comparison of Roof Relative Displacement Time History with Different Damping Coefficients Assumed

Three different material strengths for the subject building, namely, 1.0 x (design values), $4/3$ x (design values), and $3/2$ x (design values) have been tried. The results show (Figure 5.8) that strength of material had little influence on the period of

the structure or the peak roof horizontal displacement. However, it did affect the roof relative displacement in general. Higher material strength resulted in less roof displacement (except at peak roof displacement). Also higher material strength limited damage in the structure.



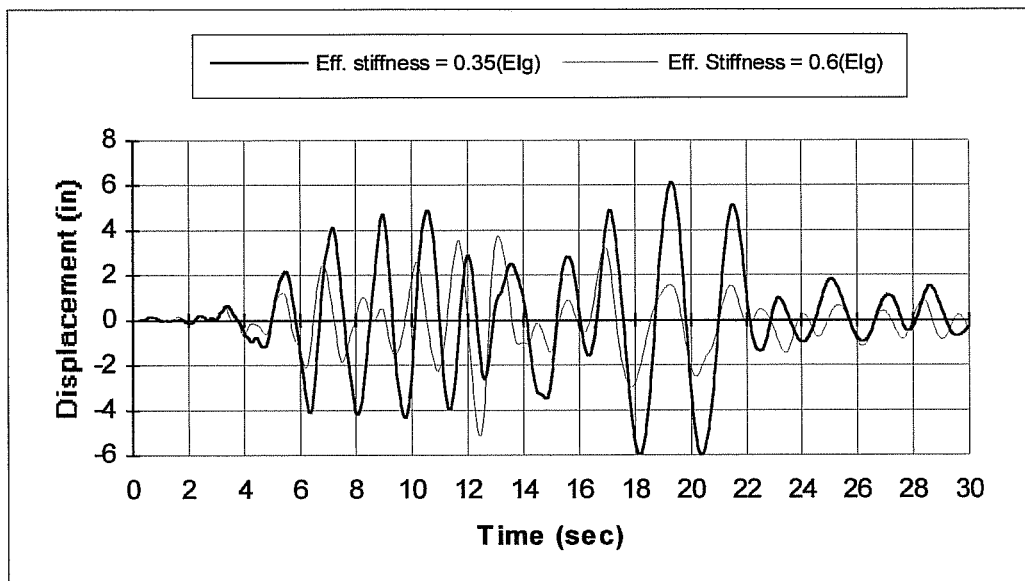
Ground motion:	1994 Northridge Earthquake.
Damping coefficients:	5% critical damping.
Effective Stiffness $(EI)_{\text{eff}}$:	$0.30(EI_g)$
Residual shear capacity:	2/3 of original shear capacity.

Figure 5.8 Comparison of Roof Relative Displacement Time History with Different Material Strength Assumed

5.2.2.3 Effective Stiffness of Members $(EI)_{\text{eff}}$

The effective stiffness of a member represents an average stiffness after the member cracks. The value of effective stiffness has been found to significantly affect

the response of the structure. For example, Figure 5.9 shows the building response to the same earthquake with different effective stiffness used. With a lower effective stiffness, the period of the structure increased. Note that the earthquake ground motion used for this study was the 1971 San Fernando Earthquake recorded at the ground floor of the building. No matter what earthquake was used, the same trend was obtained.



Ground motion:	1971 San Fernando Earthquake.
Damping coefficients:	5% critical damping.
Material strength:	$4/3 \times$ (designed value).
Residual shear capacity:	$2/3$ of original shear capacity.

Figure 5.9 Comparison of Roof Relative Displacement Time History with Different Effective Stiffness $(EI)_{\text{eff}}$ Assumed

5.2.2.4 Residual Shear Capacity

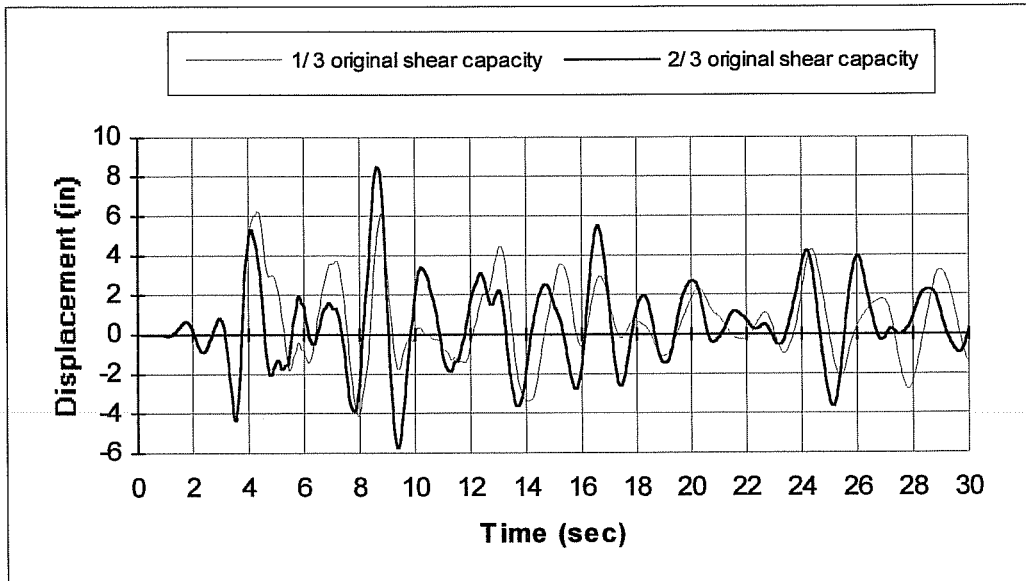
The subject building experienced shear failure of several columns between the fourth and the fifth floor levels. Test results have shown that strength and stiffness of columns reduce dramatically after shear failures occur (Figures 4.21, 4.22 and 4.23).

Different values of residual shear capacity were tried, and the results showed they had significant impact on building response after column shear failure occurred. As shown in Figure 5.10, after columns started to fail in shear at about 8.5 seconds, the period of the structure increased. The lower the residual shear capacity assumed, the more abrupt the change of period, and the longer the period of the structure during the remainder of the response became.

5.2.3 Analysis Results

The parameters chosen for this building are described in the following paragraphs.

- (1) Damping coefficients: Considering the relatively small influence of damping on the response of the building, a 5% damping coefficient was used as an average value for viscous damping for reinforced concrete structures.



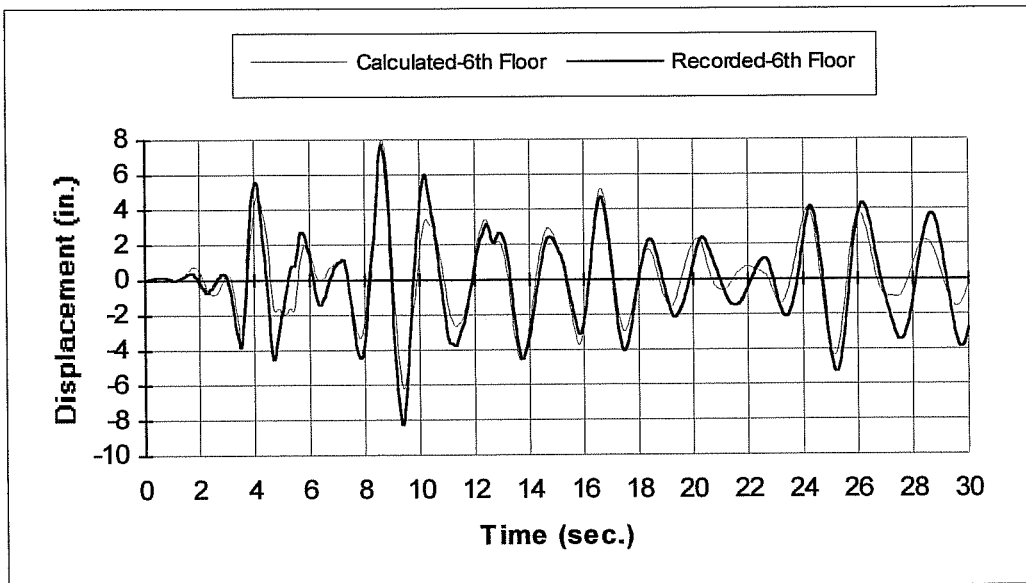
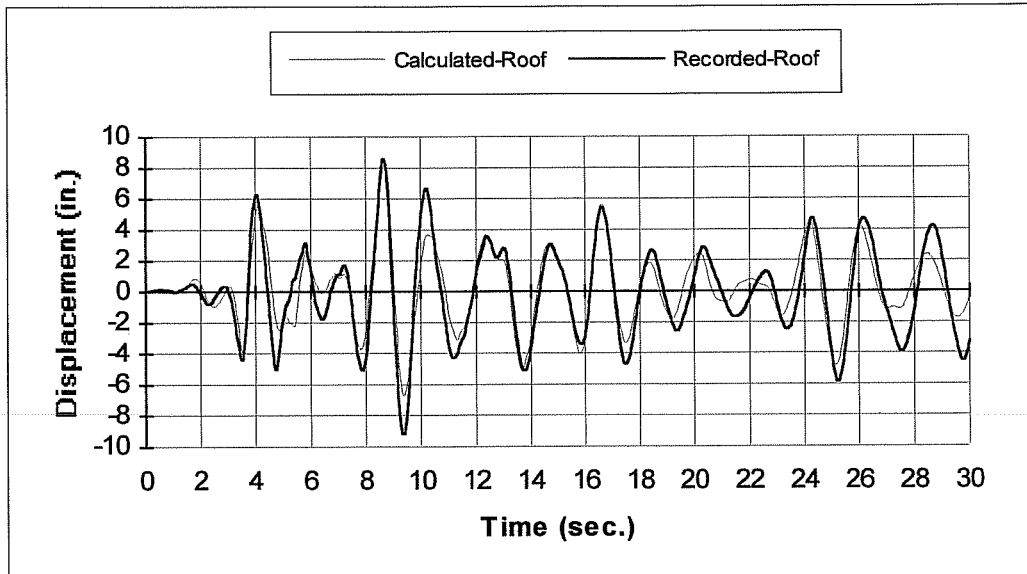
Ground motion: 1994 Northridge Earthquake.
 Damping coefficients: 5% critical damping.
 Material strength: $3/2 \times (\text{design values})$.
 Effective Stiffness $(EI)_{\text{eff}}$: $0.30(EI_g)$

Figure 5.10 Comparison of Roof Relative Displacement Time History with Different Residual Shear Capacity Assumed

- (2) Actual material strength: Considering the age of the building and the intensity of the earthquake, $3/2 \times (\text{design values})$ were used for both concrete and steel strengths to take into account the overstrength in the original material, strength gained over time, and high strain rates during the earthquake. The resulting flexural strength will be about 1.5 times nominal strength.

- (3) Effective stiffness: Effective stiffness was chosen so that the period in the calculated response time history would match the period of vibration of recorded response time history. After several trials, $0.30(EI_g)$ was chosen as the effective stiffness $(EI)_{\text{eff}}$. For simplicity, the same effective stiffness factor 0.30 was used for all members including beams and columns.
- (4) Residual shear capacity: Comparing the observed column failures with experimental results in which columns failed in shear (Section 4.3.1.3), it was assumed that the columns failed in combined shear and flexure (Figure 4.23). $2/3$ of original shear capacity was chosen as the residual shear capacity to represent the response of columns failing in a similar mode. As shown in Figure 5.1, a double member model was used for columns in the structure.

Figure 5.11 shows the comparison between the calculated roof and 6th floor relative displacement time history using the parameters described above and the recorded relative roof and 6th floor displacement time history. The recorded roof relative displacement time history was obtained by subtracting the recorded roof absolute displacement at Station S9 (Figure 3.10) from the ground absolute displacement at Station S16. The recorded 6th floor relative displacement time history was obtained by subtracting the recorded 6th floor absolute displacement at Station S10 (Figure 3.10) from the ground absolute displacement at Station S16. Since the



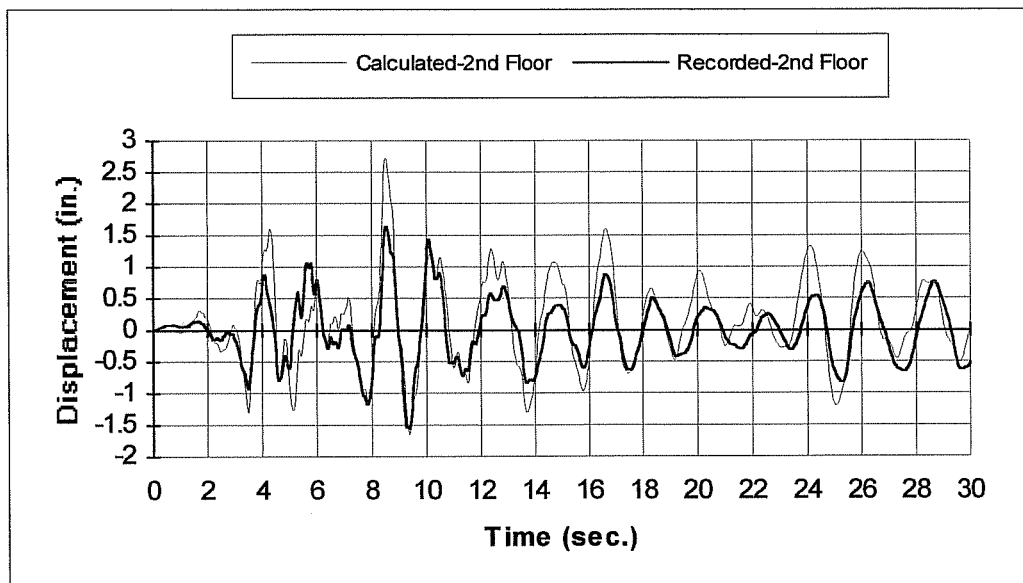
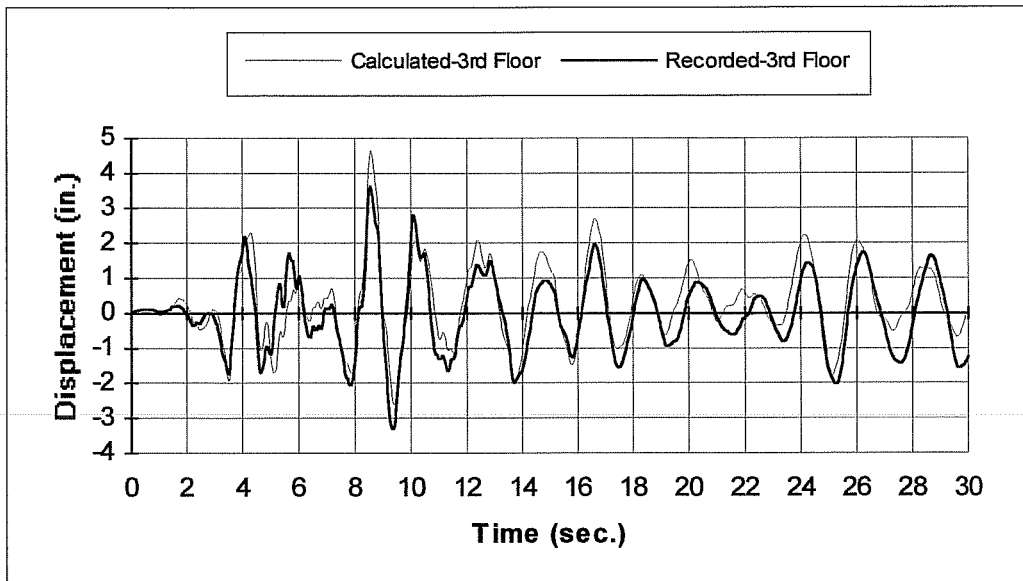
Ground motion:	1994 Northridge Earthquake.
Damping coefficients:	5% critical damping.
Material strength:	$3/2 \times$ (design values).
Effective Stiffness $(EI)_{\text{eff}}$:	$0.30(EI_g)$.
Residual shear capacity:	$2/3$ of original shear capacity.

Figure 5.11 Comparison Between Calculated and Recorded Roof and 6th Floor Relative Displacement Time Histories

analysis was two-dimensional, no torsional effects could be included. However because Stations S9 and S10 were located on the center line of the building in the longitudinal direction, the responses recorded at Stations S9 and S10 should contain negligible torsional movement in this direction. Therefore calculated data and recorded data can be compared regardless of the large torsional responses in the building.

As shown in Figure 5.11, the first thirty seconds of ground shaking were used for comparison. An integration interval of 0.005 seconds yielded sufficiently accurate results in DRAIN-2D¹⁴ and therefore it was used for this and all subsequent DRAIN-2D analyses.

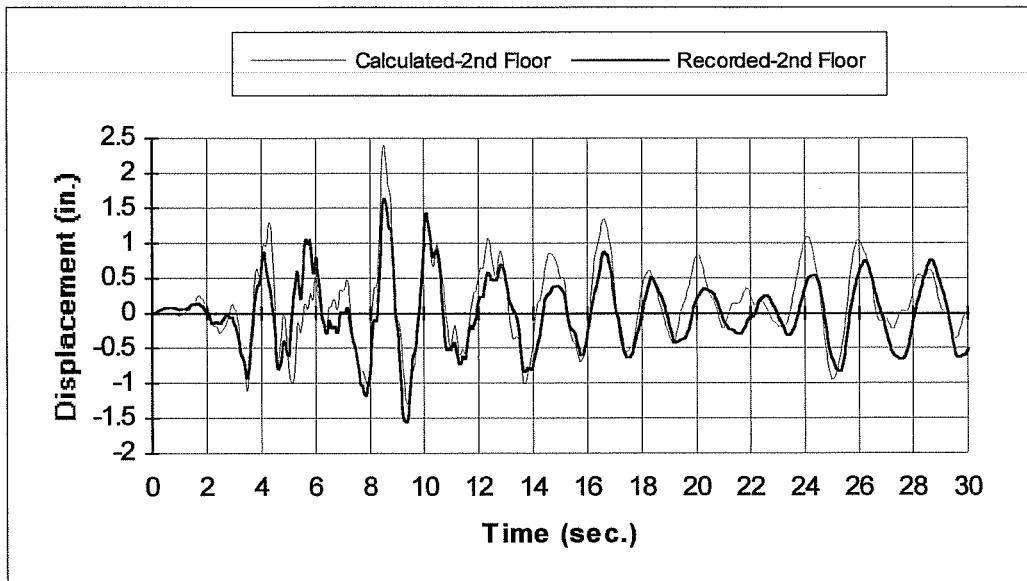
Figure 5.12 shows calculated and recorded 3rd, and 2nd floor relative displacement time histories. The recorded relative displacement time history at the given levels was obtained by subtracting ground absolute displacement at Station S16 from the 3rd floor absolute displacement at Station S11 (Figure 3.10), and the 2nd floor absolute displacement at Station S12 (Figure 3.10), respectively. Good agreement was found between calculated and recorded roof and 6th floor relative displacement time histories. However at the 3rd and 2nd floors, agreement was not as good. The discrepancy at lower floor levels may have been due to the same effective stiffness factor being used for all columns. At lower levels, columns were carrying higher axial loads, and the effective stiffness in lower stories should be higher than in upper stories.



Ground motion: 1994 Northridge Earthquake.
Damping coefficients: 5% critical damping.
Material strength: $3/2 \times (\text{design values})$.
Effective Stiffness $(EI)_{\text{eff}}$: $0.30(EI_g)$.
Residual shear capacity: $2/3$ of original shear capacity.

Figure 5.12 Comparison Between Calculated and Recorded 3rd Floor and 2nd Floor Relative Displacement Time Histories

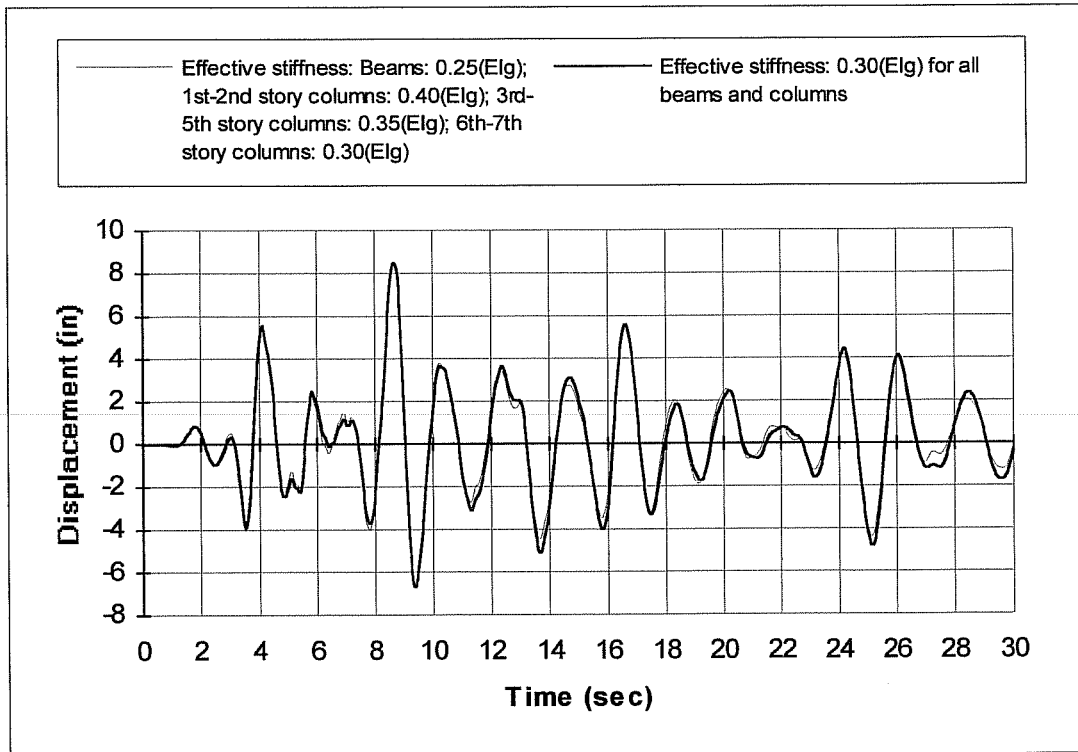
In the study, different effective stiffness factors were assigned to beams and columns to see the effects. Figure 5.13 shows the 2nd floor relative displacement time history by using different effective stiffness factors for beams and columns.



Ground motion:	1994 Northridge Earthquake.
Damping coefficients:	5% critical damping.
Material strength:	3/2x(design values).
Effective Stiffness $(EI)_{\text{eff}}$:	beams: $0.25(EI_g)$.
	columns: 1st - 2nd story: $0.30(EI_g)$.
	3rd - 5th story: $0.35(EI_g)$.
	6th - 7th story: $0.40(EI_g)$.
Residual shear capacity:	2/3 of original shear capacity.

Figure 5.13 Comparison Between Calculated and Recorded 2nd Floor Relative Displacement Time History using Different Effective Stiffness Factors

Although the difference was reduced from 67% to 47% at maximum displacements, the difference was still very large and was attributed to the fact that there were brick infill walls at the first story which added considerable stiffness and reduced deformation at the lower levels. Figure 5.14 compares the roof relative displacement using a single effective stiffness factor 0.30 for all beams and columns and using varying effective stiffness factors for beams and columns. Since using different effective stiffness factors for beams and columns will only improve the displacement in the lower floor by 14% at maximum displacement, in subsequent calculations the same effective stiffness coefficient was used for simplicity for all beams and columns. Figure 5.15 shows the calculated drift ratios at all stories. Also shown are the recorded drift ratios at the 2nd story and the 1st story. Again the small drift ratio recorded at the first story was attributed to the participation of brick infill walls in the lateral force resisting system. Also drawn in Figure 5.15 is the drift limit set by the NEHRP-94 specifications⁹. Under the drift ratios the building experienced during the 1994 Northridge Earthquake, the building was very close to collapse. If the drift limit remains under 1.5%, the building will have a better chance of withstanding the earthquake. Therefore the drift limit recommended by NEHRP-94 appears to be reasonably good at preventing collapse for this structure.



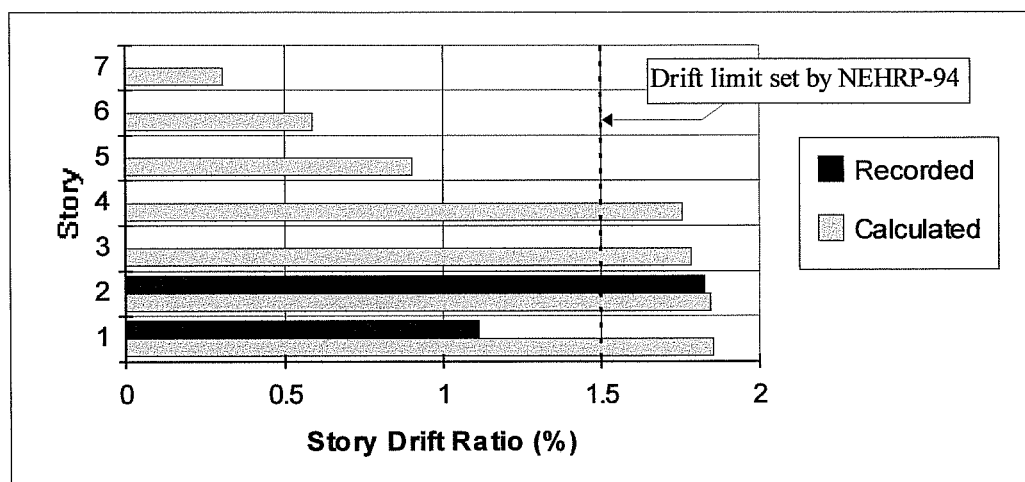
Ground motion: 1994 Northridge Earthquake.
 Damping coefficients: 5% critical damping.
 Material strength: $3/2x$ (design values).
 Residual shear capacity: $2/3$ of original shear capacity.

Figure 5.14 Comparison Between Calculated Roof Relative Displacement Time History using the Same and Different Effective Stiffness Coefficients for Beams and Columns

Figure 5.16 shows the condition of the structure at the end of calculation. Compared with the actual failure state shown in Figure 3.19, the time history analysis predicted more column shear failures. This was anticipated because the shear capacities were computed using ACI 318-95 formula (11-4) for members subject to axial compression. The ACI Code provides a fairly conservative estimate of shear

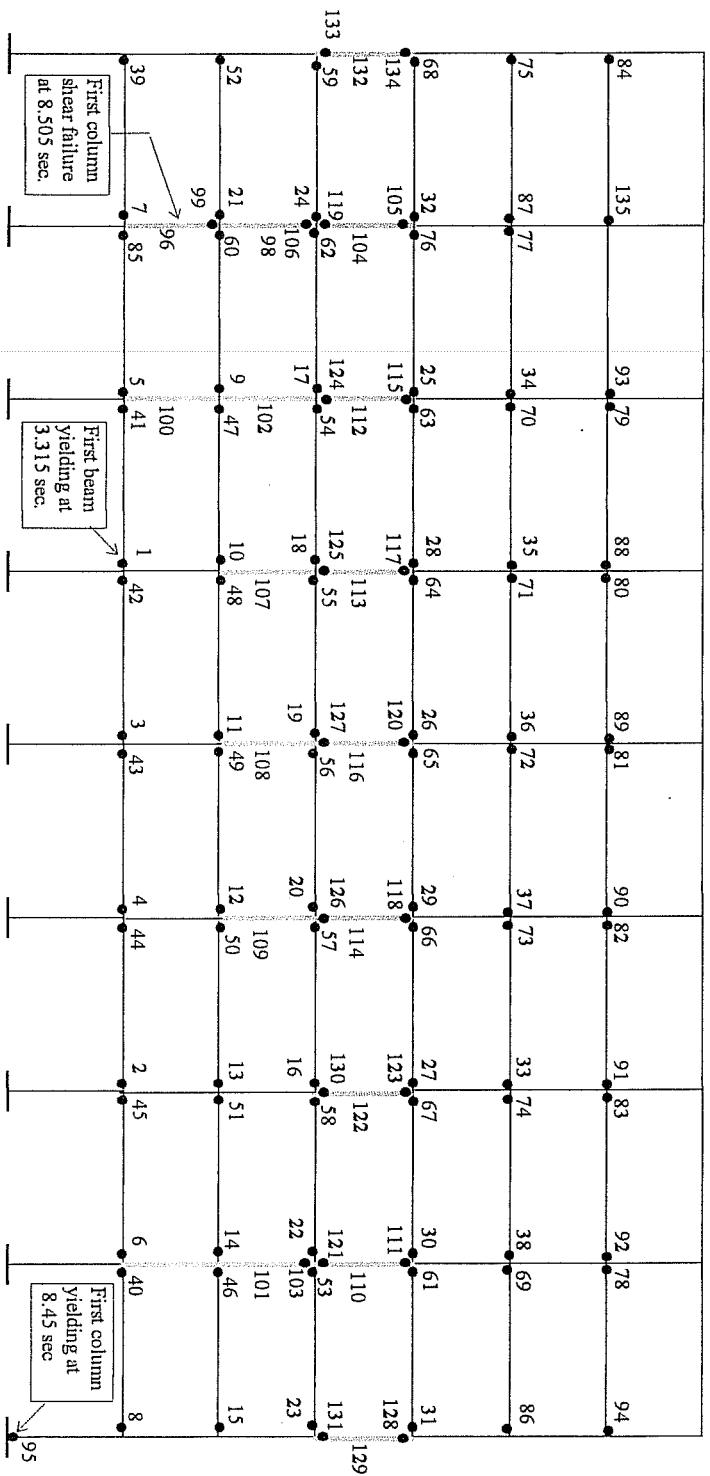
capacity. However, because the equation is widely used in design, it was adopted without any change. Nevertheless, it still demonstrated that the most severe shear failure occurred in the fourth story, which is consistent with what actually happened.

Figures 5.17 and 5.18 show the absolute acceleration time history at the roof, the 6th floor, the 3rd floor, and the 2nd floor levels. Also shown are the recorded absolute acceleration time histories at these floor levels. There is general agreement between calculated and recorded data.



Ground motion: 1994 Northridge Earthquake.
 Damping coefficients: 5% critical damping.
 Material strength: $3/2 \times$ (design values).
 Effective Stiffness $(EI)_{eff}$: $0.30(EI_g)$.
 Residual shear capacity: $2/3$ of original shear capacity.

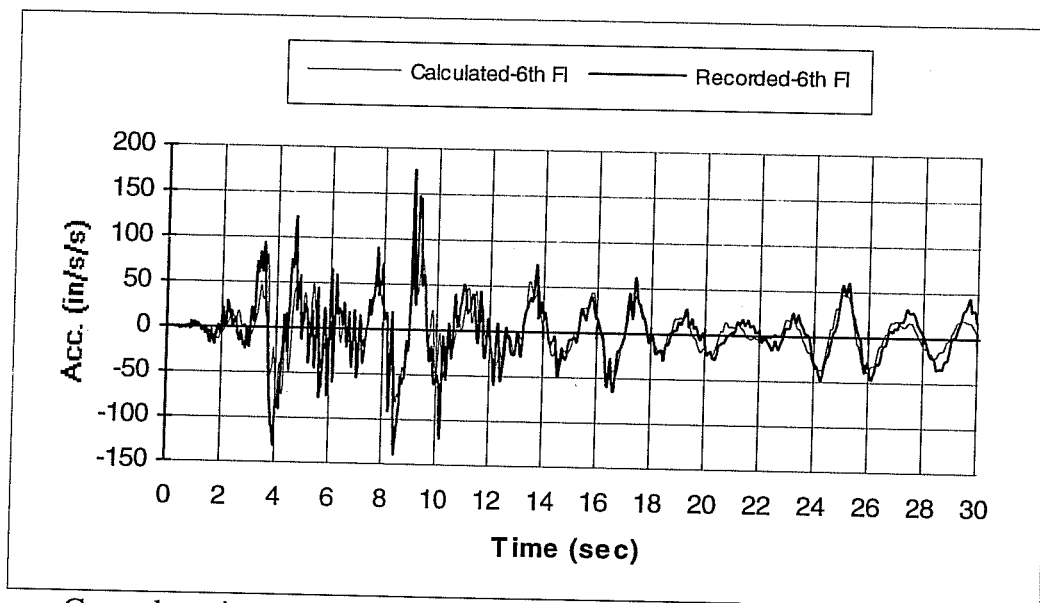
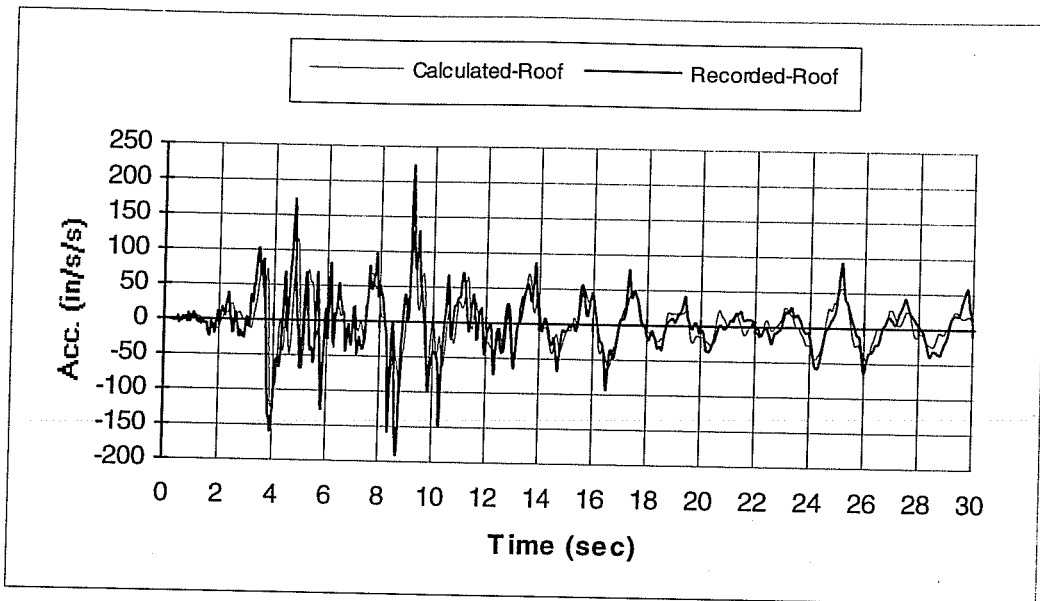
Figure 5.15 Comparison Between Calculated and Recorded Story Drift Ratio



- yielding at member end
- column failure in shear

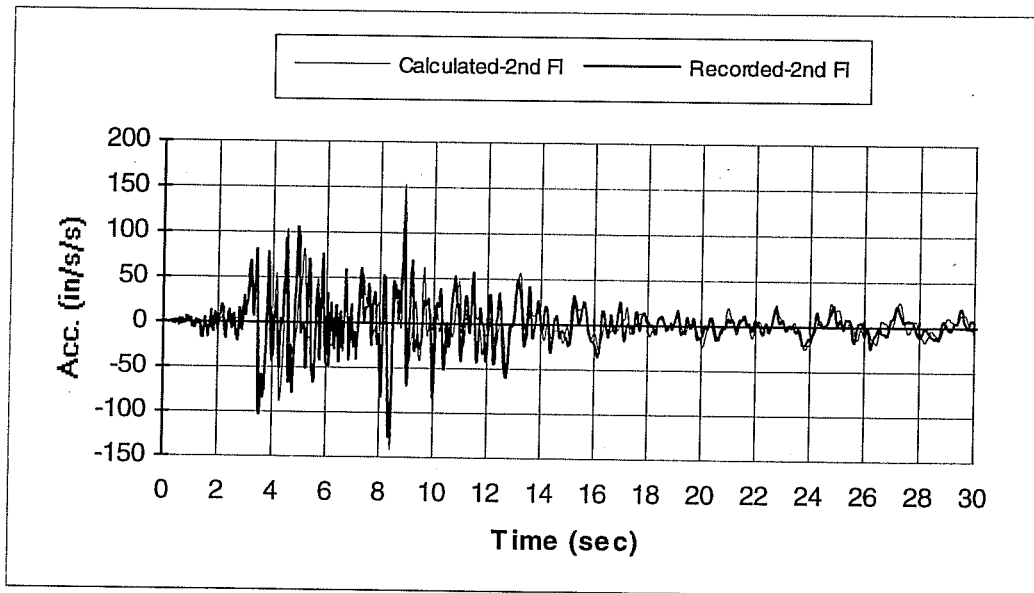
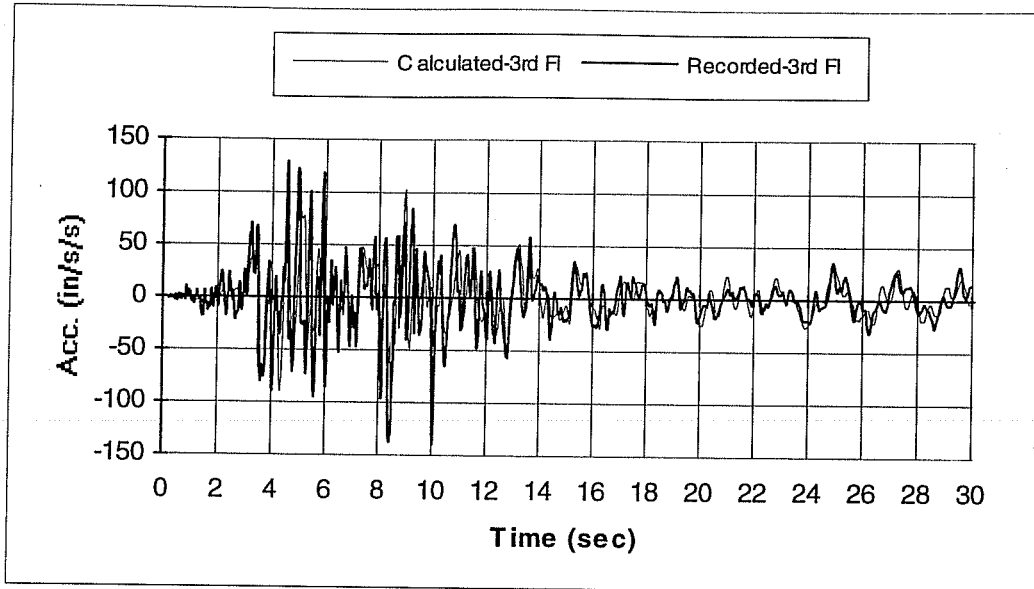
Ground motion: 1994 Northridge Earthquake.
 Damping coefficients: 5% critical damping.
 Material strength: $3/2x$ (design values).
 Effective Stiffness (EI)_{eff}: $0.30(EI_c)$.
 Residual shear capacity: $2/3$ of original shear capacity.

Figure 5.1.6 Failure Sequence from DRAIN-2D Time History Analysis. Seven-Story Hotel



Ground motion: 1994 Northridge Earthquake.
 Damping coefficients: 5% critical damping.
 Material strength: $3/2x$ (design values).
 Effective stiffness $(EI)_{\text{eff}}$: $0.30(EI_g)$.
 Residual shear capacity: $2/3$ of original shear capacity.

Figure 5.17 Comparison Between Calculated and Recorded Roof and 6th Floor Absolute Acceleration Time History



Ground motion: 1994 Northridge Earthquake.
 Damping coefficients: 5% critical damping.
 Material strength: $3/2 \times$ (design values).
 Effective stiffness $(EI)_{\text{eff}}$: $0.30(EI_g)$.
 Residual shear capacity: $2/3$ of original shear capacity.

Figure 5.18 Comparison Between Calculated and Recorded 3rd and 2nd Floor Absolute Acceleration Time History

5.3 Seven-Story Hotel in the San Fernando Earthquake

The same hotel that was severely damaged in the 1994 Northridge Earthquake survived the 1971 San Fernando Earthquake with minor structural damage. Again, two-dimensional nonlinear dynamic time history analyses were performed for the south perimeter frame in the longitudinal direction. The same structural model shown in Figure 5.1 was used here for the analyses.

5.3.1 Evaluation of Response Records

Figure 5.19 shows the relative displacement time history recorded at the roof and the 4th floor level in the east-west (longitudinal) direction. The building period of vibration in the east-west (longitudinal) direction was about 0.6 seconds in the beginning of the ground shaking. But at about 12 seconds, the period of vibration increased to 1.25 seconds. The lengthening of the building period of vibration indicates that cracking and inelastic deformation increased during the earthquake.

In the 1971 San Fernando Earthquake, there was only one sensor at each floor to record response (Figures 3.21), and no torsional movement can be evaluated.

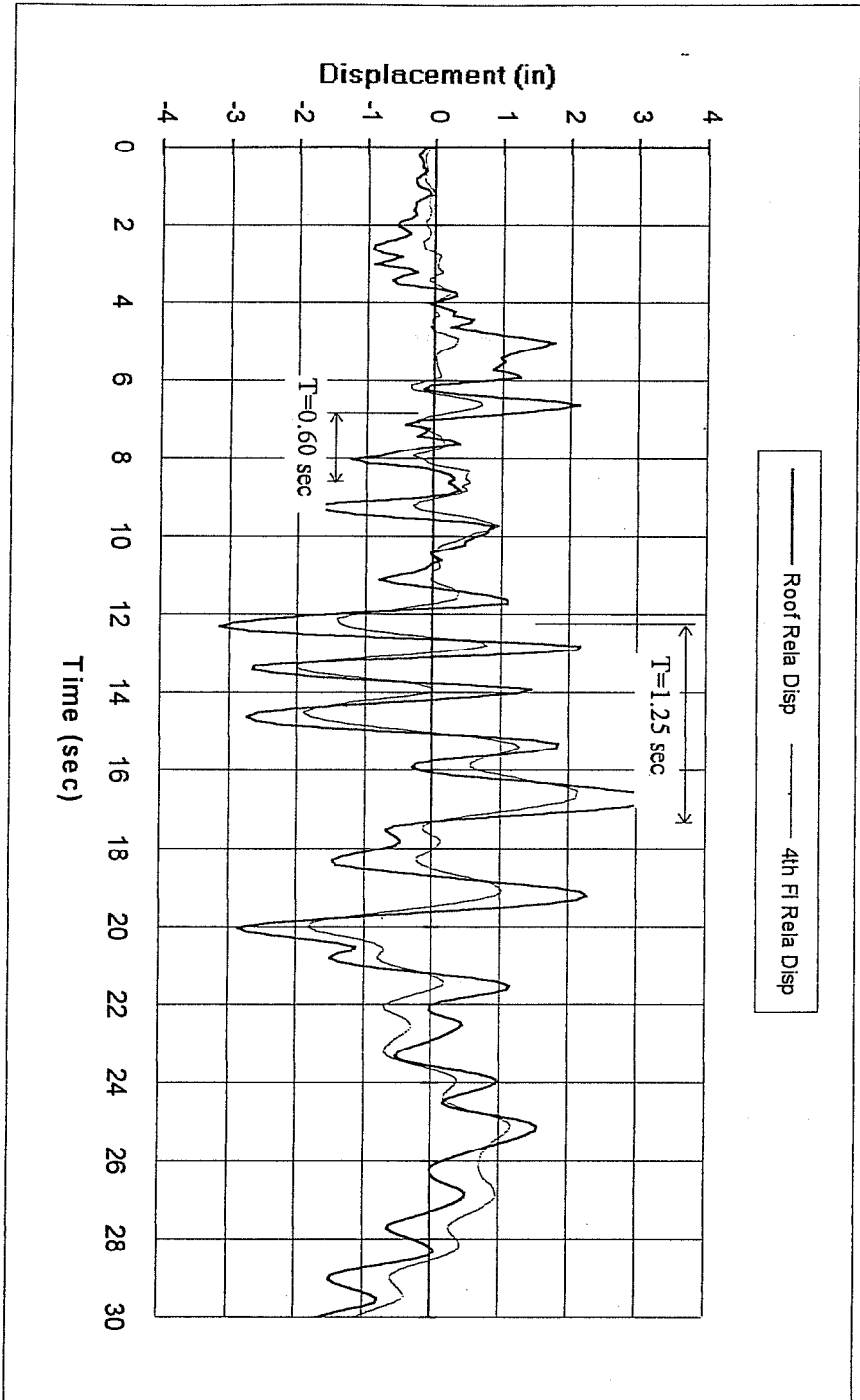


Figure 5.19 Recorded Floor Relative Displacement Time History in East-West (Longitudinal) Direction at 1971 San Fernando Earthquake

5.3.2 Analysis Results

Both DRAIN-2D and IDARC were used to analyze the response of this building under the 1971 San Fernando Earthquake, and the results were compared with recorded response. For DRAIN-2D, two options for assigning effective stiffness of members were exercised, and the results were compared.

5.3.2.1 DRAIN-2D Analyses

Using the results from Section 5.2.2, the following parameters were chosen for the building under the 1971 San Fernando Earthquake.

- (1) Damping coefficients: An average 5% damping coefficient was used as before.
- (2) Actual material strength: Considering the relatively moderate intensity of the earthquake and the age of the building, $4/3$ x (design values) were used for both concrete and steel strengths.
- (3) Residual shear capacity: $2/3$ of original shear capacity was used as residual shear capacity as before.

OPTION 1:

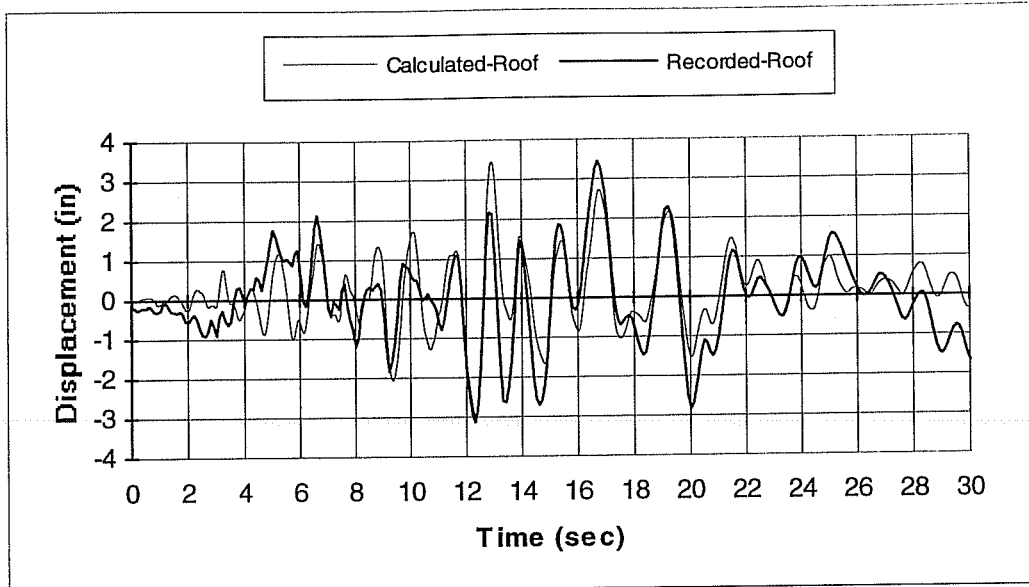
This option specified an effective flexural stiffness $(EI)_{\text{eff}}$ for cracking in the member (Section 4.3.1.2). The criterion for choosing the effective stiffness was the

calculated response time history was adjusted to produce a period of vibration that matched the period of vibration of the recorded response time history. After several trials, $0.80(EI_g)$ was chosen as the effective stiffness.

Figure 5.20 shows the comparison between the calculated roof relative displacement time history using chosen parameters and the recorded relative roof displacement time history.

Although the agreement between the calculated and the recorded roof relative displacement is not as good as that observed for the same building under the 1994 Northridge Earthquake, general agreement exists, and the maximum roof relative displacement is also predicted well.

Figure 5.21 shows the calculated and recorded relative displacement time history at the 4th floor. Once again, general agreement is observed between the calculated and the recorded 4th floor relative displacement time history. The discrepancy for the building subjected to the 1971 San Fernando Earthquake is attributed to the small magnitude of the earthquake. Non-structural elements in the structure affected response of the building more significantly, especially during the early portion of the response time history. In addition, due to the sensor location, the recorded data included the effects of building torsional movement, while the calculated displacement could not take torsional effects into account because of the nature of the two-dimensional analyses.

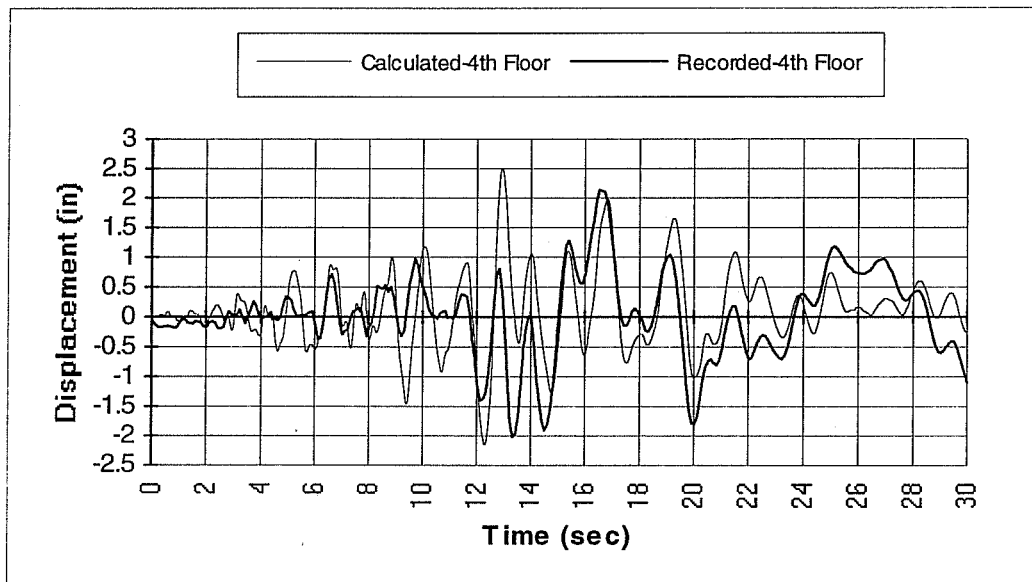


Ground motion:	1971 San Fernando Earthquake.
Damping coefficient:	5% of critical damping.
Material strength:	4/3 x (design values).
Effective stiffness $(EI)_{\text{eff}}$:	0.80(EI_g).
Residual shear capacity:	2/3 of original shear capacity.

Figure 5.20 Comparison Between Calculated and Recorded Roof Relative Displacement Time History under San Fernando Earthquake

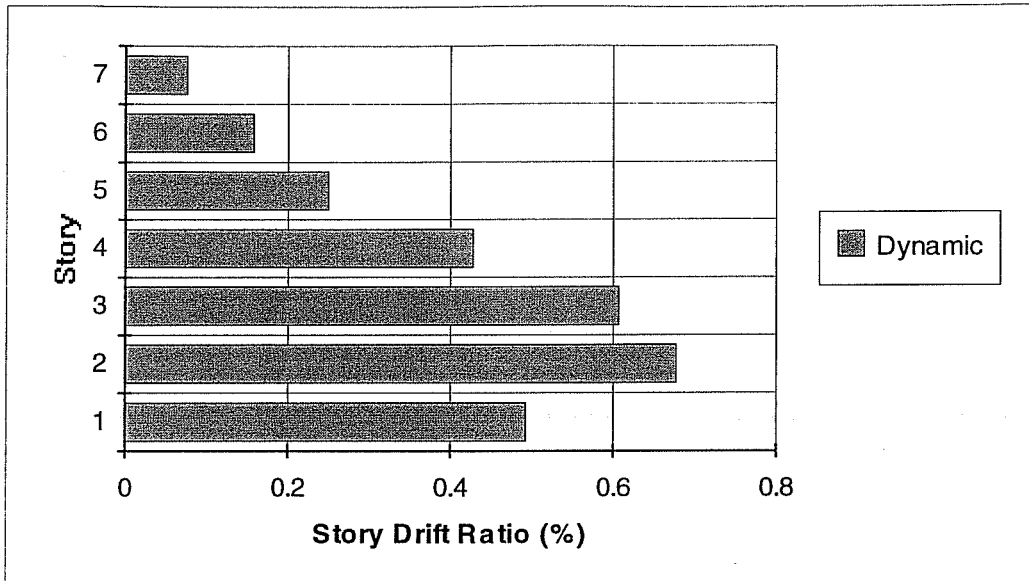
Figure 5.22 shows the calculated story drift ratio. As can be seen, story drift ratios were much smaller than those calculated from the 1994 Northridge Earthquake. In addition, all story drift ratios were less than half the limit specified in the NEHRP-94 Specifications⁹. Considering the extensive non-structural damage the building suffered after the 1971 San Fernando Earthquake, this drift limit recommended by NEHRP-94 cannot guarantee non-structural damage control. It is intended for

collapse prevention. The analytical inter-story drift ratios are higher at lower floors and explain why the most severe non-structural damage from the 1971 San Fernando Earthquake occurred at the second and third floors. The sixth and seventh floors suffered the least non-structural damage.



Ground motion:	1971 San Fernando Earthquake.
Damping coefficient:	5% of critical damping.
Material strength:	4/3 x (design values).
Effective stiffness $(EI)_{eff}$:	0.80(EI_g).
Residual shear capacity:	2/3 of original shear capacity.

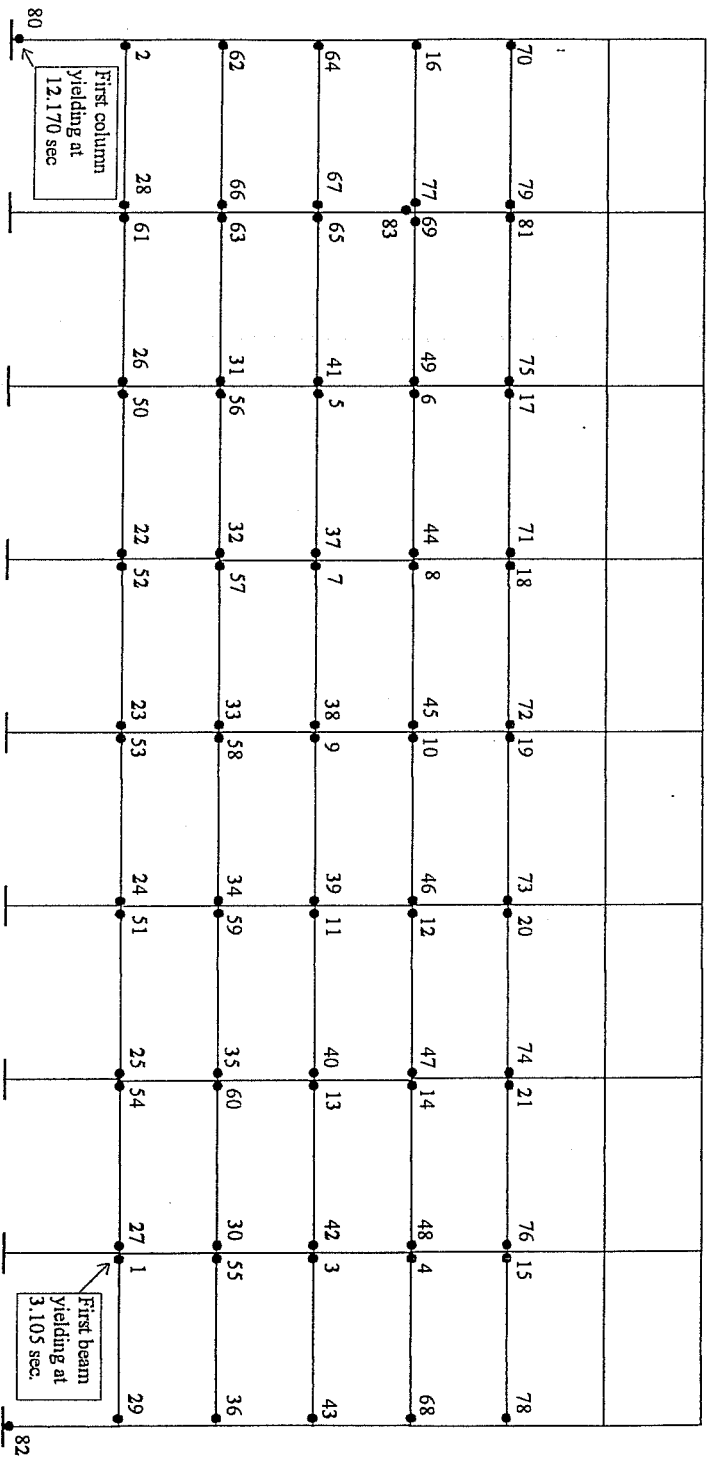
Figure 5.21 Comparison Between Calculated and Recorded 4th Floor Relative Displacement Time History under San Fernando Earthquake



Ground motion: 1971 San Fernando Earthquake.
 Damping coefficient: 5% of critical damping.
 Material strength: $4/3 \times$ (design values).
 Effective stiffness $(EI)_{eff}$: $0.80(EI_g)$.
 Residual shear capacity: $2/3$ of original shear capacity.

Figure 5.22 Calculated Story Drift Ratio for the Seven-Story Hotel under the 1971 San Fernando Earthquake

Figure 5.23 describes the calculated failure sequence of the building subject to the 1971 San Fernando Earthquake. After the 1971 San Fernando Earthquake, there were visible cracks at the second floor spandrel beam on the north side of the structure (Figure 3.25). Other cracks may have been hidden or closed after the earthquake. No columns failed in shear using the nonlinear time history analysis and none were observed in post earthquake investigations.



• yielding at member end.

- Ground motion: 1971 San Fernando Earthquake.
- Damping coefficients: 5% of critical damping.
- Material strength: $4/3 \times$ (design values).
- Effective Stiffness $(EI)_{eff}$: $0.80(EI_p)$.
- Residual shear capacity: $2/3$ of original shear capacity.

Figure 5.23 Calculated Failure Sequence for the Seven-Story Hotel under the 1971 San Fernando Earthquake

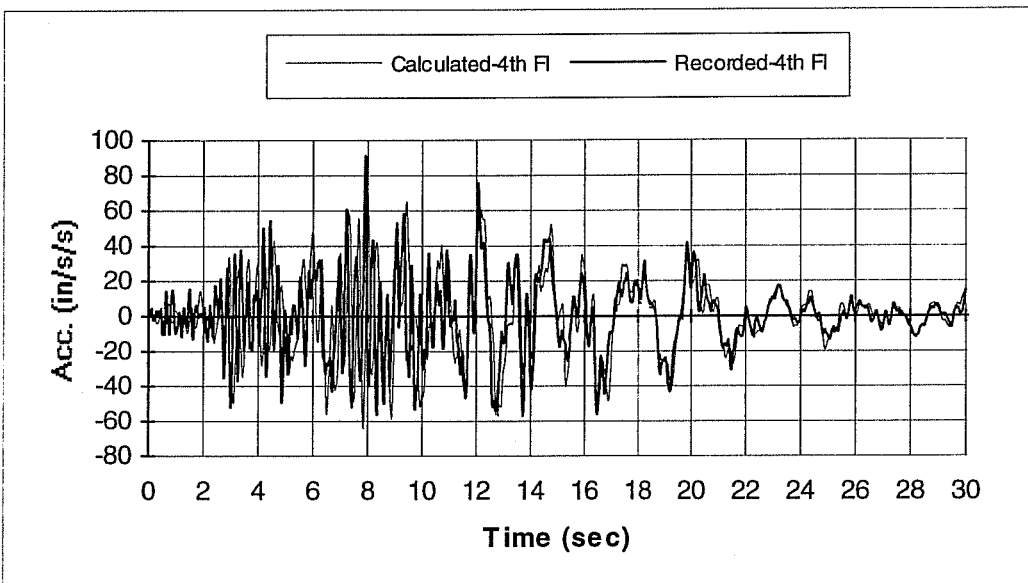
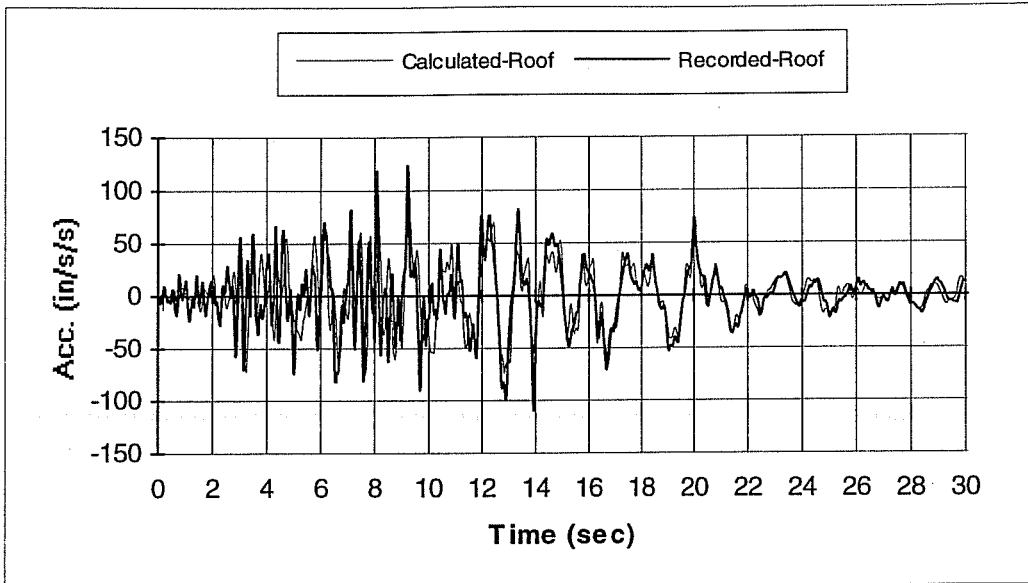
In Figure 5.24, the calculated and recorded absolute acceleration time histories at the roof and the 4th floor levels are compared. Once again, the general agreement is evident.

OPTION 2:

To pursue alternative ways of specifying effective stiffness, option 2 presented in the original DRAIN-2D users' guide³ was exercised. The effective stiffness in this option is determined by letting the equivalent member and actual member have the same tip displacement and tip rotation when the member yields at the end (Section 4.3.1.2). The results are compared in Figure 5.25.

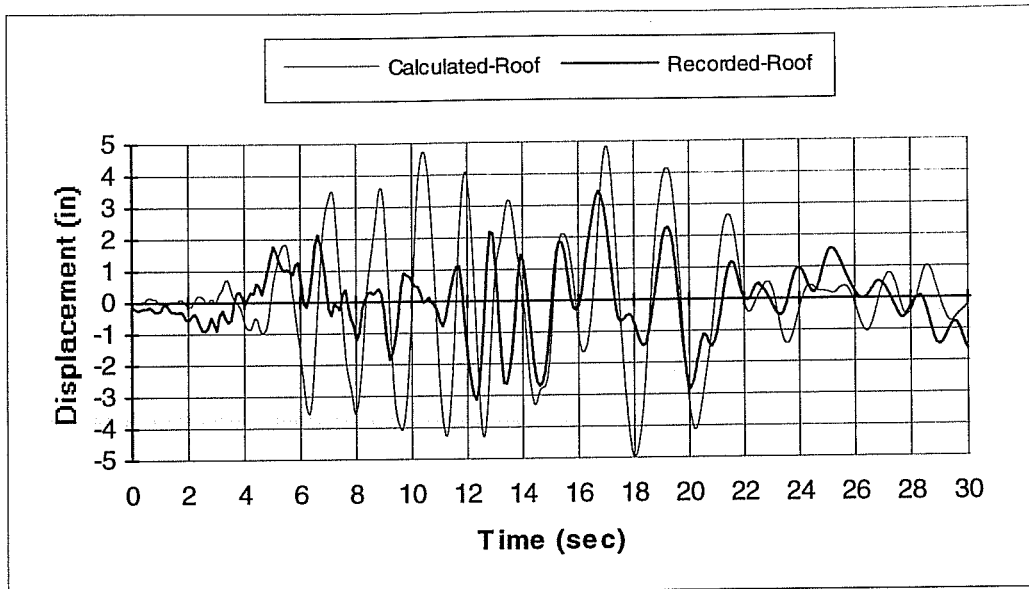
Obviously, the agreement between calculated and recorded roof relative displacement was poor using option 2. The calculated fundamental period of the structure was too long because the stiffness assigned to the member was too low. The equivalent condition set by option 2 was for member ends to reach yield. Under a moderate earthquake like the 1971 San Fernando Earthquake, many members in this building never reached yield.

Figure 5.26 shows comparisons between the calculated and recorded absolute acceleration time histories at the roof and the 4th floor levels using option 2.



Ground motion:	1971 San Fernando Earthquake.
Damping coefficient:	5% of critical damping.
Material strength:	4/3 x (design values).
Effective stiffness $(EI)_{\text{eff}}$:	0.80(EI_g).
Residual shear capacity:	2/3 of original shear capacity.

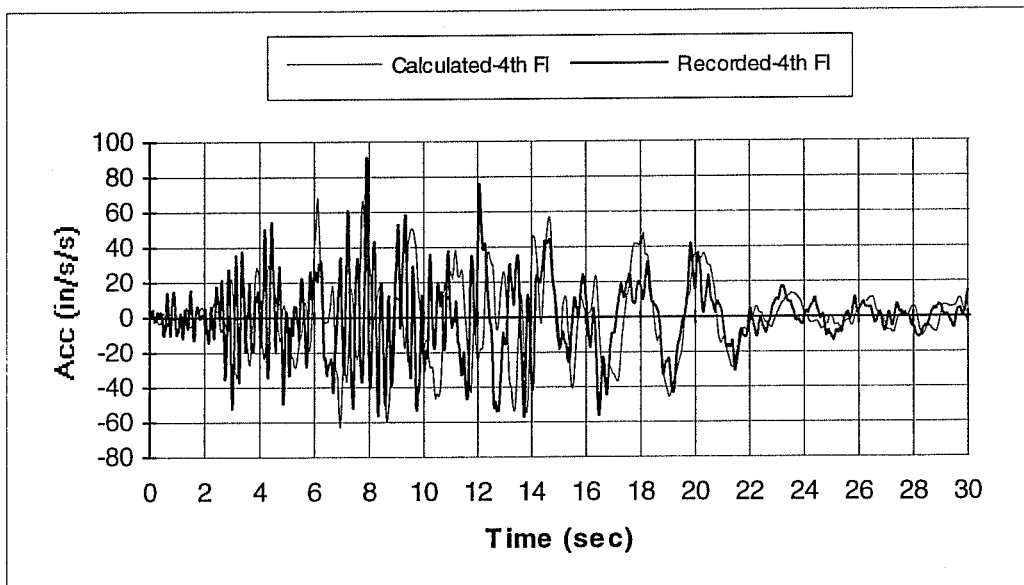
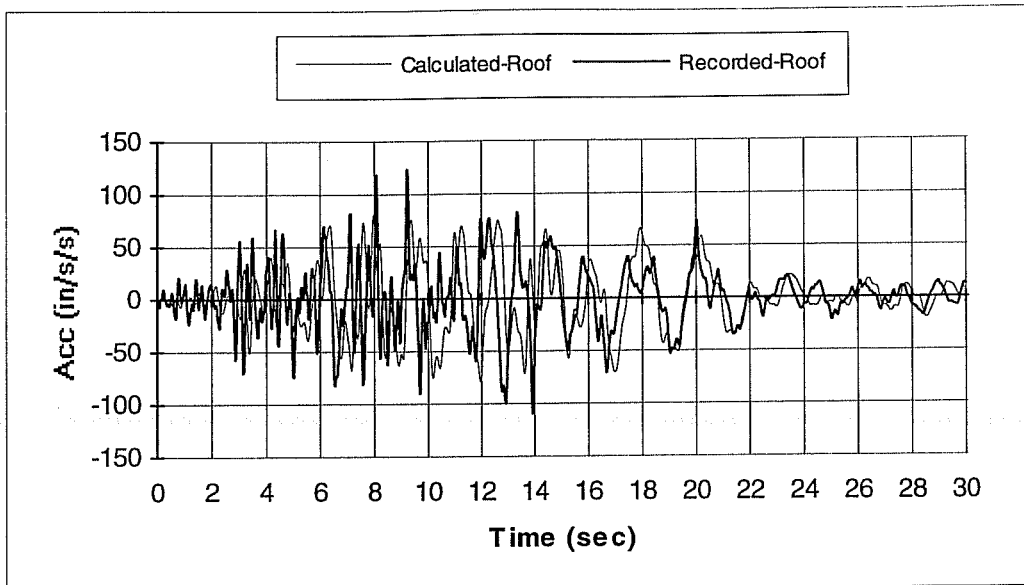
Figure 5.24 Comparison Between Calculated and Recorded Roof and 4th Floor Absolute Acceleration Time History under the 1971 San Fernando Earthquake



Ground motion:	1971 San Fernando Earthquake.
Damping coefficient:	5% of critical damping.
Material strength:	4/3 x (design values).
Effective stiffness $(EI)_{\text{eff}}$:	Option 2.
Residual shear capacity:	2/3 of original shear capacity.

Figure 5.25 Comparison Between Calculated and Recorded Roof Relative Displacement Time History under the 1971 San Fernando Earthquake using Option 2 for assigning member effective stiffness

Despite the large discrepancy between calculated and recorded roof displacement time history data, the calculated and recorded roof and the 4th floor absolute acceleration time history data show much less dramatic differences and indicate that the acceleration data are far less sensitive to stiffness than displacement data. Therefore displacement data are more valuable and more reliable in calibration and comparison for time history analyses.



Ground motion:	1971 San Fernando Earthquake.
Damping coefficient:	5% of critical damping.
Material strength:	4/3 x (design values).
Effective stiffness $(EI)_{\text{eff}}$:	Option 2.
Residual shear capacity:	2/3 of original shear capacity.

Figure 5.26 Comparison Between Calculated and Recorded Roof and 4th Floor Absolute Acceleration Time History under the 1971 San Fernando Earthquake Using Option 2 for Assigning Member Effective Stiffness

5.3.2.2. IDARC Analyses

The following parameters were chosen to use in the IDARC analyses:

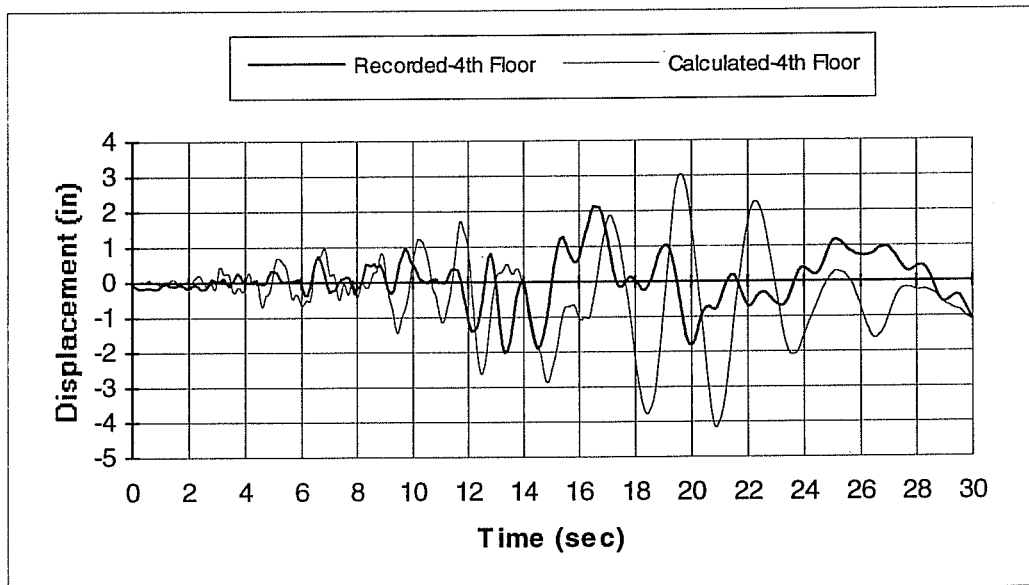
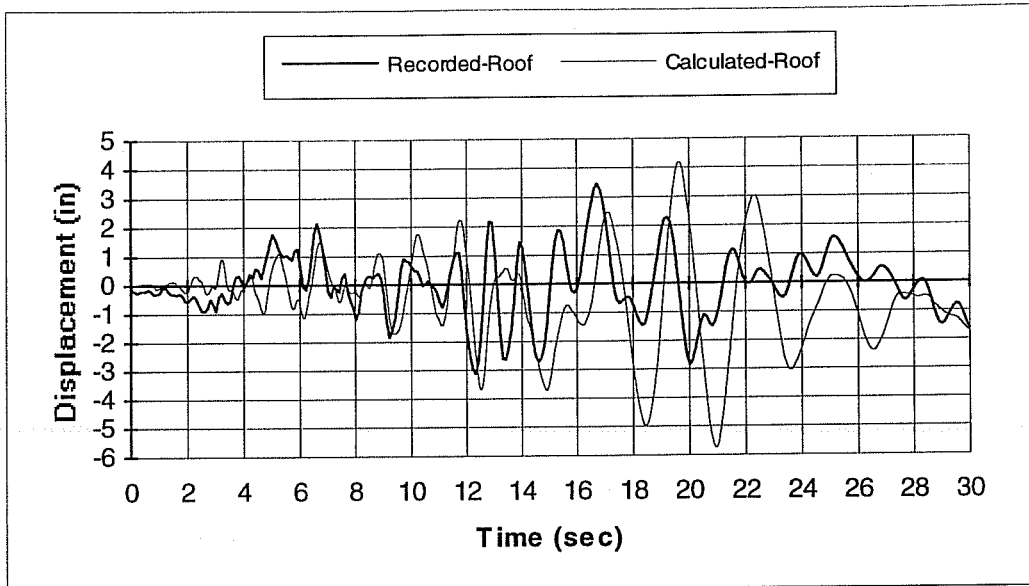
- (1) Damping coefficient: 5% of critical damping.
- (2) Material strength: Using the same argument as was used in Section 5.3.2.1 for DRAIN-2D analyses, $4/3$ x (design values) were used for both concrete and steel strengths.
- (3) Residual shear capacity: Shear failure was not taken into consideration.
- (4) Hysteretic modeling rules for beams and columns (Section 4.2.2.4):
 - Stiffness degrading parameter: $HC = 2.0$ (nominal degradation);
 - Strength deterioration parameter: $HBE = HBD = 0.0$ (no strength deterioration);
 - Slip control parameter: $HS = 0.5$ (nominal pinching).

As in DRAIN-2D analyses, part of the slab adjacent to the beam was assumed to contribute to the stiffness and strength of the beam. ACI 318-95 Code Sections 8.10.2 and 8.10.3 were used to determine the width of slab as a T-beam flange. In addition, the longitudinal reinforcement in the slab within the flange width (2#6) was added to beam top reinforcement. The same integration time step (0.005 seconds) used in DRAIN-2D was again used here. Hysteretic envelopes for beams and columns were generated by the program using a pre-processor.

In Figure 5.27, the calculated and the recorded relative displacement time histories at the roof and the 4th floor using parameters defined above are compared. The correlation between calculated and recorded responses was not as good as that obtained using DRAIN-2D analyses. Figure 5.28 shows the direct output plot by IDARC for the final failure state of the building. Although the failure predicted was consistent with the observed damage level and the results obtained from DRAIN-2D analyses, the roof maximum relative displacement predicted by the IDARC analysis was off by 67%, and the 4th floor maximum relative displacement was off by 95%. Lack of agreement in the general shape of the response trace is obvious. Different parameter values were tried to improve the results, but the change was minor.

5.4 Ten-Story Building in the Whittier Narrows Earthquake

The building was analyzed in the north-south (longitudinal) direction. In this direction, the lateral load resisting system consisted of two exterior spandrel beam-column perimeter frames and two interior slab-column frames (Figure 3.30). The building was modeled as a two-dimensional structure. The floor diaphragm was assumed to be infinitely rigid so the nodes within each floor level deformed the same amount laterally. The columns were assumed fixed at basement level.



Ground motion: 1971 San Fernando Earthquake.
 Damping coefficient: 5% of critical damping.
 Material strength: $4/3$ x (design values).
 Hysteretic modeling rules: $HC = 2.0$, $HBD = HBE = 0.0$, $HS = 0.5$

Figure 5.27 Comparisons Between Calculated and Recorded Roof and 4th Floor Relative Displacement Time History under the 1971 San Fernando Earthquake using IDARC

NOTATION:
 - = BEAM
 | = COLUMN
 x = CRACK

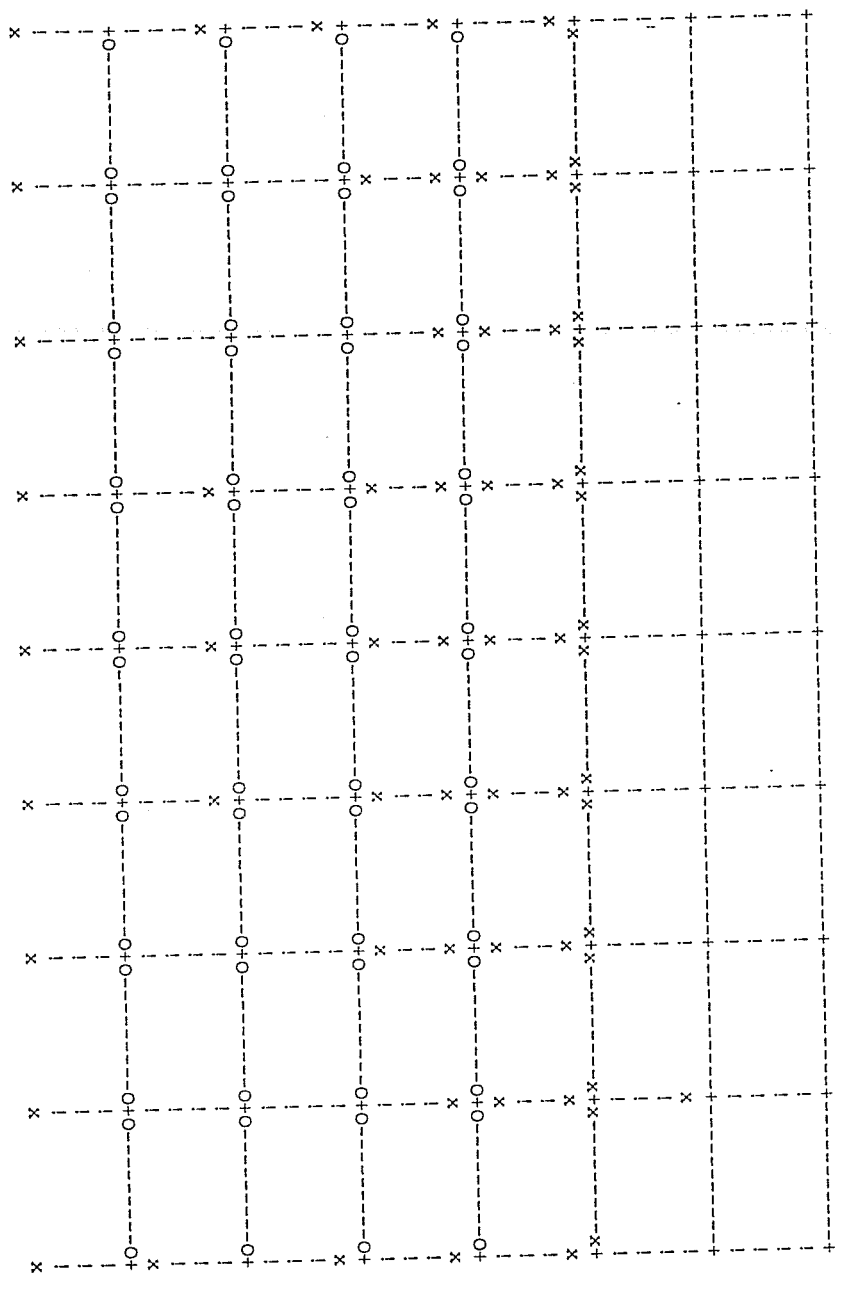


Figure 5.28 Failure State of the Seven-Story Hotel Subject to the 1971 San Fernando Earthquake from IDARC Calculation

Figure 5.29 shows the structural model for nonlinear dynamic analyses. For the exterior frame, slabs were assumed to interact with spandrel beams. The width of slabs adjacent to beams was determined using ACI 318-95 code provisions in Sections 8.10.2 and 8.10.3⁶⁹ for strength consideration. In calculating stiffness of the beam, the flange width was taken as an average of the T-beam section and the rectangular beam section to take into account positive and negative moment effects along the beam. For interior slab-column frames, previous research⁷⁰ on flat-plate frame buildings suggested that the use of an effective width based on elastic plate theory significantly overestimates the stiffness of the structure for drift ratios higher than 0.0025%. In order to account for the stiffness of the slab at large lateral drifts, an equivalent width of 36 inches, equal to $C + 3h$ (where C = column width and h = slab thickness) was recommended for this structure⁴⁹.

Slab longitudinal reinforcement within the flange width was considered as part of beam longitudinal reinforcement. Because slab reinforcement was not shown in the building information collected, it was redesigned using UBC-70⁷³, the code used for the design of this building. From the calculation, 1#4 was included in the calculation of exterior spandrel beam strength, and 3#4 were considered as interior beam reinforcement.

Because of the problems experienced with IDARC, only DRAIN-2D was used for the nonlinear dynamic time history analyses for this building.

Exterior Frame

Interior Frame

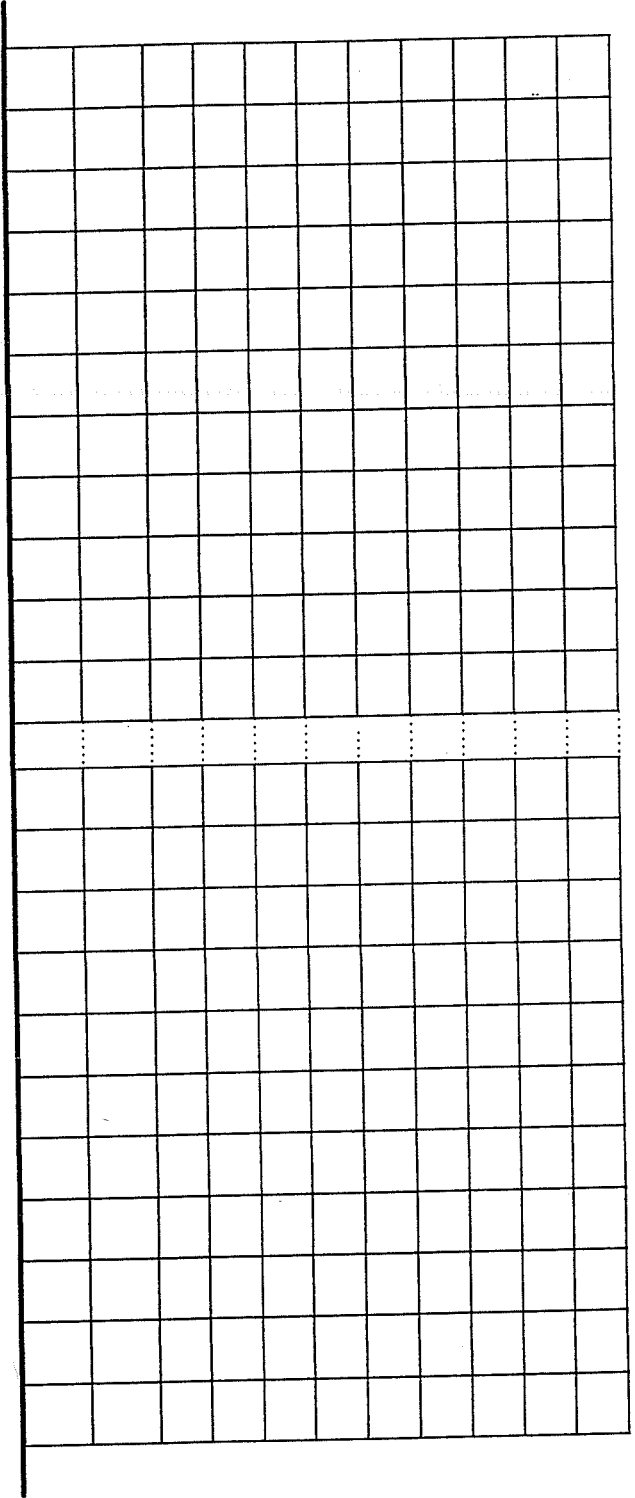


Figure 5.29 Structure Model for the Ten-Story Building

5.4.1 Evaluation of Response Records

Although the earthquake lasted about 30 seconds, the duration of strong ground motion was only about 4 seconds (Figure 3.34). Figure 5.30 shows relative displacement time history data recorded at the 10th and 5th floor levels. The period of vibration, during the strong motion part of the earthquake, appeared to be around 1.4 seconds and remained about the same thereafter. The structure response did not indicate significant changes in stiffness and is consistent with the results of an inspection of the building which indicated no visual damage to the structure.

Because there was only one sensor at each floor level, no torsional effects can be evaluated. However, the sensors at the 5th and the 10th floor were located very close to the torsional center of the building in the longitudinal direction. Therefore, the response in the longitudinal direction should not be influenced significantly by torsional effects.

5.4.2 Analysis Results

The procedure for choosing parameters was the same as outlined in Section 5.2.2. Only option 1 was used to assign the member effective stiffness.

- (1) Damping coefficient: 5% of critical damping was chosen as an average recommended value for reinforced concrete structures.

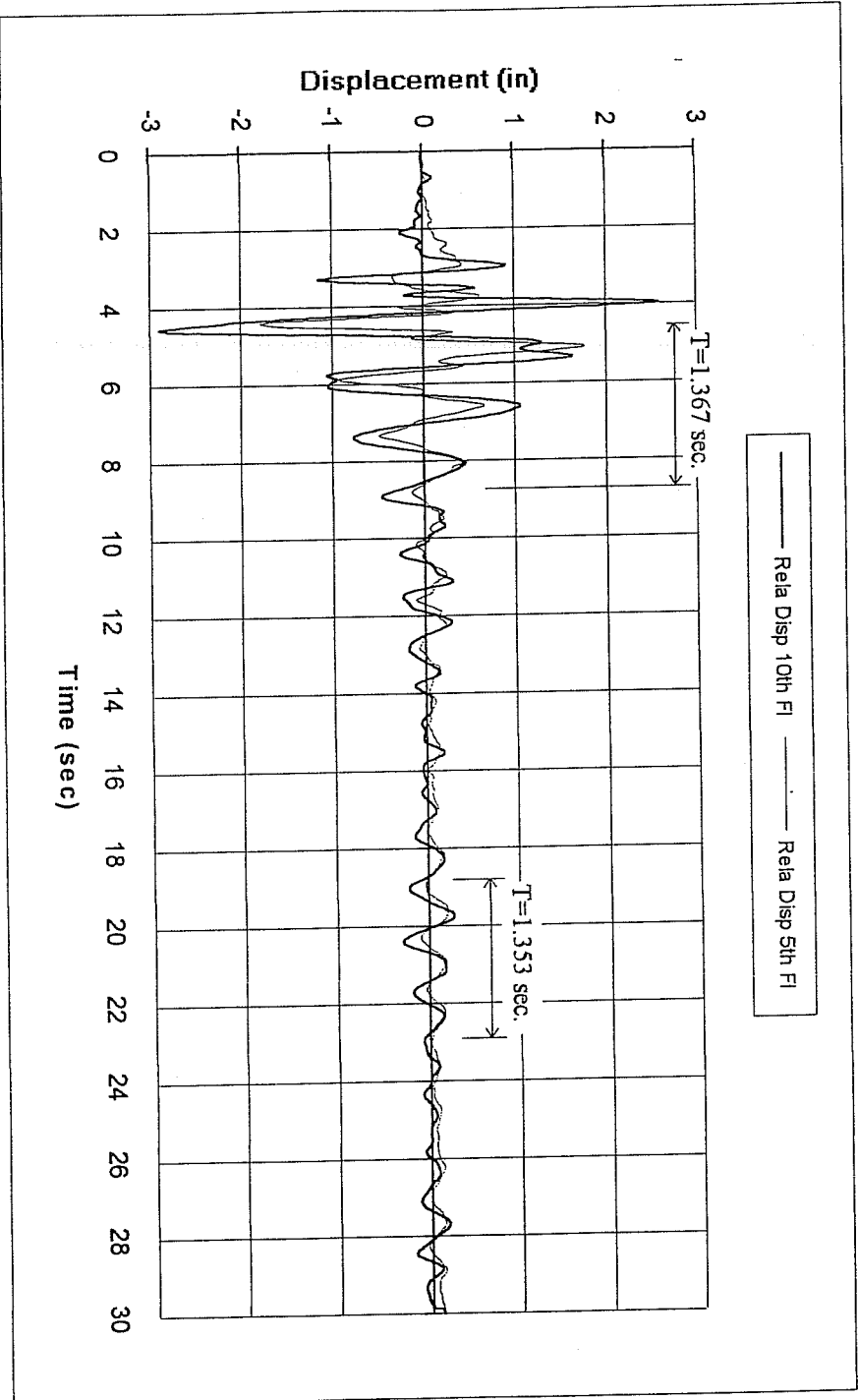


Figure 5.30 Recorded Floor Relative Displacement Time History
 in North-South (Longitudinal) Direction. 1987 Whittier Narrows Earthquake

- (2) Actual material strength: Considering the age of the building and the relatively moderate intensity of the earthquake, $4/3$ x (design values) were used for both concrete and steel strengths.
- (3) Effective stiffness: Effective stiffness was chosen so that the calculated response time history would match the recorded period of vibration. After several trials, $0.40(EI_g)$ was chosen as the effective stiffness $(EI)_{\text{eff}}$ for beams and columns.
- (4) Residual shear capacity: The structure sustained no shear failure of members. To facilitate calculations, however, $2/3$ of original shear capacity was chosen as the residual shear capacity.

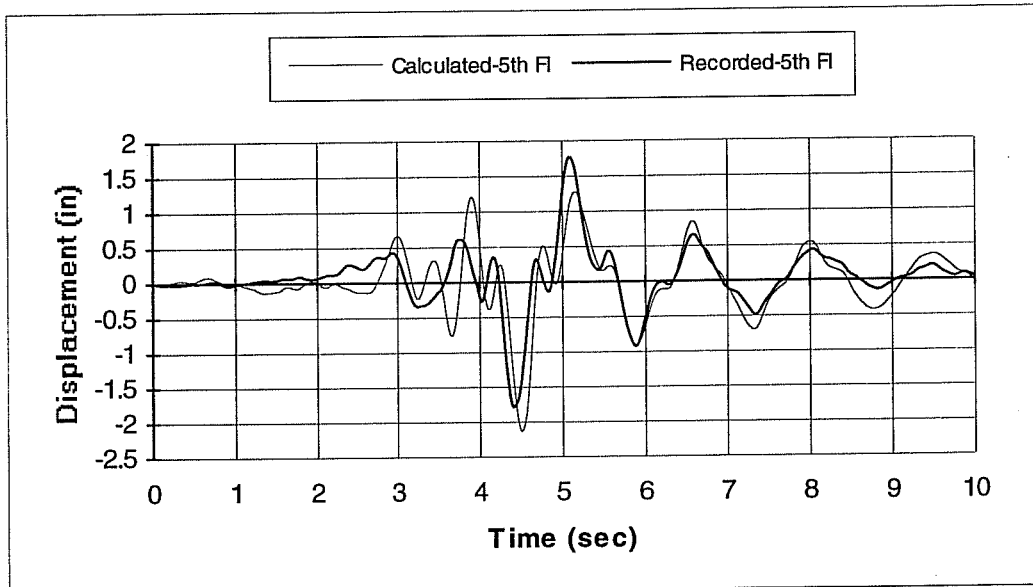
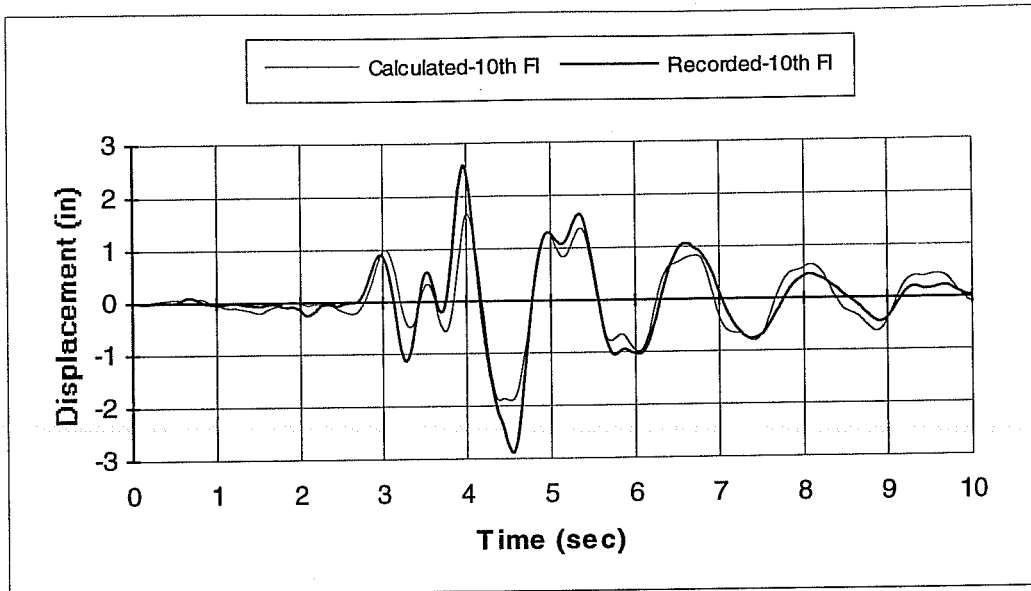
In Figure 5.31, the calculated and recorded relative displacement time histories at the 10th and 5th floor levels compare well.

Figure 5.32 shows the calculated story drift ratios. Compared with the drift ratios calculated for the seven-story hotel in the 1994 Northridge Earthquake, the story drift ratios are very small for this ten-story building in the 1987 Whittier Narrows Earthquake, and all floors meet the drift limit set by NEHRP-94 specifications. Because the first story is much taller than the rest of the stories in the building, it behaves as a soft story. Figure 5.32 shows a large inter-story drift ratio at the first story. Also from Figure 5.32, the inter-story ratios were larger in the 6th and

7th stories than in the 3rd and 4th stories, which clearly suggested participation of higher mode effects in the building response.

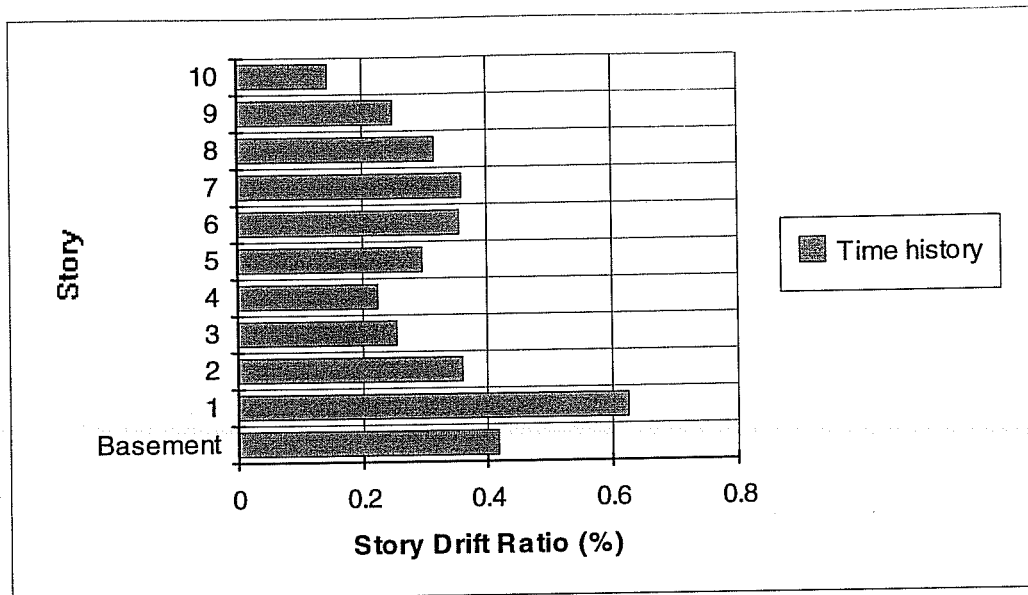
From the dynamic analysis, not only was there no shear failure in the columns, but there was no yielding at the ends of beams and columns. These results are consistent with the building condition after the earthquake.

Figure 5.33 shows a comparison of the calculated absolute acceleration time histories with the recorded absolute acceleration time histories at the 10th and the 5th floor levels, respectively. The agreement between calculated and recorded data is reasonably good, and, in particular, agreement at the 10th floor is better than at the 5th floor.



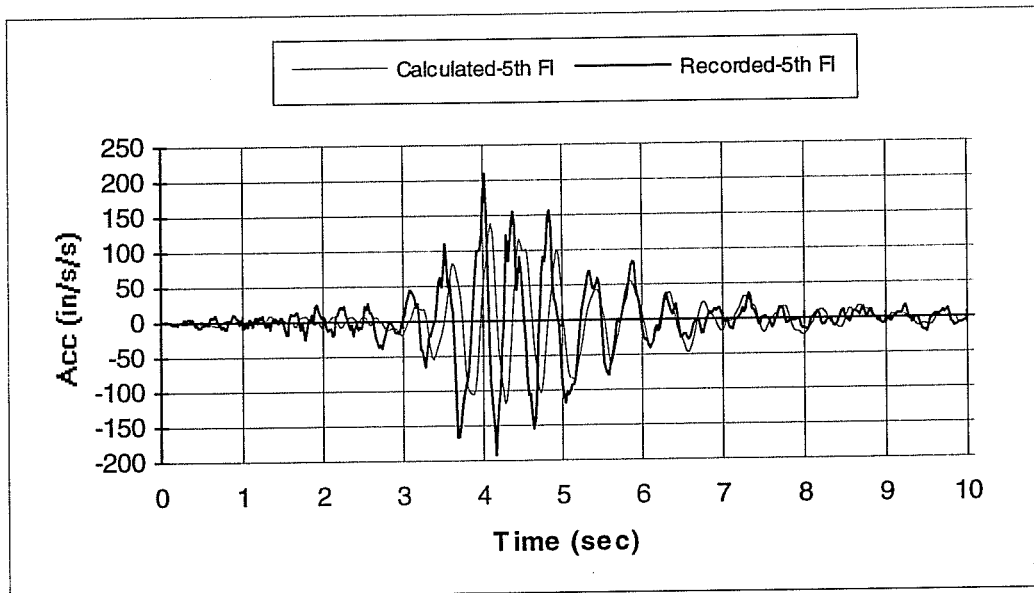
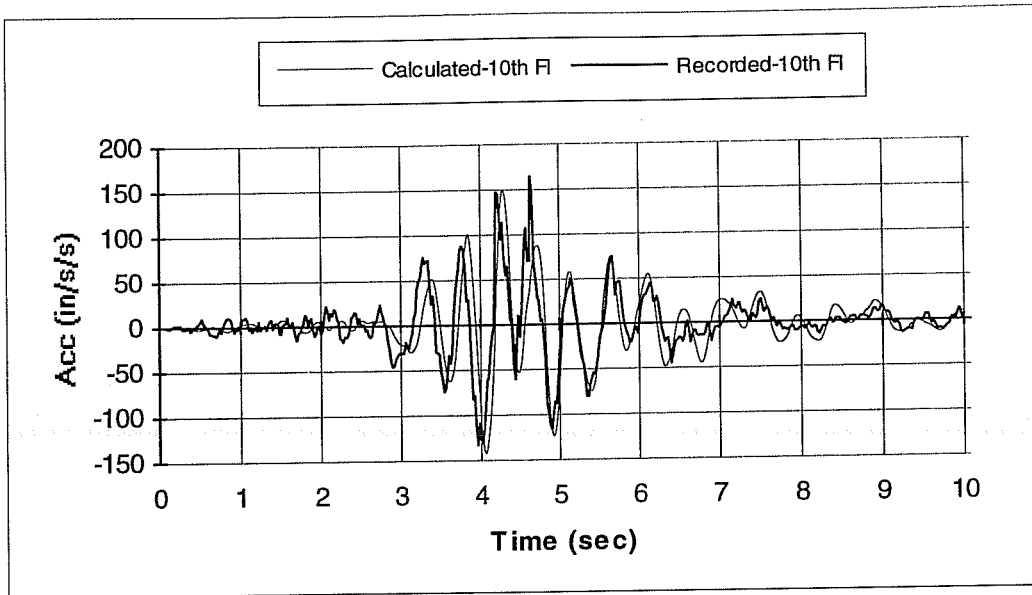
Ground motion:	1987 Whittier Narrows Earthquake.
Damping coefficient:	5% of critical damping.
Material strength:	$4/3 \times$ (design values).
Effective stiffness $(EI)_{eff}$:	$0.40(EI_g)$.
Residual shear capacity:	$2/3$ of original shear capacity.

Figure 5.31 Comparison Between Calculated and Recorded 10th and 5th Floor Relative Displacement Time History during 1987 Whittier Narrows Earthquake



Ground motion: 1987 Whittier Narrows Earthquake.
 Damping coefficient: 5% of critical damping.
 Material strength: $4/3$ x (design values).
 Effective stiffness $(EI)_{\text{eff}}$: $0.40(EI_g)$.
 Residual shear capacity: $2/3$ of original shear capacity.

Figure 5.32 Calculated Story Drift Ratios for the Ten-Story Building.
1987 Whittier Narrows Earthquake



Ground motion:	1987 Whittier Narrows Earthquake.
Damping coefficient:	5% of critical damping.
Material strength:	$\frac{4}{3}$ x (design values).
Effective stiffness $(EI)_{\text{eff}}$:	$0.40(EI_g)$.
Residual shear capacity:	$\frac{2}{3}$ of original shear capacity.

Figure 5.33 Comparison Between Calculated and Recorded Absolute Acceleration Time History at the 10th and 5th Floor. 1987 Whittier Narrows Earthquake

CHAPTER 6 NONLINEAR STATIC (PUSH-OVER) ANALYSES

6.1 General

In lieu of nonlinear dynamic time history analyses for structural seismic design and evaluation, an alternative procedure, the nonlinear static (push-over) analysis, was included in the “Guidelines for the Seismic Rehabilitation of Buildings”⁵. This procedure is described as follows:

- (1) Represent the structure in a two- or three-dimensional analytical model which includes all important linear and nonlinear behavior of the structure.
- (2) Apply lateral loads in patterns that represent approximately the relative inertial forces generated at each floor level.
- (3) Push the structure under these lateral loads to displacements that are larger than the maximum displacements expected in design earthquakes.

Figure 6.1 illustrates the push-over analysis procedure schematically. The push-over analysis provides a base shear vs. roof displacement relationship, and indicates the inelastic limit as well as lateral load capacity of the structure. The changes in slope of this curve give an indication of yielding of various structural elements.

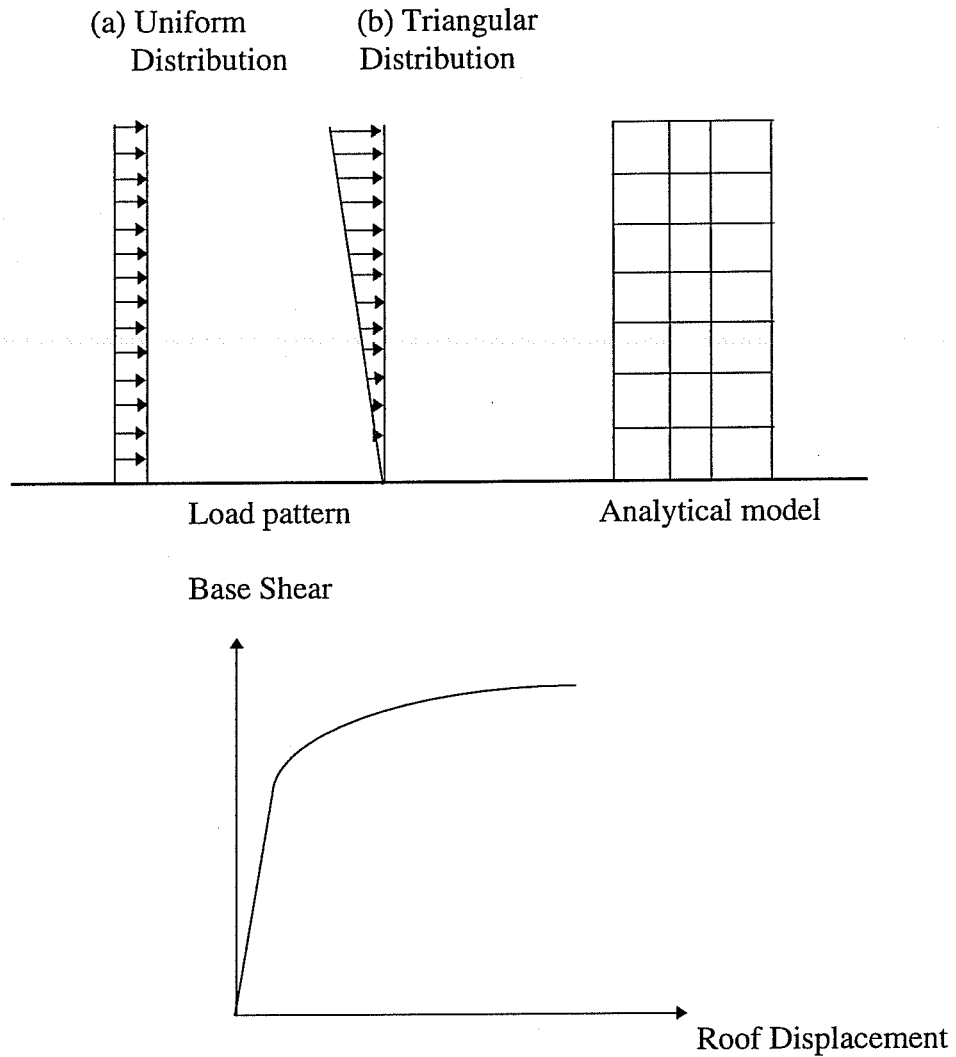


Figure 6.1 Push-Over Analysis Procedure

The objective of the push-over analysis is to estimate member forces and global as well as local deformation capacity of a structure. The information can be

used to assess the integrity of the structure. To evaluate the applicability of this simplified nonlinear analysis, two buildings analyzed in the previous chapter using nonlinear dynamic time history analyses were analyzed using push-over analyses. The strength and deformation capacity estimated using push-over analyses were compared with actual recorded strength and deformation capacity of the structures.

As in the dynamic analysis, gravity loads were applied to the structure as an initial load condition.

For consistency and for making comparisons, the same structural models used for dynamic time history analyses in Chapter 5 were used here for push-over analyses. Only program DRAIN-2D was used to perform push-over analyses.

6.2 Seven-Story Hotel

As in nonlinear time history analyses, the building was first analyzed by the push-over procedure with the material properties at the time of the 1994 Northridge Earthquake. Then the building was analyzed with the material properties at the time of the 1971 San Fernando Earthquake. Push-over results were compared with the corresponding nonlinear time history results. First, seismic design criteria according to current codes is given in the following section.

6.2.1 Current Seismic Design Criteria

According to UBC-94⁶, the seven-story hotel should be designed to resist the base shear:

$$\frac{V}{W} = ZIC / R_w \quad (6.1)$$

For this structure, $Z = 0.4$ (Zone 4);

$I = 1.0$ (Hotel);

$S_2 = 1.2$ (Soil type: 2);

$R_w = 5$ (Concrete ordinary moment frame).

So, $T = 0.030h^{3/4} = 0.03 \times 65.71^{3/4} = 0.69$ *seconds*

$$C = \frac{1.25S}{T^{2/3}} = \frac{1.25 \times 1.2}{0.69^{2/3}} = 1.92 < 2.75, \text{ OK.}$$

$$C/R_w = 1.92/5 = 0.384 > 0.075, \text{ OK.}$$

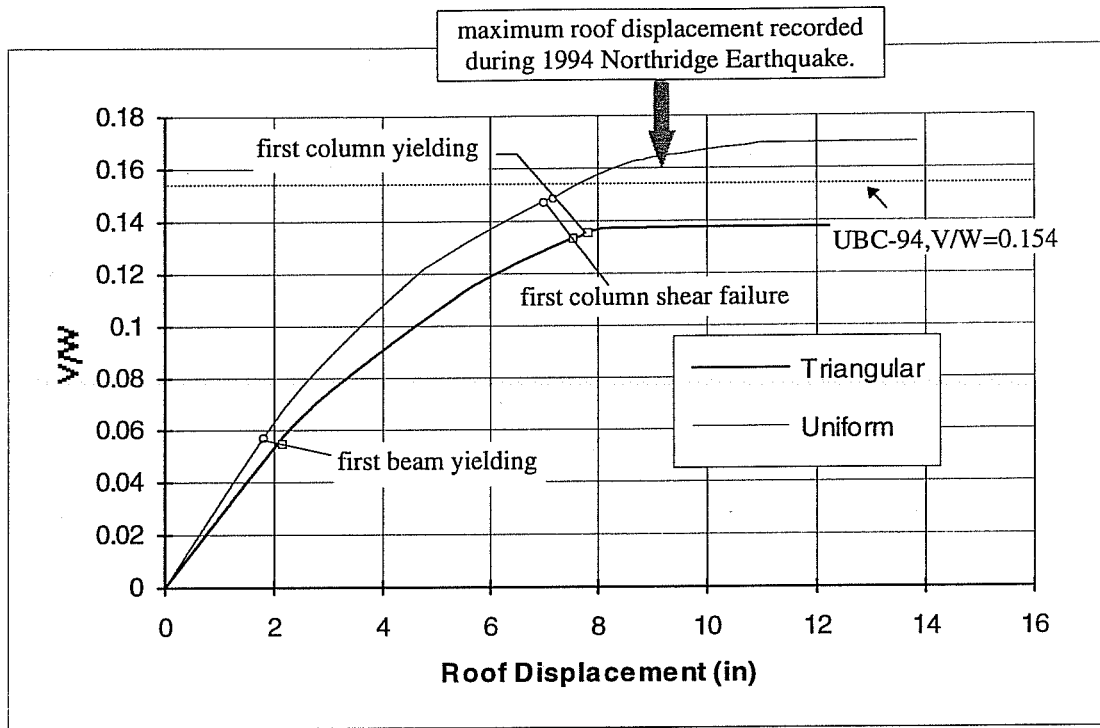
Therefore, $V/W = 0.157$.

6.2.2 1994 Northridge Earthquake

6.2.2.1 Loading Patterns

One of the questions regarding the push-over analysis is the sensitivity of results to the applied load pattern. Load patterns are intended to represent the distribution of inertial forces of design earthquakes. Since no two earthquakes have the same distribution of inertial forces, and the distribution changes with time during an earthquake, a load pattern that follows time variant distribution of inertia forces would be ideal. However, due to extra efforts required, simplified loading patterns are generally employed. Two commonly used loading patterns, namely the uniform distribution pattern and the triangular distribution pattern as shown in Figure 6.1 were studied. The triangular load distribution pattern is generally considered to reflect some higher mode effects in earthquakes.

Figures 6.2 shows (base shear V)/(weight of building W) vs. roof displacements with uniform and triangular load distribution patterns, respectively. The same parameters: $0.30(EI_g)$ as effective stiffness $(EI)_{\text{eff}}$, $3/2$ x (design values) as actual material strength, and $2/3$ of original shear capacity as residual shear capacity, were used.



Material strength: $3/2$ x (design values).
 Effective stiffness $(EI)_{eff}$: $0.30(EI_g)$.
 Residual shear capacity: $2/3$ of original shear capacity.

Figure 6.2 (Base shear V)/(Weight of building W) vs. Roof Displacement for the Uniform and Triangular Load Distribution Patterns

Also indicated on these plots is the maximum roof relative displacement recorded during the 1994 Northridge Earthquake. Push-over analyses successfully predicted that the structure almost lost its lateral load resisting capacity and shear failures of a column occurred at this displacement level.

Base shear V was calculated by summing all applied lateral forces above the ground level, and the weight of the building W was calculated by summing all

gravity loads on each floor without load factors. Because DRAIN-2D utilizes a force-control method for push-over analyses, no capacity can be calculated beyond the peak strength. So, for a uniform lateral load pattern, at a roof displacement of 10 inches, or at (V/W) of 0.167, the structure has failed. For a triangular pattern, at a roof displacement of 8 inches, or at (V/W) of 0.137, the structure failed. Therefore, from different lateral load patterns, push-over analyses indicated differences in displacement and strength capacities. A triangular pattern results in 25% less capacity in displacement and 22% less capacity in strength at structural failure than a uniform pattern.

Also shown in Figure 6.2 is the base shear coefficient obtained following UBC-94 in Section 6.2.1.1. According to UBC-94, the building is adequate under a uniform load pattern, and inadequate under a triangular load pattern. Since the building almost collapsed during the 1994 Northridge Earthquake, the UBC-94 shear approach predicted the capacity of the building reasonably well, and a triangular lateral load pattern should be considered as a more critical loading pattern for push-over analyses.

Figures 6.3 and 6.4 show the failure sequence from push-over analyses using uniform and triangular lateral load patterns, respectively. Calculation terminated at $(V/W) = 0.170$, and 0.138 for the uniform and the triangular lateral load pattern, respectively. At higher values, the structure deflected without bound with only a

small increase in lateral forces. The structure was considered to reach failure at these values. From Figures 6.3 and 6.4, the structure follows quite different failure sequences for uniform and triangular load patterns. The triangular load pattern predicts a failure sequence very close to the observed damage state of the building and to the result obtained from nonlinear time history analyses (Figure 5.16).

The maximum story drift ratios using a uniform load pattern and a triangular load pattern are plotted in Figure 6.5. Again, in Figure 6.5, maximum inter-story drift ratios were quite different for the two different load patterns. For the uniform load pattern inter-story displacement was concentrated in lower floor levels, while for the triangular load pattern inter-story displacement was concentrated in middle floor levels. Higher mode effects were better represented using a triangular load pattern. From actual damage that occurred in the building, the push-over analysis with the triangular load pattern definitely predicted the response of this building under the 1994 Northridge Earthquake better than the analysis with the uniform load pattern.

Since the maximum recorded relative displacement at the roof during the 1994 Northridge Earthquake was 9.2 inches, the inter-story drift ratios when the roof displacement reached 9.2 inches in the push-over analyses were computed. Figure 6.6 shows the drift ratios calculated for the uniform and triangular load patterns. Also plotted in the figure are the maximum drift ratios from the nonlinear dynamic analyses as well as from the recorded data. As can be seen, the triangular load values

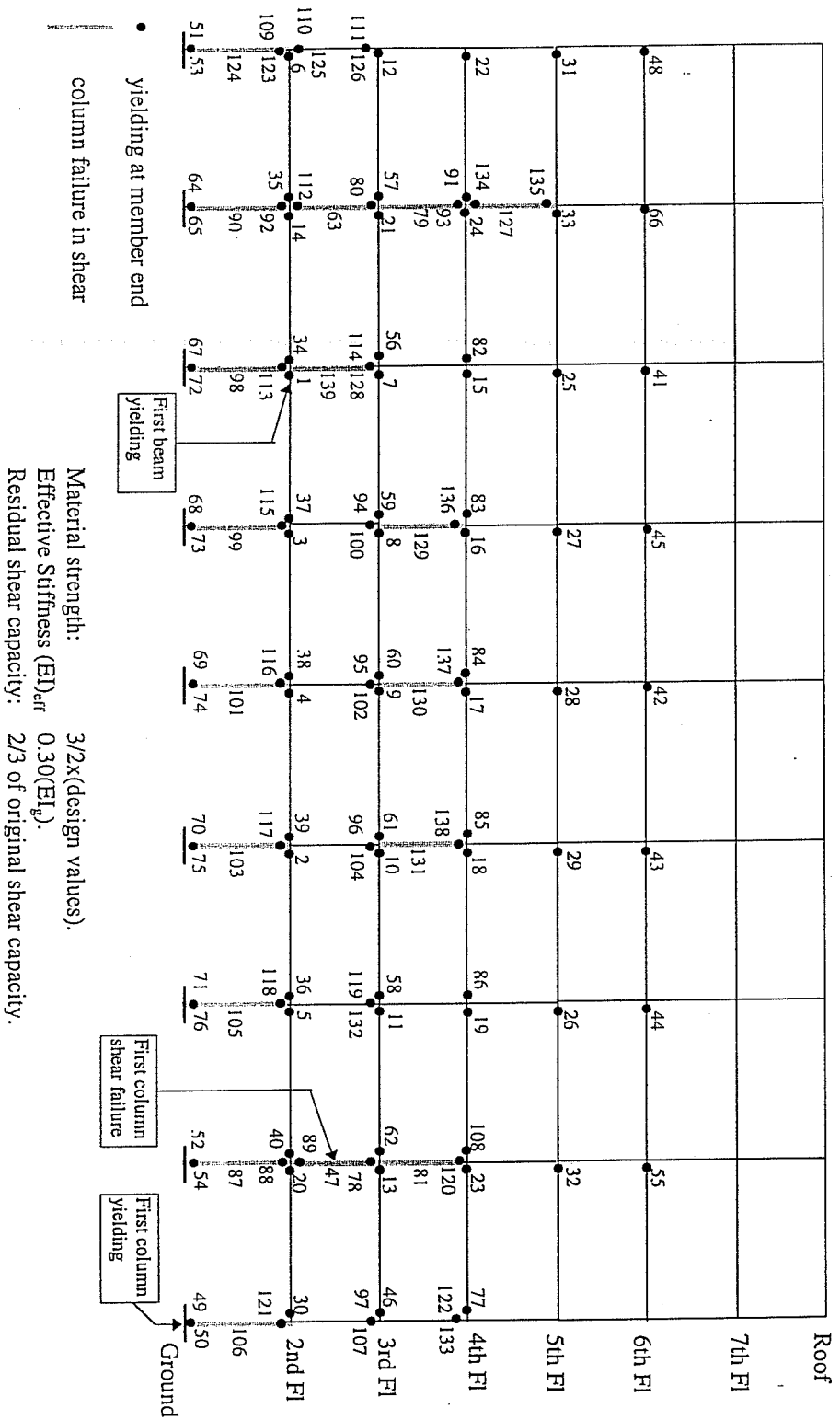


Figure 6.3 Failure Sequence from Push-Over Analysis with Uniform Lateral Load Distribution

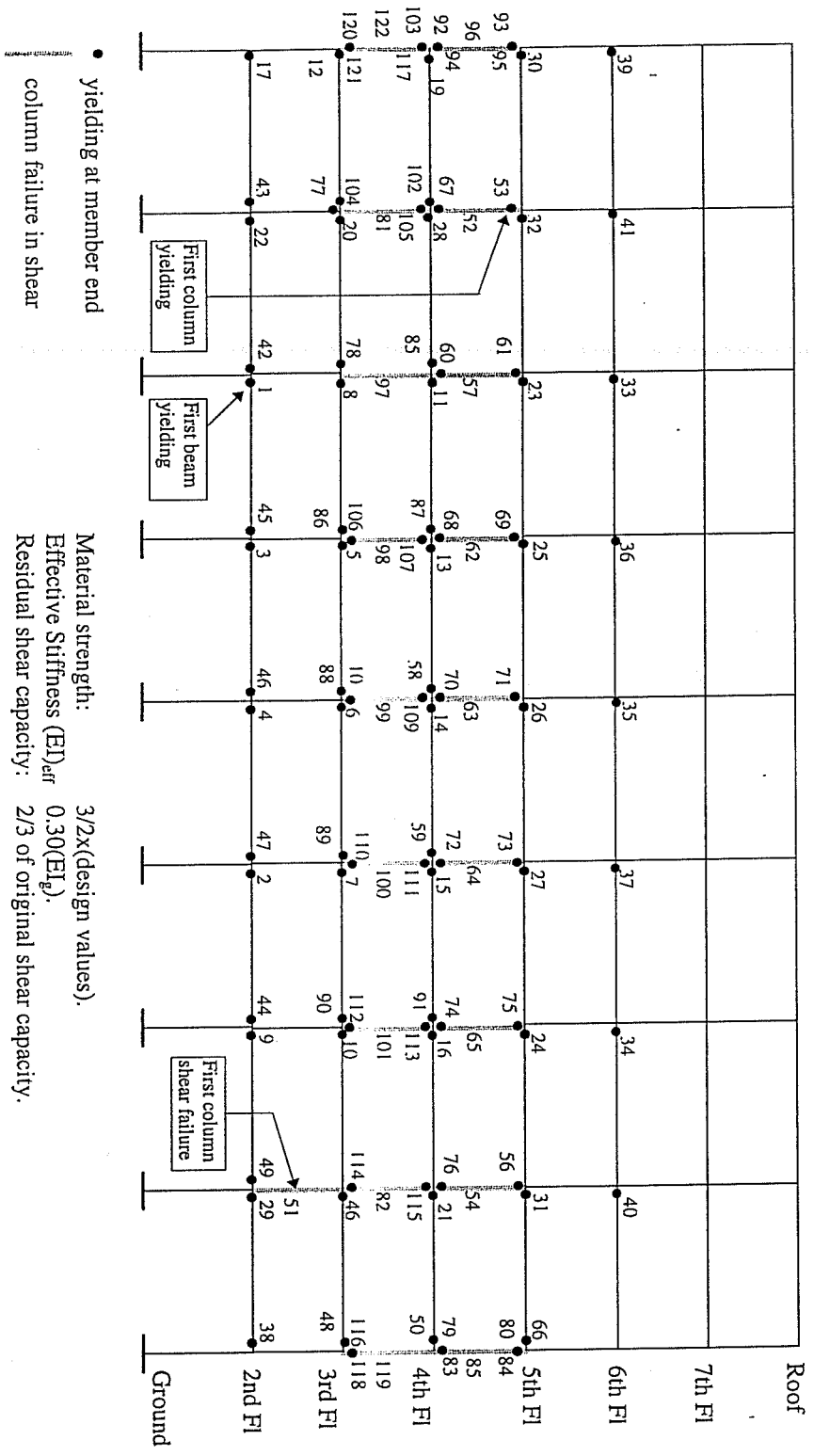
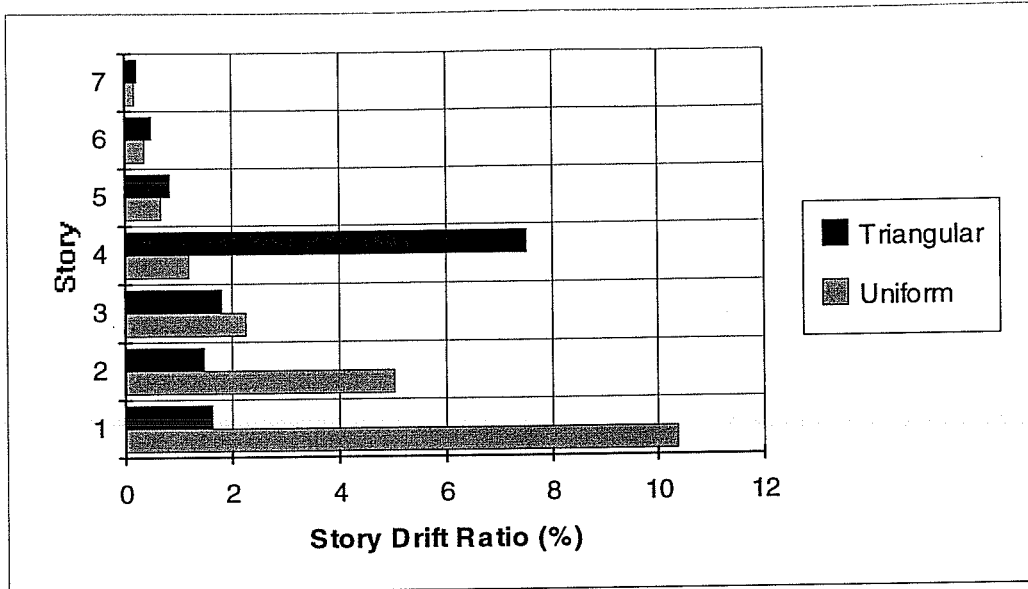


Figure 6.4 Failure Sequence from Push-Over Analysis with Triangular Lateral Load Distribution



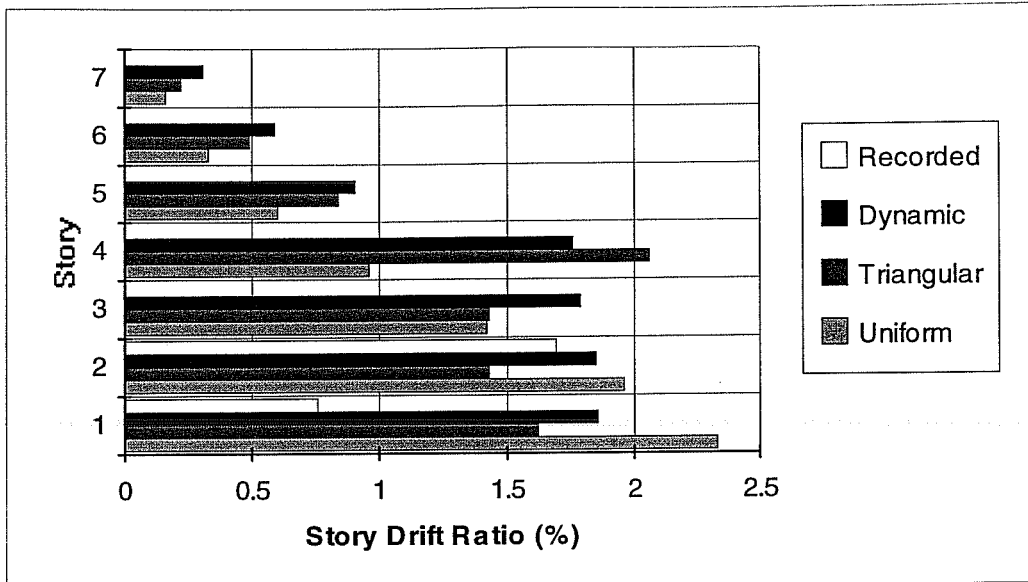
Material strength: $3/2$ x (design values).
 Effective stiffness $(EI)_{eff}$: $0.30(EI_g)$.
 Residual shear capacity: $2/3$ of original shear capacity.

Figure 6.5 Maximum Story Drift Ratios for Different Load Patterns

and the dynamic analysis results compare reasonably well in all stories, but are much larger than the observed values at the first story and are quite close at the second story.

6.2.2.2 Effects of Effective Stiffness $(EI)_{eff}$

The importance of effective stiffness has been demonstrated in dynamic time history analyses (Chapter 5). Here, again, effects of effective stiffness on push-over analyses were explored. Only Option 1 was used for assigning effective stiffness of structural elements in push-over analyses.

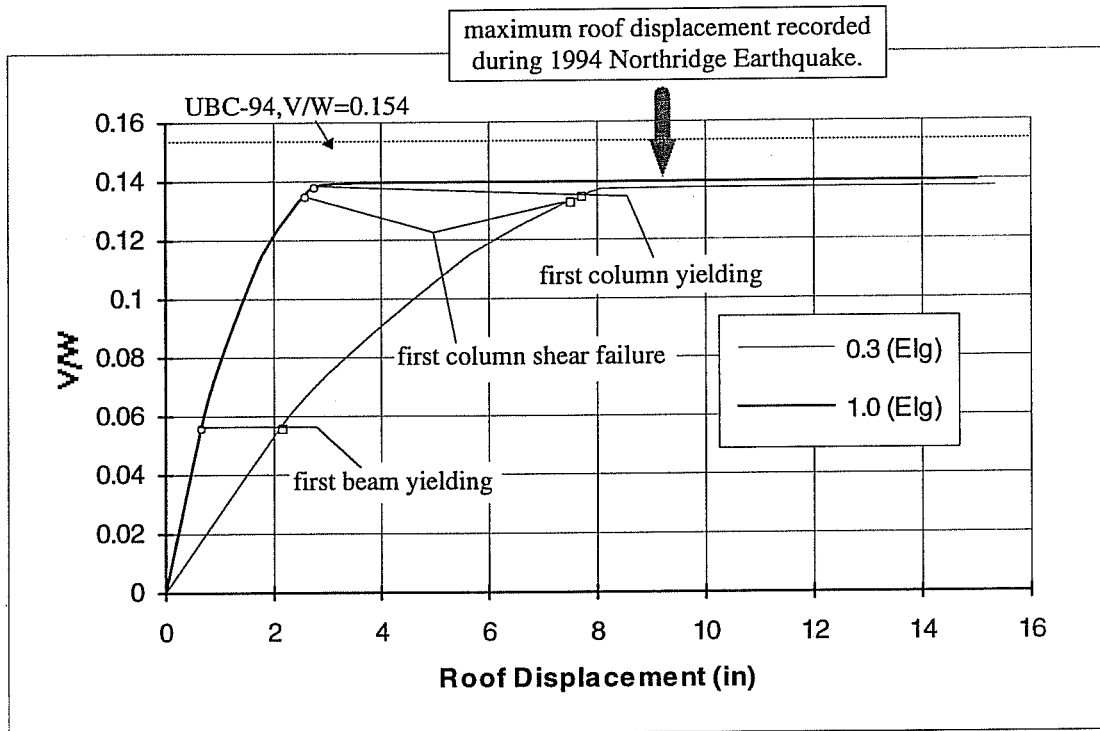


Ground motion: 1994 Northridge Earthquake.
 Damping coefficient: 5% of critical damping.
 Material strength: $3/2$ x (design values).
 Effective stiffness (EI_{eff}): $0.30(EI_g)$.
 Residual shear capacity: $2/3$ of original shear capacity.

Figure 6.6 Story Drift Ratios When Roof Relative Displacement Reaching Maximum Recorded Value For Different Load Patterns

Two different effective stiffnesses were included in the study, namely $0.30(EI_g)$ used in dynamic analyses and $1.0(EI_g)$ for gross section stiffness. Only a triangular load pattern was used for this comparison. Figure 6.7 shows the push-over analysis results using $1.0(EI_g)$ as effective stiffness. Also shown in the figure is the push-over analysis results using $0.3(EI_g)$ as effective stiffness for comparison. The different effective stiffness has a large effect on the results of the push-over analysis. The roof displacements of the building predicted by push-over analyses with different

effective stiffness values are significantly different, although strength (base shear) capacity remains almost the same.



Material strength: $3/2$ x (design values).
 Residual shear capacity: $2/3$ of original shear capacity.

Figure 6.7 (Base shear)/(Weight of building) vs. Roof Displacement with Triangular Load Pattern Using Different Effective Stiffnesses

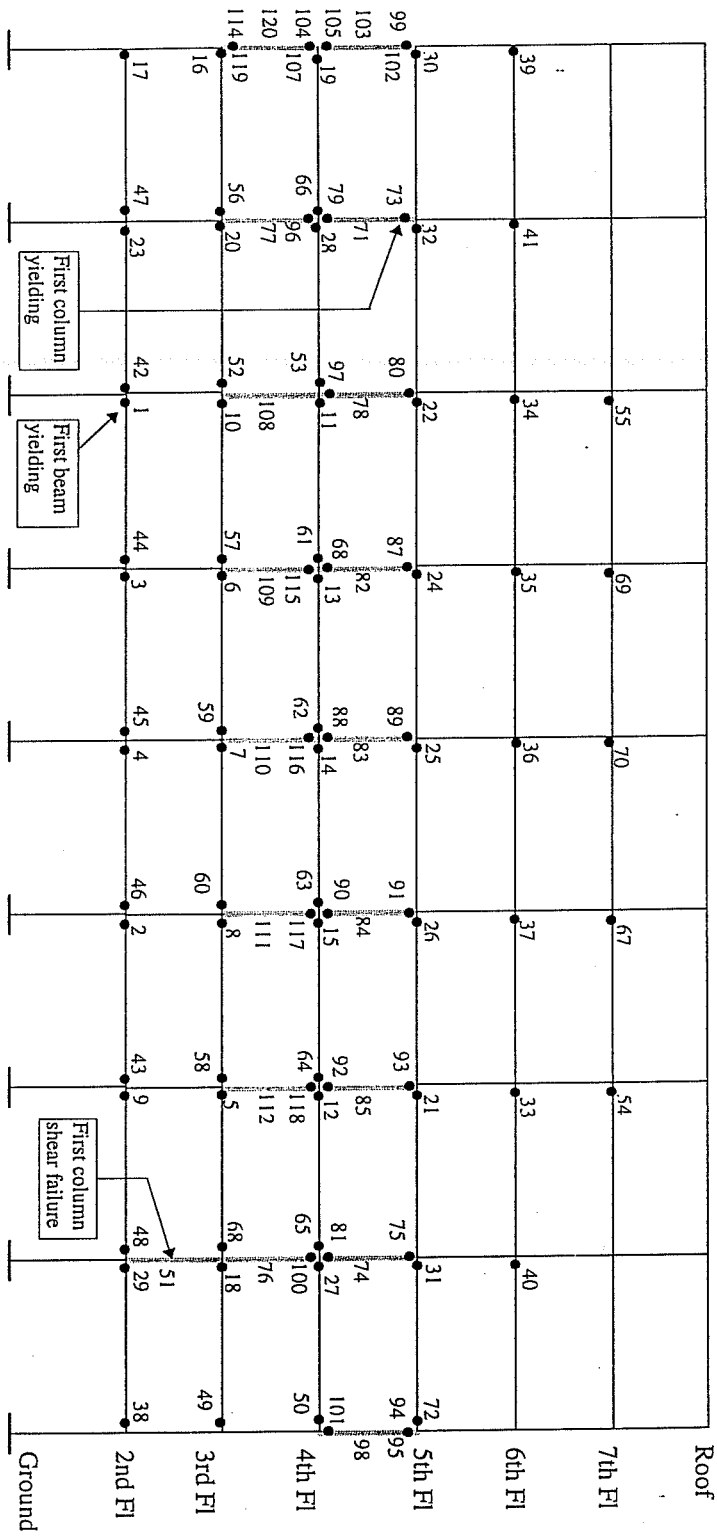
Figure 6.8 shows the failure sequence of the push-over analysis assuming $1.0(EI_g)$ as effective stiffness. Comparing Figure 6.8 with Figure 6.4, we can see that the failure sequence was almost the same with different effective stiffnesses. It is important to note that if the only objective of the push-over analysis is a

determination of capacity, stiffness is not important. However, for a design based on performance, particularly deformation response, large differences may be obtained unless stiffness is carefully considered.

6.2.3 1971 San Fernando Earthquake

This time, only effects of different loading patterns were explored, because the influence of different effective stiffness was expected to be the same for the same building. In Figures 6.9 the (base shear V)/(weight of building W) vs. roof relative displacement curves with uniform and triangular lateral load distribution patterns are plotted. The same parameters used in the 1971 San Fernando Earthquake: $0.80(EI_g)$ as effective stiffness $(EI)_{\text{eff}}$, $4/3$ x (design values) as actual material strength, and $2/3$ of original shear capacity as residual shear capacity, were used.

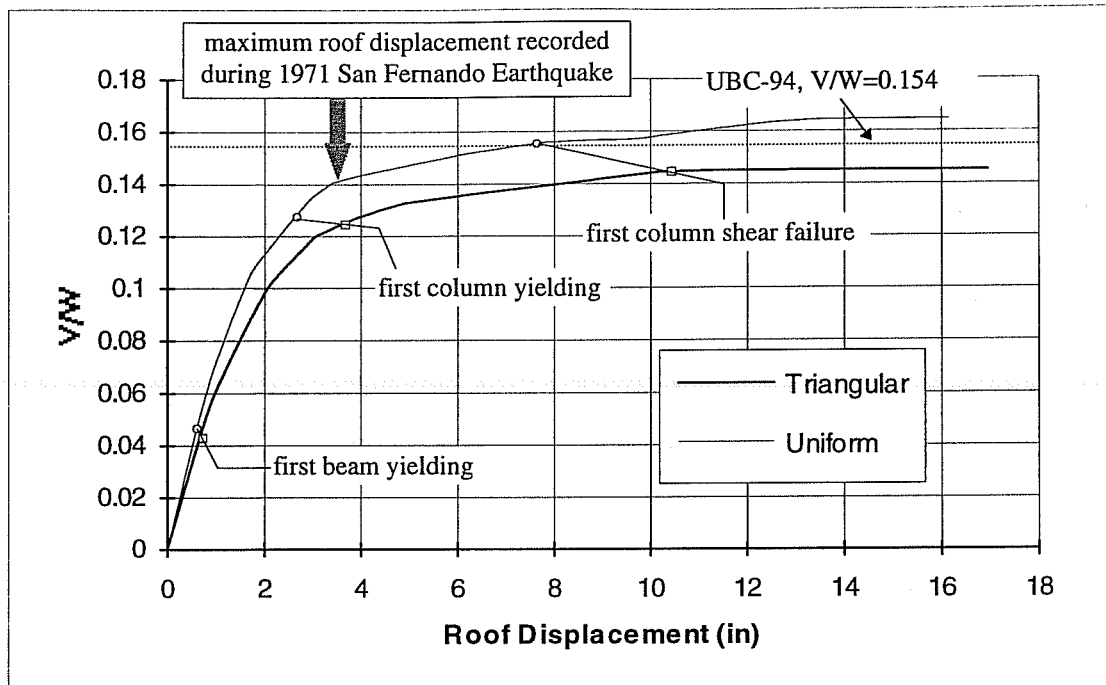
Once again, differences in V/W vs. roof displacement curves were noticeable, if not significant. The uniform lateral load pattern showed a little higher base shear capacity. The lateral deflection capacity predicted by these two different lateral load patterns was almost the same. In addition, the uniform lateral load pattern presented a little stiffer structure than the triangular pattern did. Also indicated on these figures was the actual recorded roof maximum relative displacement during the 1971 San Fernando Earthquake. Once again, push-over analyses successfully predicted that member yielding occurred, but no shear failure of columns occurred.



- yielding at member end
- column failure in shear

Material strength: $3/2 \times (\text{design values})$.
 Effective Stiffness $(EI)_{\text{eff}} = 1.0(EI_g)$.
 Residual shear capacity: $2/3$ of original shear capacity.

Figure 6.8 Failure Sequence from Push-Over Analysis with $1.0(EI_g)$ as Effective Stiffness



Material strength: $4/3$ x (design values).
 Effective stiffness $(EI)_{\text{eff}}$: $0.80(EI_g)$.
 Residual shear capacity: $2/3$ of original shear capacity.

Figure 6.9 (Base shear)/(Weight of building) vs. Roof Displacement for the Uniform and Triangular Load Distribution Patterns

In the 1971 San Fernando Earthquake, the maximum roof relative displacement was 3.4 inches. Figures 6.10 and 6.11 show the failure sequence of push-over analyses up to a roof displacement of 3.4 inches. Comparing these plots with the results from the dynamic analysis in Chapter 5 (Figure 5.23), the failure sequence predicted by push-over analyses with the triangular lateral load distribution pattern has a better agreement with the dynamic time history analysis results than the failure sequence predicted with the uniform load pattern.

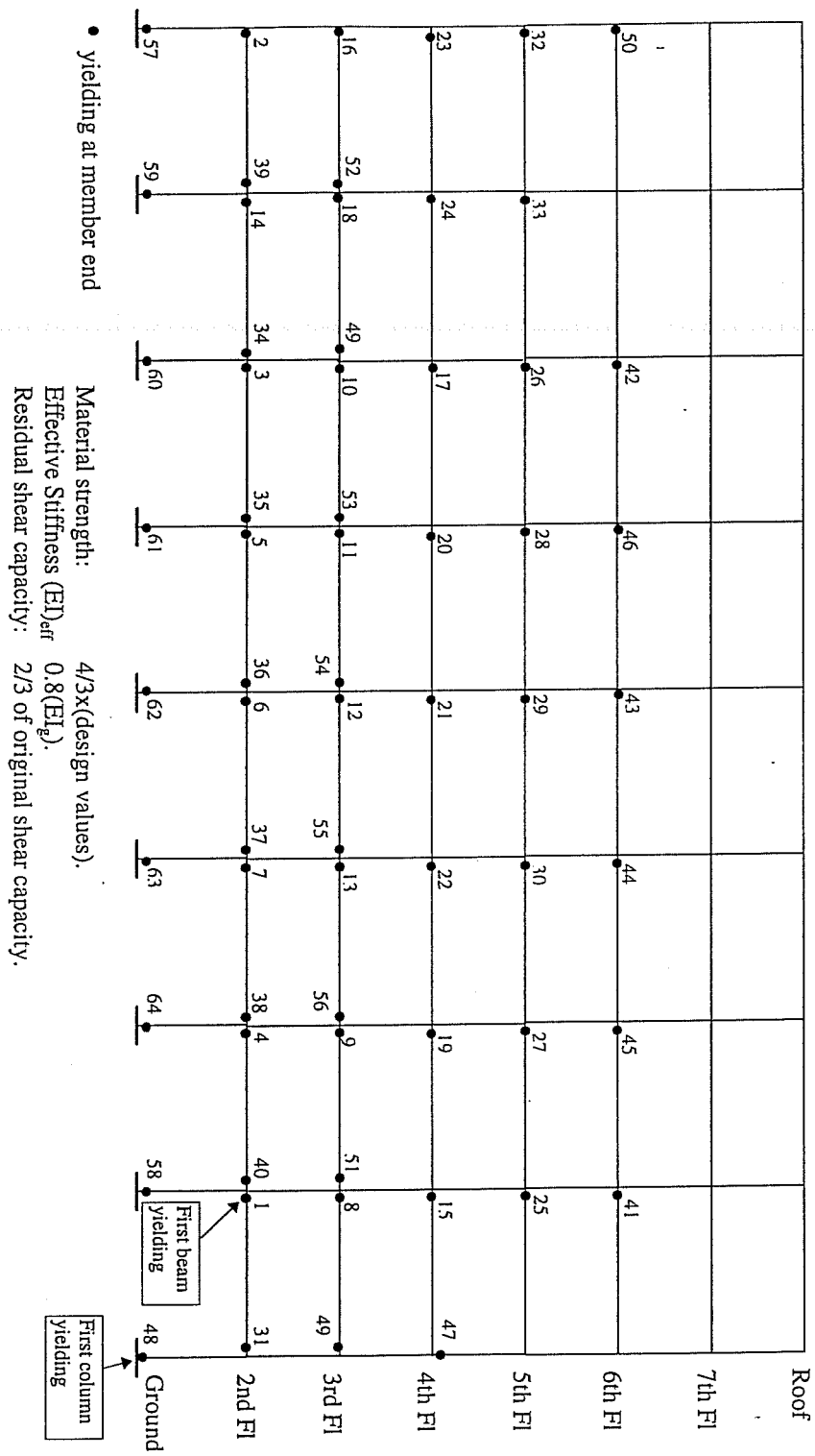


Figure 6.10 Failure Sequence Up to Roof Displacement of 3.421 inches from the Push-Over Analysis with the Uniform Lateral Load Pattern

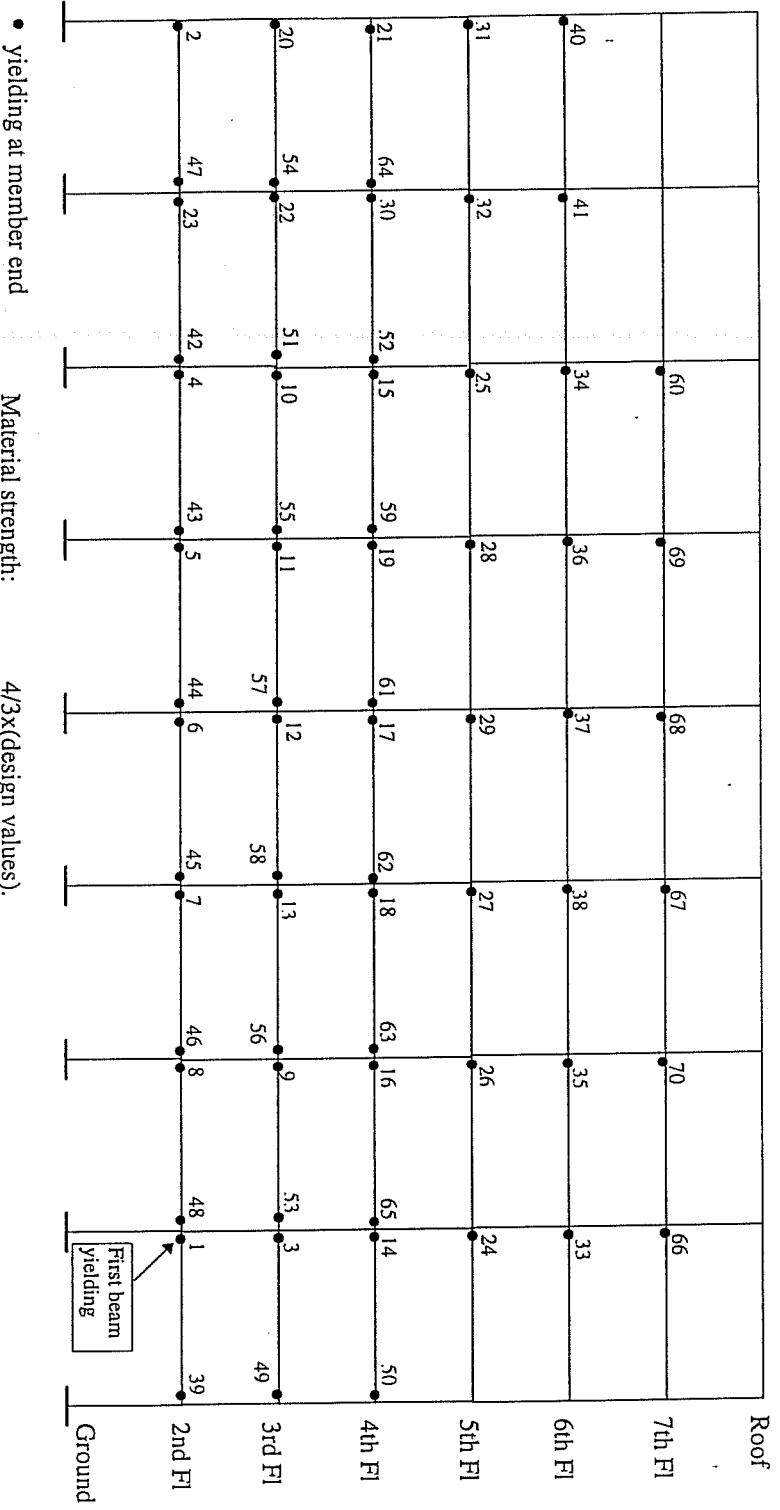
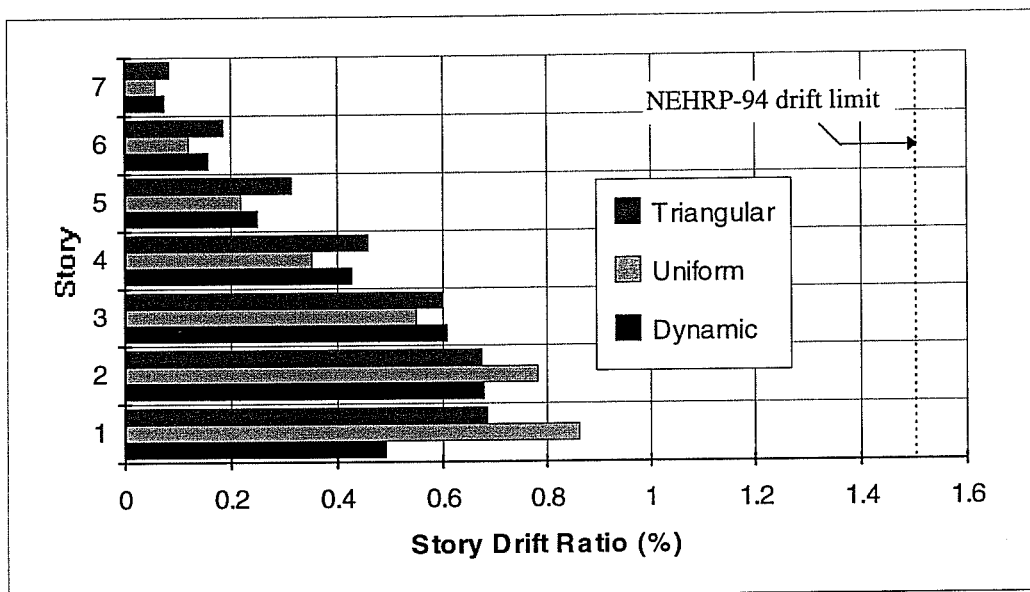


Figure 6.11 Failure Sequence Up to Roof Displacement of 3.421 inches from the Push-Over Analysis with the Triangular Lateral Load Pattern

In Figure 6.12, the maximum inter-story drift ratios between nonlinear dynamic time history analyses and nonlinear static (push-over) analyses are compared. The maximum inter-story drift ratios for push-over analyses were calculated when roof relative displacement reached 3.4 inches (the maximum roof relative displacement recorded during the 1971 San Fernando Earthquake). General agreement in inter-story drift ratios between the dynamic and the push-over analyses obviously exists, with the triangular pattern showing better correlation with the dynamic analysis.



Ground motion:	1971 San Fernando Earthquake.
Damping coefficient:	5% of critical damping.
Material strength:	4/3 x (design values).
Effective stiffness $(EI)_{\text{eff}}$:	0.80(EI_g).
Residual shear capacity:	2/3 of original shear capacity.

Figure 6.12 Story Drift Ratios When Roof Relative Displacements Reach Maximum Recorded Values For Different Load Patterns

6.3 Ten-Story Building

As in the push-over analyses for the seven-story hotel, effects of different lateral load patterns and different effective stiffnesses were analyzed for the ten-story building. The same parameters used in dynamic time history analyses were used for push-over analyses. These parameters include: $4/3$ x (design values) as actual strength of materials, $0.40(EI_g)$ as effective stiffness $(EI)_{\text{eff}}$, and $2/3$ of original shear capacity as residual shear capacity. First, the seismic design criteria according to current and former codes are discussed.

6.3.1 Seismic Design Criteria

The design base shear according to the UBC-94 Code was determined as follows:

$$\frac{V}{W} = ZIC / R_w \quad (6.1)$$

For this structure, $Z = 0.4$ (Zone 4);

$I = 1.0$ (Hotel);

$S_2 = 1.2$ (Soil type: 2);

$R_w = 5$ (Concrete ordinary moment frame).

So, $T = 0.030h^{3/4} = 0.03 \times 99.67^{3/4} = 0.946 \text{ seconds}$

$$C = \frac{1.25S}{T^{2/3}} = \frac{1.25 \times 1.2}{0.946^{2/3}} = 1.56 < 2.75, \text{ OK.}$$

$$C/R_w = 1.56/5 = 0.312 > 0.075, \text{ OK.}$$

Therefore, $V/W = 0.125$.

The (design shear V)/(weight of building W) calculated by the UBC-70 Code, the code used for original design of the building is⁴⁹:

$$V/W = 0.125$$

Corresponding load and strength reduction factors were included⁴⁹.

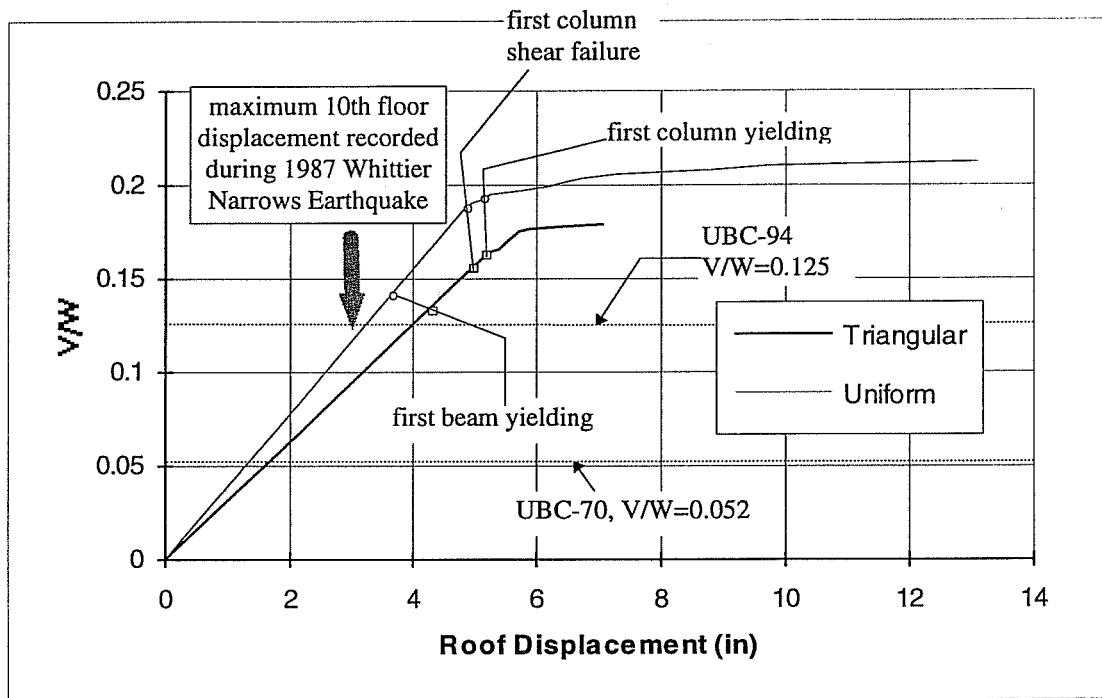
6.3.2 Loading patterns

Figure 6.13 shows the (base shear V)/(weight of building W) vs. roof relative displacement curves for uniform and triangular lateral load patterns.

Base shear V was calculated by summing all applied lateral forces above the basement level, and the weight of the building W was calculated by summing all gravity loads on each floor without load factors. Again, from different lateral load patterns, push-over analyses indicate different strengths. Under the triangular pattern, the strength is lower. However, displacement capacity using both lateral load patterns was almost the same. In addition, push-over analysis results from the triangular

lateral loading indicated a slightly softer structure than with the uniform lateral load pattern.

Also indicated on these figures is the maximum 10th floor relative displacement recorded during the 1987 Whittier Narrows Earthquake. From dynamic analyses, maximum roof displacement was only a little larger than the maximum 10th floor displacement. Therefore the recorded 10th floor maximum displacement was used as a basis for comparison.



Material strength: $4/3 \times$ (design values).
 Effective stiffness $(EI)_{eff}$: $0.40(EI_g)$.
 Residual shear capacity: $2/3$ of original shear capacity.

Figure 6.13 (Base shear)/(Weight of building) vs. Roof Displacement for the Uniform and Triangular Load Distribution Patterns. Ten-Story Building

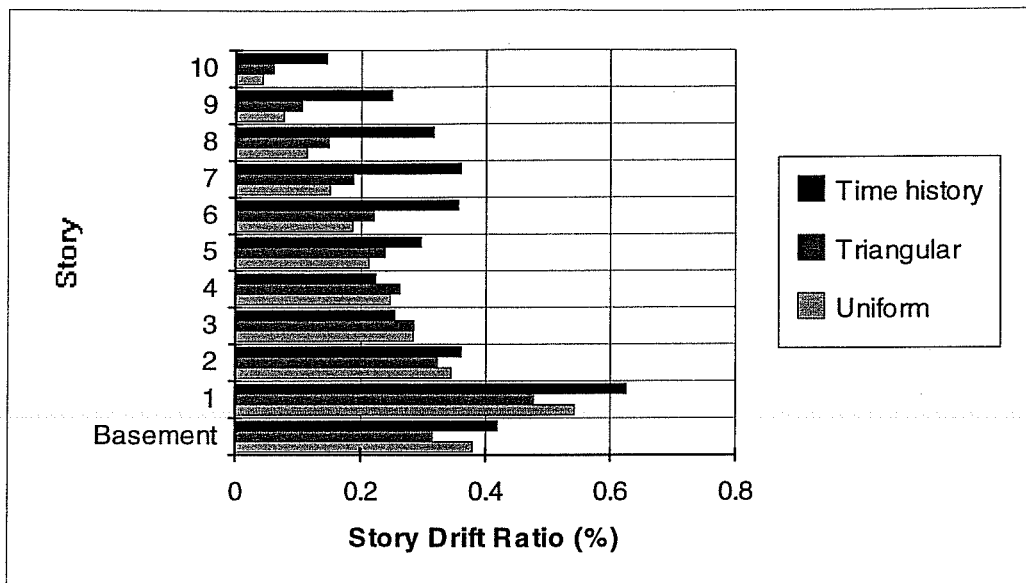
Also shown in Figure 6.13 are design shear coefficients calculated according to UBC-94 and UBC-70 Codes (Section 6.3.1). The lateral capacity of the building is well above design values for both standards.

In Figure 6.14, the maximum inter-story drift ratios computed using the dynamic analysis and the inter-story drift ratios obtained from the push-over analyses are compared. The inter-story drift ratios from push-over analyses were calculated when the 10th floor relative displacement reached 2.9 inches, the maximum 10th floor relative displacement recorded during the 1987 Whittier Narrows Earthquake.

Because the building is taller than the seven-story hotel, higher mode effects become significant. Although the inter-story drift ratios predicted by push-over analyses were close to the dynamic analysis at lower stories, the correlation in story drift ratios between the push-over analyses and the dynamic analysis at higher stories were unsatisfactory.

6.3.3 Effects of Effective Stiffness $(EI)_{\text{eff}}$

As in the case of the seven-story hotel, two different effective stiffness values were studied, namely $0.40(EI_g)$ used in dynamic analyses and $1.0(EI_g)$ for gross section stiffness. Only the triangular load pattern was used in the comparison. Figure 6.15 shows the push-over analysis results using $1.0(EI_g)$ as effective stiffness. Results using $0.4(EI_g)$ as effective stiffness are also included in the figure for comparison.

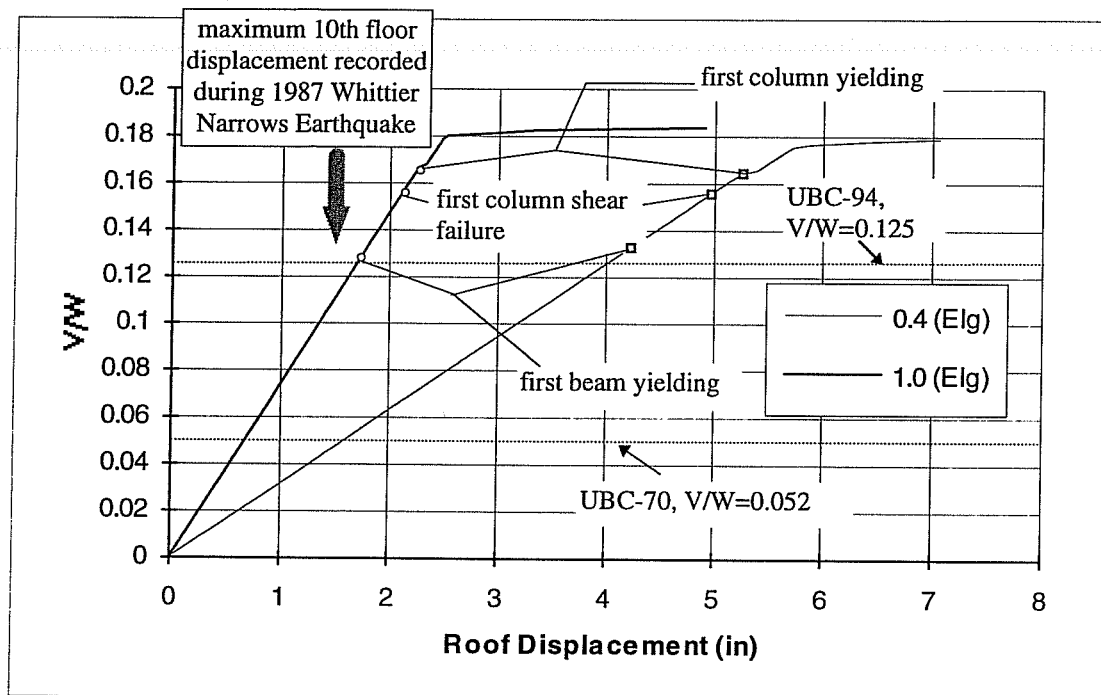


Ground motion: 1987 Whittier Narrows Earthquake.
 Damping coefficient: 5% of critical damping.
 Material strength: $4/3$ x (design values).
 Effective stiffness $(EI)_{\text{eff}}$: $0.40(EI_g)$.
 Residual shear capacity: $2/3$ of original shear capacity.

Figure 6.14 Story Drift Ratios When 10th Floor Relative Displacement Reaching Maximum Recorded Value For Different Load Patterns

From Figure 6.15, the same conclusion as in the case for the seven-story hotel can be drawn. Different effective stiffness significantly affects the push-over analysis results. Although strength (base shear) capacity was almost the same for different assumed effective stiffnesses, roof displacement capacity of the building differed very significantly for different effective stiffness. Assuming an effective stiffness of $1.0(EI)$ would have predicted that the structure suffered yielding in both beams and

columns, and shear failure in columns at a 10th floor relative displacement of less than 2.9 inches. The condition of the structure after the earthquake indicated that the structure had no visible damage.



Material strength: 4/3 x (design values).
Residual shear capacity: 2/3 of original shear capacity.

Figure 6.15 (Base shear)/(Weight of building) vs. Roof Displacement with Triangular Load Pattern Using Different Effective Stiffnesses. Ten-Story Building

CHAPTER 7

DISCUSSION OF RESULTS AND DESIGN IMPLICATIONS

7.1 General

One of the difficulties that a design engineer faces in conducting a dynamic time history analysis of structures is what earthquake ground motion should be used to obtain the largest demand on the structures. In this chapter, several representative earthquakes from the West coast of the United States were selected. The two buildings analyzed in previous chapters were studied using the selected earthquake ground motions to compare responses under different earthquake ground motions. In addition, design-spectrum-compatible earthquake ground motions were artificially generated and building responses under these artificially generated earthquakes were analyzed.

7.2 Selection of Representative Ground Motions

Despite the moderate magnitude of the ground motion recorded at ground level of the seven-story hotel (east-west direction) in the 1994 Northridge Earthquake, the building sustained significant damage. This ground motion record was considered of interest for further study. Figure 3.11 (S16(E-W)) shows the accelerogram recorded.

Ground motion recorded at the basement of the ten-story building (longitudinal direction) during the 1987 Whittier Narrows Earthquake was moderate, but the building experienced no visual damage at all. Therefore this record was also chosen for study. Figure 3.34 (Longitudinal) shows the accelerogram recorded.

The S00E component of El Centro, the Imperial Valley Earthquake of May 18, 1940, the first complete earthquake ground motion accelerogram in history was selected for this study. This record has been widely used as a typical earthquake ground motion in past research. Strong shaking lasted more than 20 seconds (Figure 7.1)

The S16E component of the Pacoima Dam records in the 1971 San Fernando Earthquake was also chosen for this study. Figure 7.2 shows the acceleration time history of the record. The record has a short strong shaking duration but a large acceleration pulse.

In Figure 7.3, pseudo acceleration response spectra for the 1994 Northridge Earthquake recorded at the ground level of the seven-story hotel and the 1987 Whittier Narrows earthquake recorded at the basement level of the ten-story building are plotted.

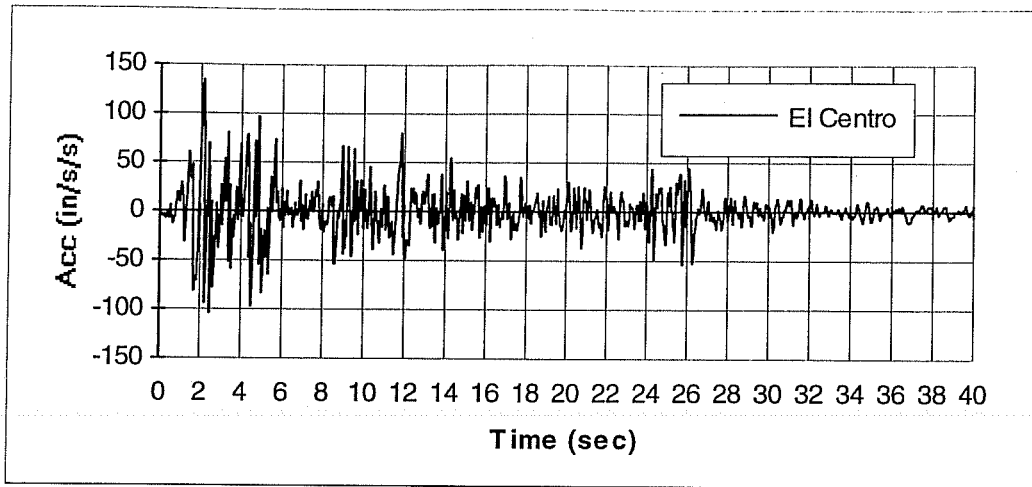


Figure 7.1 Ground Acceleration Time History of 1940 Imperial Valley Earthquake at El Centro (S00E Direction)

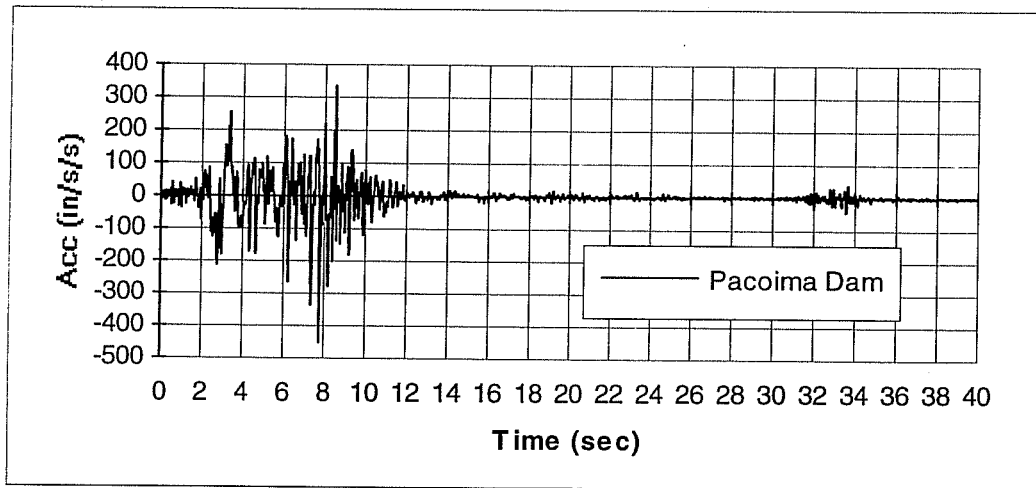


Figure 7.2 Ground Acceleration Time History in 1971 San Fernando Earthquake at Pacoima Dam (S16E Direction)

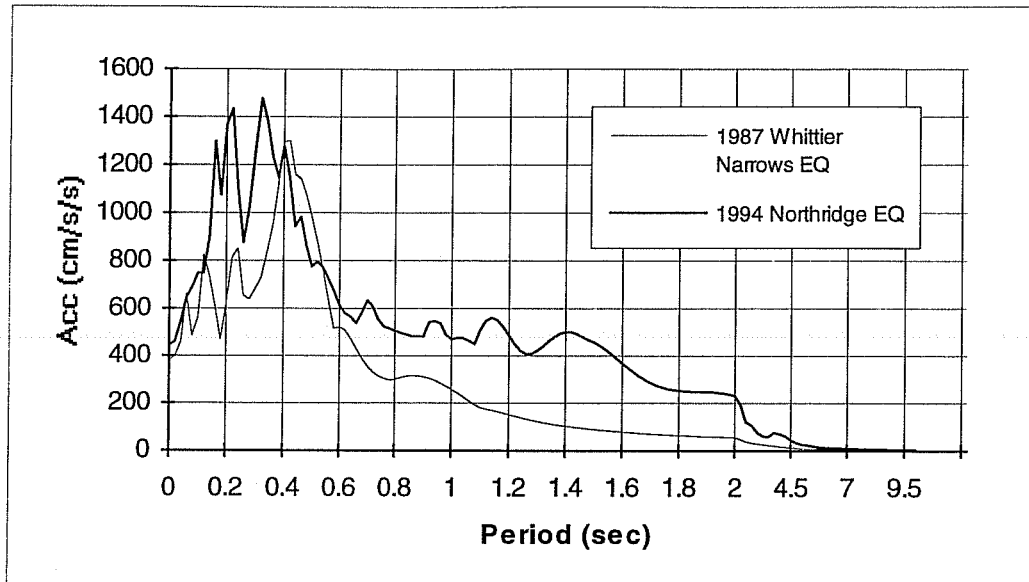


Figure 7.3 Comparison of Acceleration Response Spectra between 1994 Northridge Earthquake and 1987 Whittier Narrows Earthquake

For the seven-story hotel, the fundamental period of vibration is 1.60 seconds, and the second mode period of vibration is 0.54 seconds. The acceleration response spectrum for the 1994 Northridge Earthquake recorded at the ground level of the seven-story building indicates high responses in these periods, especially at the fundamental period of vibration. This may explain why the building suffered extensive damage during the 1994 Northridge Earthquake.

The acceleration response spectrum for the 1987 Whittier Narrows Earthquake recorded at the basement level of the ten-story building has a high pulse only at a 0.4

second period. The building fundamental period of vibration is 1.45 second, while the building second mode period of vibration is 0.47 seconds. Since the building response spectrum at the fundamental period of vibration is very low, it explains why the overall displacement and story drift ratios were small and the building sustained no damage. However, the acceleration response at the second mode period of vibration is rather high. This is consistent with the high drift ratios at higher stories indicated by dynamic calculations (Figure 6.14).

In Figure 7.4, the acceleration response spectra of all four earthquake ground motions are compared. All motions were scaled to the same peak acceleration as the 1994 Northridge Earthquake recorded at the ground level of the seven-story hotel. Also plotted in the figure was the design response spectrum adopted by the Seismology Committee of the Structural Engineers Association of California¹ and UBC-94⁶ as discussed in Chapter 2 (Figure 2.4) for deep cohesionless or stiff clay soils (soil type 2).

As is clearly shown in Figure 7.4, the UBC-94 design spectrum is lower than the Northridge and Whittier Narrows Earthquake ground motions in the short period region, but is greater in the long period region. In addition, it envelopes El Centro and Pacoima Dam records almost entirely. 5% damping was used in calculating pseudo acceleration response spectra.

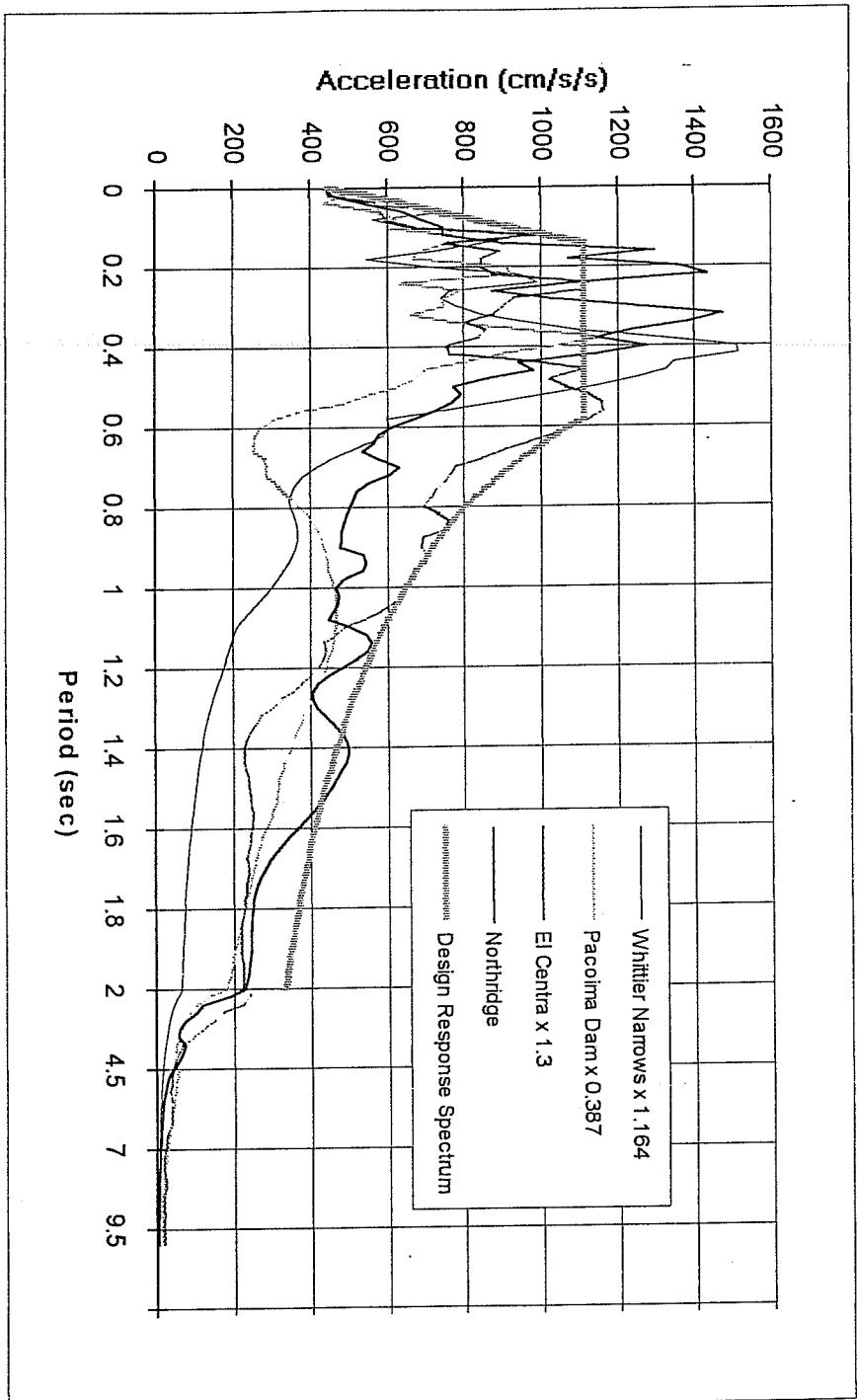


Figure 7.4 Comparison of Acceleration Response Spectra (5% Damping) among Selected Representative Earthquake Ground Motions and Design Response Spectrum for Soil Type 2

7.3 Artificially Generated Earthquake Ground Motions

Since response spectra seem to be good indications of damage potential of earthquakes, researchers have been using artificially generated design-spectrum-compatible earthquake ground motions in designing nuclear reactor facilities⁷⁴. Also the Building Code of Japan requests that high-rise buildings be subjected to structural evaluations for seismic safety through dynamic response analyses using artificially generated design-spectrum-compatible earthquake motions⁷⁵. This technique was employed in this study in selecting several critical design earthquakes.

Program SIMQKE⁷⁶ was used to synthesize the artificial earthquakes. Developed by Vanmarcke, Cornell, Gasparini, and Hou, the program was revised in September 1976 after the first version became available in August 1969. An acceleration envelope needs to be specified by users as shown in Figure 7.5. t_1 , t_2 , and t_3 are pre-specified durations for the rising portion, the flat portion, and the descending portion of the earthquake motion, respectively. Positive and negative envelopes are symmetric.

For all artificial earthquake motions generated for this study, the duration of ground motion was assumed to be 30 seconds, with the rising portion t_1 to be 2 sec. long, flat portion t_2 to be 12 sec. long, and the descending portion t_3 assumed to be 16 sec. long.

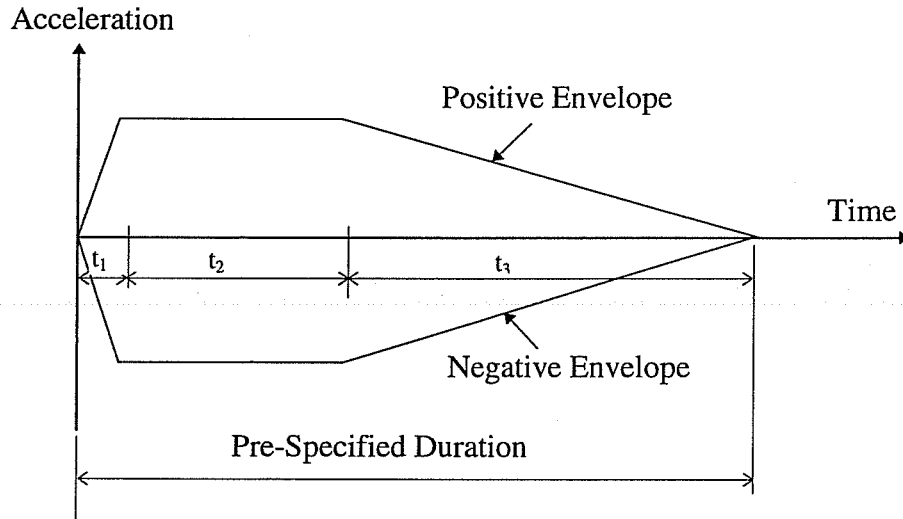
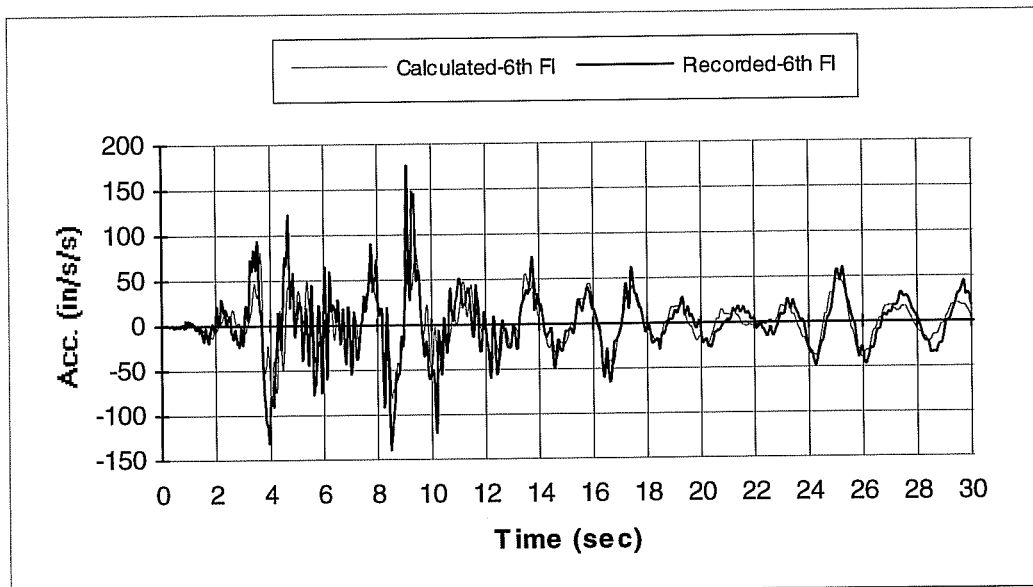
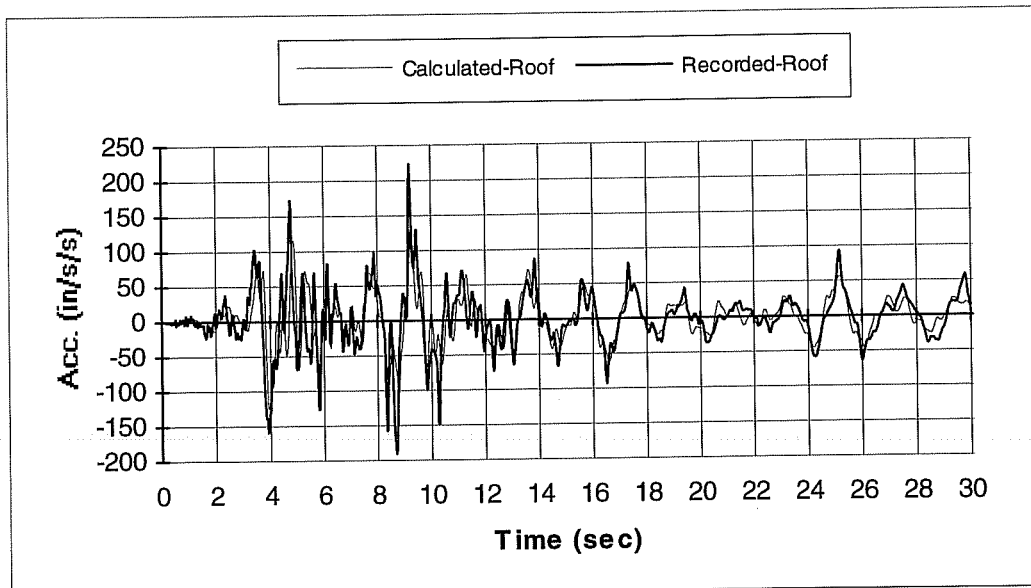


Figure 7.5 Envelopes for Artificial Earthquakes

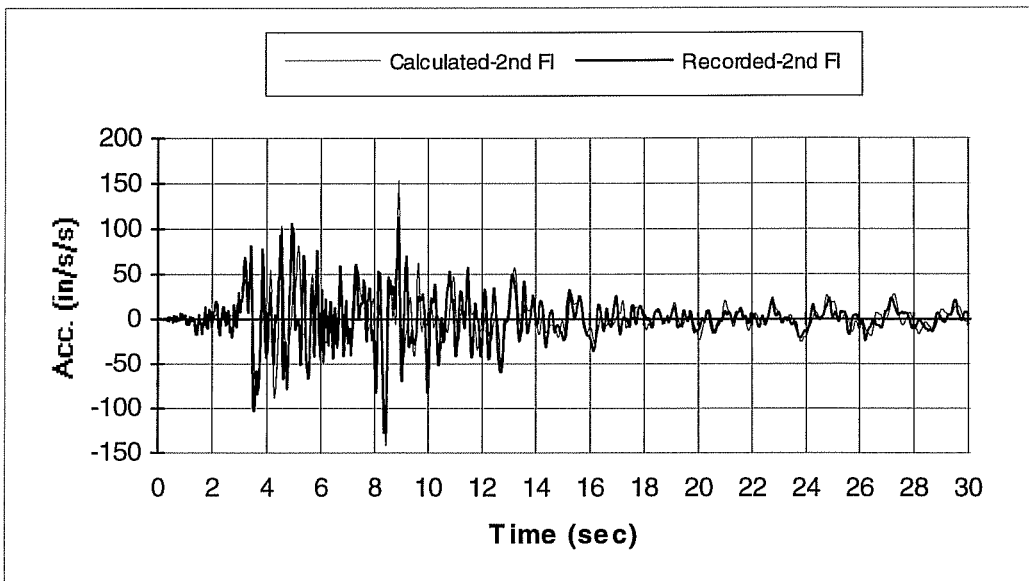
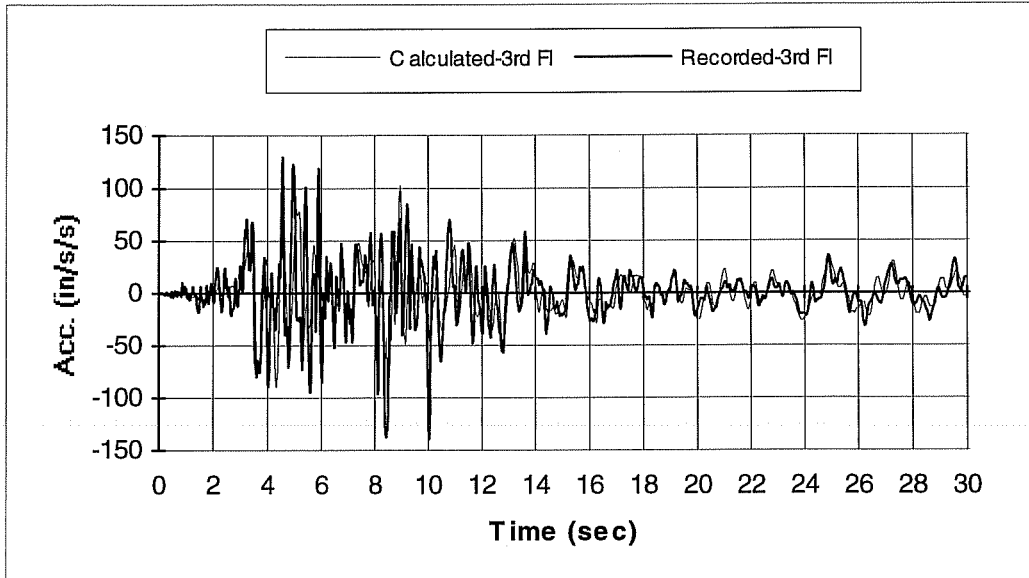
7.3.1 Design-Spectrum-Compatible Artificial Earthquake

The first artificial earthquake generated was a UBC-94 design-spectrum-compatible earthquake motion for soil type 2. Figure 7.6 is the acceleration time history of the artificial earthquake and Figure 7.7 is the pseudo acceleration response spectrum for the artificial earthquake. Peak acceleration was specified as 1g, which can be easily scaled if needed.



Ground motion: 1994 Northridge Earthquake.
 Damping coefficients: 5% critical damping.
 Material strength: $3/2 \times$ (design values).
 Effective stiffness $(EI)_{\text{eff}}$: $0.30(EI_g)$.
 Residual shear capacity: $2/3$ of original shear capacity.

Figure 5.17 Comparison Between Calculated and Recorded Roof and 6th Floor Absolute Acceleration Time History



Ground motion:	1994 Northridge Earthquake.
Damping coefficients:	5% critical damping.
Material strength:	$3/2 \times$ (design values).
Effective stiffness $(EI)_{\text{eff}}$:	$0.30(EI_g)$.
Residual shear capacity:	$2/3$ of original shear capacity.

Figure 5.18 Comparison Between Calculated and Recorded 3rd and 2nd Floor Absolute Acceleration Time History

5.3 Seven-Story Hotel in the San Fernando Earthquake

The same hotel that was severely damaged in the 1994 Northridge Earthquake survived the 1971 San Fernando Earthquake with minor structural damage. Again, two-dimensional nonlinear dynamic time history analyses were performed for the south perimeter frame in the longitudinal direction. The same structural model shown in Figure 5.1 was used here for the analyses.

5.3.1 Evaluation of Response Records

Figure 5.19 shows the relative displacement time history recorded at the roof and the 4th floor level in the east-west (longitudinal) direction. The building period of vibration in the east-west (longitudinal) direction was about 0.6 seconds in the beginning of the ground shaking. But at about 12 seconds, the period of vibration increased to 1.25 seconds. The lengthening of the building period of vibration indicates that cracking and inelastic deformation increased during the earthquake.

In the 1971 San Fernando Earthquake, there was only one sensor at each floor to record response (Figures 3.21), and no torsional movement can be evaluated.

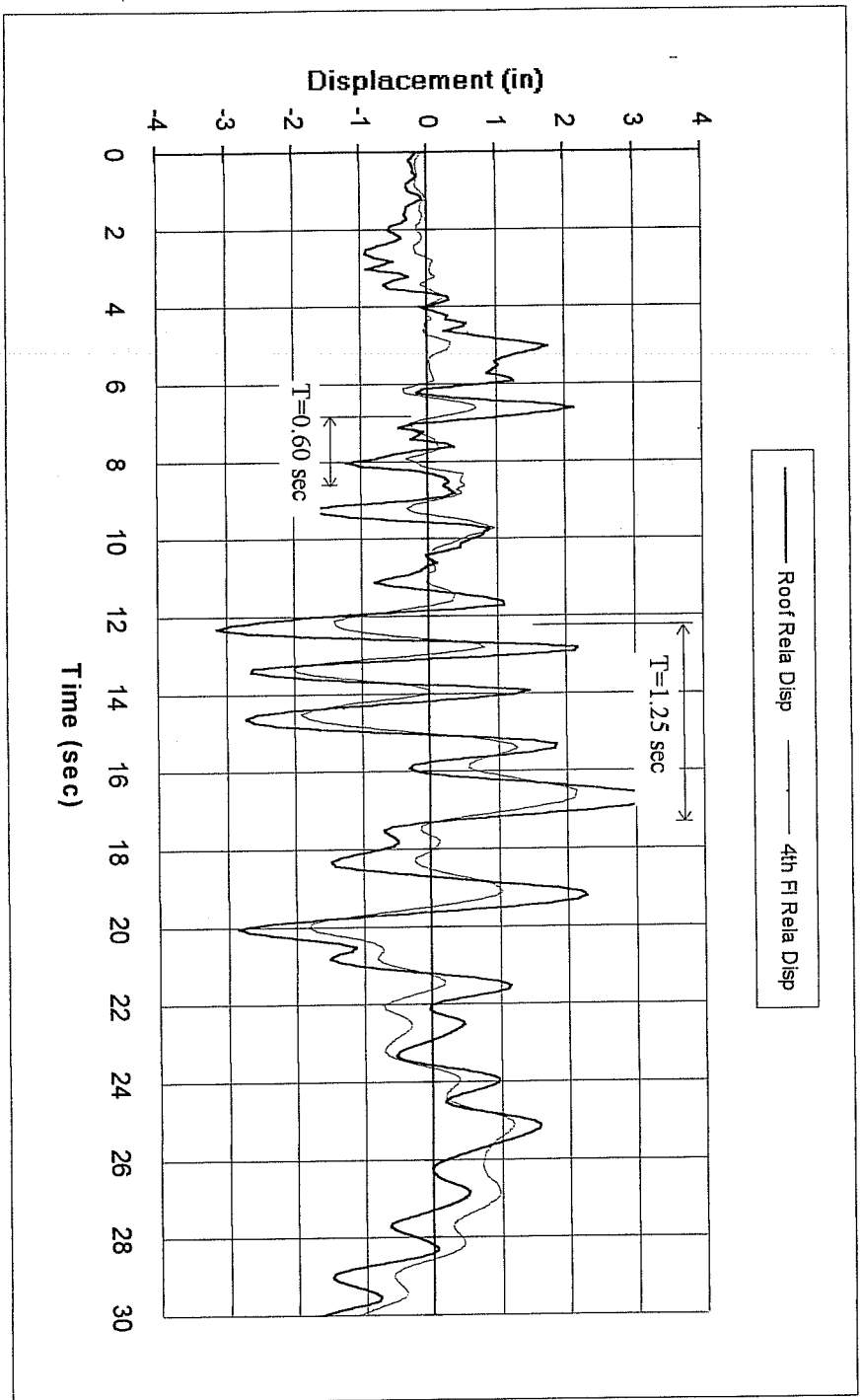


Figure 5.19 Recorded Floor Relative Displacement Time History in East-West (Longitudinal) Direction at 1971 San Fernando Earthquake

5.3.2 Analysis Results

Both DRAIN-2D and IDARC were used to analyze the response of this building under the 1971 San Fernando Earthquake, and the results were compared with recorded response. For DRAIN-2D, two options for assigning effective stiffness of members were exercised, and the results were compared.

5.3.2.1 DRAIN-2D Analyses

Using the results from Section 5.2.2, the following parameters were chosen for the building under the 1971 San Fernando Earthquake.

- (1) Damping coefficients: An average 5% damping coefficient was used as before.
- (2) Actual material strength: Considering the relatively moderate intensity of the earthquake and the age of the building, $4/3$ x (design values) were used for both concrete and steel strengths.
- (3) Residual shear capacity: $2/3$ of original shear capacity was used as residual shear capacity as before.

OPTION 1:

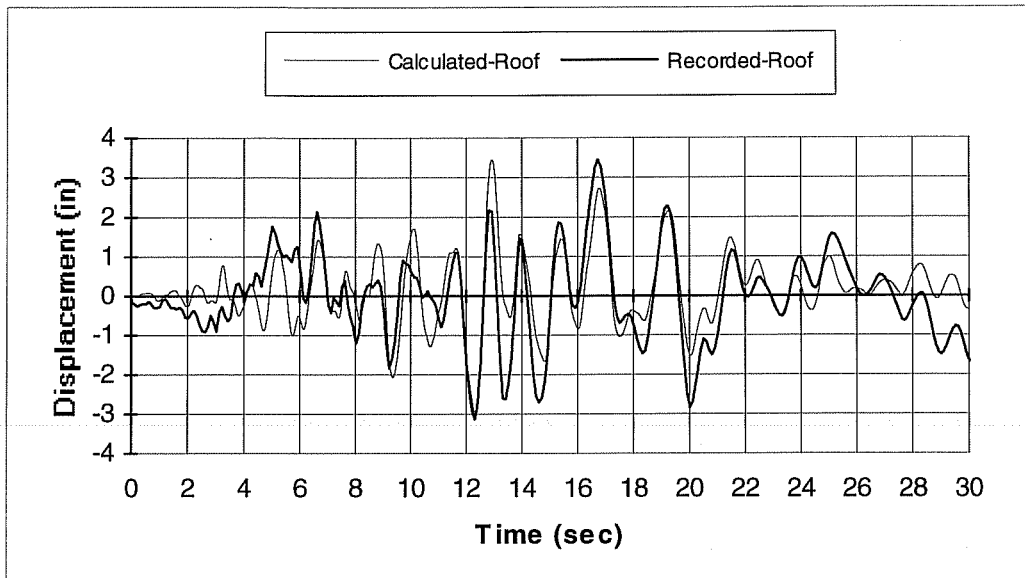
This option specified an effective flexural stiffness $(EI)_{\text{eff}}$ for cracking in the member (Section 4.3.1.2). The criterion for choosing the effective stiffness was the

calculated response time history was adjusted to produce a period of vibration that matched the period of vibration of the recorded response time history. After several trials, $0.80(EI_g)$ was chosen as the effective stiffness.

Figure 5.20 shows the comparison between the calculated roof relative displacement time history using chosen parameters and the recorded relative roof displacement time history.

Although the agreement between the calculated and the recorded roof relative displacement is not as good as that observed for the same building under the 1994 Northridge Earthquake, general agreement exists, and the maximum roof relative displacement is also predicted well.

Figure 5.21 shows the calculated and recorded relative displacement time history at the 4th floor. Once again, general agreement is observed between the calculated and the recorded 4th floor relative displacement time history. The discrepancy for the building subjected to the 1971 San Fernando Earthquake is attributed to the small magnitude of the earthquake. Non-structural elements in the structure affected response of the building more significantly, especially during the early portion of the response time history. In addition, due to the sensor location, the recorded data included the effects of building torsional movement, while the calculated displacement could not take torsional effects into account because of the nature of the two-dimensional analyses.

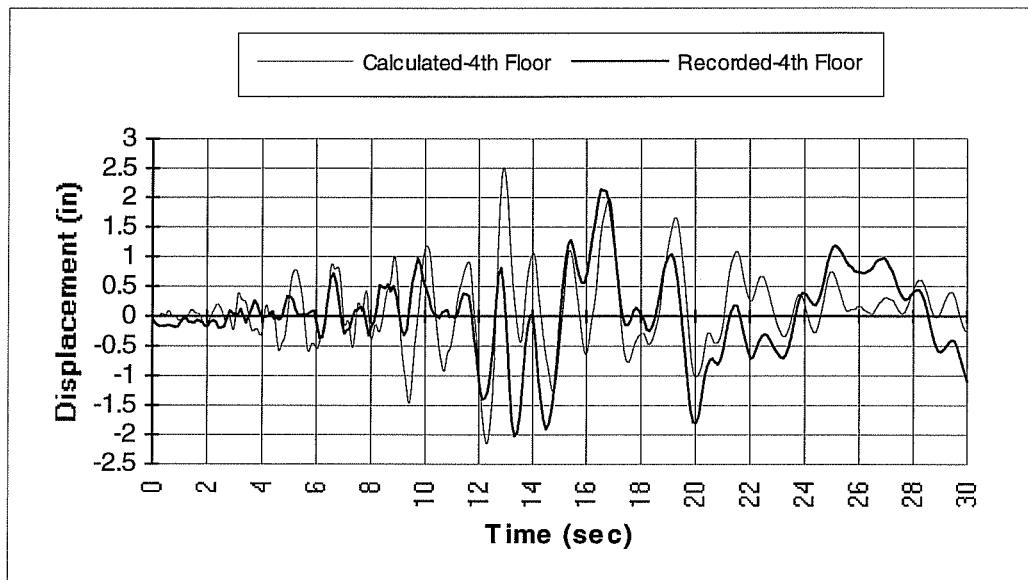


Ground motion:	1971 San Fernando Earthquake.
Damping coefficient:	5% of critical damping.
Material strength:	4/3 x (design values).
Effective stiffness $(EI)_{\text{eff}}$:	0.80(EI_g).
Residual shear capacity:	2/3 of original shear capacity.

Figure 5.20 Comparison Between Calculated and Recorded Roof Relative Displacement Time History under San Fernando Earthquake

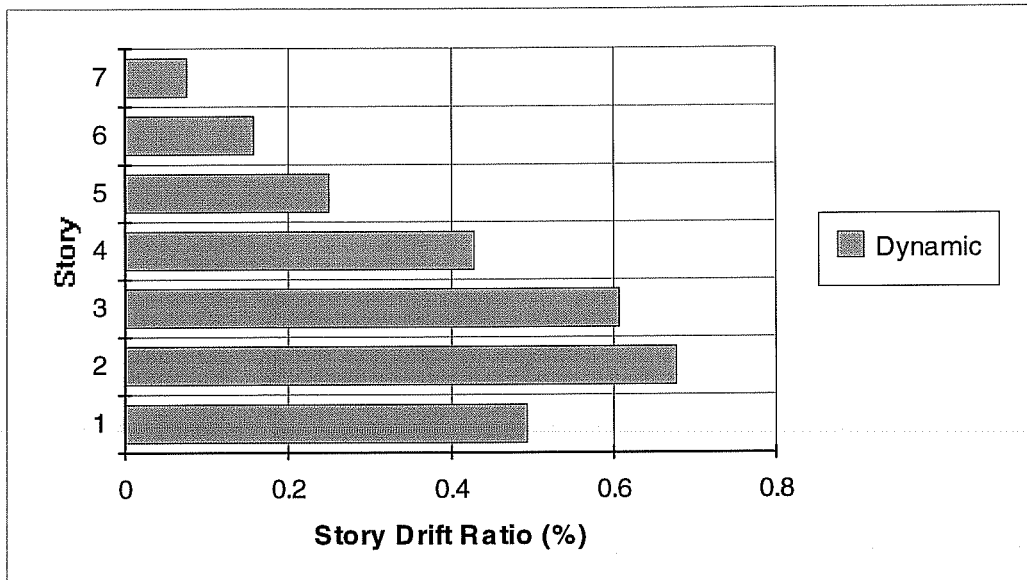
Figure 5.22 shows the calculated story drift ratio. As can be seen, story drift ratios were much smaller than those calculated from the 1994 Northridge Earthquake. In addition, all story drift ratios were less than half the limit specified in the NEHRP-94 Specifications⁹. Considering the extensive non-structural damage the building suffered after the 1971 San Fernando Earthquake, this drift limit recommended by NEHRP-94 cannot guarantee non-structural damage control. It is intended for

collapse prevention. The analytical inter-story drift ratios are higher at lower floors and explain why the most severe non-structural damage from the 1971 San Fernando Earthquake occurred at the second and third floors. The sixth and seventh floors suffered the least non-structural damage.



Ground motion:	1971 San Fernando Earthquake.
Damping coefficient:	5% of critical damping.
Material strength:	4/3 x (design values).
Effective stiffness $(EI)_{eff}$:	0.80(EI_g).
Residual shear capacity:	2/3 of original shear capacity.

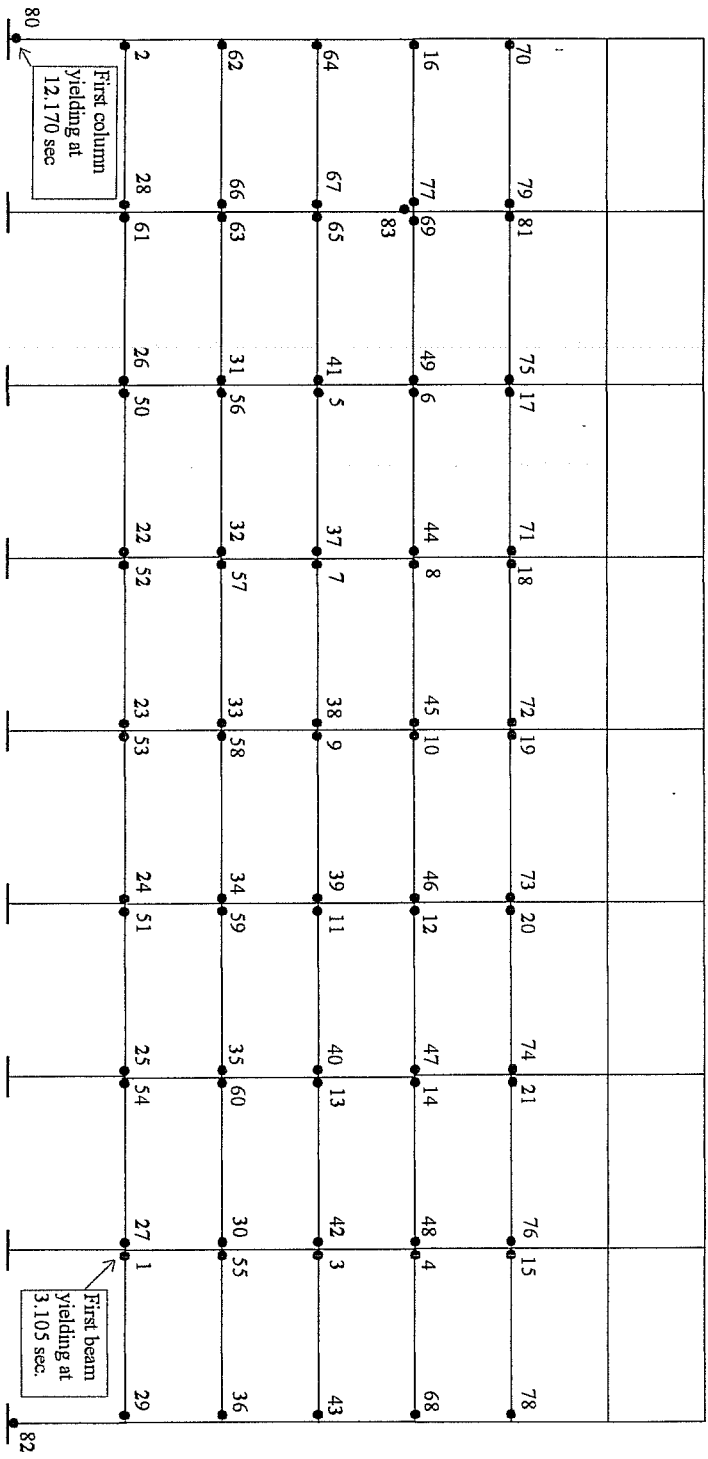
Figure 5.21 Comparison Between Calculated and Recorded 4th Floor Relative Displacement Time History under San Fernando Earthquake



Ground motion: 1971 San Fernando Earthquake.
 Damping coefficient: 5% of critical damping.
 Material strength: $4/3$ x (design values).
 Effective stiffness $(EI)_{\text{eff}}$: $0.80(EI_g)$.
 Residual shear capacity: $2/3$ of original shear capacity.

Figure 5.22 Calculated Story Drift Ratio for the Seven-Story Hotel under the 1971 San Fernando Earthquake

Figure 5.23 describes the calculated failure sequence of the building subject to the 1971 San Fernando Earthquake. After the 1971 San Fernando Earthquake, there were visible cracks at the second floor spandrel beam on the north side of the structure (Figure 3.25). Other cracks may have been hidden or closed after the earthquake. No columns failed in shear using the nonlinear time history analysis and none were observed in post earthquake investigations.



- yielding at member end
- Ground motion: 1971 San Fernando Earthquake.
Damping coefficients: 5% of critical damping.
Material strength: $4/3 \times$ (design values).
Effective Stiffness $(EI)_{eff}$: $0.80(EI_g)$.
Residual shear capacity: $2/3$ of original shear capacity.

Figure 5.23 Calculated Failure Sequence for the Seven-Story Hotel under the 1971 San Fernando Earthquake

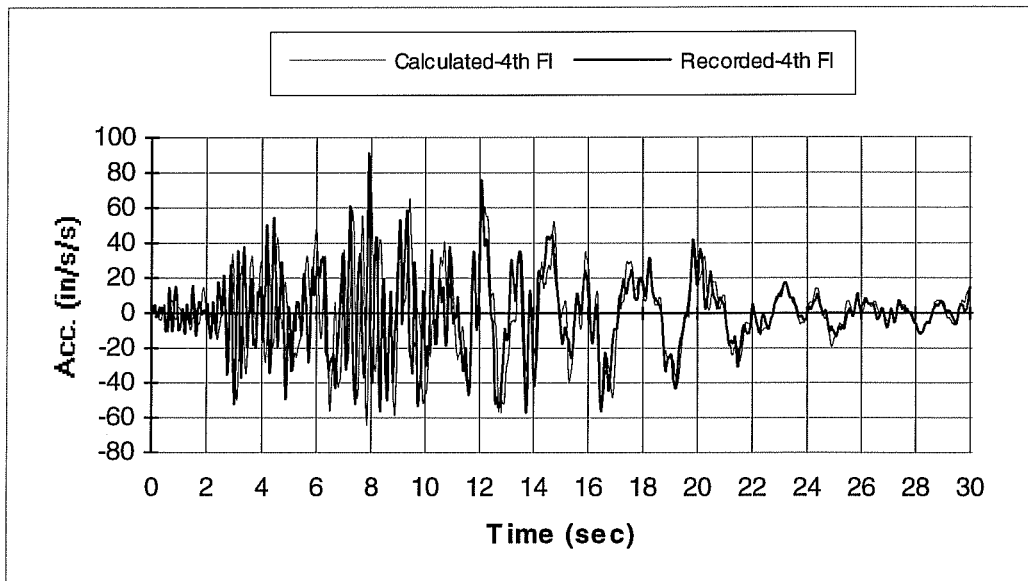
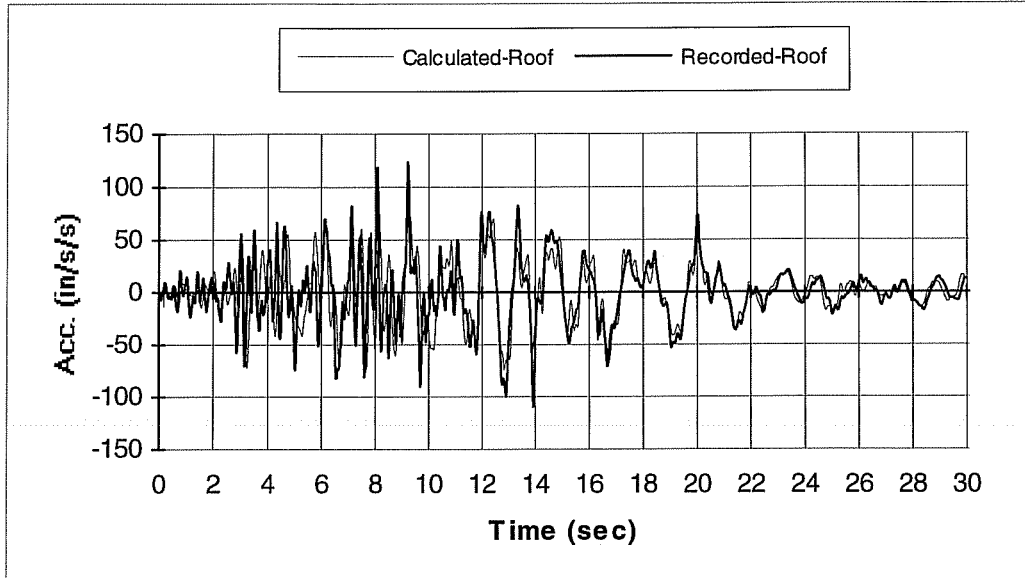
In Figure 5.24, the calculated and recorded absolute acceleration time histories at the roof and the 4th floor levels are compared. Once again, the general agreement is evident.

OPTION 2:

To pursue alternative ways of specifying effective stiffness, option 2 presented in the original DRAIN-2D users' guide³ was exercised. The effective stiffness in this option is determined by letting the equivalent member and actual member have the same tip displacement and tip rotation when the member yields at the end (Section 4.3.1.2). The results are compared in Figure 5.25.

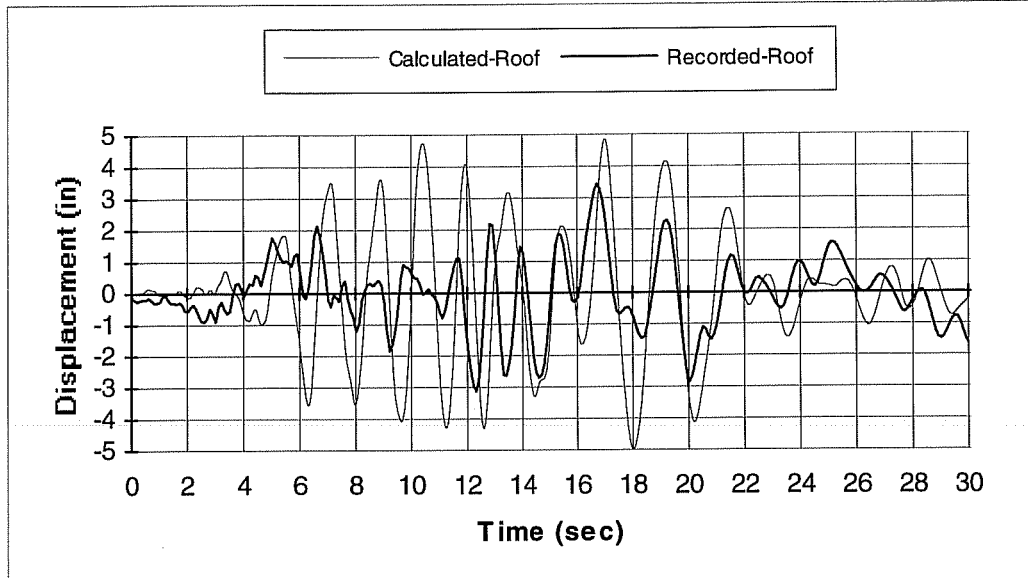
Obviously, the agreement between calculated and recorded roof relative displacement was poor using option 2. The calculated fundamental period of the structure was too long because the stiffness assigned to the member was too low. The equivalent condition set by option 2 was for member ends to reach yield. Under a moderate earthquake like the 1971 San Fernando Earthquake, many members in this building never reached yield.

Figure 5.26 shows comparisons between the calculated and recorded absolute acceleration time histories at the roof and the 4th floor levels using option 2.



Ground motion:	1971 San Fernando Earthquake.
Damping coefficient:	5% of critical damping.
Material strength:	$4/3$ x (design values).
Effective stiffness (EI_{eff}):	$0.80(EI_g)$.
Residual shear capacity:	$2/3$ of original shear capacity.

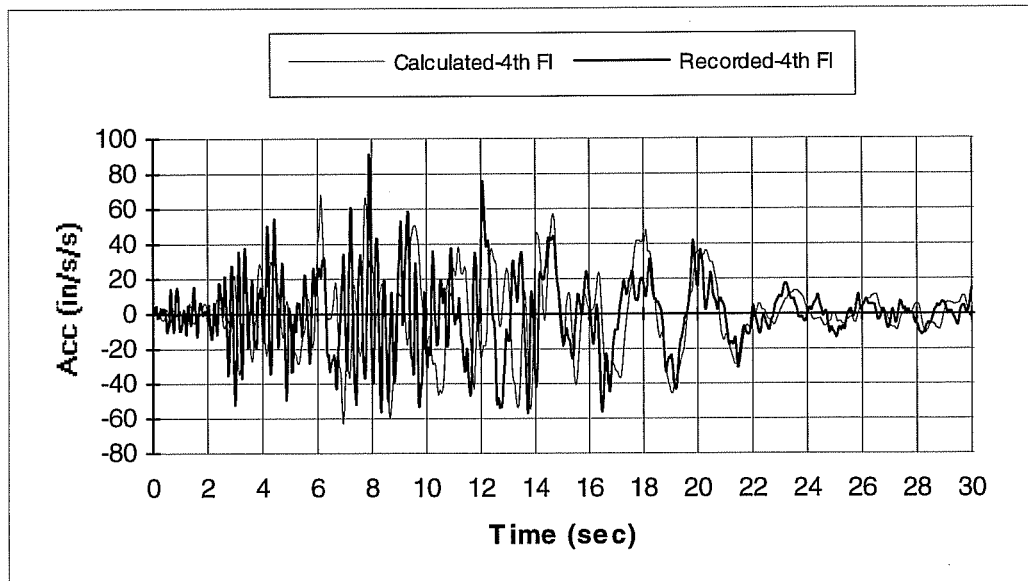
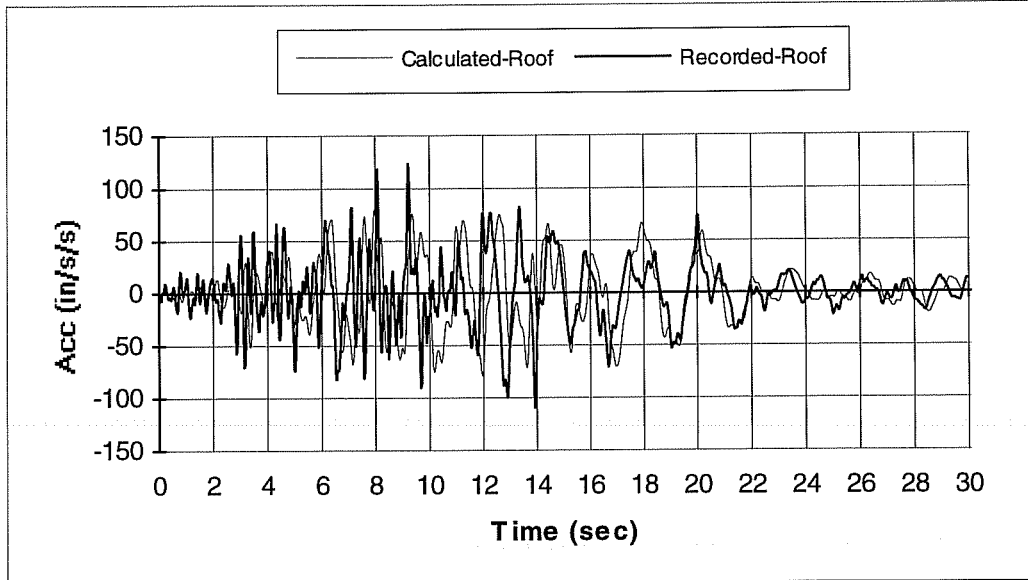
Figure 5.24 Comparison Between Calculated and Recorded Roof and 4th Floor Absolute Acceleration Time History under the 1971 San Fernando Earthquake



Ground motion:	1971 San Fernando Earthquake.
Damping coefficient:	5% of critical damping.
Material strength:	4/3 x (design values).
Effective stiffness $(EI)_{\text{eff}}$:	Option 2.
Residual shear capacity:	2/3 of original shear capacity.

Figure 5.25 Comparison Between Calculated and Recorded Roof Relative Displacement Time History under the 1971 San Fernando Earthquake using Option 2 for assigning member effective stiffness

Despite the large discrepancy between calculated and recorded roof displacement time history data, the calculated and recorded roof and the 4th floor absolute acceleration time history data show much less dramatic differences and indicate that the acceleration data are far less sensitive to stiffness than displacement data. Therefore displacement data are more valuable and more reliable in calibration and comparison for time history analyses.



Ground motion:	1971 San Fernando Earthquake.
Damping coefficient:	5% of critical damping.
Material strength:	4/3 x (design values).
Effective stiffness $(EI)_{eff}$:	Option 2.
Residual shear capacity:	2/3 of original shear capacity.

Figure 5.26 Comparison Between Calculated and Recorded Roof and 4th Floor Absolute Acceleration Time History under the 1971 San Fernando Earthquake Using Option 2 for Assigning Member Effective Stiffness

5.3.2.2. IDARC Analyses

The following parameters were chosen to use in the IDARC analyses:

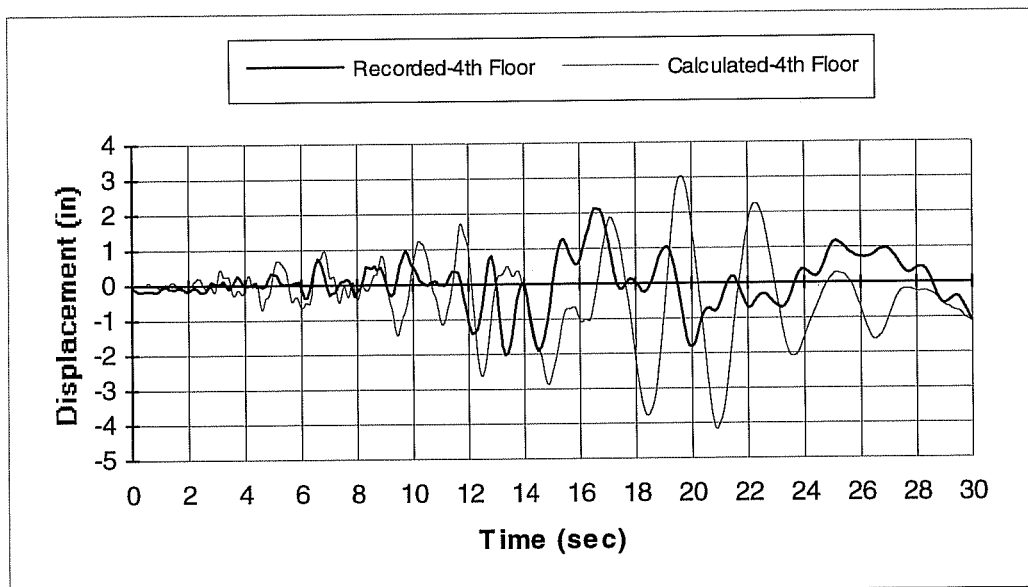
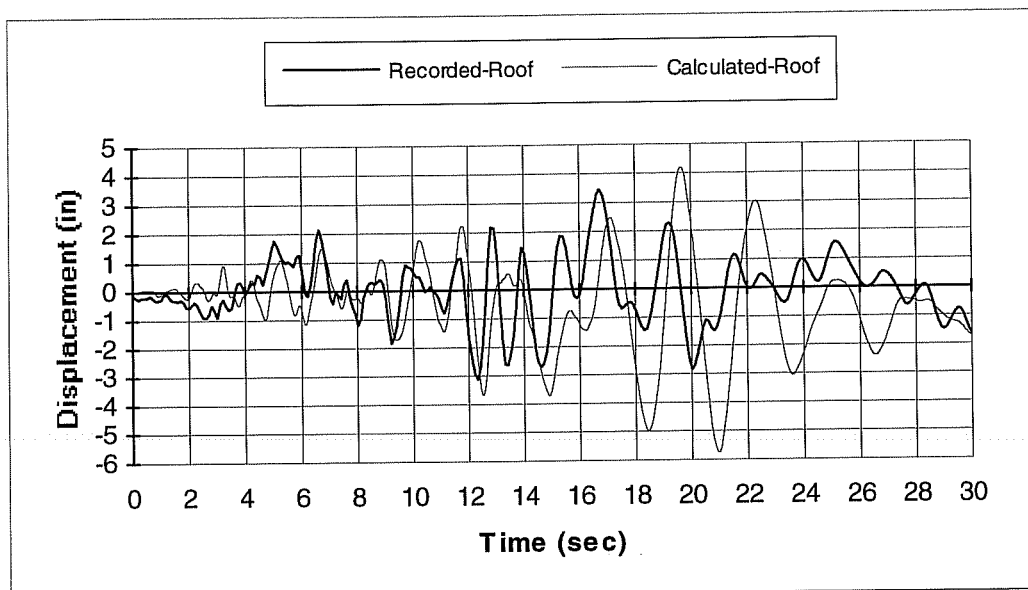
- (1) Damping coefficient: 5% of critical damping.
- (2) Material strength: Using the same argument as was used in Section 5.3.2.1 for DRAIN-2D analyses, $4/3$ x (design values) were used for both concrete and steel strengths.
- (3) Residual shear capacity: Shear failure was not taken into consideration.
- (4) Hysteretic modeling rules for beams and columns (Section 4.2.2.4):
 - Stiffness degrading parameter: $HC = 2.0$ (nominal degradation);
 - Strength deterioration parameter: $HBE = HBD = 0.0$ (no strength deterioration);
 - Slip control parameter: $HS = 0.5$ (nominal pinching).

As in DRAIN-2D analyses, part of the slab adjacent to the beam was assumed to contribute to the stiffness and strength of the beam. ACI 318-95 Code Sections 8.10.2 and 8.10.3 were used to determine the width of slab as a T-beam flange. In addition, the longitudinal reinforcement in the slab within the flange width (2#6) was added to beam top reinforcement. The same integration time step (0.005 seconds) used in DRAIN-2D was again used here. Hysteretic envelopes for beams and columns were generated by the program using a pre-processor.

In Figure 5.27, the calculated and the recorded relative displacement time histories at the roof and the 4th floor using parameters defined above are compared. The correlation between calculated and recorded responses was not as good as that obtained using DRAIN-2D analyses. Figure 5.28 shows the direct output plot by IDARC for the final failure state of the building. Although the failure predicted was consistent with the observed damage level and the results obtained from DRAIN-2D analyses, the roof maximum relative displacement predicted by the IDARC analysis was off by 67%, and the 4th floor maximum relative displacement was off by 95%. Lack of agreement in the general shape of the response trace is obvious. Different parameter values were tried to improve the results, but the change was minor.

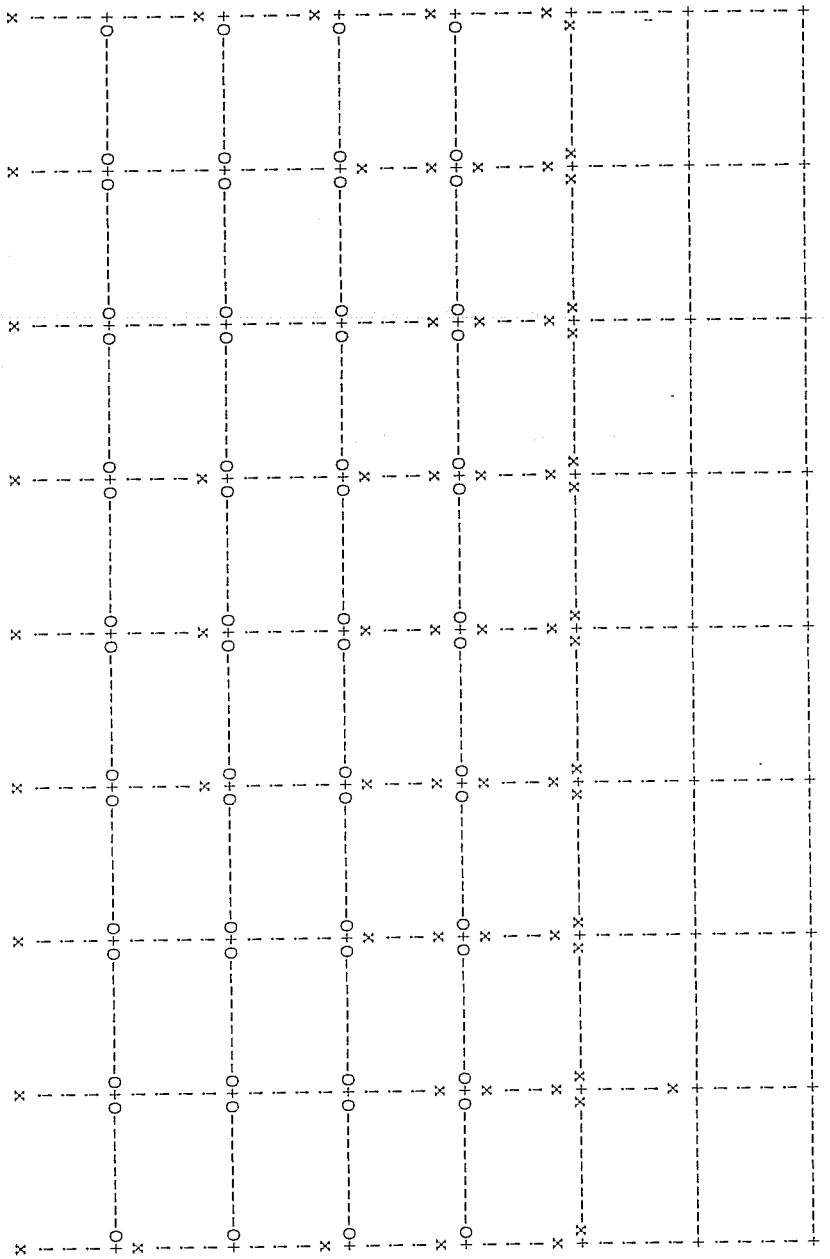
5.4 Ten-Story Building in the Whittier Narrows Earthquake

The building was analyzed in the north-south (longitudinal) direction. In this direction, the lateral load resisting system consisted of two exterior spandrel beam-column perimeter frames and two interior slab-column frames (Figure 3.30). The building was modeled as a two-dimensional structure. The floor diaphragm was assumed to be infinitely rigid so the nodes within each floor level deformed the same amount laterally. The columns were assumed fixed at basement level.



Ground motion: 1971 San Fernando Earthquake.
 Damping coefficient: 5% of critical damping.
 Material strength: $4/3 \times$ (design values).
 Hysteretic modeling rules: $HC = 2.0, HBD = HBE = 0.0, HS = 0.5$

Figure 5.27 Comparisons Between Calculated and Recorded Roof and 4th Floor Relative Displacement Time History under the 1971 San Fernando Earthquake using IDARC



NOTATION:
 - = BEAM
 + = COLUMN
 O = JOINT
 x = CRACK

Figure 5.28 Failure State of the Seven-Story Hotel Subject to the 1971 San Fernando Earthquake from IDARC Calculation

Figure 5.29 shows the structural model for nonlinear dynamic analyses. For the exterior frame, slabs were assumed to interact with spandrel beams. The width of slabs adjacent to beams was determined using ACI 318-95 code provisions in Sections 8.10.2 and 8.10.3⁶⁹ for strength consideration. In calculating stiffness of the beam, the flange width was taken as an average of the T-beam section and the rectangular beam section to take into account positive and negative moment effects along the beam. For interior slab-column frames, previous research⁷⁰ on flat-plate frame buildings suggested that the use of an effective width based on elastic plate theory significantly overestimates the stiffness of the structure for drift ratios higher than 0.0025%. In order to account for the stiffness of the slab at large lateral drifts, an equivalent width of 36 inches, equal to $C + 3h$ (where C = column width and h = slab thickness) was recommended for this structure⁴⁹.

Slab longitudinal reinforcement within the flange width was considered as part of beam longitudinal reinforcement. Because slab reinforcement was not shown in the building information collected, it was redesigned using UBC-70⁷³, the code used for the design of this building. From the calculation, 1#4 was included in the calculation of exterior spandrel beam strength, and 3#4 were considered as interior beam reinforcement.

Because of the problems experienced with IDARC, only DRAIN-2D was used for the nonlinear dynamic time history analyses for this building.

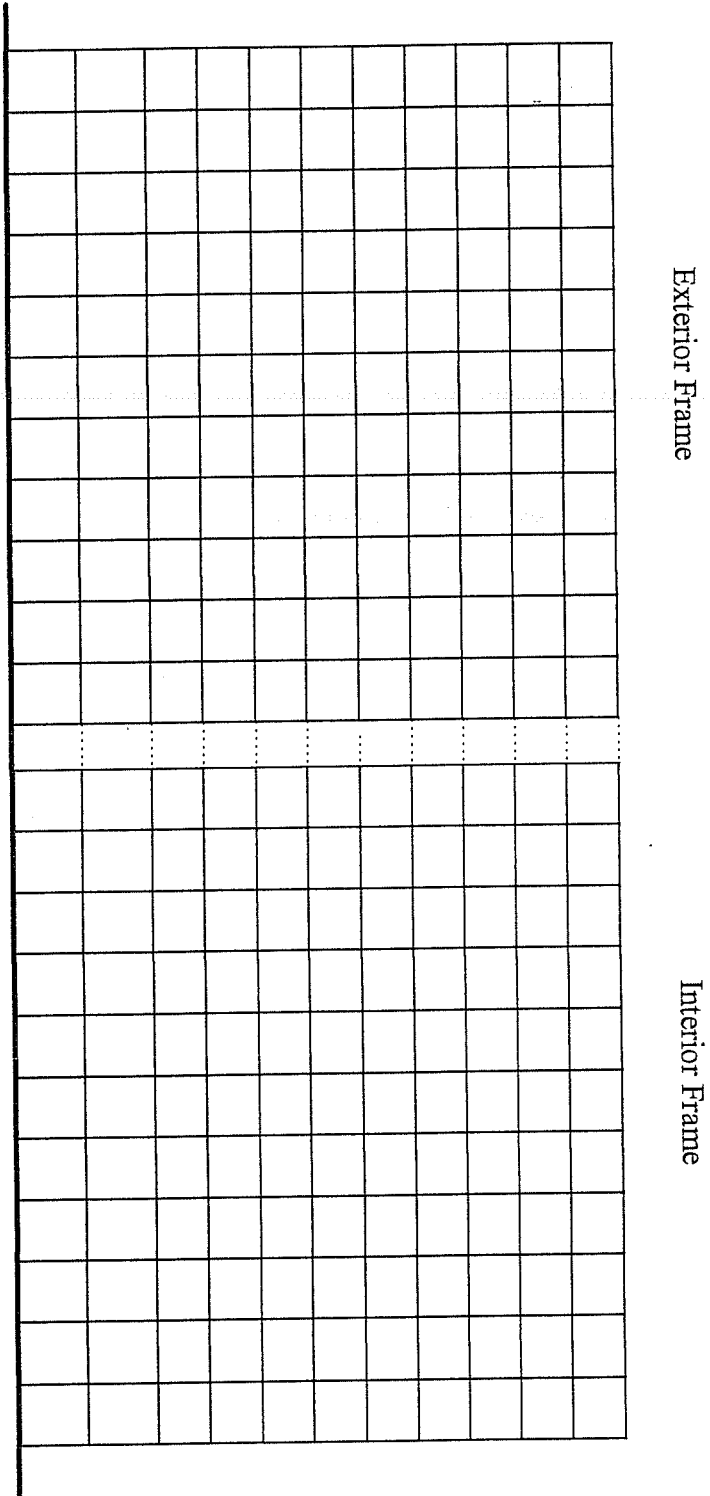


Figure 5.29 Structure Model for the Ten-Story Building

5.4.1 Evaluation of Response Records

Although the earthquake lasted about 30 seconds, the duration of strong ground motion was only about 4 seconds (Figure 3.34). Figure 5.30 shows relative displacement time history data recorded at the 10th and 5th floor levels. The period of vibration, during the strong motion part of the earthquake, appeared to be around 1.4 seconds and remained about the same thereafter. The structure response did not indicate significant changes in stiffness and is consistent with the results of an inspection of the building which indicated no visual damage to the structure.

Because there was only one sensor at each floor level, no torsional effects can be evaluated. However, the sensors at the 5th and the 10th floor were located very close to the torsional center of the building in the longitudinal direction. Therefore, the response in the longitudinal direction should not be influenced significantly by torsional effects.

5.4.2 Analysis Results

The procedure for choosing parameters was the same as outlined in Section 5.2.2. Only option 1 was used to assign the member effective stiffness.

- (1) Damping coefficient: 5% of critical damping was chosen as an average recommended value for reinforced concrete structures.

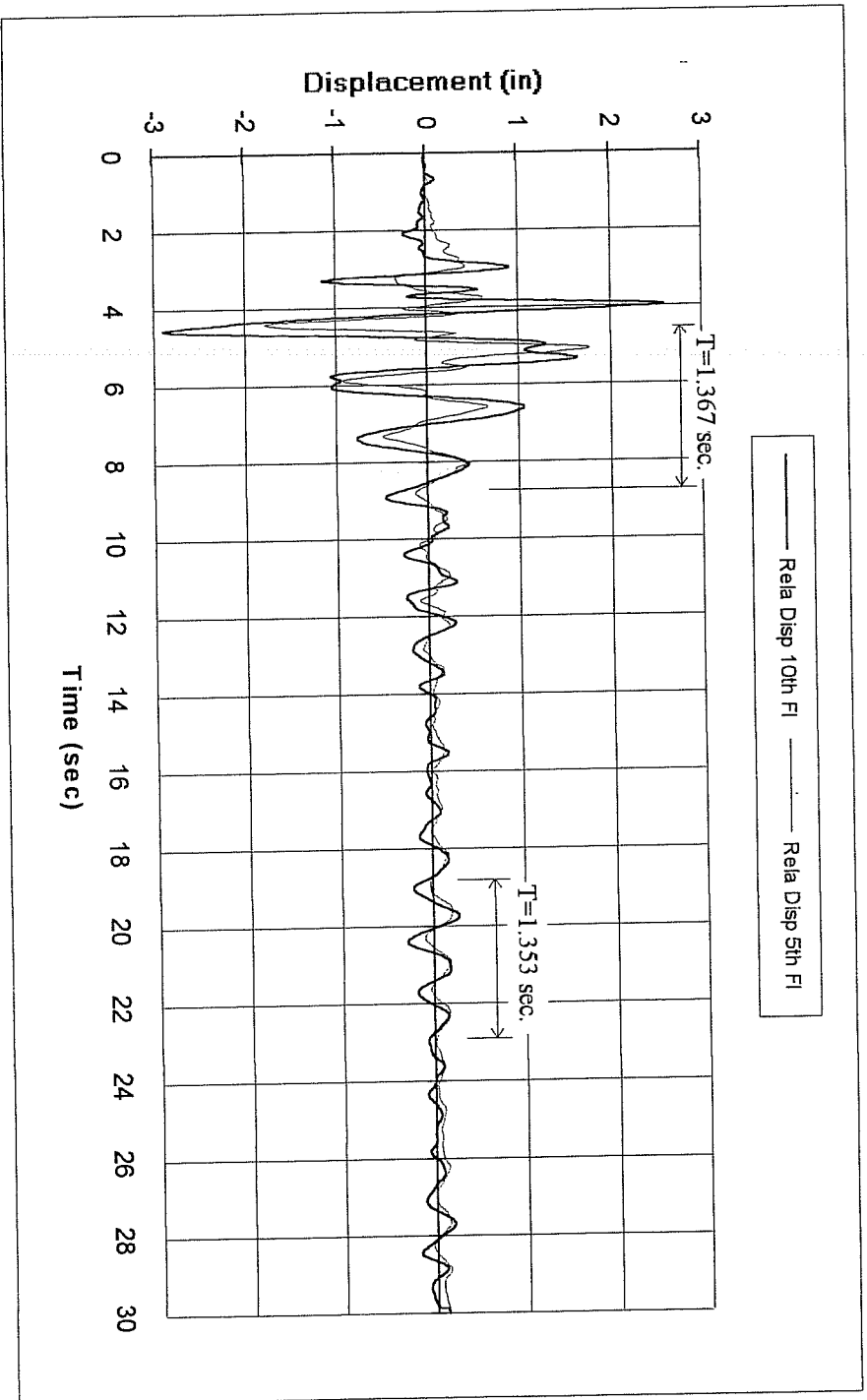


Figure 5.30 Recorded Floor Relative Displacement Time History
in North-South (Longitudinal) Direction. 1987 Whittier Narrows Earthquake

- (2) Actual material strength: Considering the age of the building and the relatively moderate intensity of the earthquake, $4/3$ x (design values) were used for both concrete and steel strengths.
- (3) Effective stiffness: Effective stiffness was chosen so that the calculated response time history would match the recorded period of vibration. After several trials, $0.40(EI_g)$ was chosen as the effective stiffness $(EI)_{\text{eff}}$ for beams and columns.
- (4) Residual shear capacity: The structure sustained no shear failure of members. To facilitate calculations, however, $2/3$ of original shear capacity was chosen as the residual shear capacity.

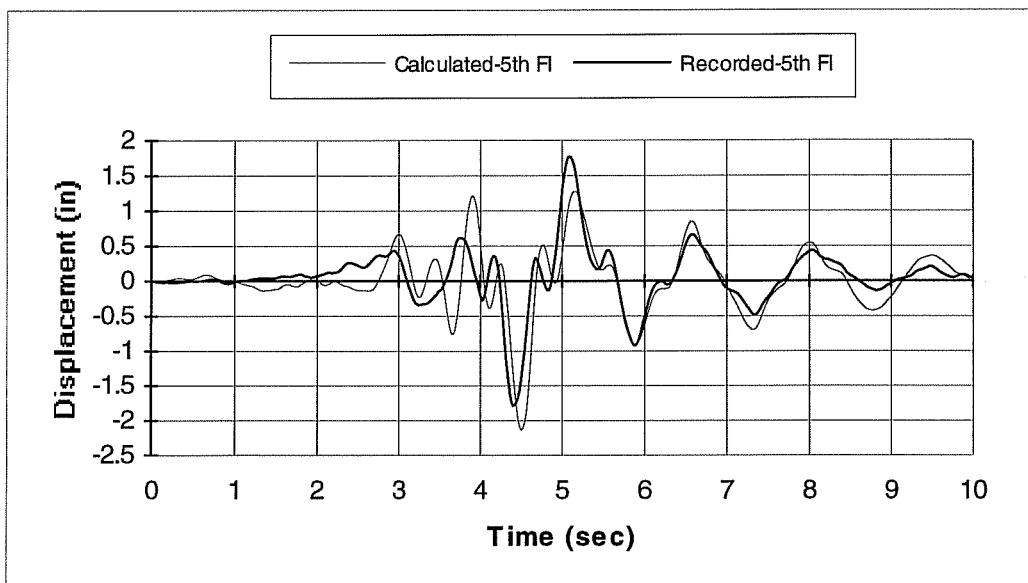
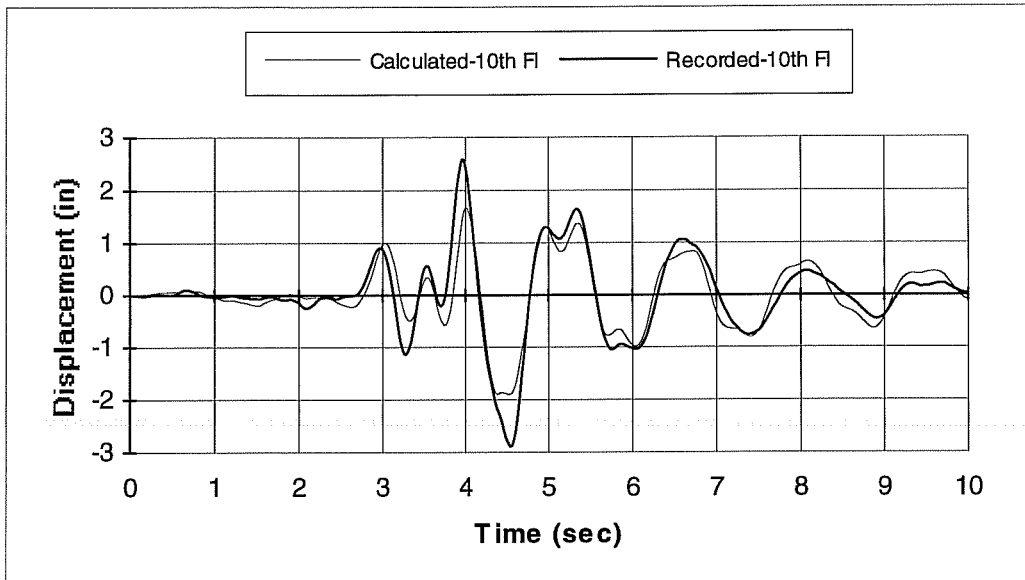
In Figure 5.31, the calculated and recorded relative displacement time histories at the 10th and 5th floor levels compare well.

Figure 5.32 shows the calculated story drift ratios. Compared with the drift ratios calculated for the seven-story hotel in the 1994 Northridge Earthquake, the story drift ratios are very small for this ten-story building in the 1987 Whittier Narrows Earthquake, and all floors meet the drift limit set by NEHRP-94 specifications. Because the first story is much taller than the rest of the stories in the building, it behaves as a soft story. Figure 5.32 shows a large inter-story drift ratio at the first story. Also from Figure 5.32, the inter-story ratios were larger in the 6th and

7th stories than in the 3rd and 4th stories, which clearly suggested participation of higher mode effects in the building response.

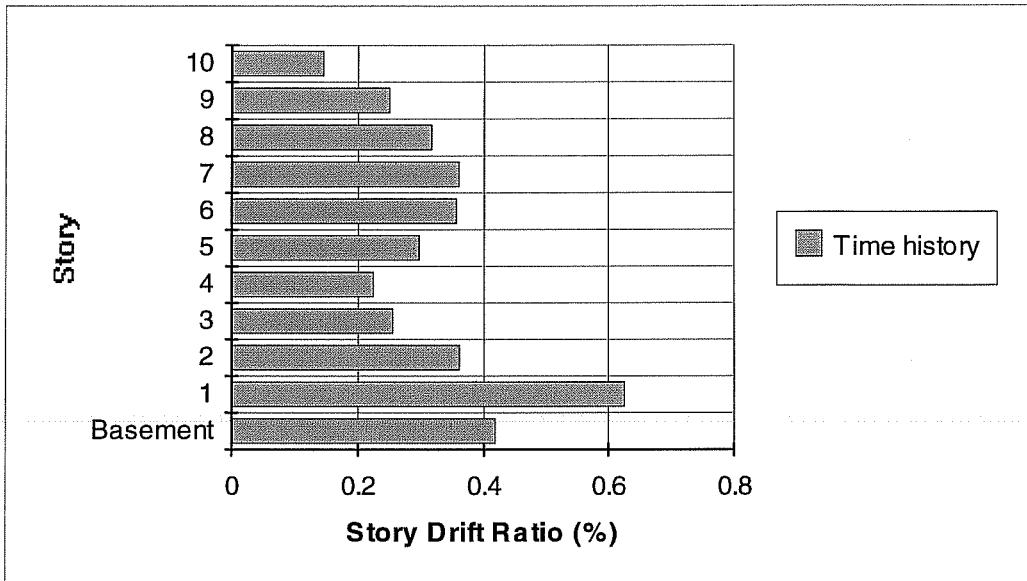
From the dynamic analysis, not only was there no shear failure in the columns, but there was no yielding at the ends of beams and columns. These results are consistent with the building condition after the earthquake.

Figure 5.33 shows a comparison of the calculated absolute acceleration time histories with the recorded absolute acceleration time histories at the 10th and the 5th floor levels, respectively. The agreement between calculated and recorded data is reasonably good, and, in particular, agreement at the 10th floor is better than at the 5th floor.



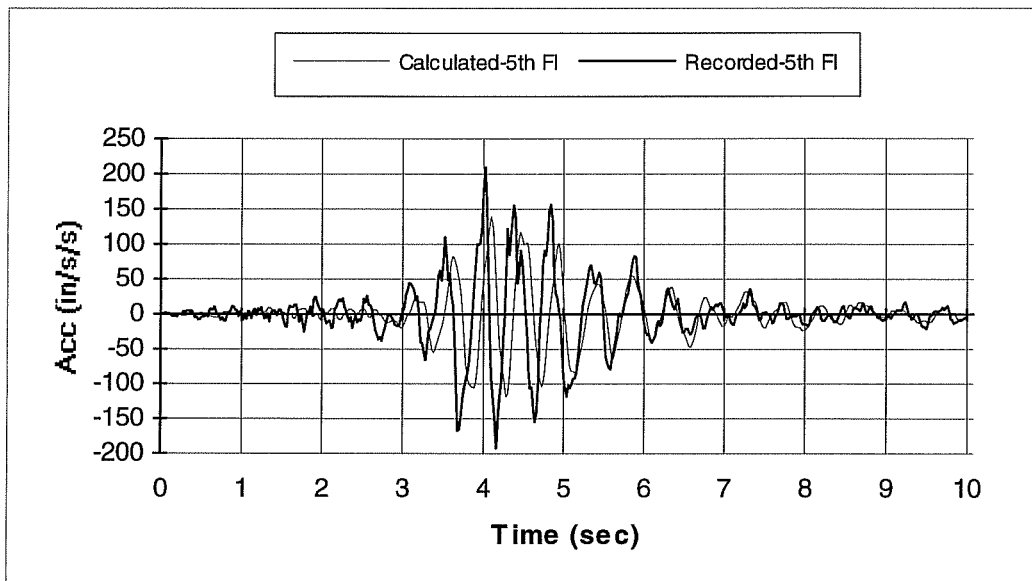
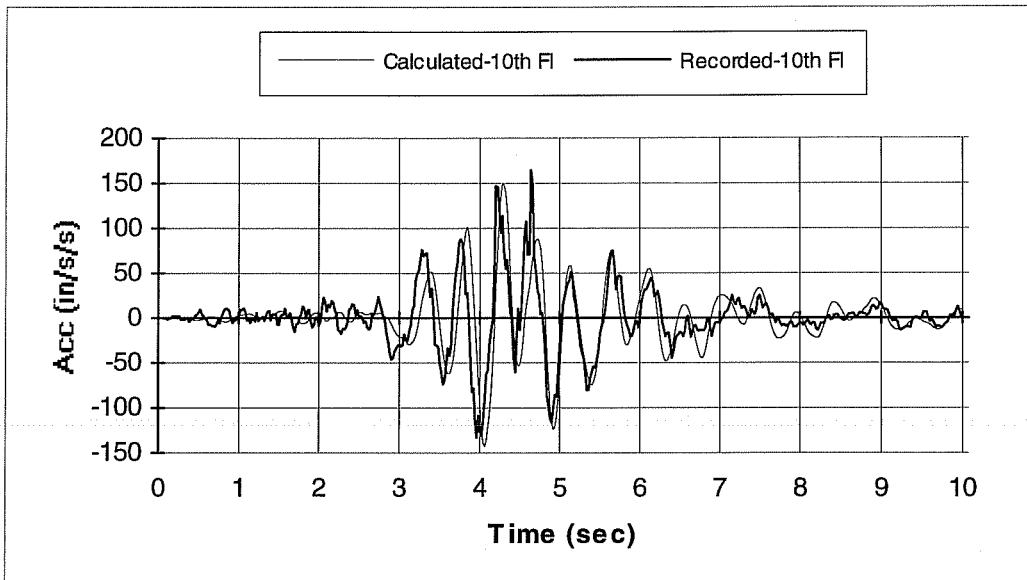
Ground motion:	1987 Whittier Narrows Earthquake.
Damping coefficient:	5% of critical damping.
Material strength:	4/3 x (design values).
Effective stiffness $(EI)_{\text{eff}}$:	0.40(EI_g).
Residual shear capacity:	2/3 of original shear capacity.

Figure 5.31 Comparison Between Calculated and Recorded 10th and 5th Floor Relative Displacement Time History during 1987 Whittier Narrows Earthquake



Ground motion: 1987 Whittier Narrows Earthquake.
 Damping coefficient: 5% of critical damping.
 Material strength: $4/3$ x (design values).
 Effective stiffness $(EI)_{\text{eff}}$: $0.40(EI_g)$.
 Residual shear capacity: $2/3$ of original shear capacity.

Figure 5.32 Calculated Story Drift Ratios for the Ten-Story Building.
1987 Whittier Narrows Earthquake



Ground motion:	1987 Whittier Narrows Earthquake.
Damping coefficient:	5% of critical damping.
Material strength:	$\frac{4}{3}$ x (design values).
Effective stiffness $(EI)_{\text{eff}}$:	$0.40(EI_g)$.
Residual shear capacity:	$\frac{2}{3}$ of original shear capacity.

Figure 5.33 Comparison Between Calculated and Recorded Absolute Acceleration Time History at the 10th and 5th Floor. 1987 Whittier Narrows Earthquake

CHAPTER 6

NONLINEAR STATIC (PUSH-OVER) ANALYSES

6.1 General

In lieu of nonlinear dynamic time history analyses for structural seismic design and evaluation, an alternative procedure, the nonlinear static (push-over) analysis, was included in the “Guidelines for the Seismic Rehabilitation of Buildings”⁵. This procedure is described as follows:

- (1) Represent the structure in a two- or three-dimensional analytical model which includes all important linear and nonlinear behavior of the structure.
- (2) Apply lateral loads in patterns that represent approximately the relative inertial forces generated at each floor level.
- (3) Push the structure under these lateral loads to displacements that are larger than the maximum displacements expected in design earthquakes.

Figure 6.1 illustrates the push-over analysis procedure schematically. The push-over analysis provides a base shear vs. roof displacement relationship, and indicates the inelastic limit as well as lateral load capacity of the structure. The changes in slope of this curve give an indication of yielding of various structural elements.

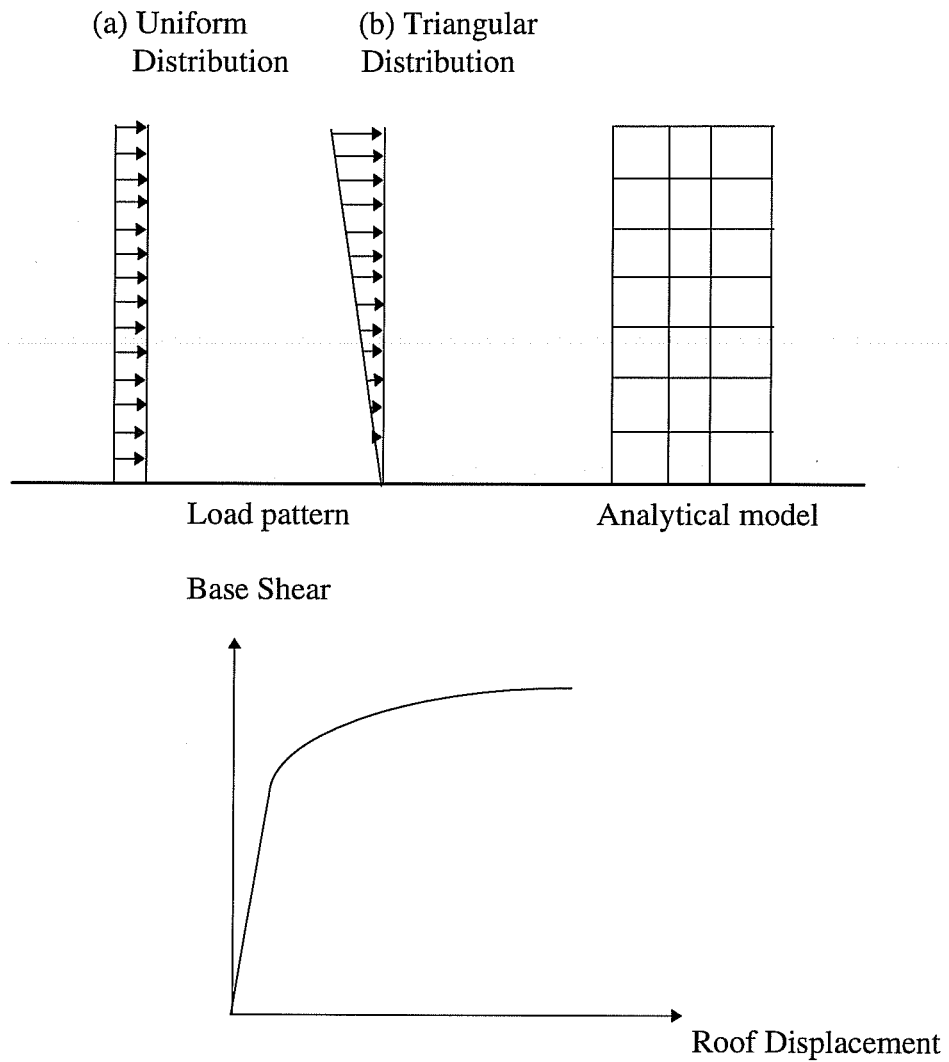


Figure 6.1 Push-Over Analysis Procedure

The objective of the push-over analysis is to estimate member forces and global as well as local deformation capacity of a structure. The information can be

used to assess the integrity of the structure. To evaluate the applicability of this simplified nonlinear analysis, two buildings analyzed in the previous chapter using nonlinear dynamic time history analyses were analyzed using push-over analyses. The strength and deformation capacity estimated using push-over analyses were compared with actual recorded strength and deformation capacity of the structures.

As in the dynamic analysis, gravity loads were applied to the structure as an initial load condition.

For consistency and for making comparisons, the same structural models used for dynamic time history analyses in Chapter 5 were used here for push-over analyses. Only program DRAIN-2D was used to perform push-over analyses.

6.2 Seven-Story Hotel

As in nonlinear time history analyses, the building was first analyzed by the push-over procedure with the material properties at the time of the 1994 Northridge Earthquake. Then the building was analyzed with the material properties at the time of the 1971 San Fernando Earthquake. Push-over results were compared with the corresponding nonlinear time history results. First, seismic design criteria according to current codes is given in the following section.

6.2.1 Current Seismic Design Criteria

According to UBC-94⁶, the seven-story hotel should be designed to resist the base shear:

$$\frac{V}{W} = ZIC / R_w \quad (6.1)$$

For this structure, $Z = 0.4$ (Zone 4);

$I = 1.0$ (Hotel);

$S_2 = 1.2$ (Soil type: 2);

$R_w = 5$ (Concrete ordinary moment frame).

So, $T = 0.030h^{3/4} = 0.03 \times 65.71^{3/4} = 0.69$ sec *onds*

$$C = \frac{1.25S}{T^{2/3}} = \frac{1.25 \times 1.2}{0.69^{2/3}} = 1.92 < 2.75, \text{ OK.}$$

$$C/R_w = 1.92/5 = 0.384 > 0.075, \text{ OK.}$$

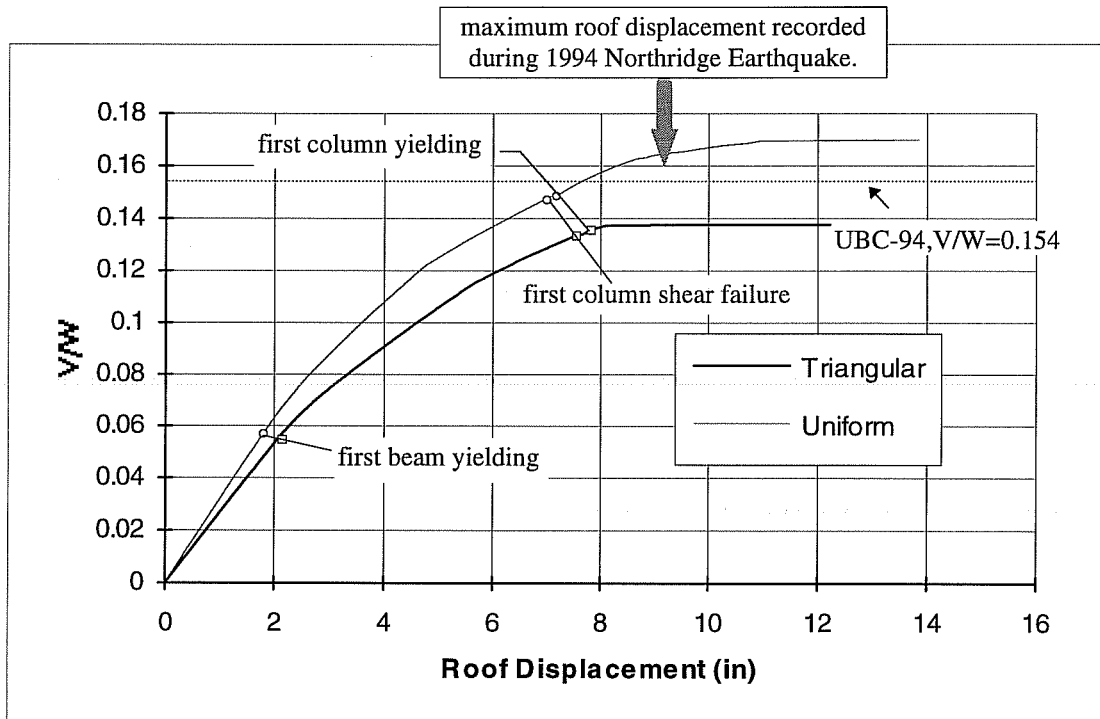
Therefore, $V/W = 0.157$.

6.2.2 1994 Northridge Earthquake

6.2.2.1 Loading Patterns

One of the questions regarding the push-over analysis is the sensitivity of results to the applied load pattern. Load patterns are intended to represent the distribution of inertial forces of design earthquakes. Since no two earthquakes have the same distribution of inertial forces, and the distribution changes with time during an earthquake, a load pattern that follows time variant distribution of inertia forces would be ideal. However, due to extra efforts required, simplified loading patterns are generally employed. Two commonly used loading patterns, namely the uniform distribution pattern and the triangular distribution pattern as shown in Figure 6.1 were studied. The triangular load distribution pattern is generally considered to reflect some higher mode effects in earthquakes.

Figure 6.2 shows (base shear V)/(weight of building W) vs. roof displacements with uniform and triangular load distribution patterns, respectively. The same parameters: $0.30(EI_g)$ as effective stiffness $(EI)_{eff}$, $3/2$ x (design values) as actual material strength, and $2/3$ of original shear capacity as residual shear capacity, were used.



Material strength: $3/2$ x (design values).
 Effective stiffness $(EI)_{\text{eff}}$: $0.30(EI_g)$.
 Residual shear capacity: $2/3$ of original shear capacity.

Figure 6.2 (Base shear V)/(Weight of building W) vs. Roof Displacement for the Uniform and Triangular Load Distribution Patterns

Also indicated on these plots is the maximum roof relative displacement recorded during the 1994 Northridge Earthquake. Push-over analyses successfully predicted that the structure almost lost its lateral load resisting capacity and shear failures of a column occurred at this displacement level.

Base shear V was calculated by summing all applied lateral forces above the ground level, and the weight of the building W was calculated by summing all

gravity loads on each floor without load factors. Because DRAIN-2D utilizes a force-control method for push-over analyses, no capacity can be calculated beyond the peak strength. So, for a uniform lateral load pattern, at a roof displacement of 10 inches, or at (V/W) of 0.167, the structure has failed. For a triangular pattern, at a roof displacement of 8 inches, or at (V/W) of 0.137, the structure failed. Therefore, from different lateral load patterns, push-over analyses indicated differences in displacement and strength capacities. A triangular pattern results in 25% less capacity in displacement and 22% less capacity in strength at structural failure than a uniform pattern.

Also shown in Figure 6.2 is the base shear coefficient obtained following UBC-94 in Section 6.2.1.1. According to UBC-94, the building is adequate under a uniform load pattern, and inadequate under a triangular load pattern. Since the building almost collapsed during the 1994 Northridge Earthquake, the UBC-94 shear approach predicted the capacity of the building reasonably well, and a triangular lateral load pattern should be considered as a more critical loading pattern for push-over analyses.

Figures 6.3 and 6.4 show the failure sequence from push-over analyses using uniform and triangular lateral load patterns, respectively. Calculation terminated at $(V/W) = 0.170$, and 0.138 for the uniform and the triangular lateral load pattern, respectively. At higher values, the structure deflected without bound with only a

small increase in lateral forces. The structure was considered to reach failure at these values. From Figures 6.3 and 6.4, the structure follows quite different failure sequences for uniform and triangular load patterns. The triangular load pattern predicts a failure sequence very close to the observed damage state of the building and to the result obtained from nonlinear time history analyses (Figure 5.16).

The maximum story drift ratios using a uniform load pattern and a triangular load pattern are plotted in Figure 6.5. Again, in Figure 6.5, maximum inter-story drift ratios were quite different for the two different load patterns. For the uniform load pattern inter-story displacement was concentrated in lower floor levels, while for the triangular load pattern inter-story displacement was concentrated in middle floor levels. Higher mode effects were better represented using a triangular load pattern. From actual damage that occurred in the building, the push-over analysis with the triangular load pattern definitely predicted the response of this building under the 1994 Northridge Earthquake better than the analysis with the uniform load pattern.

Since the maximum recorded relative displacement at the roof during the 1994 Northridge Earthquake was 9.2 inches, the inter-story drift ratios when the roof displacement reached 9.2 inches in the push-over analyses were computed. Figure 6.6 shows the drift ratios calculated for the uniform and triangular load patterns. Also plotted in the figure are the maximum drift ratios from the nonlinear dynamic analyses as well as from the recorded data. As can be seen, the triangular load values

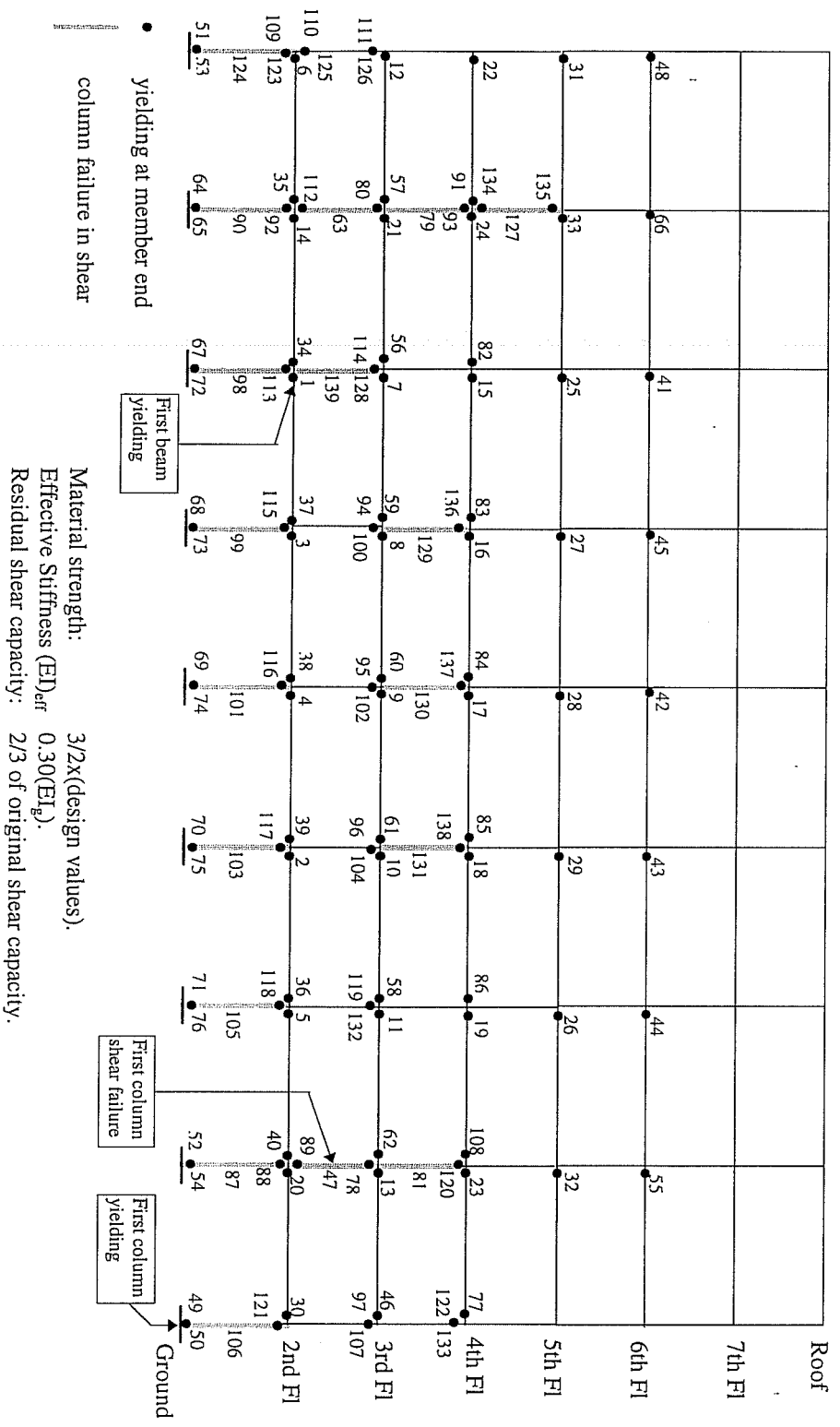


Figure 6.3 Failure Sequence from Push-Over Analysis with Uniform Lateral Load Distribution

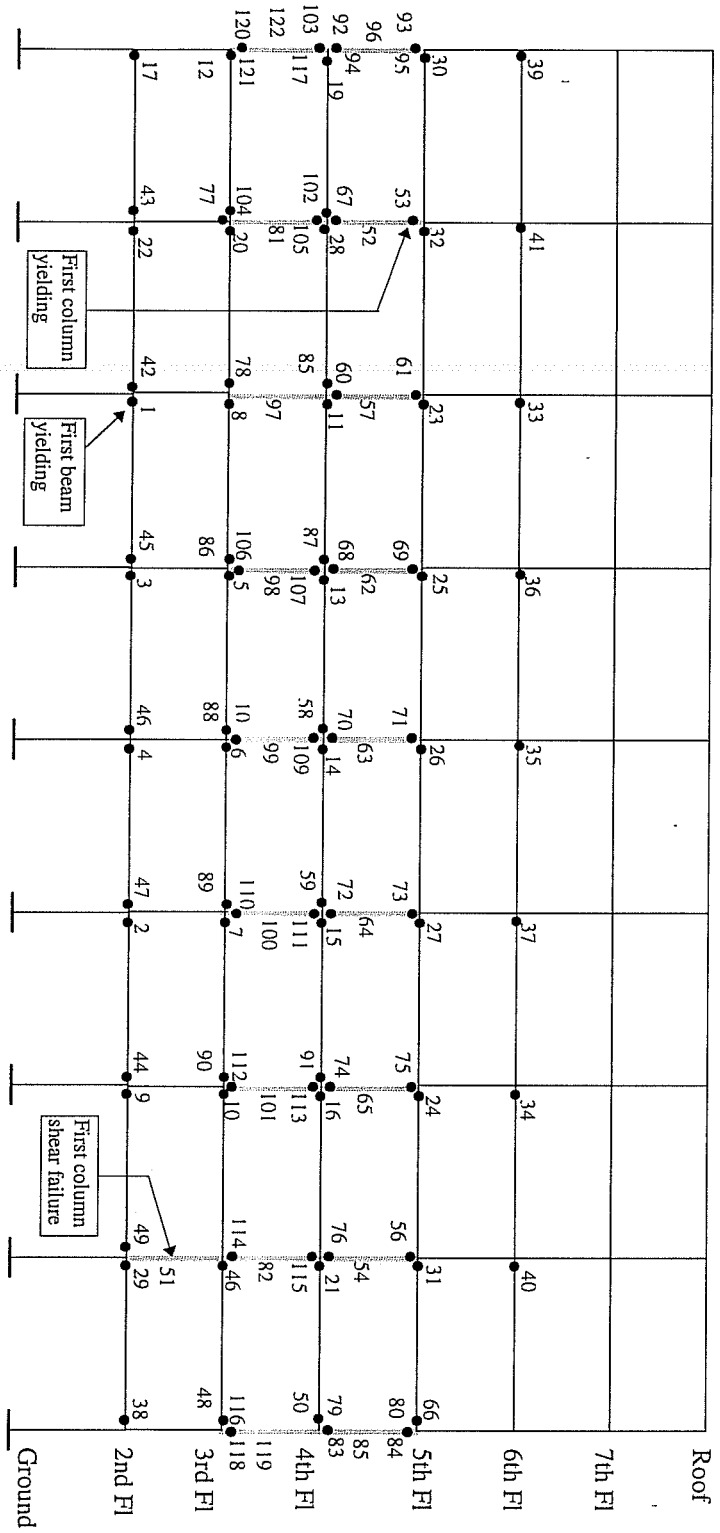
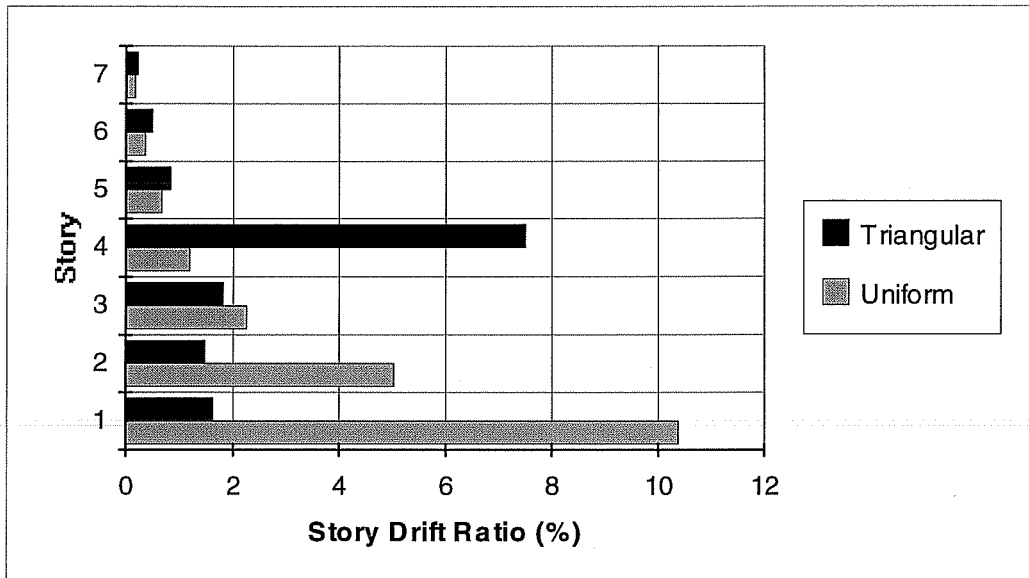


Figure 6.4 Failure Sequence from Push-Over Analysis with Triangular Lateral Load Distribution



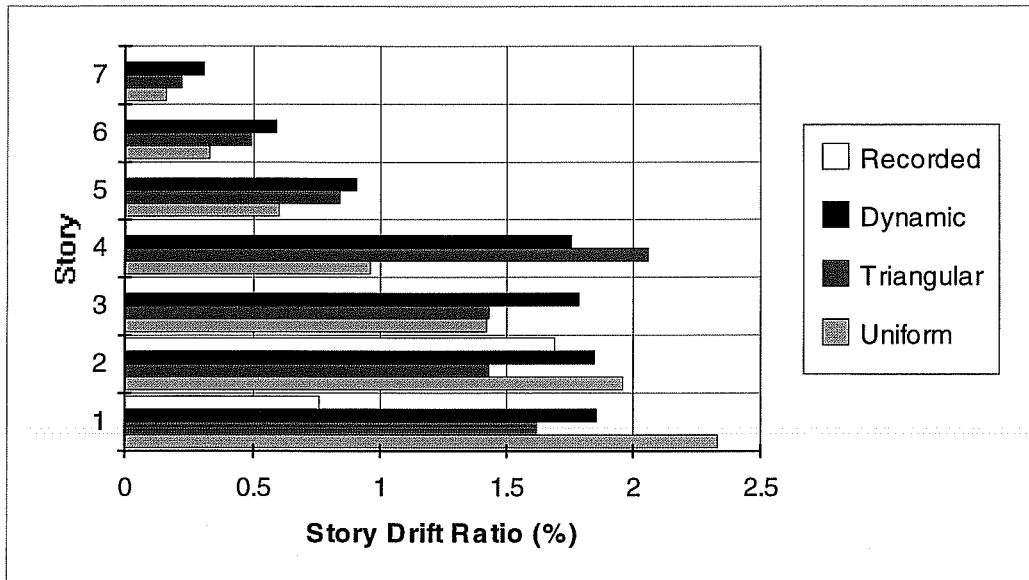
Material strength: $3/2 \times$ (design values).
 Effective stiffness $(EI)_{\text{eff}}$: $0.30(EI_g)$.
 Residual shear capacity: $2/3$ of original shear capacity.

Figure 6.5 Maximum Story Drift Ratios for Different Load Patterns

and the dynamic analysis results compare reasonably well in all stories, but are much larger than the observed values at the first story and are quite close at the second story.

6.2.2.2 Effects of Effective Stiffness $(EI)_{\text{eff}}$

The importance of effective stiffness has been demonstrated in dynamic time history analyses (Chapter 5). Here, again, effects of effective stiffness on push-over analyses were explored. Only Option 1 was used for assigning effective stiffness of structural elements in push-over analyses.

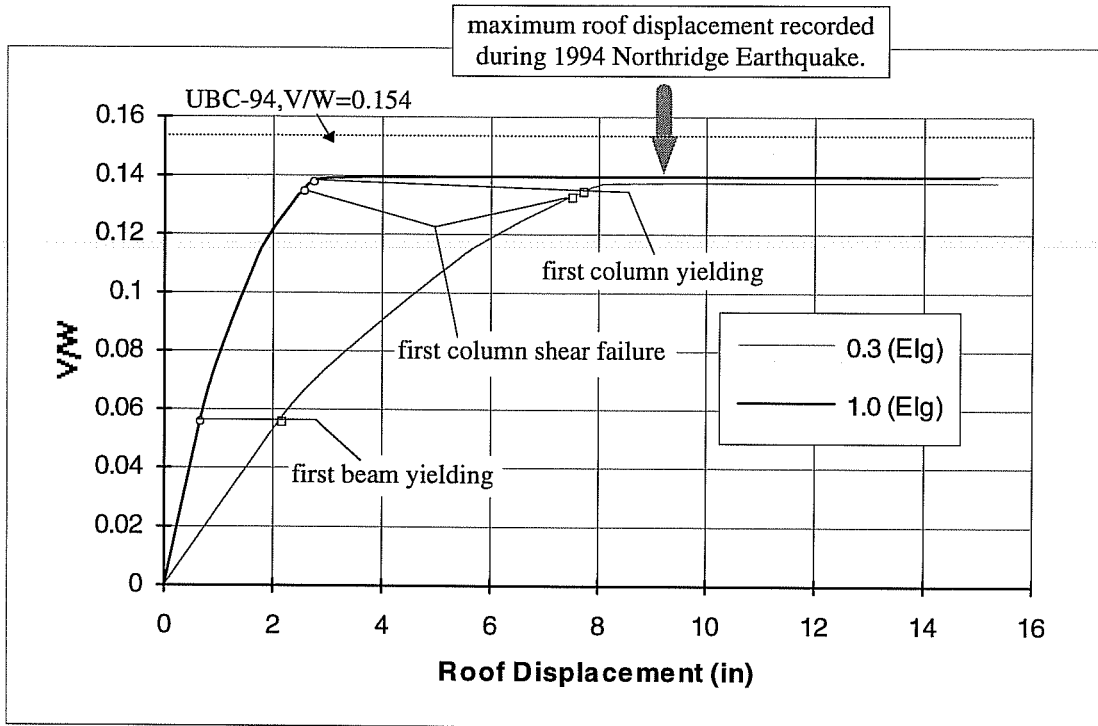


Ground motion: 1994 Northridge Earthquake.
 Damping coefficient: 5% of critical damping.
 Material strength: 3/2 x (design values).
 Effective stiffness (EI_{eff}): $0.30(EI_g)$.
 Residual shear capacity: 2/3 of original shear capacity.

Figure 6.6 Story Drift Ratios When Roof Relative Displacement Reaching Maximum Recorded Value For Different Load Patterns

Two different effective stiffnesses were included in the study, namely $0.30(EI_g)$ used in dynamic analyses and $1.0(EI_g)$ for gross section stiffness. Only a triangular load pattern was used for this comparison. Figure 6.7 shows the push-over analysis results using $1.0(EI_g)$ as effective stiffness. Also shown in the figure is the push-over analysis results using $0.3(EI_g)$ as effective stiffness for comparison. The different effective stiffness has a large effect on the results of the push-over analysis. The roof displacements of the building predicted by push-over analyses with different

effective stiffness values are significantly different, although strength (base shear) capacity remains almost the same.



Material strength: $3/2$ x (design values).
 Residual shear capacity: $2/3$ of original shear capacity.

Figure 6.7 (Base shear)/(Weight of building) vs. Roof Displacement with Triangular Load Pattern Using Different Effective Stiffnesses

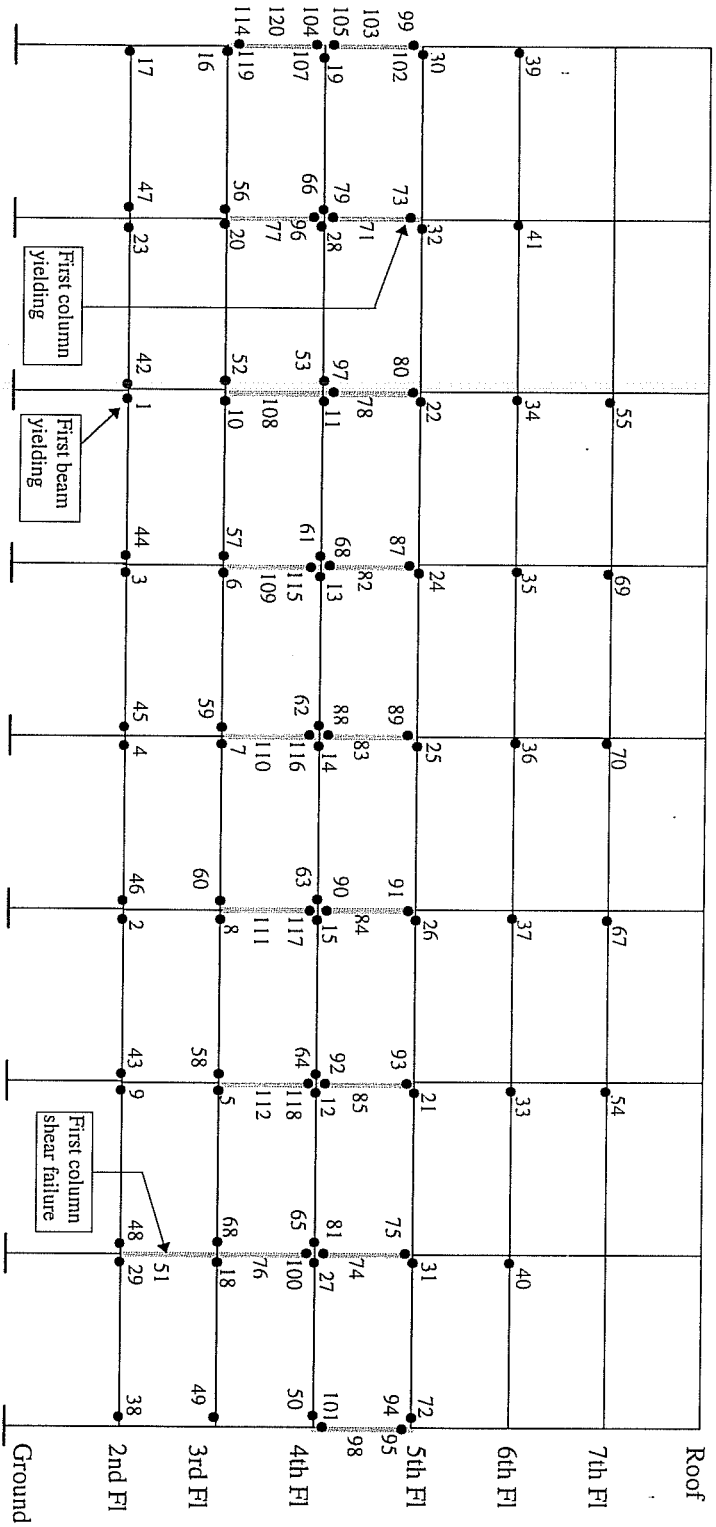
Figure 6.8 shows the failure sequence of the push-over analysis assuming $1.0(EI_g)$ as effective stiffness. Comparing Figure 6.8 with Figure 6.4, we can see that the failure sequence was almost the same with different effective stiffnesses. It is important to note that if the only objective of the push-over analysis is a

determination of capacity, stiffness is not important. However, for a design based on performance, particularly deformation response, large differences may be obtained unless stiffness is carefully considered.

6.2.3 1971 San Fernando Earthquake

This time, only effects of different loading patterns were explored, because the influence of different effective stiffness was expected to be the same for the same building. In Figures 6.9 the (base shear V)/(weight of building W) vs. roof relative displacement curves with uniform and triangular lateral load distribution patterns are plotted. The same parameters used in the 1971 San Fernando Earthquake: $0.80(EI_g)$ as effective stiffness $(EI)_{\text{eff}}$, $4/3$ x (design values) as actual material strength, and $2/3$ of original shear capacity as residual shear capacity, were used.

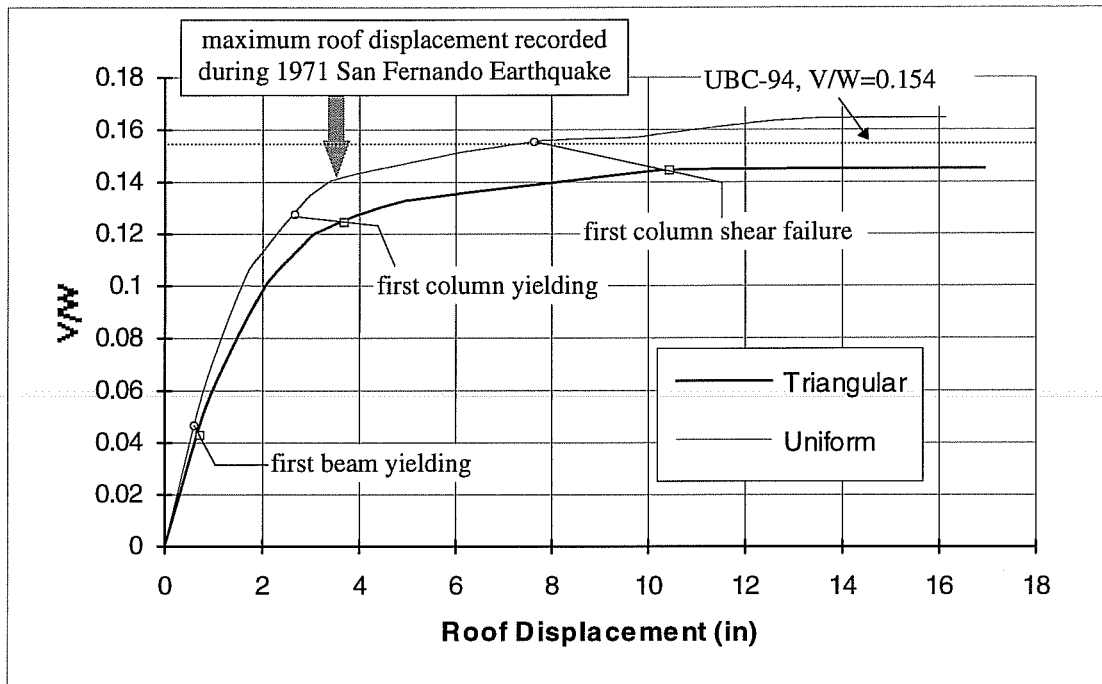
Once again, differences in V/W vs. roof displacement curves were noticeable, if not significant. The uniform lateral load pattern showed a little higher base shear capacity. The lateral deflection capacity predicted by these two different lateral load patterns was almost the same. In addition, the uniform lateral load pattern presented a little stiffer structure than the triangular pattern did. Also indicated on these figures was the actual recorded roof maximum relative displacement during the 1971 San Fernando Earthquake. Once again, push-over analyses successfully predicted that member yielding occurred, but no shear failure of columns occurred.



- yielding at member end
- column failure in shear

Material strength: $3/2 \times (\text{design values})$.
 Effective Stiffness $(EI)_{\text{eff}} = 1.0(EI_g)$.
 Residual shear capacity: $2/3$ of original shear capacity.

Figure 6.8 Failure Sequence from Push-Over Analysis with $1.0(EI_g)$ as Effective Stiffness



Material strength: $4/3$ x (design values).
 Effective stiffness $(EI)_{\text{eff}}$: $0.80(EI_g)$.
 Residual shear capacity: $2/3$ of original shear capacity.

Figure 6.9 (Base shear)/(Weight of building) vs. Roof Displacement for the Uniform and Triangular Load Distribution Patterns

In the 1971 San Fernando Earthquake, the maximum roof relative displacement was 3.4 inches. Figures 6.10 and 6.11 show the failure sequence of push-over analyses up to a roof displacement of 3.4 inches. Comparing these plots with the results from the dynamic analysis in Chapter 5 (Figure 5.23), the failure sequence predicted by push-over analyses with the triangular lateral load distribution pattern has a better agreement with the dynamic time history analysis results than the failure sequence predicted with the uniform load pattern.

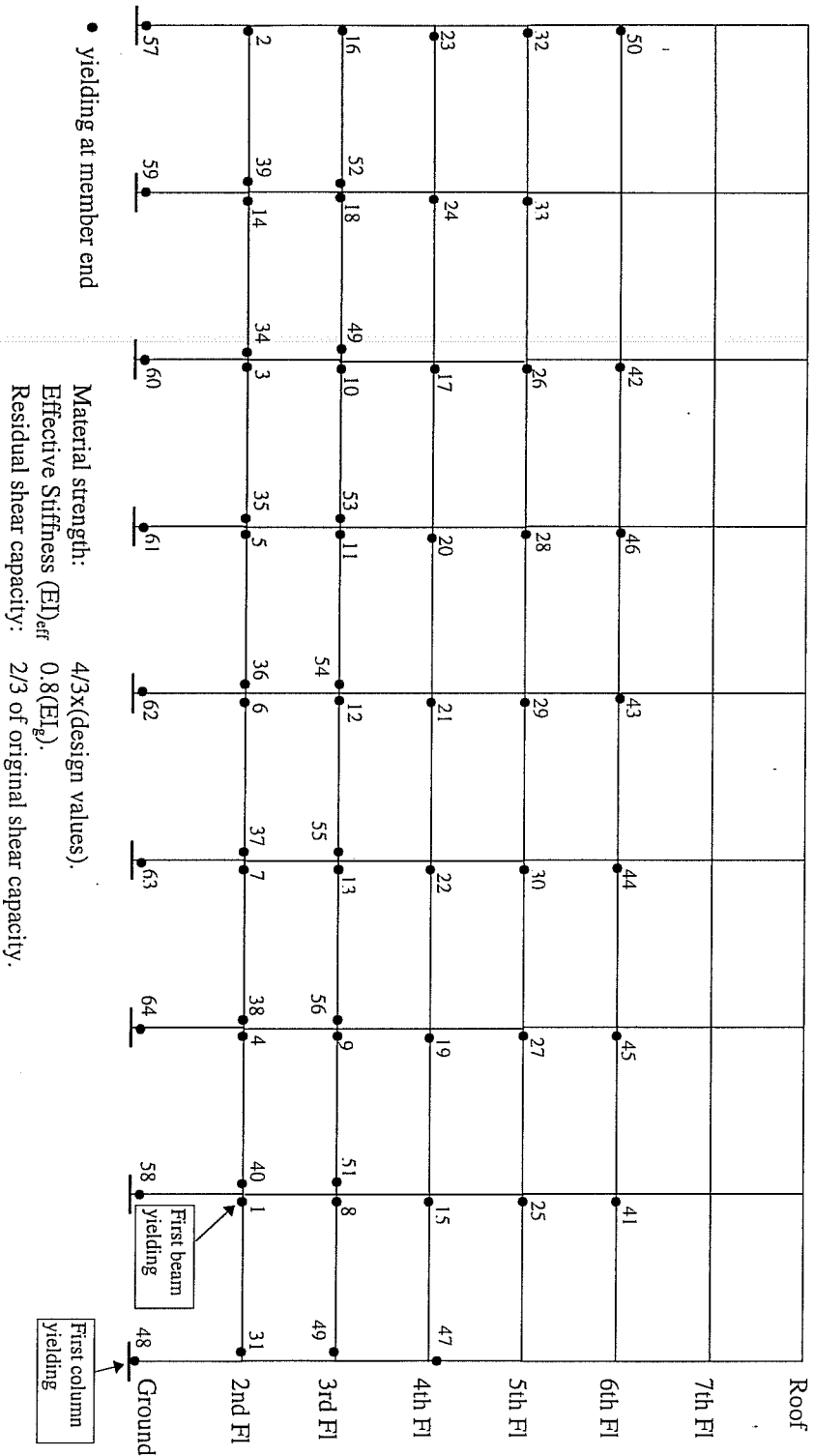
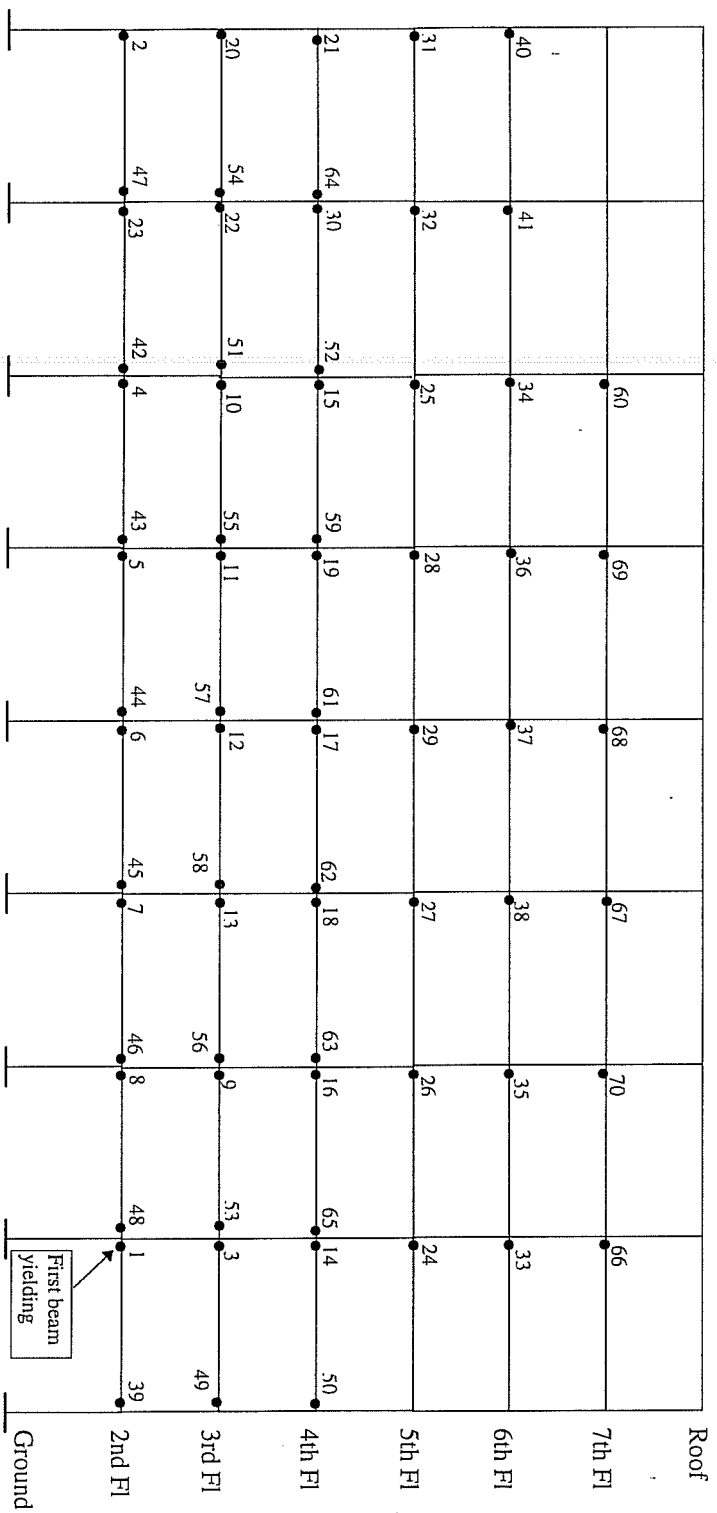


Figure 6.10 Failure Sequence Up to Roof Displacement of 3.421 inches from the Push-Over Analysis with the Uniform Lateral Load Pattern



- yielding at member end

Material strength:

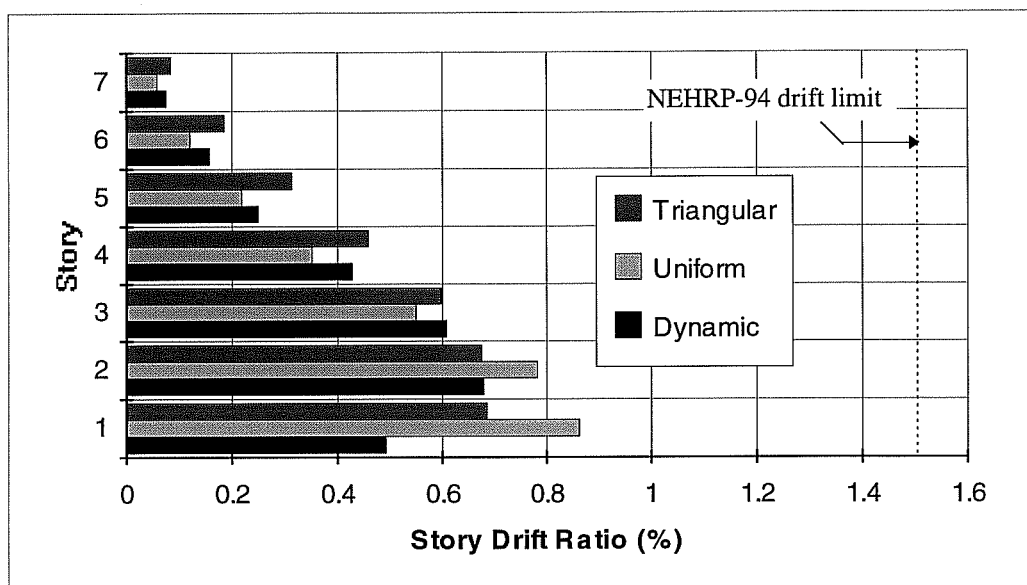
$\frac{4}{3} \times (\text{design values})$.

Effective Stiffness $(EI)_{eff}$ $0.8(EI)_g$.

Residual shear capacity: $\frac{2}{3}$ of original shear capacity.

Figure 6.11 Failure Sequence Up to Roof Displacement of 3.421 inches from the Push-Over Analysis with the Triangular Lateral Load Pattern

In Figure 6.12, the maximum inter-story drift ratios between nonlinear dynamic time history analyses and nonlinear static (push-over) analyses are compared. The maximum inter-story drift ratios for push-over analyses were calculated when roof relative displacement reached 3.4 inches (the maximum roof relative displacement recorded during the 1971 San Fernando Earthquake). General agreement in inter-story drift ratios between the dynamic and the push-over analyses obviously exists, with the triangular pattern showing better correlation with the dynamic analysis.



Ground motion: 1971 San Fernando Earthquake.
Damping coefficient: 5% of critical damping.
Material strength: $4/3$ x (design values).
Effective stiffness $(EI)_{eff}$: $0.80(EI_g)$.
Residual shear capacity: $2/3$ of original shear capacity.

Figure 6.12 Story Drift Ratios When Roof Relative Displacements Reach Maximum Recorded Values For Different Load Patterns

6.3 Ten-Story Building

As in the push-over analyses for the seven-story hotel, effects of different lateral load patterns and different effective stiffnesses were analyzed for the ten-story building. The same parameters used in dynamic time history analyses were used for push-over analyses. These parameters include: $4/3 \times$ (design values) as actual strength of materials, $0.40(EI_g)$ as effective stiffness $(EI)_{\text{eff}}$, and $2/3$ of original shear capacity as residual shear capacity. First, the seismic design criteria according to current and former codes are discussed.

6.3.1 Seismic Design Criteria

The design base shear according to the UBC-94 Code was determined as follows:

$$\frac{V}{W} = ZIC / R_w \quad (6.1)$$

For this structure, $Z = 0.4$ (Zone 4);

$I = 1.0$ (Hotel);

$S_2 = 1.2$ (Soil type: 2);

$R_w = 5$ (Concrete ordinary moment frame).

$$\text{So, } T = 0.030h^{3/4} = 0.03 \times 99.67^{3/4} = 0.946 \text{ sec onds}$$

$$C = \frac{1.25S}{T^{2/3}} = \frac{1.25 \times 1.2}{0.946^{2/3}} = 1.56 < 2.75, \text{ OK.}$$

$$C/R_w = 1.56/5 = 0.312 > 0.075, \text{ OK.}$$

Therefore, $V/W = 0.125$.

The (design shear V)/(weight of building W) calculated by the UBC-70 Code, the code used for original design of the building is⁴⁹:

$$V/W = 0.125$$

Corresponding load and strength reduction factors were included⁴⁹.

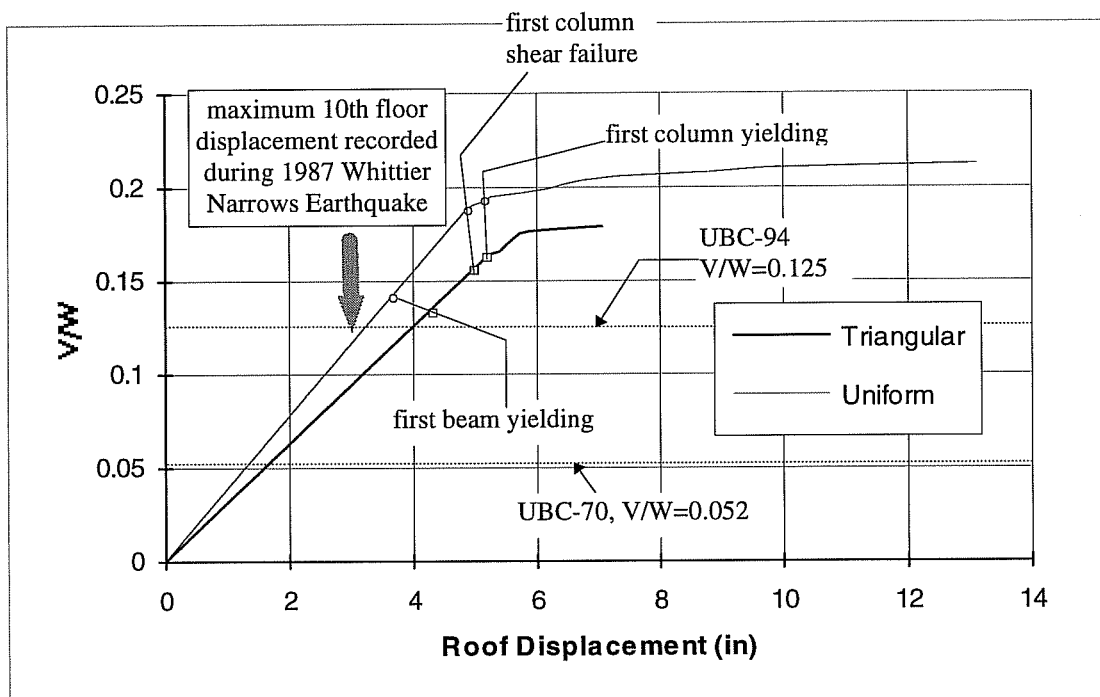
6.3.2 Loading patterns

Figure 6.13 shows the (base shear V)/(weight of building W) vs. roof relative displacement curves for uniform and triangular lateral load patterns.

Base shear V was calculated by summing all applied lateral forces above the basement level, and the weight of the building W was calculated by summing all gravity loads on each floor without load factors. Again, from different lateral load patterns, push-over analyses indicate different strengths. Under the triangular pattern, the strength is lower. However, displacement capacity using both lateral load patterns was almost the same. In addition, push-over analysis results from the triangular

lateral loading indicated a slightly softer structure than with the uniform lateral load pattern.

Also indicated on these figures is the maximum 10th floor relative displacement recorded during the 1987 Whittier Narrows Earthquake. From dynamic analyses, maximum roof displacement was only a little larger than the maximum 10th floor displacement. Therefore the recorded 10th floor maximum displacement was used as a basis for comparison.



Material strength: $4/3$ x (design values).
 Effective stiffness $(EI)_{\text{eff}}$: $0.40(EI_g)$.
 Residual shear capacity: $2/3$ of original shear capacity.

Figure 6.13 (Base shear)/(Weight of building) vs. Roof Displacement for the Uniform and Triangular Load Distribution Patterns. Ten-Story Building

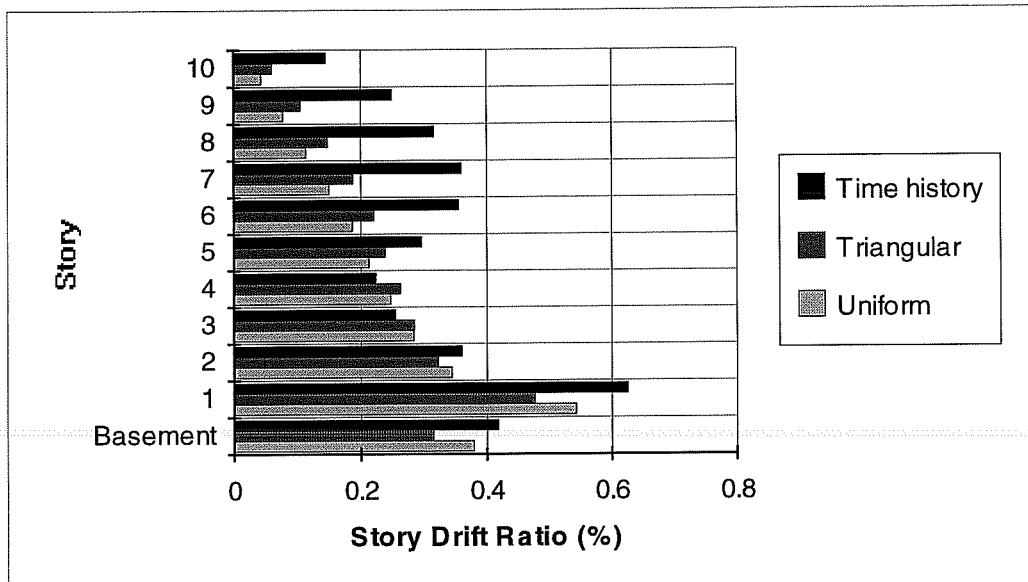
Also shown in Figure 6.13 are design shear coefficients calculated according to UBC-94 and UBC-70 Codes (Section 6.3.1). The lateral capacity of the building is well above design values for both standards.

In Figure 6.14, the maximum inter-story drift ratios computed using the dynamic analysis and the inter-story drift ratios obtained from the push-over analyses are compared. The inter-story drift ratios from push-over analyses were calculated when the 10th floor relative displacement reached 2.9 inches, the maximum 10th floor relative displacement recorded during the 1987 Whittier Narrows Earthquake.

Because the building is taller than the seven-story hotel, higher mode effects become significant. Although the inter-story drift ratios predicted by push-over analyses were close to the dynamic analysis at lower stories, the correlation in story drift ratios between the push-over analyses and the dynamic analysis at higher stories were unsatisfactory.

6.3.3 Effects of Effective Stiffness $(EI)_{\text{eff}}$

As in the case of the seven-story hotel, two different effective stiffness values were studied, namely $0.40(EI_g)$ used in dynamic analyses and $1.0(EI_g)$ for gross section stiffness. Only the triangular load pattern was used in the comparison. Figure 6.15 shows the push-over analysis results using $1.0(EI_g)$ as effective stiffness. Results using $0.4(EI_g)$ as effective stiffness are also included in the figure for comparison.

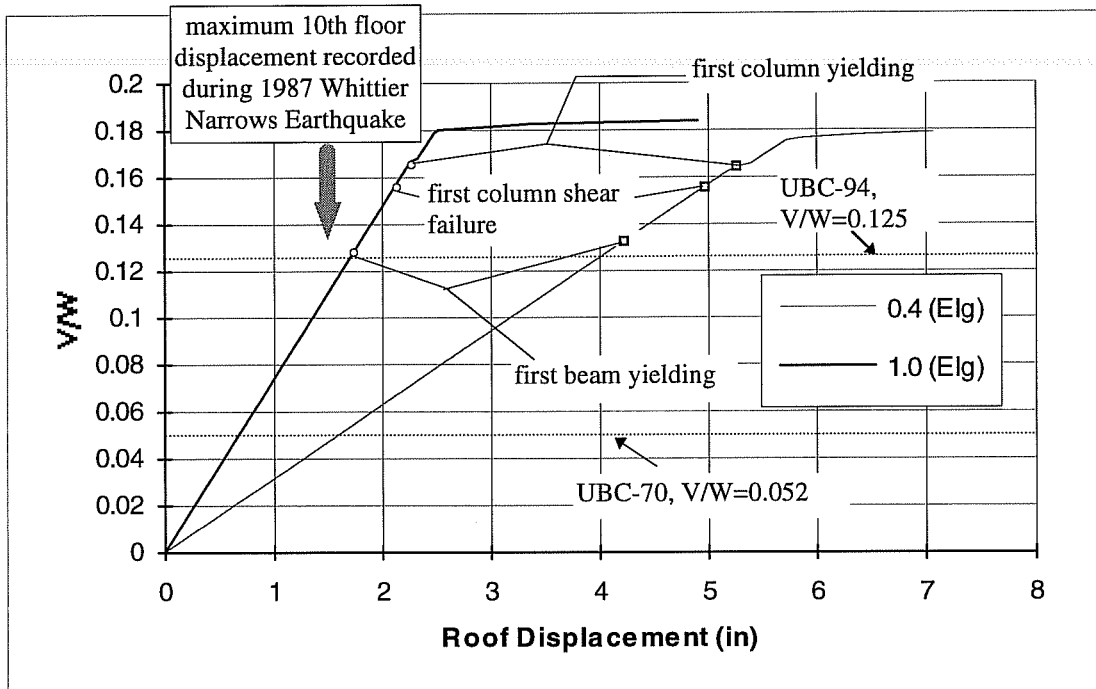


Ground motion: 1987 Whittier Narrows Earthquake.
 Damping coefficient: 5% of critical damping.
 Material strength: $4/3$ x (design values).
 Effective stiffness $(EI)_{\text{eff}}$: $0.40(EI_g)$.
 Residual shear capacity: $2/3$ of original shear capacity.

Figure 6.14 Story Drift Ratios When 10th Floor Relative Displacement Reaching Maximum Recorded Value For Different Load Patterns

From Figure 6.15, the same conclusion as in the case for the seven-story hotel can be drawn. Different effective stiffness significantly affects the push-over analysis results. Although strength (base shear) capacity was almost the same for different assumed effective stiffnesses, roof displacement capacity of the building differed very significantly for different effective stiffness. Assuming an effective stiffness of $1.0(EI)$ would have predicted that the structure suffered yielding in both beams and

columns, and shear failure in columns at a 10th floor relative displacement of less than 2.9 inches. The condition of the structure after the earthquake indicated that the structure had no visible damage.



Material strength: $4/3 \times$ (design values).
 Residual shear capacity: $2/3$ of original shear capacity.

Figure 6.15 (Base shear)/(Weight of building) vs. Roof Displacement with Triangular Load Pattern Using Different Effective Stiffnesses. Ten-Story Building

CHAPTER 7

DISCUSSION OF RESULTS AND DESIGN IMPLICATIONS

7.1 General

One of the difficulties that a design engineer faces in conducting a dynamic time history analysis of structures is what earthquake ground motion should be used to obtain the largest demand on the structures. In this chapter, several representative earthquakes from the West coast of the United States were selected. The two buildings analyzed in previous chapters were studied using the selected earthquake ground motions to compare responses under different earthquake ground motions. In addition, design-spectrum-compatible earthquake ground motions were artificially generated and building responses under these artificially generated earthquakes were analyzed.

7.2 Selection of Representative Ground Motions

Despite the moderate magnitude of the ground motion recorded at ground level of the seven-story hotel (east-west direction) in the 1994 Northridge Earthquake, the building sustained significant damage. This ground motion record was considered of interest for further study. Figure 3.11 (S16(E-W)) shows the accelerogram recorded.

Ground motion recorded at the basement of the ten-story building (longitudinal direction) during the 1987 Whittier Narrows Earthquake was moderate, but the building experienced no visual damage at all. Therefore this record was also chosen for study. Figure 3.34 (Longitudinal) shows the accelerogram recorded.

The S00E component of El Centro, the Imperial Valley Earthquake of May 18, 1940, the first complete earthquake ground motion accelerogram in history was selected for this study. This record has been widely used as a typical earthquake ground motion in past research. Strong shaking lasted more than 20 seconds (Figure 7.1)

The S16E component of the Pacoima Dam records in the 1971 San Fernando Earthquake was also chosen for this study. Figure 7.2 shows the acceleration time history of the record. The record has a short strong shaking duration but a large acceleration pulse.

In Figure 7.3, pseudo acceleration response spectra for the 1994 Northridge Earthquake recorded at the ground level of the seven-story hotel and the 1987 Whittier Narrows earthquake recorded at the basement level of the ten-story building are plotted.

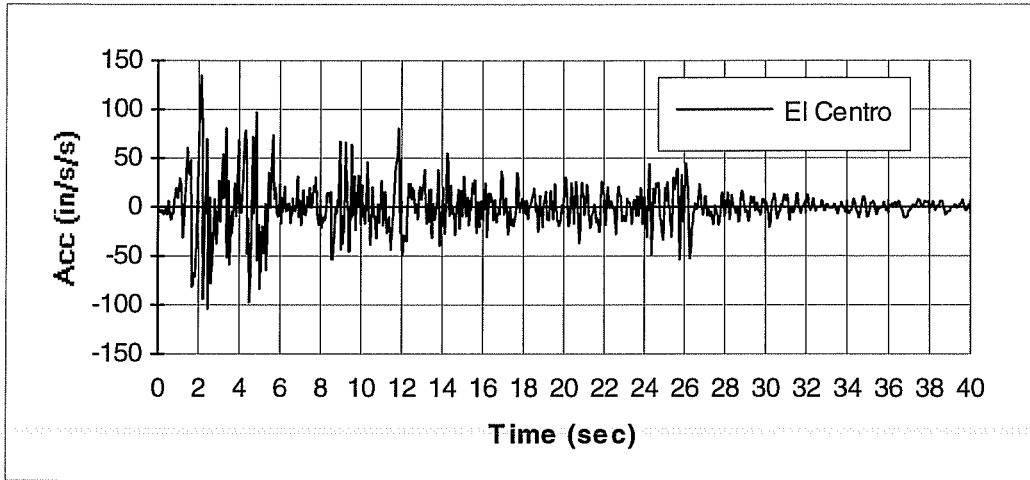


Figure 7.1 Ground Acceleration Time History of 1940 Imperial Valley Earthquake at El Centro (S00E Direction)

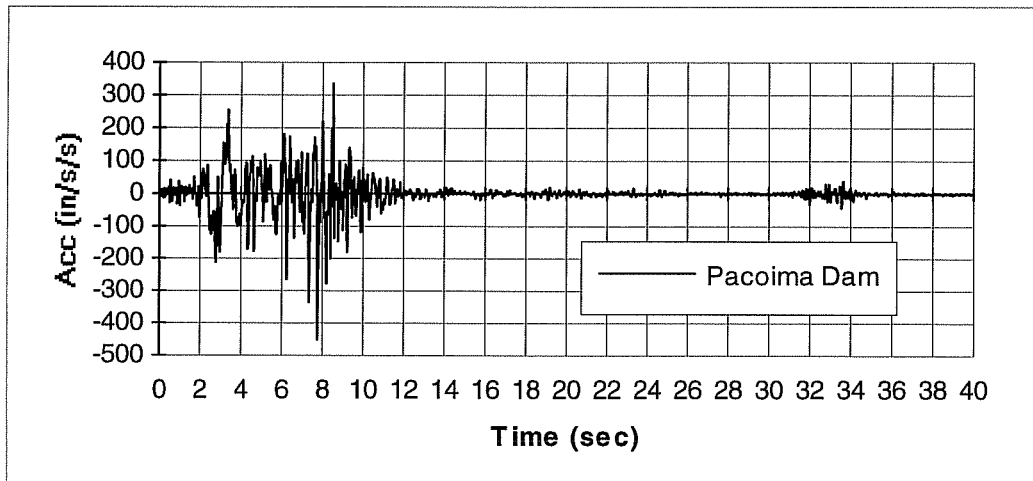


Figure 7.2 Ground Acceleration Time History in 1971 San Fernando Earthquake at Pacoima Dam (S16E Direction)

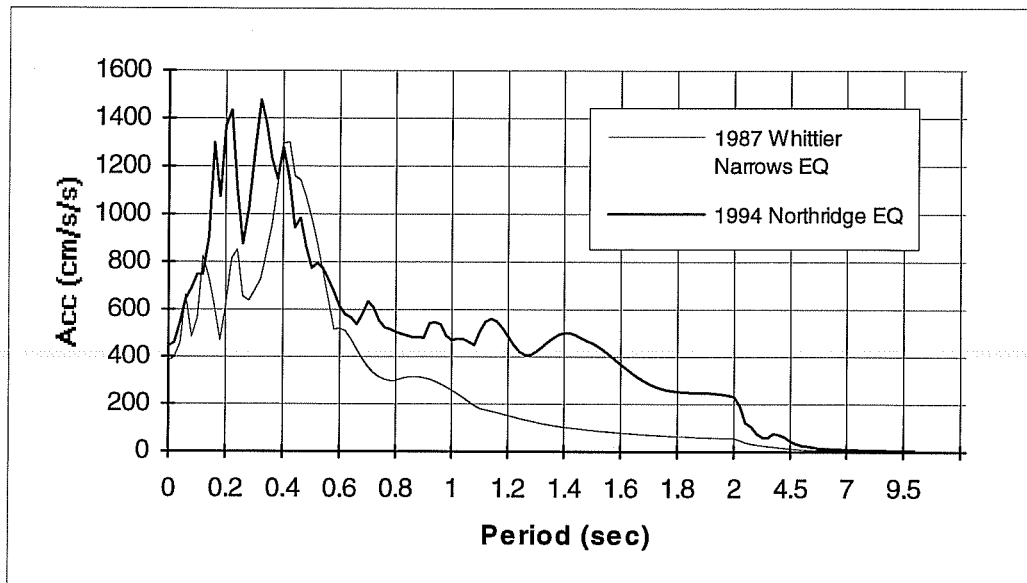


Figure 7.3 Comparison of Acceleration Response Spectra between 1994 Northridge Earthquake and 1987 Whittier Narrows Earthquake

For the seven-story hotel, the fundamental period of vibration is 1.60 seconds, and the second mode period of vibration is 0.54 seconds. The acceleration response spectrum for the 1994 Northridge Earthquake recorded at the ground level of the seven-story building indicates high responses in these periods, especially at the fundamental period of vibration. This may explain why the building suffered extensive damage during the 1994 Northridge Earthquake.

The acceleration response spectrum for the 1987 Whittier Narrows Earthquake recorded at the basement level of the ten-story building has a high pulse only at a 0.4

second period. The building fundamental period of vibration is 1.45 second, while the building second mode period of vibration is 0.47 seconds. Since the building response spectrum at the fundamental period of vibration is very low, it explains why the overall displacement and story drift ratios were small and the building sustained no damage. However, the acceleration response at the second mode period of vibration is rather high. This is consistent with the high drift ratios at higher stories indicated by dynamic calculations (Figure 6.14).

In Figure 7.4, the acceleration response spectra of all four earthquake ground motions are compared. All motions were scaled to the same peak acceleration as the 1994 Northridge Earthquake recorded at the ground level of the seven-story hotel. Also plotted in the figure was the design response spectrum adopted by the Seismology Committee of the Structural Engineers Association of California¹ and UBC-94⁶ as discussed in Chapter 2 (Figure 2.4) for deep cohesionless or stiff clay soils (soil type 2).

As is clearly shown in Figure 7.4, the UBC-94 design spectrum is lower than the Northridge and Whittier Narrows Earthquake ground motions in the short period region, but is greater in the long period region. In addition, it envelopes El Centro and Pacoima Dam records almost entirely. 5% damping was used in calculating pseudo acceleration response spectra.

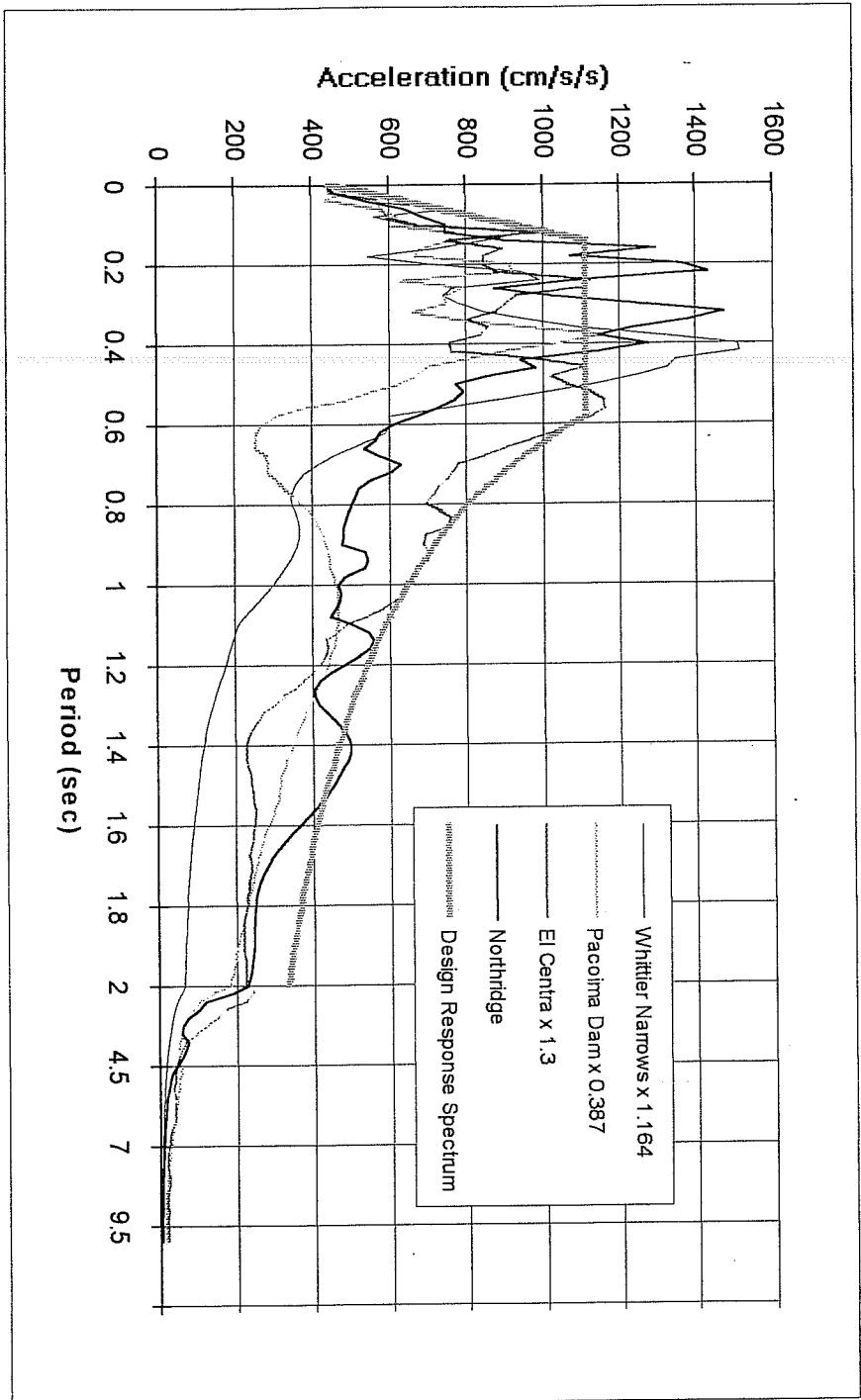


Figure 7.4 Comparison of Acceleration Response Spectra (5% Damping) among Selected Representative Earthquake Ground Motions and Design Response Spectrum for Soil Type 2

7.3 Artificially Generated Earthquake Ground Motions

Since response spectra seem to be good indications of damage potential of earthquakes, researchers have been using artificially generated design-spectrum-compatible earthquake ground motions in designing nuclear reactor facilities⁷⁴. Also the Building Code of Japan requests that high-rise buildings be subjected to structural evaluations for seismic safety through dynamic response analyses using artificially generated design-spectrum-compatible earthquake motions⁷⁵. This technique was employed in this study in selecting several critical design earthquakes.

Program SIMQKE⁷⁶ was used to synthesize the artificial earthquakes. Developed by Vanmarcke, Cornell, Gasparini, and Hou, the program was revised in September 1976 after the first version became available in August 1969. An acceleration envelope needs to be specified by users as shown in Figure 7.5. t_1 , t_2 , and t_3 are pre-specified durations for the rising portion, the flat portion, and the descending portion of the earthquake motion, respectively. Positive and negative envelopes are symmetric.

For all artificial earthquake motions generated for this study, the duration of ground motion was assumed to be 30 seconds, with the rising portion t_1 to be 2 sec. long, flat portion t_2 to be 12 sec. long, and the descending portion t_3 assumed to be 16 sec. long.

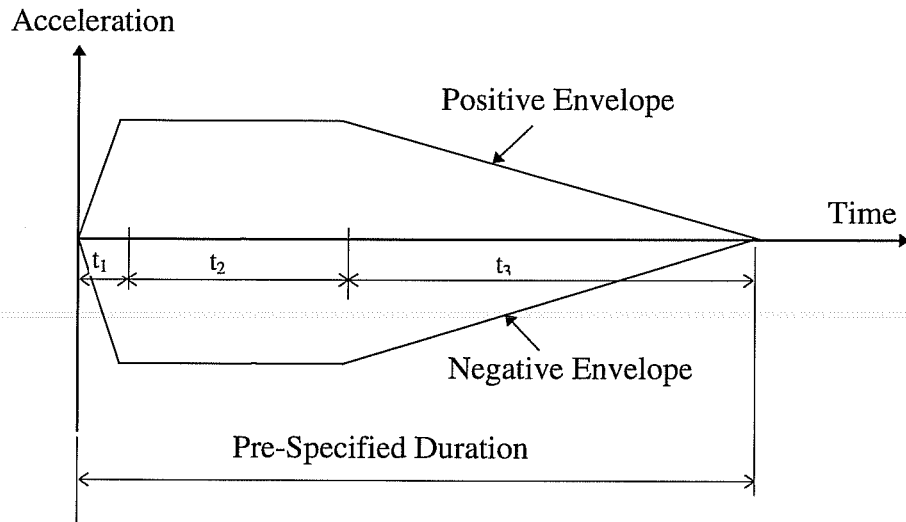


Figure 7.5 Envelopes for Artificial Earthquakes

7.3.1 Design-Spectrum-Compatible Artificial Earthquake

The first artificial earthquake generated was a UBC-94 design-spectrum-compatible earthquake motion for soil type 2. Figure 7.6 is the acceleration time history of the artificial earthquake and Figure 7.7 is the pseudo acceleration response spectrum for the artificial earthquake. Peak acceleration was specified as 1g, which can be easily scaled if needed.

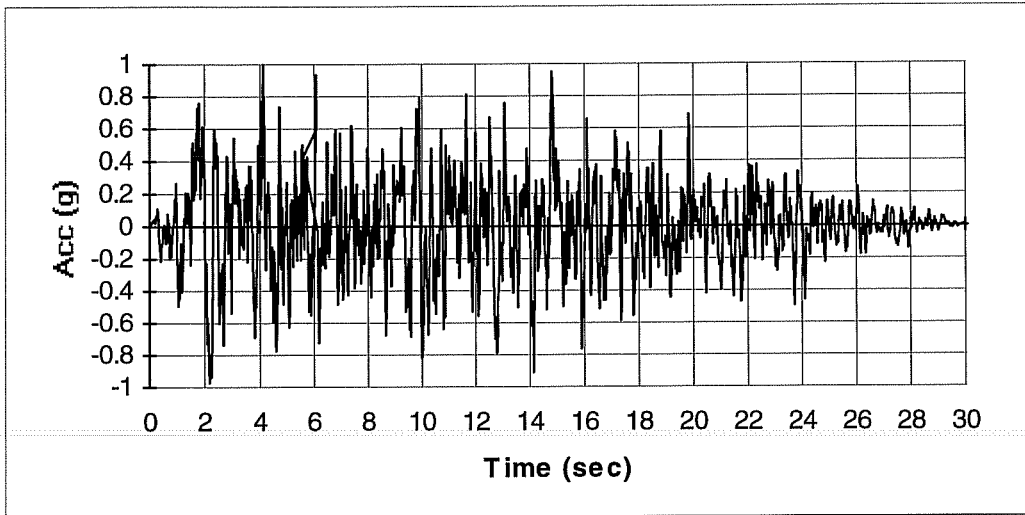


Figure 7.6 UBC-94 Design-Spectrum-Compatible Artificial Earthquake for Soil Type 2

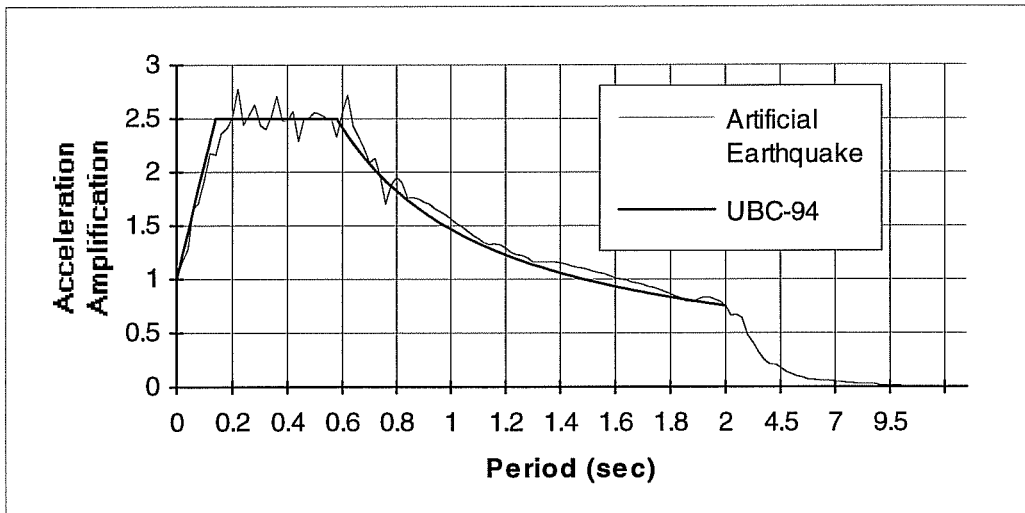


Figure 7.7 Pseudo Acceleration Response Spectrum for UBC-94 Design-Spectrum Compatible Artificial Earthquake

Although the match between actual pseudo acceleration response spectrum and the target UBC-94 smoothly curved design spectrum can be improved by performing more iterations, an absolute match is impossible and unnecessary.

7.3.2 Site-Dependent, Spectrum-Compatible Artificial Earthquake

As noted in Figure 7.4, the UBC-94 design spectrum is not an envelope spectrum for all the possible earthquakes. In looking for solutions for most critical design earthquakes, the site-dependent spectra from research work by Seed et. al.²² were utilized in this study.

Figure 7.8 shows the results obtained by Seed et. al. for stiff soil (soil type 2) after statistical analyses of the spectral shapes of 104 ground motion records from 23 earthquakes, mostly in the western part of the United States.

Figure 7.9 shows the artificial earthquake synthesized using SIMQKE for a site-dependent spectrum on firm soil after Seed, et. al.²² with mean plus one standard deviation. Again, 30 seconds was specified as the duration of the earthquake, with 2 seconds for the rising portion, 12 seconds for the flat portion, and 16 seconds for the descending portion.

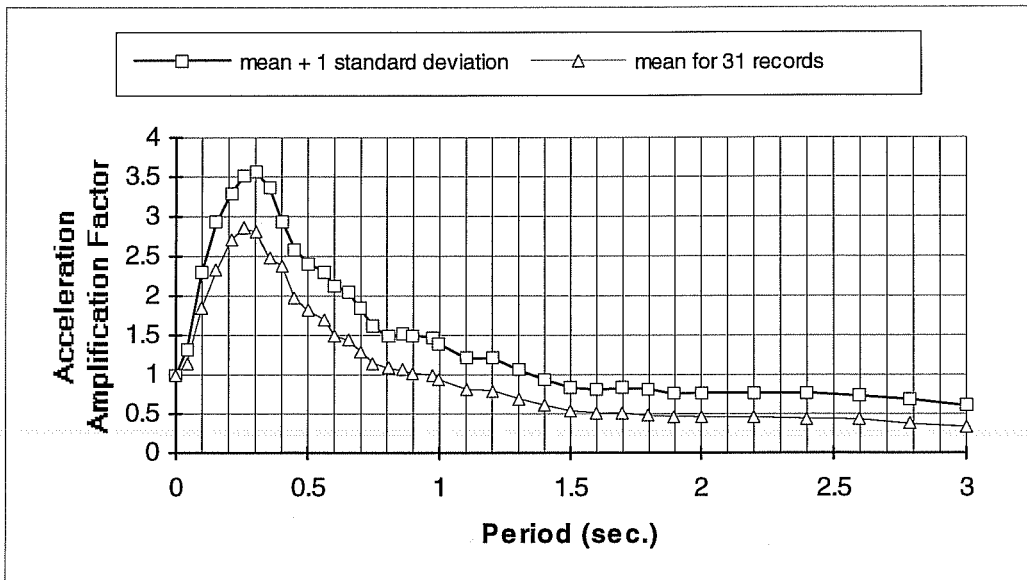


Figure 7.8 Normalized Acceleration Spectra for Stiff Soil (5% Damping) after Seed, et. al.²²

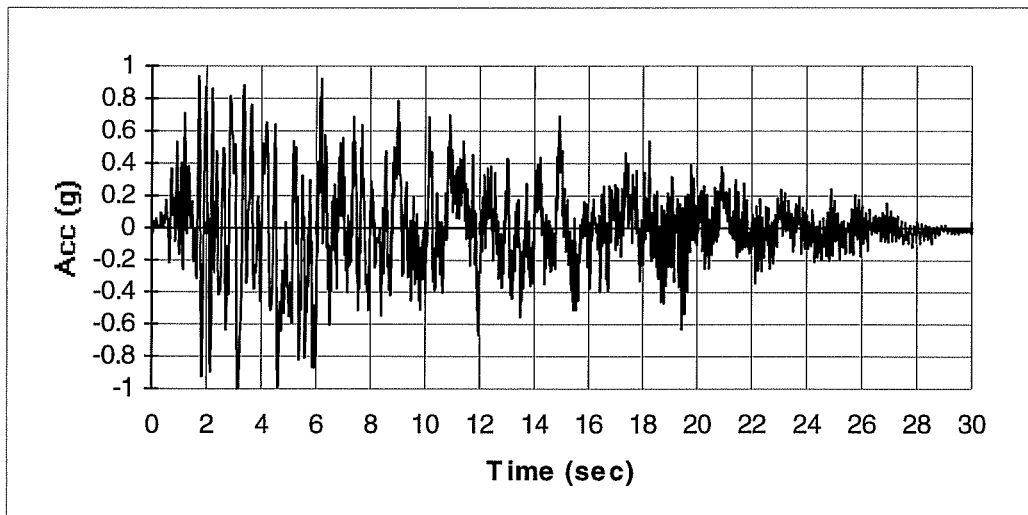


Figure 7.9 Site-Dependent, Spectrum-Compatible Artificial Earthquake after Seed, et. al.²² for Firm Soil (Soil Type 2) with Mean Plus One Standard deviation

In Figure 7.10, the pseudo acceleration response spectra for the 1994 Northridge Earthquake recorded at the ground level of the seven-story hotel, 1987 Whittier Narrows Earthquake recorded at the basement level of the ten-story building, and the artificially generated site-dependent spectrum for firm soil after Seed, et. al. with mean plus one standard deviation are compared. All the earthquakes were scaled to the same peak acceleration as that for the 1994 Northridge Earthquake recorded at the ground floor level.

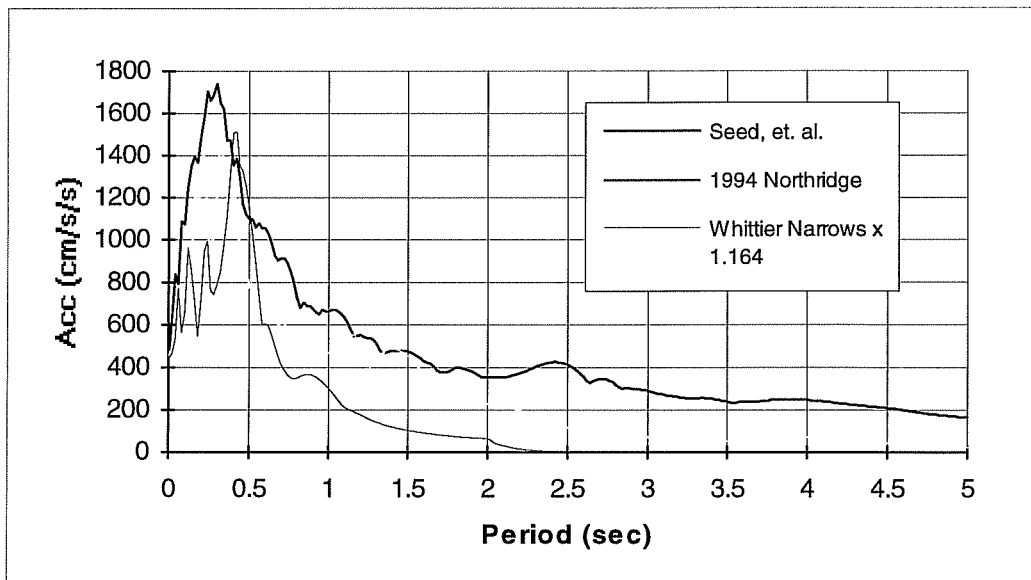


Figure 7.10 Comparison of Response Spectra Between 1994 Northridge, 1987 Whittier Narrows and Site-Dependent, Spectrum-Compatible Artificial Earthquake for Firm Soil (Soil Type 2) with Mean Plus One Standard Deviation

Apparently the artificial earthquake motion generated after Seed, et. al. for mean plus one standard deviation envelopes the other two earthquakes. In the following sections, the building responses to these artificially generated earthquake ground motions were compared with the building responses to the four selected real earthquake ground motions.

7.4 Effects of Different Earthquake Ground Motions on Building Responses

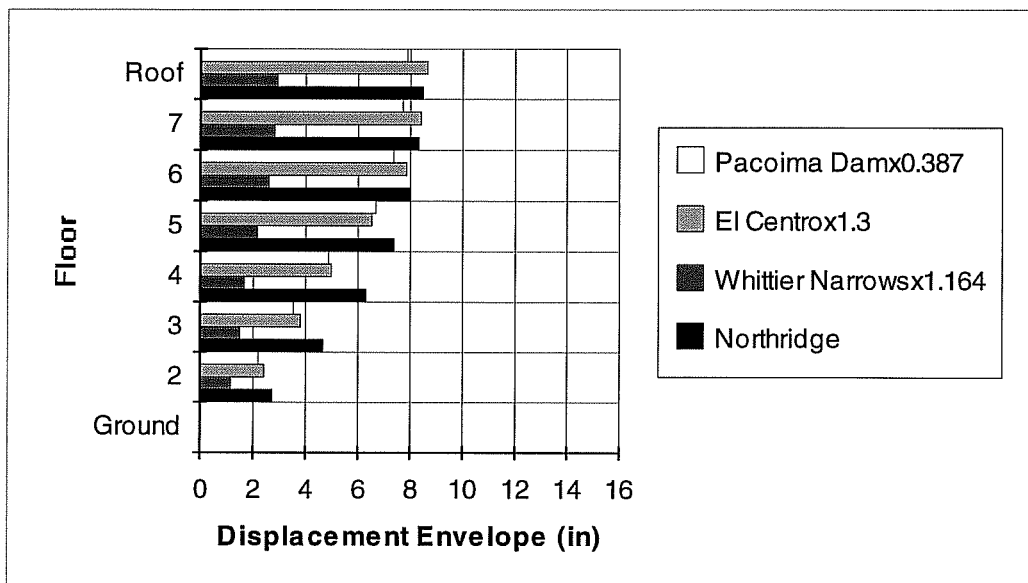
The two buildings analyzed in the previous chapters, namely the seven-story hotel and the ten-story building, were used to study the effects of different earthquake ground motions on structural responses. The same structural models and the same parameters used for dynamic analyses were used here in order to compare. In addition, all earthquake ground motions used for the same building were scaled to the same peak acceleration as that in the corresponding earthquake that occurred at that building.

7.4.1 Seven-Story Hotel

The parameters used here were the same as that used for the building subjected to the 1994 Northridge Earthquake, including: 5% for damping ratio, $0.30(EI_g)$ for effective stiffness $(EI)_{eff}$, $3/2$ x (design values) for actual material strength, and $2/3$ of original shear capacity for residual shear capacity. All the

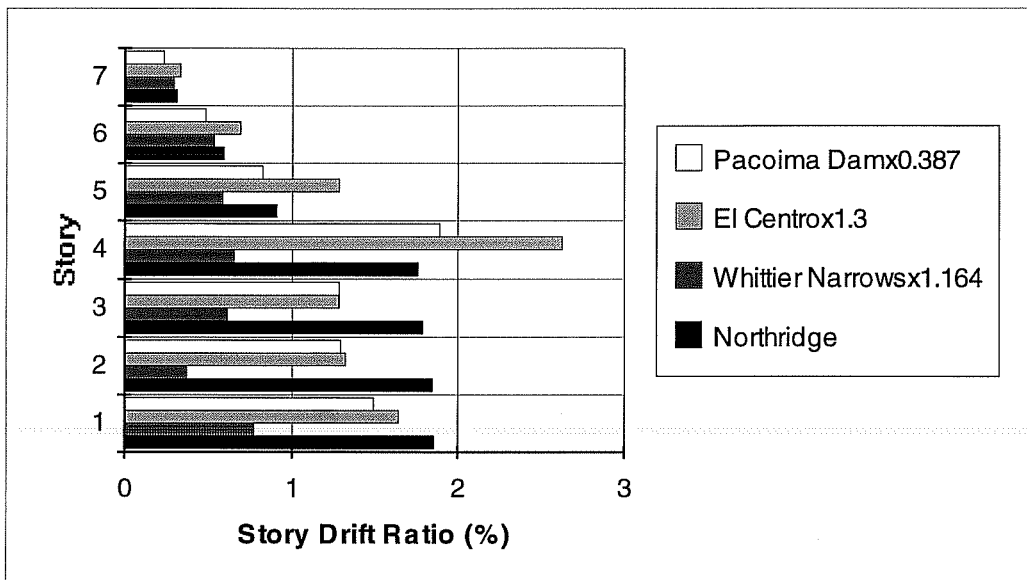
earthquake ground motions used for comparison were scaled to 175.0 in/s/s, the maximum ground acceleration the building experienced during the 1994 Northridge Earthquake.

Figure 7.11 shows the building lateral displacement envelopes for four earthquakes. Figure 7.12 is a plot of inter-story drift ratios for the selected earthquake ground motions. The 1987 Whittier Narrows Earthquake recorded at the basement of the ten-story building had the least impact on the building response. The inter-story drift ratios (Figure 7.12) also indicate that the Whittier Narrows ground motion has



Damping coefficient: 5% of critical damping.
 Material strength: 3/2 x (design values).
 Effective stiffness $(EI)_{eff}$: $0.30(EI_g)$.
 Residual shear capacity: 2/3 of original shear capacity.

Figure 7.11 Floor Relative Displacement Envelopes for the Selected Earthquake Ground Motions. Seven-Story Hotel



Damping coefficient: 5% of critical damping.
 Material strength: $3/2$ x (design values).
 Effective stiffness $(EI)_{eff}$: $0.30(EI_g)$.
 Residual shear capacity: $2/3$ of original shear capacity.

Figure 7.12 Story Drift Ratios for the Selected Four Real Earthquake Ground Motions. Seven-Story Hotel

noticeable higher mode effects. This can be explained from the response spectrum shown in Figure 7.4. At a second mode period of 0.54 seconds, the acceleration response spectrum reached a high value, while at the building fundamental period of 1.60 seconds, the response spectrum gave a rather low value. From the failure state of the seven-story hotel subjected to the 1987 Whittier Narrows Earthquake shown in Figure 7.13, the building can survive the 1987 Whittier Narrows Earthquake, even if

the peak acceleration of the earthquake is the same as the 1994 Northridge Earthquake.

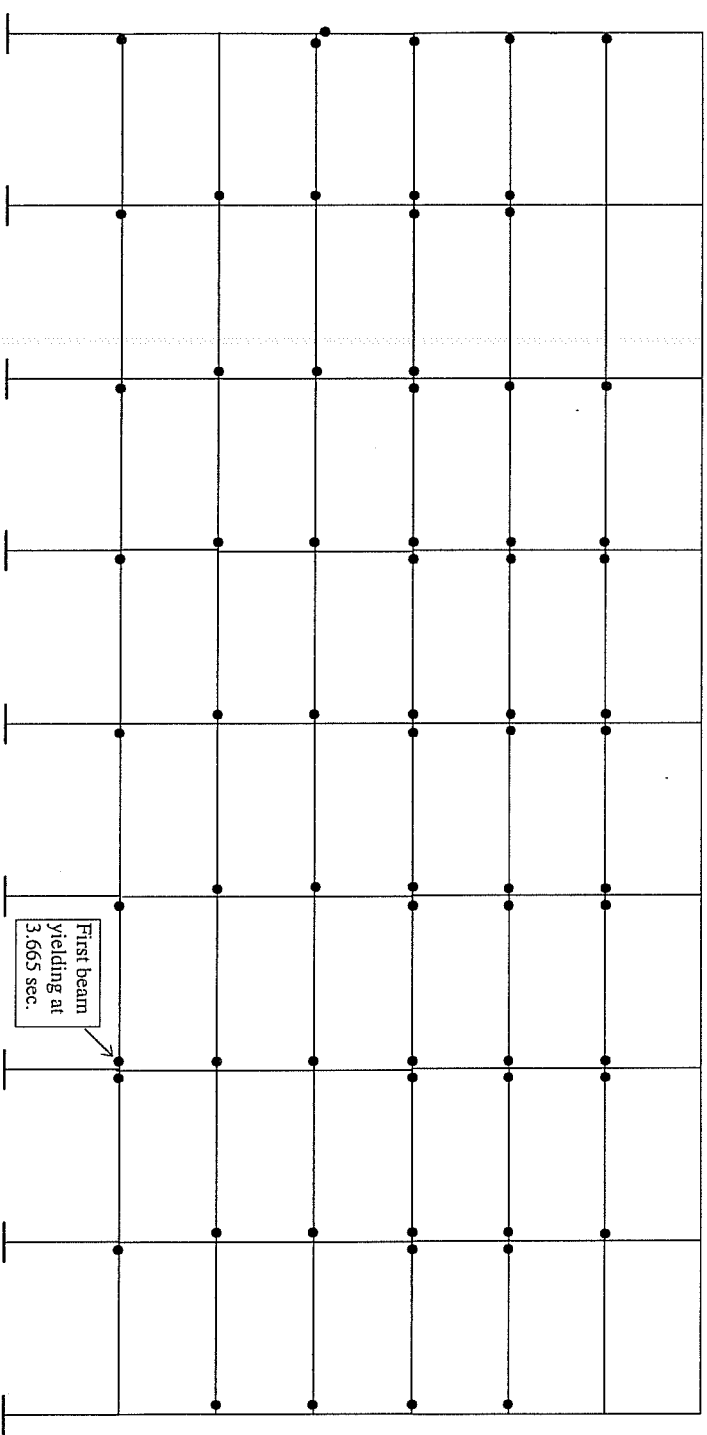
The acceleration response spectrum for the El Centro record (Figure 7.4) has a little lower value than that of the 1994 Northridge Earthquake at the building's fundamental period of vibration. It has a very high value at the second mode period of vibration. That leads to responses (floor displacement envelope and maximum inter-story drift ratios as shown in Figures 7.11 and 7.12) at upper floor levels higher than those of the 1994 Northridge record. The high second mode response also explains the failure state of the building shown in Figure 7.14. Comparing results with those shown in Figure 5.16 (the failure state of the building subjected to the 1994 Northridge Earthquake), we see that shear failure of columns moves from the third and the fourth stories in the 1994 Northridge Earthquake to the fourth and the fifth stories in the case of the 1940 Imperial Valley Earthquake at El Centro.

The Pacoima Dam record from the 1971 San Fernando Earthquake shows very small high mode effects (Figure 7.12), and this result can also be explained from the acceleration response spectrum (Figure 7.4). Despite the small high mode effects observed, the shear failure of columns between the fourth and the fifth floor levels (Figure 7.15) was indicated. Another noteworthy observation is that in spite of the significant differences among acceleration response spectra, all selected earthquake motions indicated highest maximum inter-story drift ratios and column failures

between the fourth and the fifth floor levels (Figures 7.13, 7.14, 7.15, 7.16, and 7.17). Other researchers have suggested that column failures between the fourth and the fifth floor level were due to high mode effects of 1994 Northridge Earthquake. It was concluded from this study that the primary reason for columns failing between the fourth and the fifth floor levels is the change of reinforcement (both longitudinal and transverse). The strength (mainly shear capacity) changed between the fourth and the fifth floor levels of the structure.

In Figures 7.18 and 7.19, the floor displacement envelopes and maximum inter-story drift ratios for the 1994 Northridge Earthquake recorded at the ground level of the seven-story hotel, the UBC-94 design-spectrum-compatible artificial earthquake and the site-dependent, spectrum-compatible artificial earthquake after Seed, et. al. with mean plus one standard deviation are compared.

High building responses under the artificial earthquakes, especially the site-dependent earthquake with mean plus one standard deviation, are obvious. While maximum inter-story drift ratios at the fifth and the sixth stories due to the UBC-94 design-spectrum-compatible artificial earthquake are less than those due to the 1994 Northridge Earthquake, a site-dependent, spectrum-compatible artificial earthquake produced the highest responses of the building in every story and on every floor.



• yielding at member end

Ground motion: 1987 Whittier Narrows Earthquake x 1.164.
 Damping coefficients: 5% critical damping.
 Material strength: $3/2 \times$ (design values).
 Effective stiffness $(EI)_{eff}$: $0.30(EI_g)$.
 Residual shear capacity: $2/3$ of original shear capacity.

Figure 7.13 Failure state of the Seven-Story Hotel Subject to 1987 Whittier Narrows Earthquake
 Scaled to Peak Acceleration of 175.0 in/s/s.

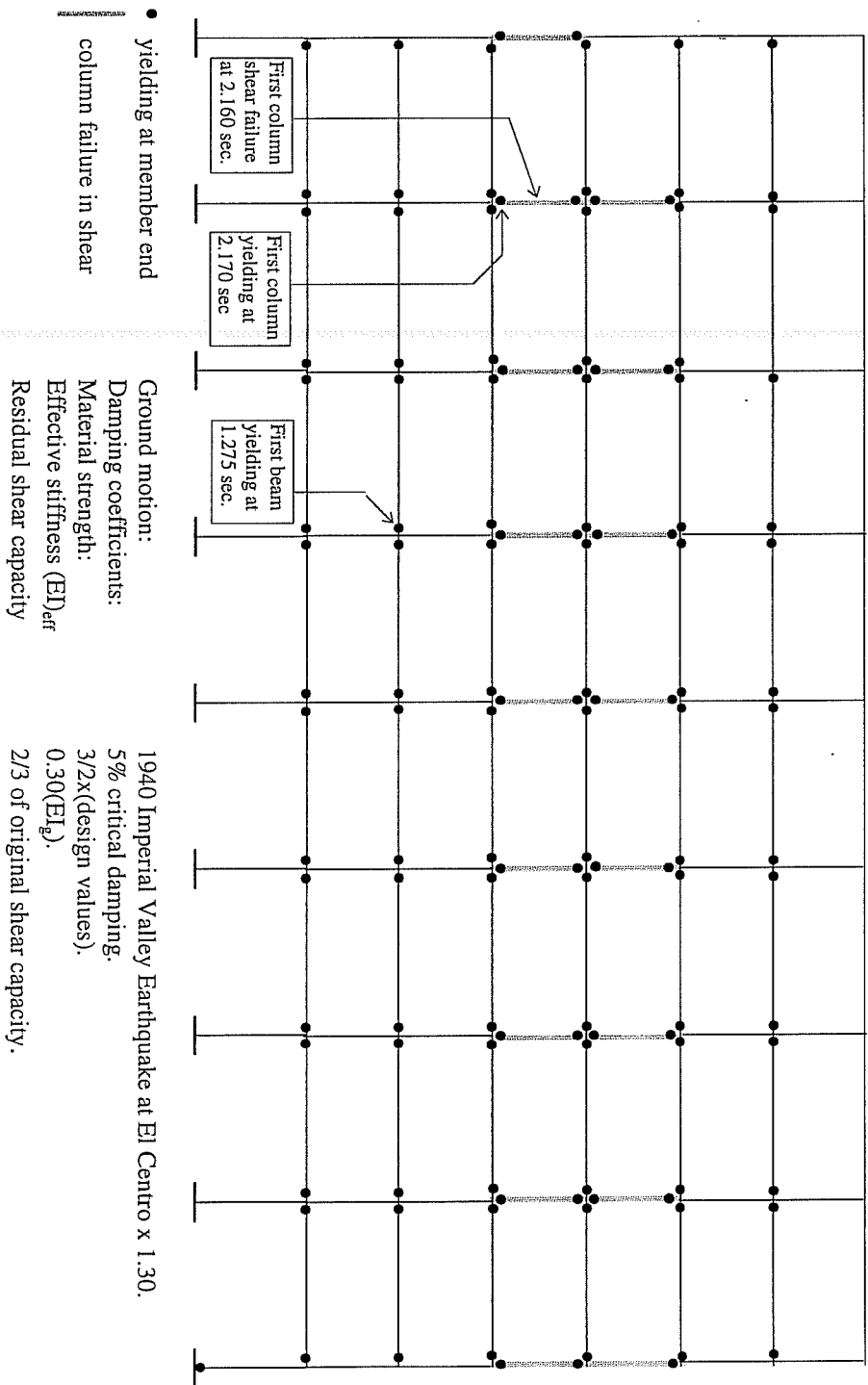
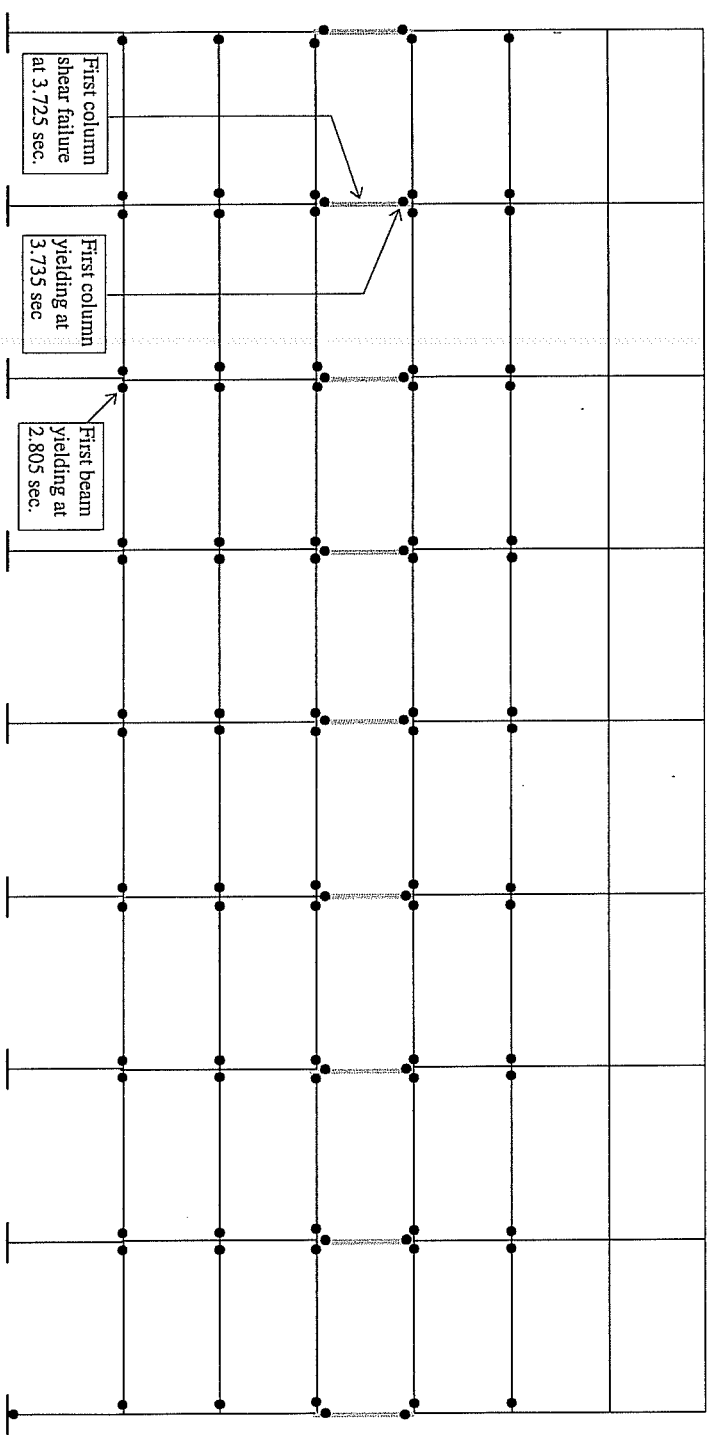


Figure 7.14 Failure state of the Seven-Story Hotel Subject to 1940 Imperial Valley Earthquake
 Recorded at El Centro Scaled to Peak Acceleration of 175.0 in/s/s.



- yielding at member end
 - column failure in shear
- Ground motion : 1971 San Fernando Earthquake at Pacoima Dam.
- Damping coefficients: 5% critical damping.
- Material strength: $3/2 \times$ (design values).
- Effective stiffness $(EI)_{eff}$: $0.30(EI_g)$.
- Residual shear capacity : $2/3$ of original shear capacity.

Figure 7.15 Failure state of the Seven-Story Hotel Subject to 1971 San Fernando Earthquake Recorded at Pacoima Dam Scaled to Peak Acceleration of 175.0 in/s/s.

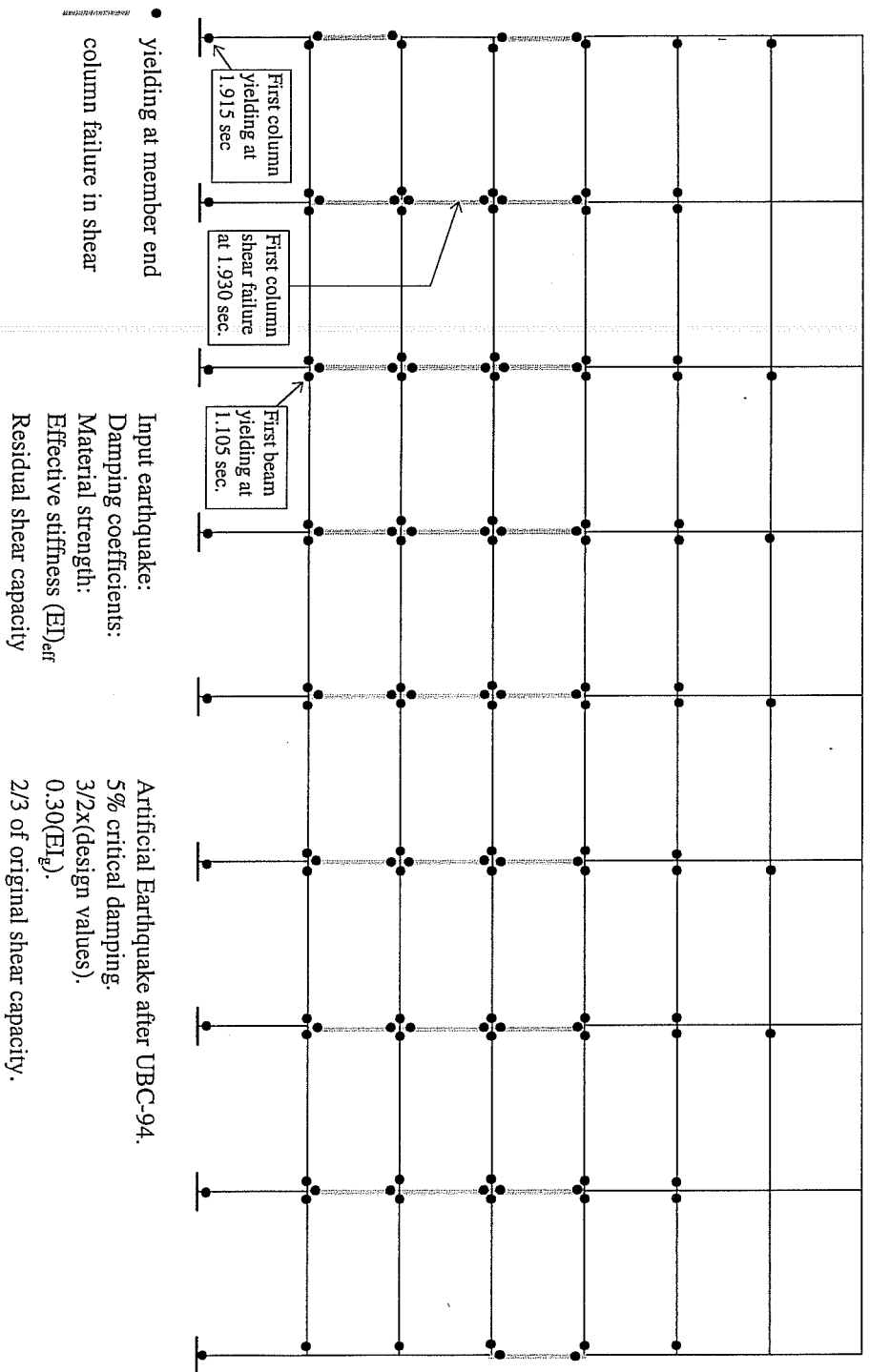


Figure 7.16 Failure state of the Seven-Story Hotel Subject to UBC-94 Design-Spectrum Compatible Earthquake Scaled to Peak Acceleration of 175.0 in/s/s.

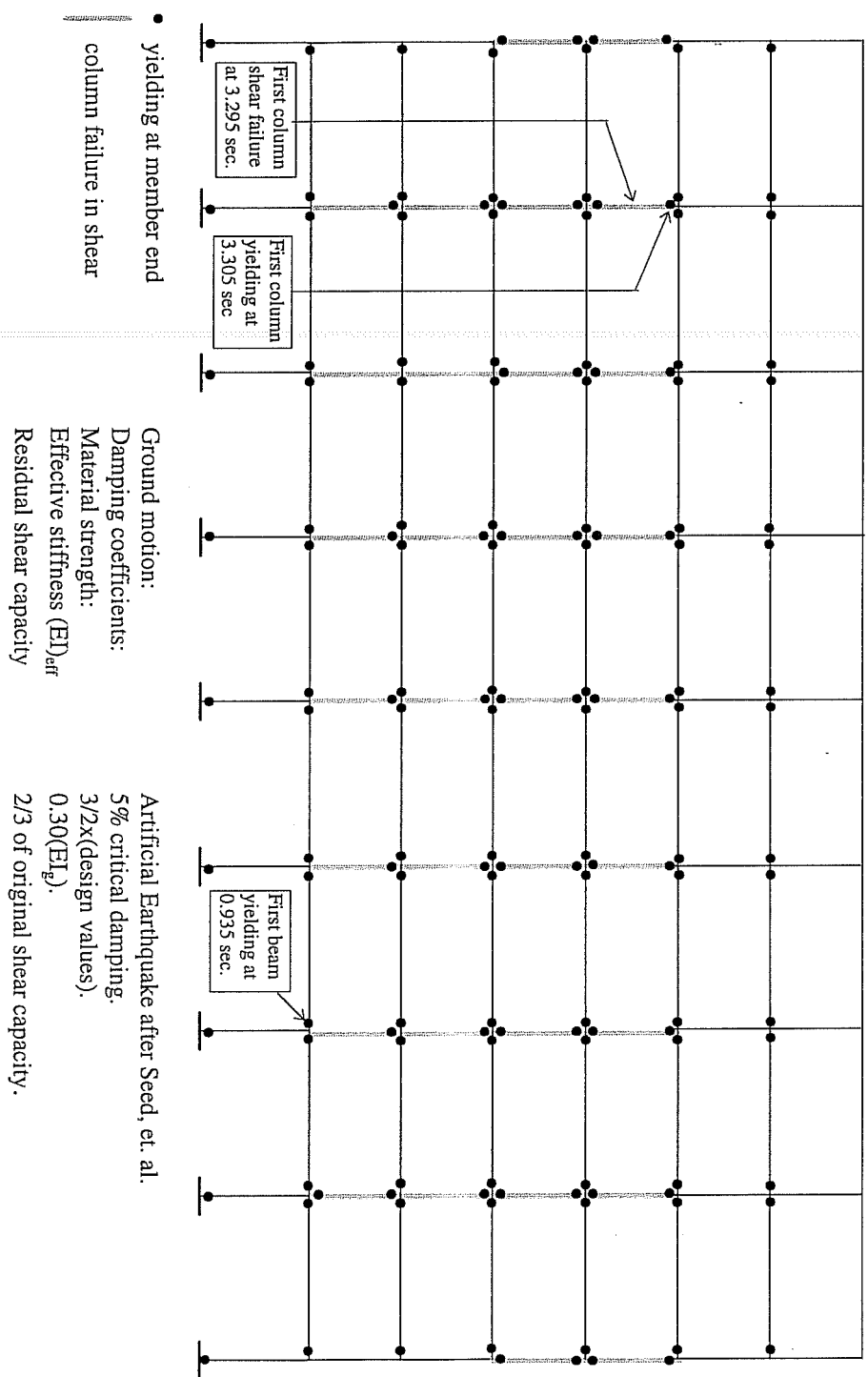
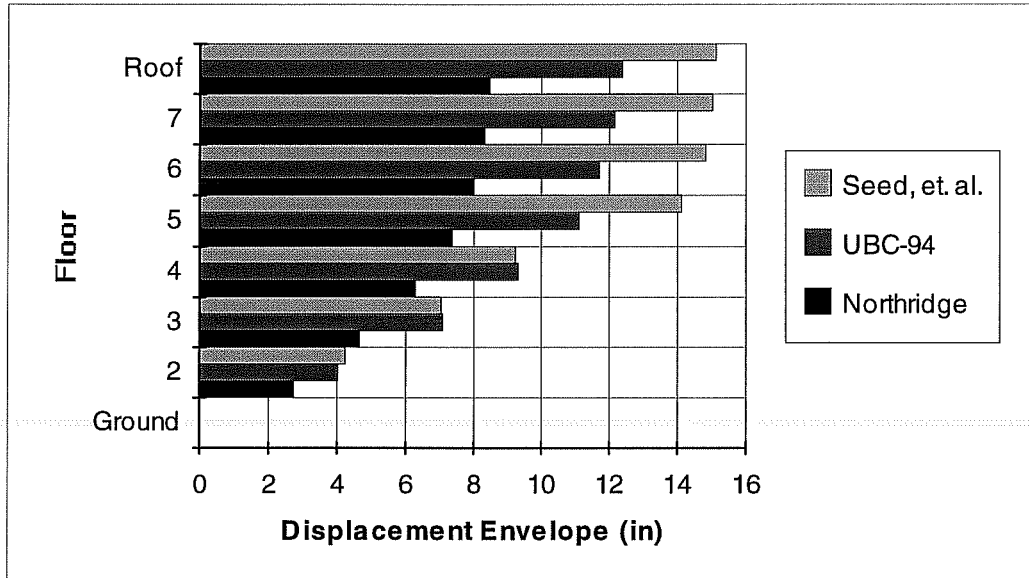


Figure 7.17 Failure state of the Seven-Story Hotel Subject to Site-Dependent, Spectrum-Compatible Earthquake after Seed, et. al. Scaled to Peak Acceleration of 175.0 in/s/s.

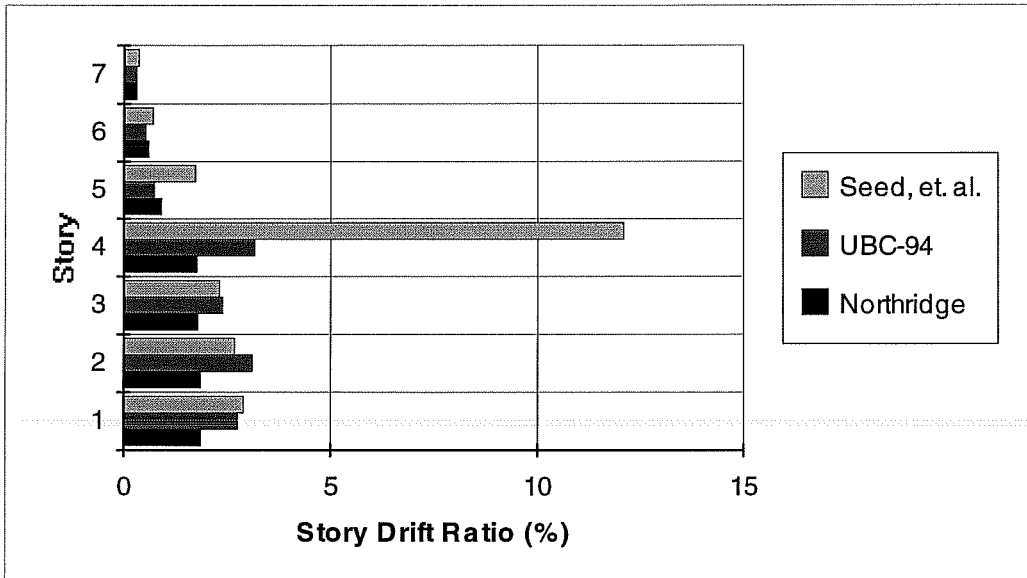


Damping coefficient: 5% of critical damping.
 Material strength: $3/2$ x (design values).
 Effective stiffness $(EI)_{\text{eff}}$: $0.30(EI_g)$.
 Residual shear capacity: $2/3$ of original shear capacity.

Figure 7.18 Floor Relative Displacement Envelopes for the 1994 Northridge Earthquake and artificial Earthquake Ground Motions. Seven-Story Hotel

7.4.2 Ten-Story Building

The same parameters used for the building subjected to the 1987 Whittier Narrows Earthquake were used here for consistency and comparison. Those parameters include: 5% for damping ratio, $0.40(EI_g)$ for effective stiffness $(EI)_{\text{eff}}$, $4/3$ x (design values) for actual material strength, and $2/3$ of original shear capacity for residual shear capacity. All the earthquake ground motions used for comparison were

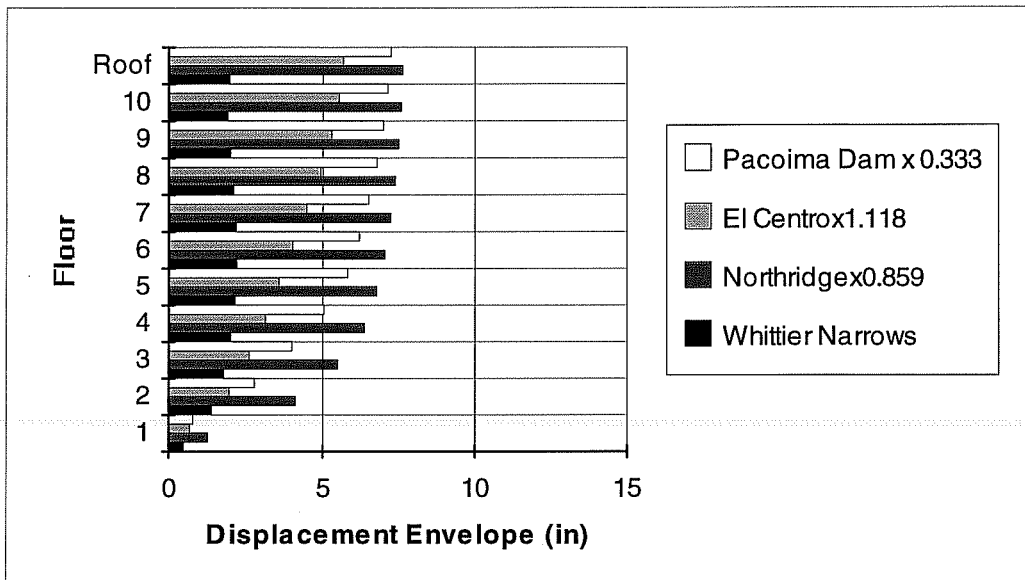


Damping coefficient: 5% of critical damping.
 Material strength: $3/2$ x (design values).
 Effective stiffness $(EI)_{\text{eff}}$: $0.30(EI_g)$.
 Residual shear capacity: $2/3$ of original shear capacity.

Figure 7.19 Story Drift Ratios for the 1994 Northridge Earthquake and artificial Earthquake Ground Motions. Seven-Story Hotel

scaled to 150.3 in/s/s, the maximum ground acceleration recorded at the basement floor of the building during the 1987 Whittier Narrows Earthquake.

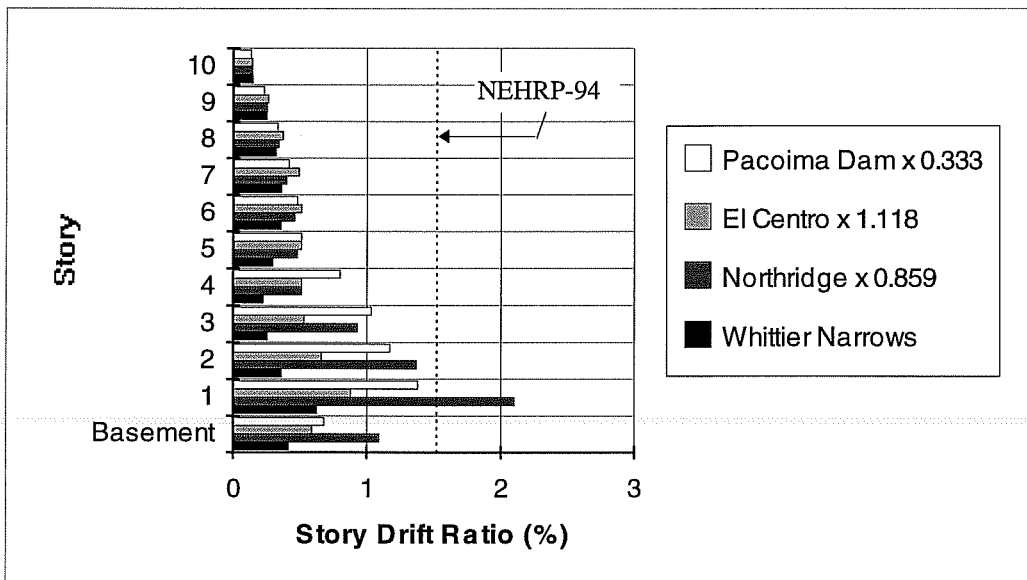
Figure 7.20 shows the building lateral displacement envelopes for the four selected real earthquakes. Figure 7.21 is a plot of maximum inter-story drift ratios for these selected earthquake ground motions.



Damping coefficient: 5% of critical damping.
 Material strength: $4/3$ x (design values).
 Effective stiffness $(EI)_{eff}$: $0.40(EI_g)$.
 Residual shear capacity: $2/3$ of original shear capacity.

Figure 7.20 Floor Relative Displacement Envelopes for the Selected Four Earthquake Ground Motions. Ten-Story Building

The 1987 Whittier Narrows Earthquake recorded at the basement of the ten-story building had the least impact on building response because of its low responses at 1.45 seconds (Figure 7.4), the fundamental period of vibration of the building. The inter-story drift ratios (Figure 7.21) indicate that the 1987 Whittier Narrows Earthquake recorded at the basement of the ten-story building has the most significant high mode effects. The reason for this is that the acceleration response spectrum of



Damping coefficient: 5% of critical damping.
 Material strength: $4/3$ x (design values).
 Effective stiffness $(EI)_{\text{eff}}$: $0.40(EI_g)$.
 Residual shear capacity: $2/3$ of original shear capacity.

Figure 7.21 Story Drift Ratios for the Selected Four Real Earthquake Ground Motions. Ten-Story Building

this record has a high peak at 0.47 seconds which is the second mode period of vibration of the building.

Also shown on Figure 7.21 is the maximum inter-story drift ratio recommended in the NEHRP-94 specifications⁹. Except for the first story in the building subjected to the 1994 Northridge Earthquake recorded at the ground floor level of the seven-story hotel, inter-story drift ratios of the ten-story building satisfy code requirements for all other selected earthquake ground motions.

Comparing floor relative displacement envelopes and maximum inter-story drift ratios for the two buildings subjected to different earthquake ground motions, the same earthquake ground motion has different effects on different buildings. For the seven-story hotel, the El Centro record had a significant impact on the building, especially on the fourth story drift ratio, while the Pacoima Dam record had less significant impact on the building. However, for the ten-story building, the Pacoima Dam record had much more significant impact on the building than the El Centro record. Overall, the 1994 Northridge record produced high responses for both buildings.

Figure 7.22 through 7.24 show the failure state of the building subjected to the 1994 Northridge Earthquake recorded at the ground floor of the seven-story hotel, the 1940 Imperial Valley Earthquake recorded at El Centro, and the 1971 San Fernando Earthquake recorded at Pacoima Dam, respectively. The building sustained no visible structural damage after the 1987 Whittier Narrows Earthquake. As we can see, the building would not have survived without failure of structural elements if any of the other selected ground motions with the same peak acceleration as that recorded during 1987 Whittier Narrows Earthquake had occurred.

Exterior Frame

Interior Frame

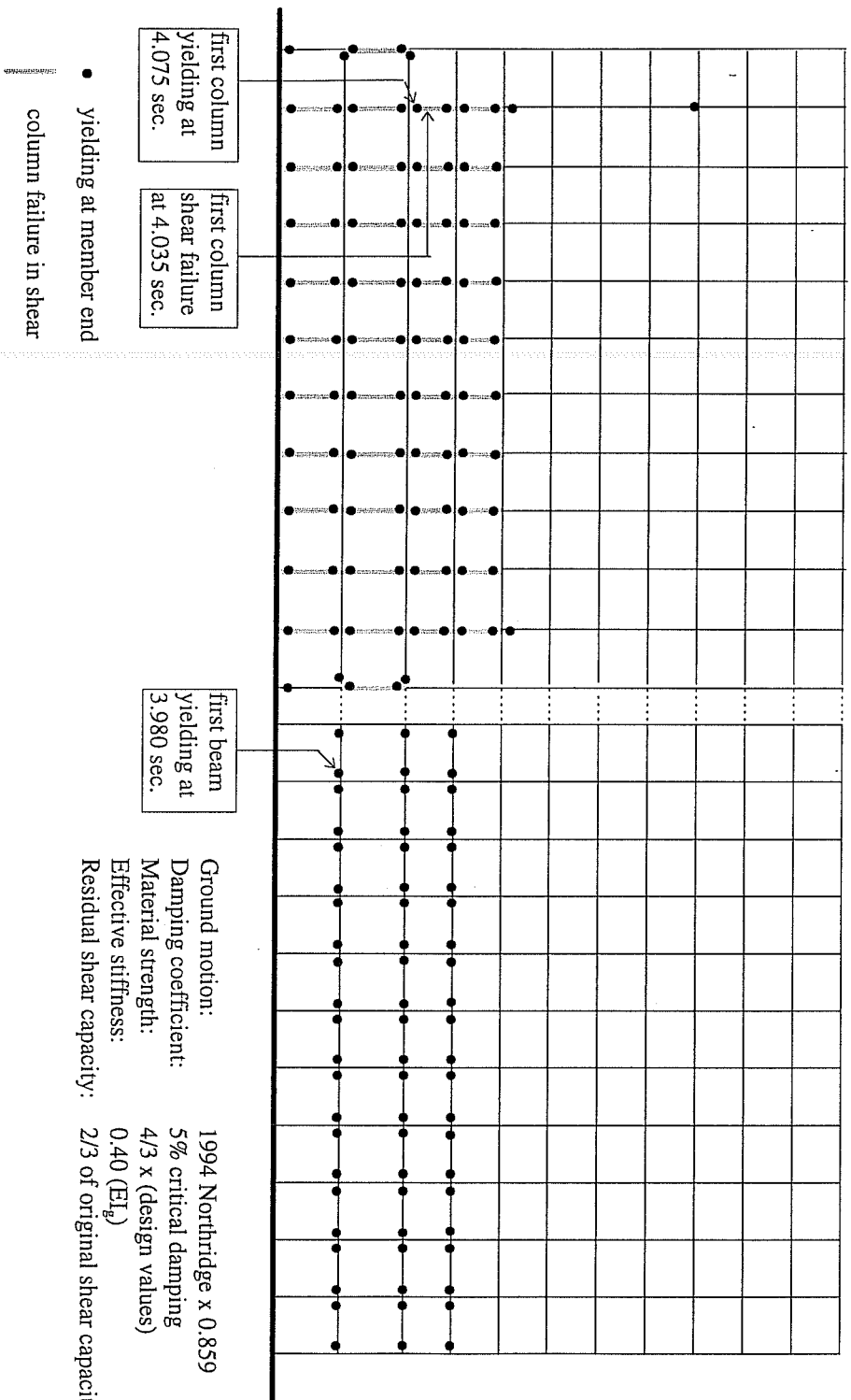


Figure 7.22 Failure state of the Ten-Story Building Subjected to 1994 Northridge Earthquake Recorded at the ground floor of the seven-story hotel Scaled to Peak Acceleration of 150.3 in/s/s

Exterior Frame

Interior Frame

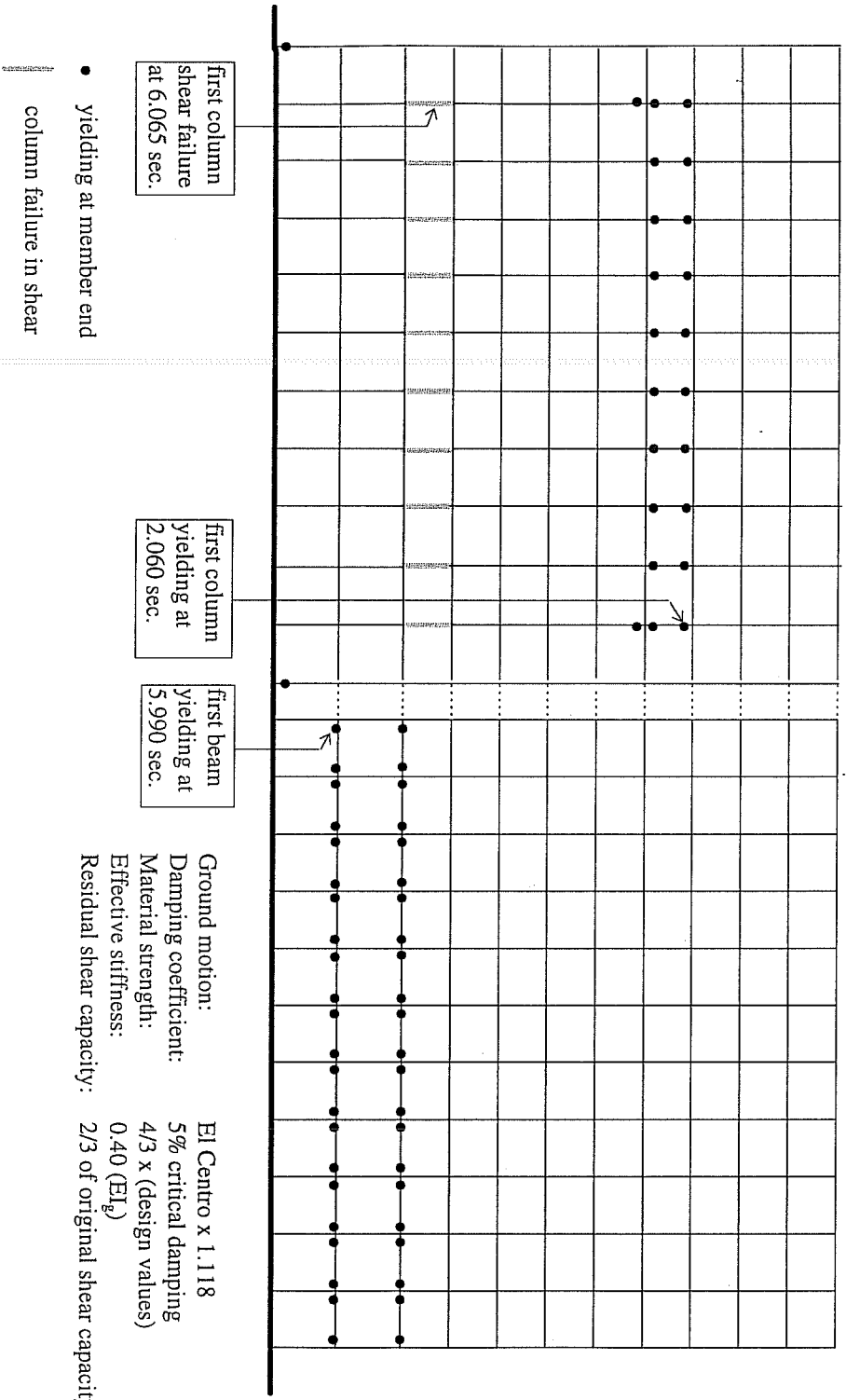


Figure 7.23 Failure State of the Ten-Story Building Subjected to 1940 Imperial Valley Earthquake
 Recorded at El Centro Scaled to Peak Acceleration of 150.3 in/s/s

Exterior Frame

Interior Frame

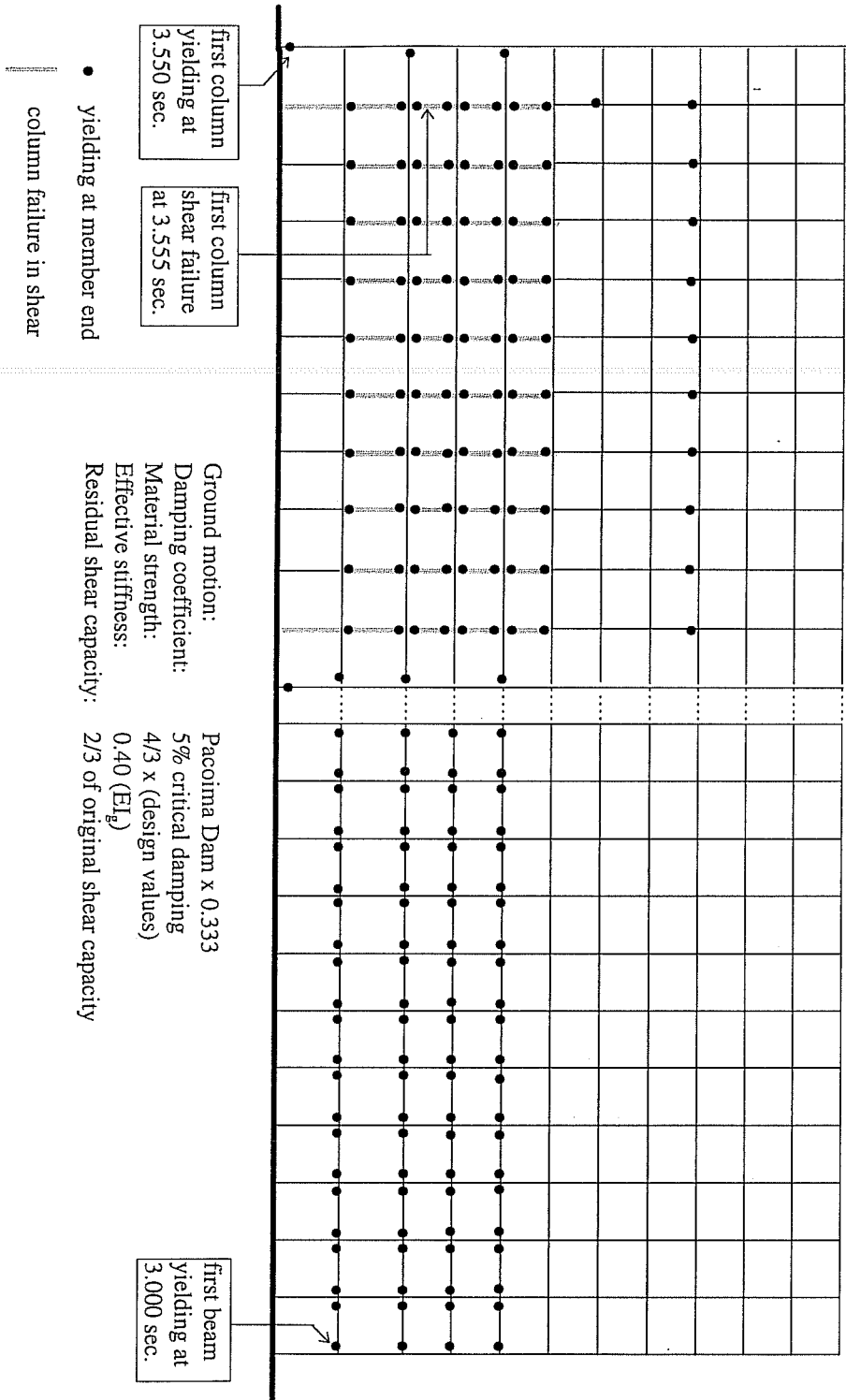
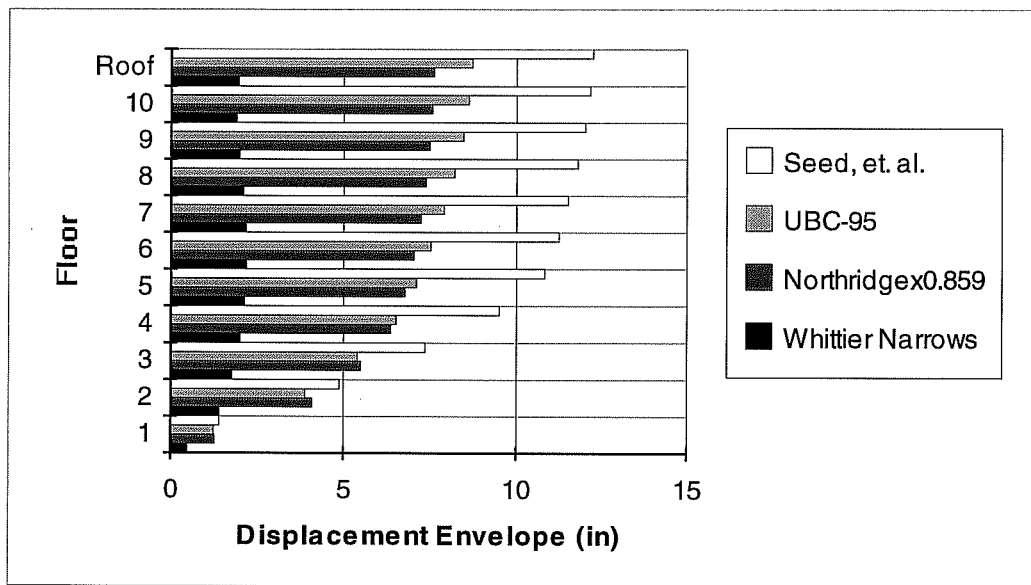


Figure 7.24 Failure State of the Ten-Story Building Subjected to 1971 San Fernando Earthquake
Recorded at Pacoima Dam Scaled to Peak Acceleration of 150.3 in/s/s

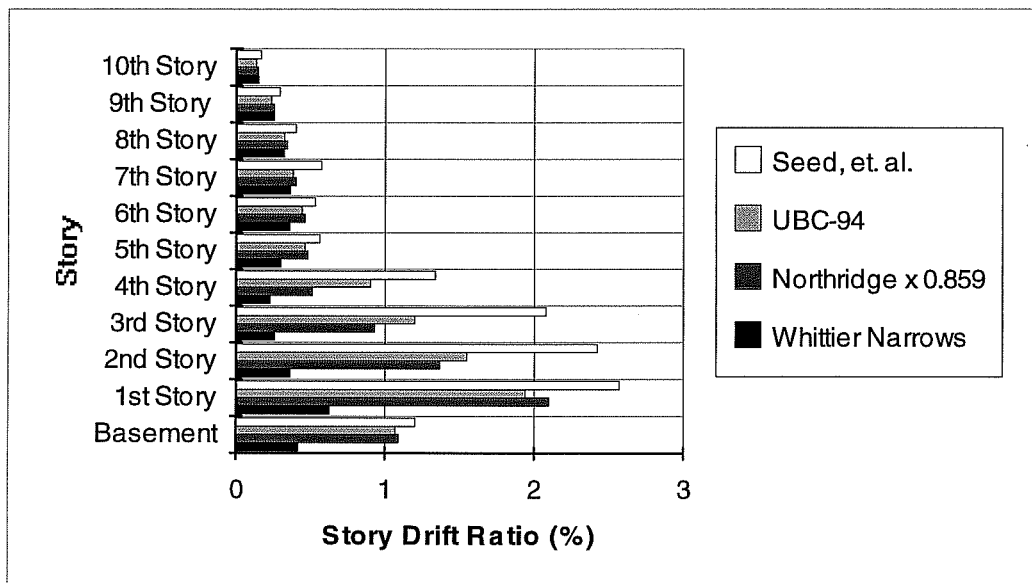
Building responses to artificial earthquakes were also studied. Figures 7.25 and 7.26 show floor displacement envelopes and maximum inter-story drift ratios for the 1987 Whittier Narrows Earthquake recorded at the basement of the ten-story building, the artificial earthquakes, and the 1994 Northridge Earthquake recorded at the ground floor. Responses produced by these spectrum-compatible artificial earthquakes are very significant. Compared with building responses to the 1994



Damping coefficient: 5% of critical damping.
 Material strength: 4/3 x (design values).
 Effective stiffness $(EI)_{\text{eff}}$: $0.40(EI_g)$.
 Residual shear capacity: 2/3 of original shear capacity.

Figure 7.25 Floor Relative Displacement Envelopes for the Real Earthquake and Artificial Earthquake Ground Motions. Ten-Story Building

Northridge Earthquake and the UBC-94 design-spectrum-compatible artificial earthquake, the 1994 Northridge Earthquake produces higher responses than the UBC-94 design-spectrum-compatible artificial earthquake does at lower story levels. However, the site-dependent, spectrum compatible artificial earthquake produces envelope responses considering selected earthquakes representative of the West coast of the United State and a UBC-94 design-spectrum-compatible artificial earthquake.



Damping coefficient: 5% of critical damping.
 Material strength: 3/2 x (design values).
 Effective stiffness $(EI)_{\text{eff}}$: $0.30(EI_g)$.
 Residual shear capacity: 2/3 of original shear capacity.

Figure 7.26 Story Drift Ratios for the 1987 Whittier Narrows, 1994 Northridge and Artificial Earthquake Ground Motions. Ten-Story Building

In Figures 7.27 and 7.28, failure states of the building subjected to artificial earthquakes are illustrated. Once again, the site-dependent, spectrum-compatible artificial earthquake represents the most critical earthquake.

Exterior Frame

Interior Frame

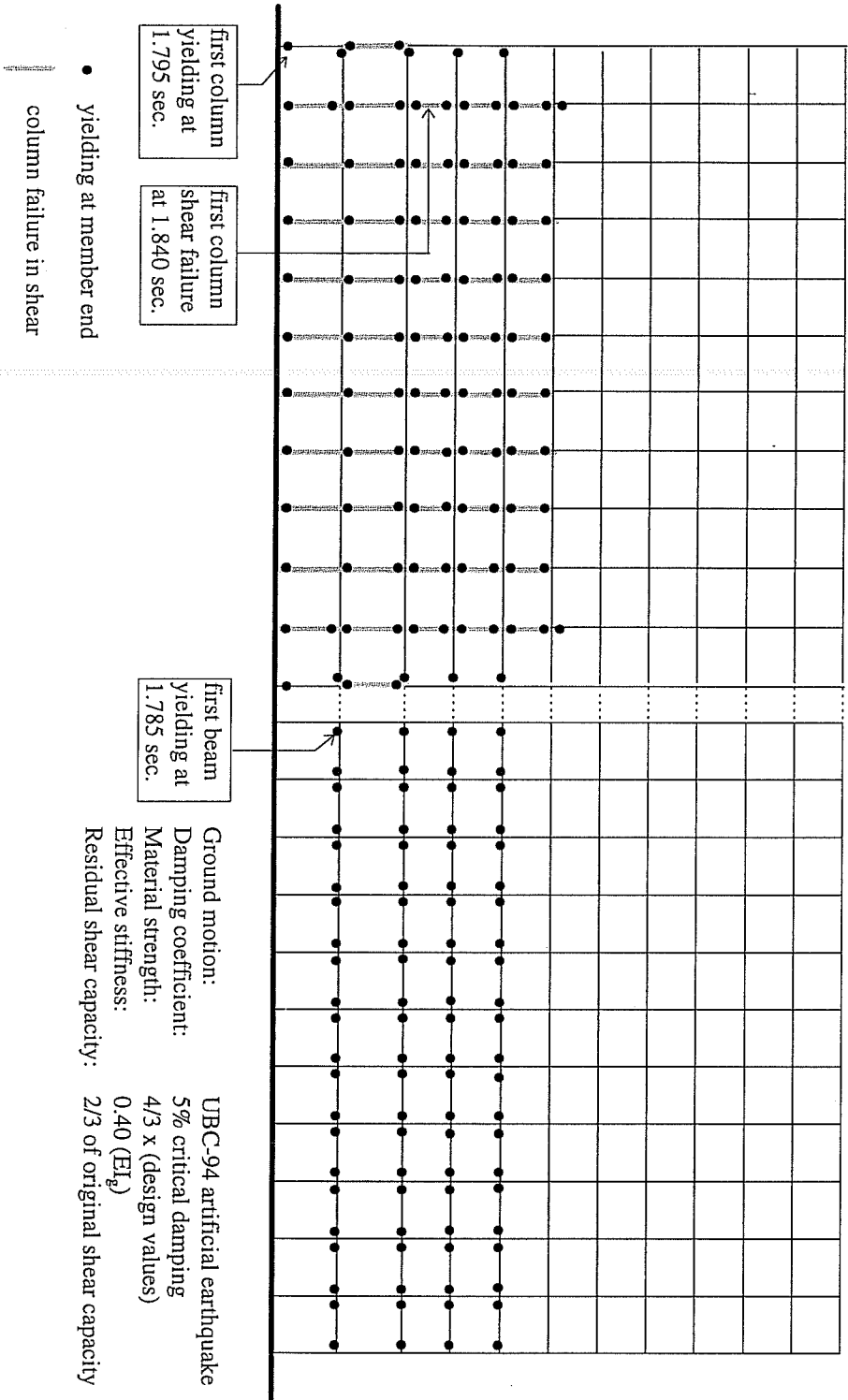


Figure 7.27 Failure State of the Ten-Story Building Subjected to UBC-94 Design-Spectrum Compatible Earthquake Scaled to Peak Acceleration of 150.3 in/s/s

Exterior Frame

Interior Frame

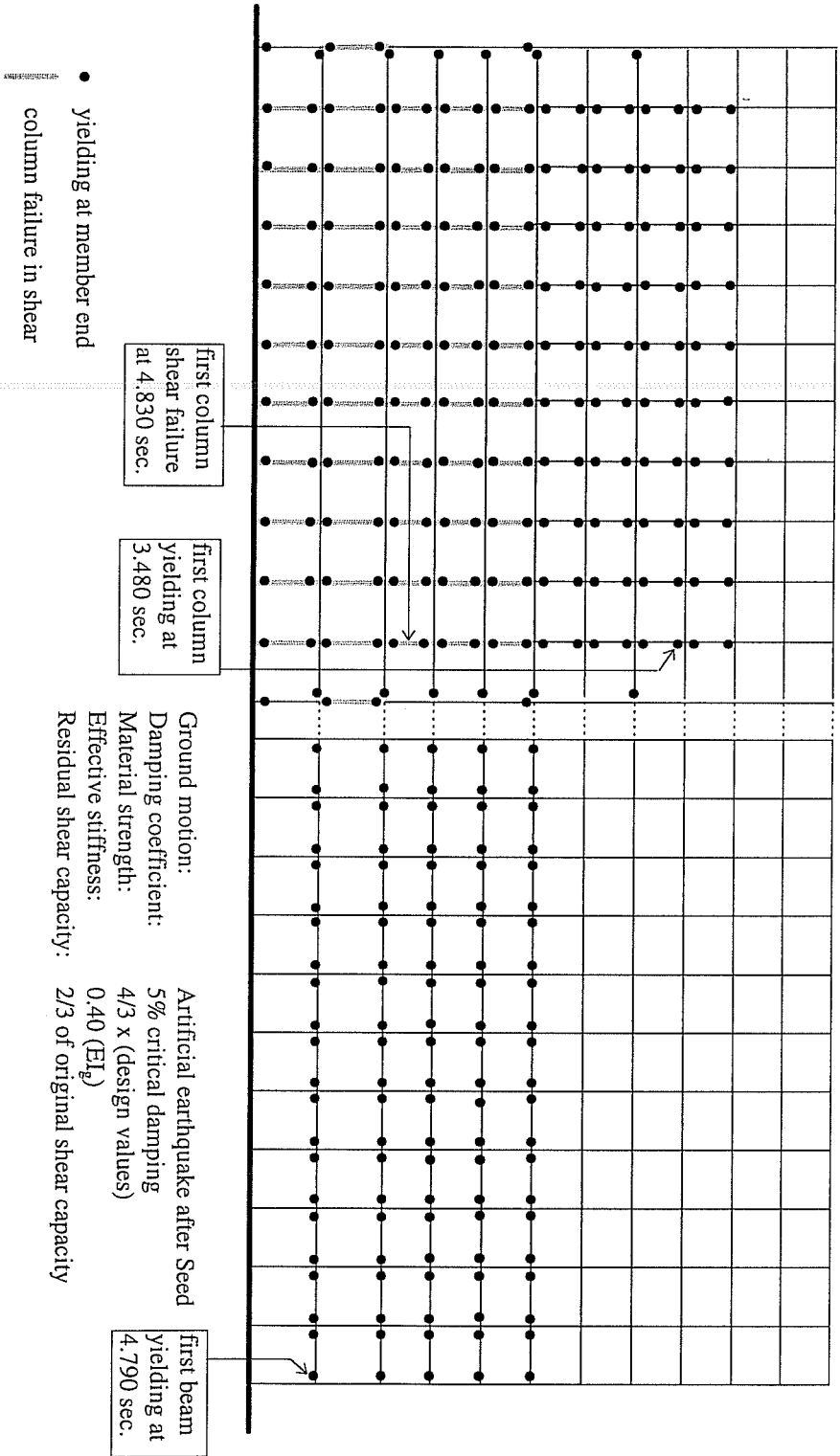


Figure 7.28 Failure State of the Ten-Story Building Subjected to Site-Dependent, Spectrum-Compatible Artificial Earthquake Scaled to Peak Acceleration of 150.3 in/s/s

CHAPTER 8 CONCLUSIONS

8.1 Summary

The capability of nonlinear analyses to predict responses of buildings under earthquake generated ground motions is assessed in this study. The equivalent lateral force procedure for seismic design in current building codes of the United States and most other countries is based on implicit consideration of inelastic structural response in the event of severe earthquakes. The extensive damage and economic losses that occurred during the 1994 Northridge and other recent moderate earthquakes have indicated that the equivalent lateral force procedure is inadequate in controlling non-structural damage in buildings. Non-structural damage can be controlled by limiting displacements, such as inter-story drift ratios, that the building will experience during earthquakes. Information on the amount and change of deformations and internal forces in structures can be explicitly obtained from nonlinear dynamic time history analyses. The applicability and accuracy of nonlinear analyses are evaluated, and significance of parameters included in nonlinear analyses is studied in this research.

The objective of this study is to demonstrate the capacity of nonlinear analyses to predict performance of reinforced concrete structures subjected to various earthquake ground motions, and to provide guidance on use of nonlinear time history

analyses for designing and evaluating new, existing, or retrofitted buildings in seismic zones to meet various performance requirements.

Two reinforced concrete moment resisting frame buildings (a seven-story hotel and a ten-story building) were analyzed using three earthquake records, and analysis results were compared with recorded responses during these earthquakes.

Nonlinear Analysis Programs

Two nonlinear programs, namely DRAIN-2D and IDARC, were studied. Differences between these two programs include the element model used for reinforced concrete frame members and the hysteretic rules used for cyclic loading. From the examples used in this study, the nonlinear time history results from DRAIN-2D correlated better with the recorded data than the results from IDARC. A number of parameters affecting the nonlinear analysis results, such as damping coefficients, actual strength of materials, effective stiffness and residual shear capacity were investigated.

Shear Failure Model

The seven-story hotel experienced several column shear failures during the 1994 Northridge Earthquake. A simplified shear failure model was proposed in the study. Each column was divided into two parallel sub-members. After the shear

capacity of the original column element was exceeded, one sub-member lost its lateral load resisting capacity by changing from a flexural member to a truss member. The shear capacity of the other sub-member was set to a very large value so it would not fail in shear, and the strength of this sub-member represented a residual shear capacity of the original column. The column element could sustain large lateral deformations through yielding of plastic hinges at ends of the element. By changing the magnitude of residual shear capacity, the simplified model could be varied to represent different types of shear failure of reinforced concrete members. The results indicated that the model was simple, convenient and effective. Better results could be obtained by adding additional sub-members to represent other behavioral characteristics.

Nonlinear Dynamic Time History Analyses -- Seven Story Hotel

The seven-story hotel was located at 8244 Orion Avenue, Van Nuys, California. It was severely damaged during the 1994 Northridge Earthquake. The damage consisted primarily of shear failure of columns in the fourth story. Nonlinear time history analyses were conducted on the south perimeter frame in the longitudinal direction where most of the damage occurred. From the analyses, it was found that the primary reason for failure of columns was inadequate shear capacity compared to the flexural capacity of the columns. The primary reason that most of the column

shear failures occurred at the fourth story was a change in column shear capacity (mainly the shear reinforcement) at the fourth floor level.

Infill masonry walls located at the east end of the building at the first story along the north perimeter frame were found to participate in the lateral force resisting system but were not considered as such in the original design. Because of the torsional effects created by these infill walls, the south perimeter frame suffered more damage than the north perimeter frame.

The drift ratio limit recommended by the NEHRP-94 was exceeded at the first through fourth stories from dynamic analyses.

Comparisons between the calculated and the recorded response data indicated that the nonlinear dynamic time history analysis produced satisfactory results. Relative floor displacement time history data seemed more sensitive than absolute acceleration time history data. The failure state of the building calculated from the time history analyses predicted more shear failures than what were observed. This was anticipated because the calculated shear capacity was very conservative. Nevertheless, the analyses did predict that the most extensive column shear failures would occur at the fourth story.

The hotel survived the 1971 San Fernando Earthquake with minor structural damage. The south perimeter frame of the building was analyzed in the longitudinal direction. Because of the small magnitude of ground motion, the analyses indicated

that no column shear problems should have occurred and the condition of the building after the 1971 San Fernando Earthquake indicated no column distress. The comparison between the calculated and the recorded response data was satisfactory, except that floor displacements were not in as good agreement as was found for the 1994 Northridge Earthquake. The difference was attributed to the relatively small earthquake ground motion and the more significant influence of non-structural elements on the response of the building at low deformation levels.

Although the drift ratios calculated from the time history analysis using the 1971 records were all less than the design drift limit set by the NEHRP-94 specification, the building sustained extensive non-structural damage. Therefore the drift limit recommended by the NEHRP-94 specifications cannot guarantee damage control. Rather, it is aimed at preventing building collapse.

Nonlinear Dynamic Time History Analyses -- Ten-story Building

Another building chosen for the study is a ten-story reinforced concrete building located at 7215 Bright Avenue, Whittier, California. The building was analyzed in the longitudinal direction in which the lateral force resisting system consists of moment frames. The comparison between the calculated and the recorded response data was satisfactory. The time history analysis indicated neither column shear failure nor member yielding occurred in the structure, which is consistent with

the building condition after the earthquake. The calculated inter-story drift ratios were relatively small, which explains why the building sustained no damage. Because the building is taller, the higher mode effects were noticeable.

Nonlinear Static Push-Over Analyses

Nonlinear static (push-over) analyses were also performed on these two buildings, and the results were consistent. Two commonly used lateral force patterns were studied, namely a uniform loading pattern and an inverted triangular loading pattern. Only DRAIN-2D was used for push-over analyses. For the buildings studied, the triangular loading pattern produced results which correlated better with recorded data and with results from nonlinear dynamic time history analyses. In addition, the triangular load pattern created a more critical condition than the uniform loading pattern. The study also indicated that the level of effective stiffness assumed significantly affected the push-over analysis results. With a proper level of effective stiffness, push-over analysis results were consistent with the dynamic analysis results and the recorded building response data.

Ground Motions

To compare the effects of different input earthquake ground motions, five representative earthquake ground motions were selected. The responses of the two buildings subjected to the various ground motions were studied using nonlinear time history analyses. Different building responses to different earthquake ground motions were explained using acceleration response spectra.

Since response spectra seemed to be a good indication of damage potential of earthquakes, response-spectrum-compatible artificial earthquakes were used in selecting the most critical design earthquakes. Two design spectra were used. One was the UBC-94 design spectrum, and the other was a site-dependent response spectrum after Seed, et al with mean-plus-one standard deviation. Results showed that the artificial earthquake generated according to site-dependent response spectrum with mean-plus-one standard deviation after Seed, et al²² created the largest demand on both buildings.

8.2 Conclusions

Based on the analyses performed on the selected buildings under different earthquake ground motions, the following are the most important conclusions obtained from this study.

8.2.1 Nonlinear Dynamic Time History Analyses

- (1) A proper effective stiffness value was needed to obtain results from DRAIN-2D which correlated with observed response and damage patterns. The effective stiffness had to be reduced as the magnitude of the earthquake ground motion increased. A simple effective stiffness factor for all beams and columns was sufficient to produce satisfactory results but results could be improved by assuming different effective stiffness factors for beams and columns.
- (2) Analysis results from IDARC correlated less well with the recorded response data for the examples used in this study, although IDARC has a more sophisticated and more modern element model.
- (3) By using a simplified shear failure model, DRAIN-2D satisfactorily predicted the location of shear failures, and the response of the building after shear failures. The response of the seven-story hotel proved this simplified shear failure model was efficient and accurate.
- (4) The analysis indicated that the primary reason for damage in the seven-story hotel during the 1994 Northridge Earthquake was the sudden change in shear capacity (longitudinal and transverse reinforcement in columns) which occurred at the fourth floor level.

- (5) Nonlinear dynamic time history analyses could predict the responses of reinforced concrete frame structures with satisfactory accuracy provided proper assumptions for critical properties were made. Sensitivity studies are needed to understand importance and influence of parameters.
- (6) The design drift limit recommended by the NEHRP-94 specification is aimed at preventing buildings from collapse and is not intended for non-structural damage control. A more restricted design drift ratio is desirable in order to prevent extensive damage and large economic losses related to excessive displacement, especially in the event of moderate earthquakes.

8.2.2 Nonlinear Static Push-Over Analyses

- (1) The nonlinear static (push-over) analysis procedure can predict structural capacity in terms of strength and deformation. However, as in dynamic time history analyses, a proper effective stiffness must be assumed to produce results using DRAIN-2D which correlate with observed responses. For example, from analysis results, $0.30(EI_g)$ was found appropriate for effective stiffness for the seven-story hotel in the 1994 Northridge Earthquake, $0.80(EI_g)$ for the seven-story hotel in the 1971 San Fernando Earthquake, and $0.40(EI_g)$ for the ten-story building in the 1987 Whittier Narrows Earthquake.

- (2) Different lateral force patterns in the static push-over analysis create different results. From the examples used in this study, the results using the triangular lateral force pattern correlated better with recorded data and with results from the dynamic analysis. In addition, the triangular lateral force pattern indicated a lower lateral load resisting capacity of the structure than the uniform lateral force pattern. Therefore, the triangular lateral force pattern is recommended for static push-over analyses.
- (3) For taller buildings, nonlinear static push-over analyses failed to reproduce the high mode effects in building responses with the lateral force patterns used. Therefore, the static push-over analysis procedure is recommended only for low-rise buildings, perhaps less than seven stories in height. For buildings taller than seven stories, a dynamic time history analysis may be needed.

8.2.3 Most Critical Earthquake Ground Motions

- (1) The response of two buildings subjected to different earthquake ground motions could be explained using acceleration response spectra, suggesting that acceleration response spectra serve as a simple, yet effective indicator of damage potential of earthquakes.

- (2) Design-spectrum-compatible artificial earthquakes produced the highest building responses from the examples studied.
- (3) The best approach of selecting the most critical design earthquake ground motions is to use a suite of records. Spectrum-compatible artificial earthquakes should be used with caution because they tend to yield very conservative results.

8.3 Suggestions for Further Research

After completing the research for this study, needs for further research in the following areas include:

- (1) A better element model is desirable. The element model used in DRAIN-2D needs a pre-determined effective stiffness for each member; information not available at the beginning of the calculation. IDARC uses an element model which does not require information about effective stiffness, but the results from IDARC were not satisfactory.
- (2) More case studies are needed in order to calibrate accuracy of nonlinear dynamic time history analysis results before the nonlinear time history analysis method can be used in routine design.
- (3) A three dimensional nonlinear dynamic time history analysis program must be developed for irregular structures with significant torsional responses.

REFERENCES

1. Seismology Committee, Structural Engineers Association of California, "Recommended Lateral Force Requirements and Commentary", San Francisco, California, 1989.
2. Earthquake Engineering Research Institute, "Northridge Earthquake January 17, 1994", Oakland, California, 1994.
3. Kannan, A. E., and Powell, G. H., "DRAIN 2D: A General Purpose Program for Dynamic Analysis of Inelastic Plane Structures", *Reports No. EERC 736 and EERC 73 22*, University of California at Berkeley, April 1973 (Revised September 1973 and August 1975).
4. Sashi K. Kunnath and Andrei M. Reinhorn, "IDARC2D Version 3.1 - Inelastic Damage Analysis of RC Building Structures", September 1994.
5. ATC-33.03, "Guidelines for the Seismic Rehabilitation of Buildings (75% complete draft), Volume I: Guidelines", Applied Technology Council, Redwood City, California, October 1995.
6. International Conference of Building Officials (ICBO), Uniform Building Code, Whittier, California, 1994.
7. Building Officials & Code Administrators International, The BOCA National Building Code, Country Club Hills, IL, 1993.
8. Southern Building Code Congress International (SBCCI), Standard Building Code, Birmingham, AL, 1993.
9. Building Seismic Safety Council, NEHRP Recommended Provisions for the Development of Seismic Regulations for Buildings, FEMA-222, Washington, DC, 1994.
10. Applied Technology Council, Tentative Provisions for the Development of Seismic Regulations for Buildings, ATC 3-06, Washington, DC, 1978.
11. Earthquake Engineering Research Institute, Loma Prieta Earthquake Reconnaissance Report, *Earthquake Spectra*, Supplement to Volume 6, May 1990.

12. Clough, R. W., and Benuska, K. L., "Earthquake Performance of High-Rise Buildings", *Report to the Federal Housing Administration*, T. Y. Lin and Associates, Van Nuys, CA, October 1965.
13. Jordan, R. M., "Evaluation of Strengthening Schemes for Reinforced Concrete Moment Resisting Frame Structures Subjected to Seismic Loads", *Ph.D. Dissertation*, The University of Texas at Austin, Austin, TX, May 1991.
14. Pincheira, J. A., and Jirsa, J. O., "Seismic Strengthening of Reinforced Concrete Frames Using Post-Tensioned Bracing Systems", *PMFSEL Report N. 92-3*, The University of Texas at Austin, Austin, TX, December 1992.
15. Chopra, A. K., "Dynamics of Structures, A Primer", *Monograph Series*, Earthquake Engineering Research Institute, Berkeley, CA, 1981.
16. Clough, R. W., and Penzien, J., "Dynamics of Structures", McGraw-Hill Book Co., New York, NY, 1975.
17. Biggs, J. M., "Introduction to Structural Dynamics", McGraw-Hill Book Co., New York, NY, 1964.
18. Newmark, N. M., and Rosenblueth, E., "Fundamentals of Earthquake Engineering", Prentice-Hall, Inc., Englewood Cliffs, NJ, 1971.
19. Biot, M. A., "A Mechanical Analyzer for Prediction of Earthquake Stresses", *Bulletin of the Seismological Society of America*, Vol. 31, pp.151-171, 1941.
20. Biot, M. A., "Analytical and Experimental Methods in Engineering Seismology", *Proceedings of ASCE*, Vol. 68, pp.49-69, 1942.
21. Housner, G. W., "An Investigation of the Effects of Earthquakes on Buildings", *Ph.D. Thesis*, California Institute of Technology, Pasadena, CA, 1941.
22. Seed, H. B., Ugas, C., and Lysmer, J., "Site-Dependent Spectra for Earthquake-Resistance Design", *Bulletin of the Seismological Society of America*, Vol. 66, pp.221-243, 1976.

23. US Nuclear Regulatory Commission, "Combination of Modes and Spatial Components in Seismic Response Analysis", Regulatory Guide 1.92, Washington, DC, 1976.
24. Crandall, S. H. and Mark, W. D., "Random Vibration in Mechanical Systems", Academic Press, New York, NY, 1973.
25. Bendat, J. S. and Piersol, A. G., "Random Data: Analysis and Measurement Procedures", Wiley-Interscience, New York, NY, 1971.
26. Newmark, N. M. and Hall, W. M., "Earthquake Spectra and Design", *Monograph Series*, Earthquake Engineering Research Institute, Berkeley, CA, 1982.
27. Mahin, S. A. and Bertero, V. V., "An Evaluation of Inelastic Seismic Design Spectra", *Journal of the Structural Division*, ASCE, Vol. 107, No. ST9, September, 1981, pp. 1777-1795.
28. Shibata, A. and Sozen, M. A., "The Substitute-Structure Method for Seismic Design in Reinforced Concrete", *Journal of the Structural Division*, ASCE, Vol. 102, No. ST1, January 1976, pp. 1-18.
29. Gulkan, P. and Sozen, M. A., "Response and Energy Dissipation of Reinforced Concrete Frames Subjected to Strong Base Motions", *Structural Research Series No. 377*, University of Illinois, Urbana, IL, May 1971.
30. Saiidi, M. and Sozen, M. A., "Simple and Complex Models for Nonlinear Seismic Response of Reinforced Concrete Structures", *Structural Research Series No. 465*, University of Illinois, Urbana, IL, August 1979.
31. Bathe, K. J., "Finite Element Procedures in Engineering Analysis", Prentice-Hall, Inc., Englewood Cliffs, NJ, 1982.
32. Housner, G. W., "Interaction of Building and Ground During an Earthquake", *Bulletin of Seismological Society of America*, Vol. 47, No. 3, 1957, pp.179-186.
33. Hudson, D. E., "A Comparison of Theoretical and Experimental Determinations of Building Response to Earthquakes", *Proceedings of Second World Conference on Earthquake Engineering*, Tokyo, Japan, 1960, II, 1105-1120.

34. Murphy, L. M., ed., "San Fernando, California, Earthquake of February 9, 1971", Vol. 1, U.S. Department of Commerce, Washington, D.C., 1973.
35. Wood, J. H., "Analysis of the Earthquake Response of a Nine-story Steel Frame Building during the San Fernando Earthquake", *Report No. EERL 72-04*, Oct. 1972, Caltech, Pasadena, California.
36. Abdel-Ghaffar, A. M., "Engineering Data and Analyses of the Whittier, California, Earthquake of January 1, 1976", *Report No. EERL 77-05*, Nov. 1977, Caltech, Pasadena, California.
37. Miller, R. K., "The Santa Barbara Earthquake of 13 August 1978", *Earthquake Engineering and Structural Dynamics*, Vol. 7, 1979, pp. 491-506.
38. Earthquake Engineering Research Institute, "Reconnaissance Report Imperial County, California, Earthquake October 15, 1979", Feb. 1980, Berkeley, California.
39. Pardoen, G. C., Hart, G. C., and Bunce, B. T., "Earthquake and Ambient Response of El Centro County Services Building", *Proceedings of Second Specialty Conference on Dynamic Response of Structures*, Atlanta, Georgia, Jan. 1981, American Society of Civil Engineers, New York, pp. 164-173.
40. Saïidi M., "Seismic Study of Imperial County Services Building", *Proceedings of Second Specialty Conference on Dynamic Response of Structures*, Atlanta, Georgia, Jan. 1981, American Society of Civil Engineers, New York, pp.431-444.
41. Seekins, L. C., Brady, A. G., Carperter, C. and Brown, N., "Digitized Strong Motion Accelerograms of North and Central American Earthquakes 1933-1986", *USGS CD-ROM DDS-7*, Boulder, Colorado, 1992.
42. Naeim, F. and Anderson, A. G., "Classification and Evaluation of Earthquake Records for Design", *Report No. CE 93-08*, Department of Civil Engineering, University of Southern California, 1993.
43. Naeim, F., "Selection of Earthquake Records for Seismic Design of Tall Buildings", *The Structural Design of Tall Buildings*, Vol. 2, No. 4, Dec. 1993. pp. 255-293.

44. Applied Technology Council, "Post-Earthquake Safety Evaluation of Buildings", ATC-20, Redwood City, CA, 1989.
45. Islam, M. S., "Holiday Inn", *Northridge Building Case Studies Project (Second Drift)*, Sacramento, CA., September 1994. pp. 1.14-1 - 1.14-49.
46. Dames and Moore, "Report of Foundation Investigation, Proposed Seven-Story Motel, Roscoe Boulevard and Orion Avenue, Panorama City, Los Angeles", Feb. 1966, 12pp. plus appendix.
47. Procella, R. L., Etheredge, E. C., Maley, R. P., and Acosta, A. V., "Accelerograms Recorded at USGS National Strong-Motion Network Stations During the $M_S = 6.6$ Northridge, California Earthquake of January 17, 1994", *U. S. Geological Survey Open File Report 94-141*, 1994
48. Hart, G. C., Thurston, S. J., and Englekirk, R. E., "Seismic Evaluation of a Tall Reinforced Concrete Frame Building", *Seismic Engineering: Research and Practice, Proceedings of the ASCE Structures Conference '89, San Francisco, California*, pp. 277-286, May, 1989.
49. Miranda, E., and Bertero, V. V., "Evaluation of Seismic Performance of A Ten-Story RC Building During The Whittier Narrows Earthquake", *Report UCB/EERC-91/10*, University of California at Berkeley, CA, 1991.
50. Jones, L., and Hakusson, E., "The Whittier Narrows Earthquake, California Earthquake of October 1, 1987 - Seismology", *Earthquake Spectra*, Vol.4, No. 1, pp. 43-53, February, 1988.
51. Etheredge, E., Porcella, R., "Strong-Motion Data from the October 1st, 1987 Whittier Narrows Earthquake", *Open-file Report 88-38*, Department of Interior, U.S. Geological Survey, Menlo Park, California, January, 1988.
52. Park, Y. J., Reinhorn, A. M., and Kunnath, S. K., "IDARC: Inelastic Damage Analysis of Reinforced Concrete Frames-Shearwall Structures", *Technical Report NCEER-87-0008*, State University of New York at Buffalo, Buffalo, NY, 1987.
53. Alvarez, R. J., and Birnstiel, C., "Inelastic Analyses of Multistory Frames", *Journal of Structural Division*, ASCE, 95(11), 1969, pp. 2477-2503.

54. Bouadi, A., "Use of Eccentrically Braced Frames (EBFS) for Seismic Strengthening of Reinforced Concrete Frames", *Ph.D. Dissertation*, The University of Texas at Austin, Austin, TX, August 1994.
55. Wilson, E. L., "A Method of Analysis for the Evaluation of Foundation-Structure Interaction", *Proceedings, Fifth World Conference on Earthquake Engineering*, Santiago, Chile, January 1969, pp. A-6, 87-46, 99.
56. Giberson, M. F., "Two Nonlinear Beams with Definition of Ductility", *Journal of the Structural Division*, ASCE, Vol. 95, February 1969, pp. 137-157.
57. Takeda, T., Sozen, M. A., and Nielsen, N., "Reinforced Concrete Response to Simulated Earthquakes", *Journal of the Structural Division*, ASCE, Vol. 96, December 1970, pp. 2557-2573.
58. Kunnath, S. K., Reinhorn, A. M., and Park, Y. J., "Analytical Modeling of Inelastic Seismic Response of R/C Structures", *Journal of Structural Engineering*, ASCE, Vol. 116, No. 4, 1990, pp. 996-1017.
59. Vision 2000 Committee, "VISION 2000, Performance Based Seismic Engineering of Buildings", Structural Engineers Association of California (SEAOC), Sacramento, CA, April 1995.
60. Bathe, K. J., "Finite Element Procedures in Engineering", Prentice-Hall, Englewood Cliffs, NJ, 1982.
61. Kunnath, S. K., Reinhorn, A. M., and Abel, J. F., "A Computational Tool for Evaluation of Seismic Performance of Reinforced Concrete Buildings", *Computers & Structures*, Vol. 4, No. 1, 1991, pp. 157-173.
62. Kent, D. C., and Park, R., "Flexural Members with Confined Concrete", *Journal of the Structural Division*, ASCE, Vol. 97,(7), 1971, pp. 1969-1989.
63. Farahany, M. M., "Computer Analysis of Reinforced Concrete Cross Sections", *M.Sc. Thesis*, The University of Texas at Austin, May 1977.
64. Lu, Zhan-Qin, Chen Jia-Kui, "Aseismic Behavior of RC and SRC Shore Columns", *Concrete Shear in Earthquake*, Elsevier Applied Science, London, and New York, 1992, pp.65-74

65. Umehara, H. and Jirsa, J. O., "Shear Strength and Deterioration of Short Reinforced Concrete Columns under Cyclic Deformations", *PMFSEL Report* 823, The University of Texas at Austin, July 1982, 256pp.
66. Mirza, S. H., et at, "Statistical Description of Strength of Concrete", *ASCE Journal of Structural Division*, June 1979, pp. 1021-1037.
67. Pauley, T. and Priestly, M. J. N., "Seismic Design of Reinforced Concrete and Masonry Buildings", John Wiley & Sons, Inc., 1992.
68. John A. Blume & Associates Engineers, "Holiday Inn", *San Fernando, California, Earthquake of February 9, 1971*, NOAA Report, 1973.
69. ACI Committee 318, "Building Code Requirements for Structural Concrete (ACI 318-95) ad Commentary (ACI 318R-95)", American Concrete Institute, Framington Hills, MI, 1995.
70. Moehle, J. P., and Diebold, J. W., "Lateral Load Response of Flat-Plane Frame", *Journal of Structural Engineering*, Vol. 111, No. 10, pp. 2149-2164, October, 1985.
71. Lawson, R. S., Vance, V., and Krawinkler, H., "Nonlinear Static Push-Over Analysis - Why, When, and How?", *Proceedings of the Fifth U.S. National Conference on Earthquake Engineering*, Earthquake Engineering Research Institute, Vol. 1, pp. 283-292., 1994.
72. Lew, H. S., Leyendecker, E. V., and Dikkers R. D., "Engineering Aspects of the 1971 San Fernando Earthquake", *Building Science Series 40*, U.S. Department of Commerce, December 1971.
73. International Conference of Building Officials (ICBO), Uniform Building Code, 1970 Edition, Pasadena, California, 1971.
74. Levy, S. and Wilkinson, J. P. D., "Generation of Artificial Time-History, Rich in All Frequencies, From Given Response Spectra", *Nuclear Engineering and Design*, North-Holland Publishing Company, 38 (1976), pp. 241-251.
75. Okawa, Izuru, Kitagawa, Yoshikazu, Kashima, Toshihide, and Koyama, Shin, " A Guideline for Composing Design Earthquake Ground Motion for Dynamic Analysis of Buildings", *The Fifth U.S. National Conference on*

Earthquake Engineering, Vol. II, July 10-14, 1994, Chicago, Illinois, pp. 273-282.

76. Roesset, J. M., SIMQKE - Simulation of Earthquake Ground Motions, (private communication), The University of Texas at Austin, June, 1995.

VITA

Yonghui Roger Li was born in Hefei, Anhui Province, The People's Republic of China on July 3, 1963, the son of Fukun Li and Keling Zhang. After completing his study at Hefei No. 8 High School, Hefei, Anhui in 1981, he entered Tongji University in Shanghai, P. R. of China, where he received the degree of Bachelor of Science in Civil Engineering with honor. In 1988 he received the degree of Master of Engineering from the same university. Then he worked for three years in universities before he entered the Graduate School of Syracuse University, New York, where he obtained the degree of Master of Science in Civil Engineering. In September 1993, he entered the Ph.D. program in the Graduate School of the University of Texas at Austin.

Permanent Address: 20 Jinzhei Road, Building 15, #201

Hefei, Anhui Province, The People's Republic of China

This dissertation was typed by the author.

